SIMULATION, MODELING AND EXPERIMENTAL VALIDATION OF SEMICONDUCTOR BASED THERMOELECTRIC GENERATOR

A

Ph.D. THESIS

Submitted in partial fulfillment of the requirements for the award of the degree

of

DOCTOR OF PHILOSOPHY

in

ENERGY CENTRE

by

SANJEEV KUMAR BHUKESH
(Sch. No. 163118003)

MAULANA AZAD
NATIONAL INSTITUTE OF TECHNOLOGY
BHOPAL – 462 003 (INDIA)
SEPTEMBER 2023

MAULANA AZAD NATIONAL INSTITUTE OF TECHNOLOGY, BHOPAL

DECLARATION

I hereby certify that the work which is being presented in the thesis entitled "**Simulation, Modeling and Experimental Validation of Semiconductor Based Thermoelectric Generator**" in partial fulfillment of the requirements for the award of the Degree of Doctor of Philosophy and submitted in the Energy Centre of the Maulana Azad National Institute of Technology, Bhopal is an authentic record of my own work carried out during the period from July 2016 to June 2023 under the supervision of **Dr. Anil Kumar**, Associate Professor, Department of Mechanical Engineering, Delhi Technological University, Delhi and **Dr. Suresh Kumar Gawre**, Assistant Professor, Department of Electrical Engineering, Maulana Azad National Institute of Technology, Bhopal.

The matter presented in this thesis has not been submitted by me for the award of any other degree of this or any other Institution.

Sanjeev Kumar Bhukesh
(Scholar no. 163118003)
Energy Centre, MANIT Bhopal

This is to certify that the above statement made by the candidate is correct to the best of my knowledge.

Date:

Dr. Anil Kumar
Associate Professor
Dept. of Mechanical Engg.
Delhi Technological University, Delhi (India)

Dr. Suresh Kumar Gawre
Assistant Professor
Dept. of Electrical Engg.
MANIT, Bhopal

The Ph.D. Viva-Voice Examination of **Sanjeev Kumar Bhukesh**, Research Scholar, has been held on……………………………………..

Signature of Supervisors

Signature of External Examiner

ABSTRACT

According to the **UNFCCC COP-27** agenda, producing clean energy has become the main initiative of every country. One promising kind of renewable energy is the thermoelectric generator. There are many facets to a thermoelectric generator, such as the principle of thermoelectricity, the history of solar and waste heat based thermoelectric power generation, thermoelectric hybrid systems, thermoelectric materials (silicon, ceramics, and polymers) in conventional, segmented, and "cascaded arrangement, operating temperature range, figure of merit, popular modeling and simulation tools, environmental impact, future improvements, exploitation of TEGs in a wide variety of applications", and so on (automotive engines and aerospace). Thermoelectric generator (TEG) heat recovery systems and the potential of TEG to produce energy from the human body are also discussed, as is the performance of different solar concentrators (parabolic dish, Fresnel lens, solar furnace, etc. with their optical concentration). In this research, numerical simulation of a Giant Water Lens Solar Thermoelectric Generator (GWLSTEG) system has been carried out, that employs a giant water lens as a solar concentrator and a mid-temperature nanostructured Bi_2Te_3 thermoelectric module (TEM). The two different soft-wares;Sol-Trace for ray tracing through the water lens and COMSOL for simulation of the Bi_2Te_3 module have been used. Following the simulated values, manufactured a similar giant water lens as a solar concentrator to focus the sun rays on an aluminium receiver plate integrated with Bi_2Te_3 TEM and experiments were conducted. Heat flux intensity is noticed to have increased four to five folds, i.e., from 1135 to 4580 W/m^2, through the water lens concentrator. Maximum temperature on the hot junction achieved is 225^{o}C (498K) and maximum temperature difference of 190^{o}C (463K) is achieved between the hot and cold junctions. The system was able to attain a maximum overall system efficiency of 12.04%. Also, it can be noticed that these parameters show maximum values at the time of the day when the relative humidity and velocity of the air is lowest, i.e., 12.5% at 14:00 hrs, and also the maximum power output obtained through the device is 7W. After experimenting, suggestions have also been given to provide a better software simulation alternative to carry out evaluations and modifications in the process of GWLSTEG functioning in order to get the same results to save time while making it

more cost-effective. This research helps academia, researchers, and industrialist with deep insights into customization of TEG projects in qualitative and quantitative ways before actual realization.

ACKNOWLEDGMENT

I would like to thank **Dr. Anil Kumar** and **Dr. Suresh Kumar Gawre** for their support and guidance as my supervisors and advisors throughout this project duration. I would also like to thank all my colleagues for encouraging me to get involved in this project.

I would also like to thank **Mr. P. V. S. L. Narsimham (Chairman)**, **Mr. P. S. Sampath (Managing Director), Mr. A. P. Srinivas Rao Mohan (Manager Operations) Tee-wave Power Tech, Hyderabad.**

I express my deep sense of gratitude to **Dr. Karunesh Kumar Shukla** (Director MANIT Bhopal) and **Dr. Prashant Baredar** (Head, Energy Centre, MANIT Bhopal), for his continued encouragement & permission to carry out this work at ***M.A.N.I.T. Bhopal***.

Last but not the least, I would like to thank my spiritual guru- Shri **Premanand Govind Sharan Ji Maharaj**, my family (my mother- Shrimati **Kamlesh Devi**, father- Shri **Prem Kishore**, Sister- **Ruby**, Brother- **Krishan Kant**) and friends for their unlimited support, encouragement and patience all the way throughout this Ph.D. project period.

Sanjeev Kumar Bhukesh

TABLE OF CONTENTS

TABLE OF CONTENTS

LIST OF FIGURES

LIST OF TABLES

LIST OF SYMBOLS AND ABBREVIATIONS

Nomenclature		Unit
A	Area	m^2
C	Velocity of light in vacuum	m/s
C_H	Specific heat capacity	J/(kg K)
C_{th}	Thermal concentration ratio	
C_{geo}	Geometrical concentration Ratio	
C_{opt}	Optical concentration Ratio	
$\vec{D}$	Electric flux density	C/m^2
$\vec{E}$	Electric field Intensity	N/C or V/m
f	Focal Length of the lens	m
H	Height of parabolic lens	m
h_{conv}	Convection coefficient	$W/(m^2 K)$
I	Current	A
I_P	Current at maximum power	A
I_b	Beam radiation on water lens surface	W/m^2
I_c	Concentrated solar radiation on absorber surface	W/m^2
I_d	Diffused radiation to atmosphere	W/m^2
I_g	Global incoming solar radiation	W/m^2
$\vec{J}$	Electric current density	A/m^2
k	Thermal conductivity	W/mK
K	Overall thermal conductance	W/K
n	Refractive index	1.12

P	Power	W
R	TEG module internal resistance	Ω
R_L	Load resistance	Ω
R_c	Radius of Curvature	m
s	Seebeck coefficient	V/K
T_h	Hot side temperature	K
T_c	Cold side temperature	K
T	Mean temperature	K
ΔT	Temperature difference between hot and cold side	K
T_{sun}	Temperature of Sun's outer surface	5778 K
V	Volume of parabolic giant water lens	
V_a	Velocity of air	m/s
V_L	Load voltage	V
V_{oc}	Open circuit voltage/No load voltage	V
ΔV	Change in voltage with change in temperature	V
Z	Figure of merit	1/K
ZT	Dimensionless figure of merit at highest mean temperature	
Greek Symbols:		
α_{ab}	Absorptance of the absorber	
σ_{sb}	Stefan Boltzmann constant	5.67×10^{-8} W m^{-2} K^{-4}
Φ	Electric scalar potential	V
ρ_d	Density of the TE material	kg/m^3
ρ	Resistivity	Ω-m

μ	Thomson coefficient	V/K
τ_l	Net transmittance of lens	
τ_w	Transmittance of water	
τ_P	Transmittance of LLDPE cover/Polythene/Plastic	
ε	Emittance	
ε_d	Dielectric permitivity	farad per meter (F/m)
η_{ot}	Optothermal efficiency	%
η_{te}	Thermoelectric efficiency	%
η_{opt}	Optical efficiency	%
η_{sys}	Overall efficiency of the GWLSTEG system	%
ψ_{sys}	Exergy efficiency of the GWLSTEG system	%
Subscripts:		
a	Ambience/Atmosphere/Surroundings	
ab	Absorber surface	
c	Cold Side of the absorber	
conv.	Convective	
h	Hot Side of the absorber	
in	Input to the system	
l	LLDPE lens	
mod	TEG module	
n	n-Type semiconductor	
out	Output from the system	
p	p-Type semiconductor	
rad.	Radiative	

w	Water	

Abbreviation:

ATEG	Annular Thermoelectric Generator
B-HSTEG	Hybrid Solar Thermoelectric Generator Without Evacuated Glass Tube
EGR	Exhaust Gas Recirculation (EGR)
ETC	Electric Turbo-Compound
ETEG	Exhaust based TEG
FEA	Finite Element Analysis
HFSF	High Flux Solar Furnace
GWLSTEG	Giant water lens solar concentrated thermo electric generator
LCZ	Low Convective Zone
$LCCO_2$	Life Cycle CO2 Emissions
LED	Light Emitting Diode
LLDPE	Linear Low Density Polyethylene
PCM	Phase Change Material
PV-TCS	Photovoltaic- Thermoelectric Cooling system
PV-TGS	Photovoltaic- Thermoelectric Generation system
RSTEG	Refracted Solar Thermoelectric Generator
STE	Solar Thermal Electric
STEG	Solar Thermoelectric Generator
STEPG	Solar-Based Thermoelectric Power Generation
TEG	Thermoelectric Generator
TEM	Thermoelectric Module
TEPG	Thermoelectric Power Generation
V-HSTEG	V-Hybrid Solar Thermoelectric Generator With Evacuated Glass Tube

Chapter 1

INTRODUCTION

On this planet 'earth' where petroleum derivatives command as vital energy sources, there is requirement for technically and economically feasible sustainable power sources. The procedures through which petroleum derivatives are produced don't happen sufficiently quickly to renew their sources to fulfil the needs of society and burning of non-renewable energy sources produces carbon dioxide, carbon mono-oxide, an ozone harming gas responsible for boosting the temperature of the 'Earth', means pollution and emission of heat, caused by the usage of conventional technologies result in global warming [1],[2].

By the end of year 2050, the number of people living in cities is projected to increase to 9 billion worldwide. In order to provide food security and better nutrition for a rising population, governments and non-government organizations throughout the globe are focusing on a greater sources of agriculture (for food) [3]. On the other hand, there will be a corresponding rise in electricity demand [4]. Therefore in addition to conventional fuels i.e, coal, diesel, etc., even biogas is also being used for electricity production [5], [6], [7]. Therefore the research for cleaner, more sustainable sources has become a worldwide concern in view of exponentially raising cost of energy and the environmental concerns caused due to slapdash use of fossil fuel [8]**.**

The aim of availing green and clean options can be better served by converting the solar and waste thermal energy into useful electrical energy, i.e., Thermoelectric Power [9]. Among the practically available technologies for the solution TEGs are expanding interest in light of the fact that these solid state devices can change heat released from various sources into electric power utilizing the Seebeck effect. The conduction of charge carriers takes place due to temperature difference between hot side and cold side. The most important part of any TEG is thermoelectric modules which is solid-state integrated circuit that utilizes Seebeck effect out of three thermoelectric effects known as the Peltier, Seebeck and Thomson impacts/effects.

Peltier effect is reciprocal to the Seebeck effect, discovered in 1830. As indicated by this, heat is absorbed or generated whenever a current passes through a junction between different materials, depending on the direction of the current. Thus, if a current is forced through a thermocouple by connecting an electrical source, one junction will become cold and will thus absorb energy from the ambient, and the other junction will become hot and dissipate heat to the surroundings. This principle can be used for evacuation of heat (i.e, cooling/refrigeration) from one area and releasing it to another area (i.e heating) through electrical means. This principle is being used to maintain cold and hot chambers in service carts used by airhostess [10]**.**

Peltier coolers, also known as thermoelectric coolers, are cooling devices commercialized to exhibit high performance, dissipate high heat flux precisely at a very low temperature. The thermoelectric device carries the higher temperature on the surface; by pumping heat to maintain a particular junction temperature, it serves its purpose as temperature regulator [11]**.**Thermoelectric coolers, when used with air or liquid cooling, allow for a negative temperature gradient to be created and thermal resistance to be decreased. The effectiveness of a heat exchanger's hot side is affected by the thermoelectric generator's output [12]**.**

The heat required at the hot junction of TEG may be provided by (i) burning fossil fuel (gas or oil fire) (ii) concentrated solar power (iii) decay of radioisotope (iv) decay of nuclear fuel (v) power plants (vi) factories- industrial machines (vii) motor vehicles- exhaust of automobiles (vii) computers (ix) human bodies etc. Conventional heat engines are used in solar thermal technology to convert a temperature difference into electricity. TEGs may use this temperature difference to generate electricity [13], but these are comparatively smaller in size, so less electricity is produced. A series of thermocouples may be effective, but they are often more costly[14]. The numerous focal points of this energy transformation incorporate green technology, solid state operation, the non-appearance of poisonous residuals, immense adaptability, the absence of moving parts or chemical reaction, silent operations, due to the absence of any mechanical movement and long life (20-25 years) [15], [16], [17]. It can be extensively used in isolated places and remote areas where energy conversion technologies are unavailable [18].

The various aspects of any TEG device development are; TE material, synthesis of high FOM thermoelectric materials, techniques of achieving high ZT (i.e improving power factor or by reduction in thermal conductivity), design criteria of the TEG, operating temperature range of TEG, performance, efficiency of waste heat recovery system, Solar radiation, environmental aspect, advancement, hybrid system, modelling, simulation, cost and applications of TEGs in different areas [19].

The essential parts of any TE module are TE legs, copper or any highly conductive substrate and ceramic plate. The legs are made up of TE element (n-type as well as p-type) [20],whose figure of merit/thermoelectric efficiency is an important factor and legs are alternately connected i.e. thermally in parallel and electrically in series [10]. A basic TEG generally comprises one set of thermocouples. The voltage and power yield of one set is little. A few such units might be associated with arrangement to get a workable voltage. The workable voltage depends on the TE properties of the thermoelectric material i.e, Seebeck coefficient (s), thermal conductivity (k) and electrical conductivity (σ) and FOM (ZT). ZT, which signifies the figure of merit, governs the TEM efficiency as $ZT=s^2T/k\rho$. In this expression, electrical resistivity (ρ) is the reciprocal of electrical conductivity (σ). Peak ZT values of 0.5–2.0 have been observed in thermoelectric materials so far, resulting in poor conversion efficiency and relegating these materials to some specialized uses. The Seebeck effect of metallic TE element is found low. The Seebeck coefficient (s, μv/k) and the FOM (ZT) for some metals are as; for Bismuth; -75, 0.208, for Nickel; -18, 0.112×10^{-1}, for Copper; +2.5, 0.231×10^{-3} etc [13][21][22].

Setting up an appropriate correlation among various TE physical parameters like electrical conductivity, Seebeck coefficient, and thermal conductivity for a crystalline structure is an ultimate requirement for creating TE materials with unrivaled functioning. A high Seebeck coefficient (s), low thermal conductivity (k) and high electrical conductivity (σ) are alluring for TE materials. In this way, an appropriate balance between Seebeck coefficient, thermal conductivity and electrical conductivity of a material is required to optimize these TE properties. By and large, as of now the research has concentrated on creating different TE structures and highly efficient TE materials, because the significance of this parameter (efficiency) is all around remembered; it is a built up, pervasive, routinely utilized parameter for material, devices, hardware and process portrayal both in the thermoelectric industry and in research activities [13] [23].

Semiconductor materials have considerably higher TE coefficients. Extrinsic Semiconductor materials (binary compounds) produced using bismuth (Bi), antimony (Sb), tellurium (Te) and selenium (Se) have high FOM and are utilized in TE legs. Lead telluride is the most usually utilized material at temperature underneath 600 ^{o}C. In this range of temp, the FOM (ZT) for lead telluride is in the range of 0.2 to 0.8. This is an intermetallic compound containing around 61.9% Pb and 38.1% Te in its pure form. Both lead and tellurium are soluble to a little degree in PbTe. An abundance of Te prompts a p-type semiconductor, while an over-abundance of Pb prompts an n-type material. Silicon germanium (Si-Ge) combinations are the best materials in the high temperature range (over 600 ^{o}C). They likewise have great mechanical properties-high mechanical strength, low coefficient of thermal expansion and light in weight [24]**.**

A highly efficient TE element delivers a net voltage of around 300-500 µv per degree Kelvin. A module (thermopile) is formed by series connection of large number of such elements. In a typical commercial module, an electrical output of 10W at 6V and with 100 ^{o}C at the hot junction is acquired. The thermal efficiency of a TEG is generally very low (around 8%). Higher efficiencies of the order of 14% are being endeavoured to make it compete with solar PV systems [25][26]**.**

As a result of the high cost of TE material, these generators are not widely utilized as a part of commercial applications. In the low Power range (1W-1000W), fossil fuel based TEG utilizing gas as a fuel might be more sparing than IC-engine driven generators. It provides a handy, reliable and simple auxiliary source of standby power, particularly for remote zones. Because of their reliability and robustness, these are utilized as part of military applications. Kerosene fuelled thermoelectric generators are being utilized by peasants in remote territories of Siberia. Radioisotope (polonium)-fuelled and nuclear fuelled TEG have been utilized as a part of space applications, for example; moon probes, satellites and weather stations. High cost and low efficiency are main disadvantages of TEGs [27]**.**

Since 1821, when Thomas Seebeck first used a temperature gradient to produce the electric potential, scientists have been aware of the thermoelectric effect. However, limited efficiency confined their use to thermocouple sensors and specialized fields like space exploration [28]. The explorers of deep space exploration from NASA chose thermoelectric because of their reliability and resistance to the elements [29]. The 'cordless-Electric Company' manufactured a model 'TEG-5000' of a thermoelectric generator. Like the transistor or microchip, this electric generator is solid state, makes no noise, and has no moving parts. This generator consumes natural gas or propane. The efficiency is asserted to be 12%. This generator has the output of 5 KW, 115 V, 60 HZ enough to power an average US house. Weighing only 27 pounds, the generator can be carried like a briefcase; with the push of a button, it delivers full electric power in just 20 seconds [24]**.**

Nowadays, the applications of thermoelectric generators are seen in every sector of various industries worldwide. As far as applications of TEG are concerned, low power applications of TEG can be seen in wrist watches (1µW-10µW), in microelectronics-CPU cooling (10µW-100µW), in consumer application-wine cooler (100µW-10mW), in space for electrical power and cooling-voyager (10mW-1W), in remote wireless sensors-network (1W-10W), in biomedical devices-pacemaker (10W-1kW), and on large scale waste heat recovery-transport vehicle (1kW-10-kW) [30].

As far as waste heat recovery is discussed, nearly 70% of world energy is known to be wasted. TEGs have been employed in automobiles for many reasons, like reducing carbon emissions and enhancing the engine's overall efficiency. Challenges and opportunities present for ETC and TEG systems used in compact cars powered through an SI engine that is turbocharged and an analysis for investigating the advantages attained by the ETC and TEG was carried out. This analysis was conducted through a dynamic engine vehicle model and validated against the available transient experimental data and steady-state data [31]. In a model experimental analysis for heavy-duty DE (Diesel engine) and TEM test rig was made over the EGR path, and a good agreement was observed with a simulated one. Both the models were equipped with the prototype TEG[32].

In a waste heat recovery system, fin-type heat exchanger is found comparatively more efficient and compact than the tube heat exchanger [33]. The FEA method through ANSYS, COMSOL 5.4 Multi-physics and MATLAB etc. are used for the analysis of TEG under the non-uniform and transient heat flux in waste heat recovery [34]. An advanced model of irreversible TEG was developed. The results exhibited that the law of external heat transfer affects the optimal performance and the characteristic of TE device. With the law of Newtonian heat transfer, the maximum efficiency and the output power are found maximum as compared to the various laws of heat transfer [35]. Another, one of the methods that have been in practice is the use of segmented TE leg to maximize efficiency. A mathematical model of the segmented TEG based on those TE materials which have low temperature was developed. The outcome shows that maximum conversion efficiency and output power of the segmented TEG is more significant when coolant is brought into use for the cooling source. For the heat source, diesel engine is used [36].

TEGs were installed in Porsche car. Results from this TEG system, installed in Porsche 944's exhaust were published in 2008, around 29 years after the system first installed. In this system, HI-Z Technology enabled TEG to generate 200W of power by conversion of heat. With a vision of generating 1kW of power, 2 years down the line, they mounted a TEG on a Truck, but initially, they generated only 400W of power. After a series of improvements and achieving the 1KW target, many problems were faced with applying new HZ-14 converters during durability tests [20].

The TEGs were modified and remodeled for hybrid sports utility vehicles to generate 180W of power, and to be capable of charging 300 V batteries. TEGs were implemented in displacement engines in Marlow, Visteon, BMW and BSST industries and their results were published in DEER conference [20],[37]**.** To reduce greenhouse gas emissions and current daily average demand for gasoline by up to 5%, the United States had set a target to implement TEGs in 90% of cars for the internal cooling system, and hence the dependence on conventional air conditioning will be reduced [9]**.** TE module's efficiency of conversion significantly affects the overall efficiency as well as the cost. To attain the targeted efficiency, it is practically approached to generate electrical power and thermal energy and apply co-generation within a single system [38].

TEGs have also entered the space industry. Voyager I space probe used thermoelectric modules for the first time to meet the demands of energy in outer space, making it simple, lightweight and increasing the efficiency of the space probe [39]**.** Nuclear Batteries that convert heat into electrical energy are broadly termed as

Radioisotope Thermoelectric Generators (RTG). Since safety and reliability are the primary concern of a space mission, RTG thermocouples use decomposition of radioactive plutonium-238 as the hot and outer space as cold junctions of a thermocouple, respectively [40]**.** Optimization and improvisation of RTG resulted in creating Radioisotope thermoelectric generator with multiple applications (MMRTG), which is more flexible and reliable in meeting the demands of a variety of missions like generating electricity on small scale and also capable of quickly generating 100W, because of its modular design, it works equally well in the vacuum of space, as it does on planets. MMRTG also ensures a higher degree of safety and optimization of energy levels to a minimum lifespan of 14 years and a reduced weight. MMRTG consists of 4.8kg of plutonium dioxide, which initially produces 120W of electric power and 2000W of thermal power with the help of specially designed modules with general purpose heat source [39].

Furthermore, it reduces electricity consumption and uses the available energy in aircraft, making it commercially viable by reducing gaseous pollutants and reducing operational costs. Also, refrigeration systems with TEG modules used in the aviation industry are portable, lightweight, and with reduced power consumption as compared with conventional refrigerating systems [41]**.** TEG being more reliable, efficient, compact and minimum maintenance makes it safer assessment. Despite being less efficient and high cost, it reduces weight and fuel consumption in aviation industry, by about 0.5%, which is making it cost-effective for the aviation industry [42]**.**

The application of TEGs can also be seen in residential areas in the form of wall mounted TEG and wood-stove TEG and because of the demand for new and more efficient techniques for energy conservation and generation, more and more research is being carried out on the application of thermoelectric modules, which resulted from the creation of alternatives like TEG installed in walls of the buildings and usage of the waste heat in industry as well as in residential facilities [43].

TEG in a wood stove is one of the most predominant applications to revive the waste heat and generation of electrical power. Initially, in 2002 HI-Z technology developed a wood stove TEG, which can generate around 20W of power with 12-14Vcc of output voltage[44]**.** Furthermore, one of the researchers used a conventional wood stove which consists of the hottest region at the top of the furnace and the cooler part below the ash pit. Based on the results of several experiments, it is concluded that TE modules should be placed near the upper right corner of the wood-stove to get the best temperature gradient. With a temperature difference of 152 ^{o}C between the hot side (275 °C) and the cold side (123 °C), an open-circuit voltage of 4.1V is produced. With 2 modules connected in series increased to 5.5 V and to 5.7 V with 3 modules electrically connected in series. The prediction of the addition of 4.1V with every module collapsed because the decrement of temperature takes place with increment of every module leads to the decrement of the hot surface temperature [45]**.**

Also, commercially available modules were tested for rural applications to avail at a lower cost. Method of mounting thermoelectric modules experimental tests were conducted on TE modules based on bismuth telluride to gauge their efficiency. If anyone wants the most efficient TEG power system, there will be need to make sure that heat is being transferred effectively from the module's input to its output [46], and also the location of the proposed system becomes important that can be decided by multiple simulation results. TE modules can be used conveniently. However, the heat exchanger should be designed and manufactured at local workshop as per the need for this. Generated electricity can feed the electric fan of the cook-stove and increase the efficiency of combustion and reduce the fuel consumption and emission of greenhouse gases. Extra electrical power will be supplied to power LEDs [47].

If a building is outfitted with TEGs, the sunlight streaming in through the windows can be harnessed to power electronics and appliances. Here TEG generates electrical energy with the help of the temperature difference in the exterior and interior of the room [48]. For the experimental verification of the concept, a room with a dimension of 4.5m × 3m × 3m was under observation and the thickness of the walls was considered as 0.5m using only one side of the room average temperature difference was 18 °C taking a time period of 6 months and TE modules were deployed to the only one wall out of four. 18 °C was the average temperature difference recorded for six months of the year between the interior and exterior. The power developed during the process, by one module was found to be 5W. If we consider that all the walls produce the same temperature difference, we can install many modules to meet the energy demands of the appliances in a building [49]**.**

For the sake of proper utilization of the resources and improving the overall efficiency of the industrial plant and proper utilization of waste heat is very important. A TEG is can be mounted on furnaces to utilize the waste heat to produce electrical energy. Furthermore, a TEG can be mounted on the exterior of a device exposed to a hot surface, by allowing the heat collection block to absorb residual heat from industrial ducts and chimneys [20]. The advanced thermoelectric micro-generation work developed by WULF GLATZ contributed to developing small, rigid, versatile, and flexible low maintenance thermoelectric materials. As a result the power generated got doubled, when nickel-copper alloy was replaced with bismuth tellurium in devices which use the same principle [50]. Also, devices like "green thermoelectric generators" are capable of sequestering the heat from any source and generating power and ultimately reducing the environmental temperature [46]**.**

For a low temperature gradient processing, several researches are being carried out to develop appropriate thermoelectric materials that may utilize the Seebeck effect. It can be seen in a rectangular shaped box fabricated with a provision of channels for air circulation and forced ventilation, having insulation on the outside and layers of the generator panels are exposed to hot air, air flows by alternate counter-current procedure resulting in linear decrement of temperature, thereby using a certain part of air to generate electricity and other parts of it passed to next line of channel. Temperature drop takes place between parallel channels; two adjacent channels create a temperature difference resulting in generation of electricity. Generally, in a heat exchanger unit with several stages, forced air is used to move heat around. Also, the specific output power is a function of the thickness of p-type material and n-type material [20], [51]**.**

A TE module can be coupled with an autonomous sensor to absorb heat from a heat source. It will allow the TEG to make enough voltage to power the sensor without an outside source of power**.** The TE module TGM-254-1.0-1.3 with dimension (40mm × 40mm × 3.6mm) has 254 n-p pairs connected electronically in series and thermally in parallel**.** The maximum voltage (V), output current (I), and yield (η) were all checked [44][52]. In another system, the module was heated with the help of a heater and heat sink was deployed to the opposite side for cooling purposes. A temperature difference could be maintained to produce desired power. NTC thermistors were used to quantify the temperature on both sides. Temperature difference ΔT varies in the range 0 °C to 13 °C. When the temperature difference was found to be less than 3 °C, the DC-DC converter turned off. This condition does not enable the TEG to produce voltage. A step-up converter as an assistance source is connected when the temperature reaches above 4 °C. Above ΔT 8.5 °C, the situation to turn on step-up converter completely arises and then the sensor takes power from TEG only. 2.1 V is the value of voltage of TEG that is required to stay connected to the sensor observed on test. At this voltage, temperature sensor and microcontroller can be supplied with a power of 0.9 mW and a current of 0.4 mA [53]**.**

With the development of small thermo-elements and semiconductors, it is now possible to utilize a very small amount of heat to generate electric power, which eventually can run power devices such as wireless sensors, watches, mobile phones etc [54]. Companies like Micropelt, Nextreme and Thermo-Life, with the help of several techniques use thin films to manufacture micro-thermoelectric generators and modules. Leading watch manufacturers like Seiko and Citizen worked on developing technology that can power a wristwatch by converting radiated body heat, i.e. thermal energy to electrical energy**.** There are several applications of using human body as a source of thermal energy, which is the result of development and improvement of micro TEGs [20],[55].

Bert Gyselinckx's group played a significant role in designing TEG that can be used in network made of body sensors. When these were placed at most convenient places of body to obtain maximum human thermal energy, these devices were initially able to obtain an output voltage of 2.4V and stored an average of 100 μW power in a battery by using bismuth telluride (Bi_2Te_3) TEG [56]**.** Leading to further development in a similar area, A TEG-powered health monitoring system was developed by the J. Penders group. Which consist of a pulse type generator that powers a wireless pulse oximeter and a wireless monitoring system. But instead of placing TEG on head, it is mounted on wrist for a voltage of 4V and the power developed was 30 μW/cm^2 **[37].** The amount of oxygen in the blood is measured by the sensor that is placed on the finger on the left side. The oximeter is fed by the bracelet placed on the right side due to ΔT between an individual's pulse and the surrounding environment [20][37][57]**.**

Solar energy's immense benefits such as renewable, renewable source, pollution-free source, and sustainable energy sources, have garnered a lot of attention during the last several decades [58]. Many methods exist for collecting solar energy directly, like photovoltaics and solar thermals are the most common (mostly make use of "concentrated solar power"). Photovoltaic system has also proven its utility in water pumping [59]. Every country is trying to integrate its renewable power system with conventional power system to meet the energy demand, however, when these renewable energy sources are combined with the traditional electric power grid, they have both positive and negative effects [60].

Solar energy has a big solution being a promising option for the field captured by photovoltaics. TEGs and solar thermal power can be integrated on the consumer-scale to industrial-scale. However solar thermal systems have a natural advantage of utilization of all the wavelengths of incoming radiation. An attempt at theoretical and analytical investigation of renewable power source based Thermoelectric Generator (STEG) around the globe has also been made and thermo-electrics are being investigated as a feasible power solution for small scale to large scale application [61]. The concentrator, absorber and thermoelectric modules are the main components of any STEG. "solar thermoelectric generators (STEGs)" are now being evaluated as a viable option for producing electrical power [13].

For solar TE modules direct, radiations are needed for maximum rated power, so solar tackers are used to achieve maximum efficiency. Solar tracking system increases the cost of TEG power. Researchers have compared solar panels with TEGs. The comparison study dealt with efficiency, power generation capability and capacity, cost, size, potential consumer applications, and system installation complexity to generate power.it is found that TEG perform better in each aspect in different environmental condition.

In 1888, Weston developed and patented a system that focused sunlight onto a black absorber surface of a thermoelectric module, marking the beginning of the era of STEG design [13]. Then, an STEG was presented, which consisted of a battery for storing the produced electrical energy, a pump for sending the cooling water towards the TE module's cold side, and a customizable monitoring device. Coblentz, in the year 1913, made an experiment and published the results of a STEG comprised of 100 ^{o}C of hot side temperature[62],[63]. Coblentz did not report the device's experimental efficiency, though. The 1st experimental report on the efficiency of STEG was provided by Maria Telkes in the year 1954, by utilizing the flat plate collectors combined with the ZnSb/ BiSb thermocouple [63], [64], [65]. The efficiency of this device was 0.6% without the addition of a focusing lens and 3.4% with lens [13]. Until 2011, parabola troughs made up 96.3% of all CSPs, and their greatest efficiency was 21.0% [66][67][68]. Meanwhile, the resultant system's electrical efficiency falls between 10% and 15%. One important issue is that CSPs can only harvest DNI rays, therefore their efficiency drops when the sky is overcast[69] [28].

Until the year 2011, the results demonstrated by Telkes in the year 1954, weren't surpassed. In the year 2011, Kraemer et al. surpassed these results with an experiment demonstrating an efficiency of 4.6% with nanostructured STEG with Bi_2Te_3 [70][71]. The selective absorber in the presented design acted as a heat concentrator, and the vacuum enclosure helped in reducing losses due to conduction and convection [13]. They created a STEG on a flat screen using nanostructured thermoelectric materials and a selective absorber. In addition, Kraemer et al. anticipated that a better efficient material has a "ZT = 2" along with an "optical concentration" of 10 would have an efficiency of 14 % [72][73].

STEG was reported by G. Chen, in the year 2011, where he used a "thorough CPM approach" for highlighting the most important variables of the design [74]. In this study, Chen argues for boosting the STEG's efficiency by increasing the net flux into the thermal concentrator using a selective absorber. For a module running at 527 ^{o}C with an average ZT of 1, Chen anticipated that STEG efficiency of about 12 % is possible with "10-fold optical concentration and 200-fold thermal concentration". In a subsequent publication, Bi_2Te_3 and skutterudite were cascaded and segmented in a STEG with selective surface absorber for improvement, by McEnaney et al. [72]. The anticipated maximum efficiency of the cascaded scheme was 16% at 600 ^{o}C. To catch the whole spectrum of light and to achieve efficiency of 15% "high-temperature STEG" was developed comprising a "segmented n-type leg" made of La_3Te_4 and skutterudite, and a p-type leg made of skutterudite and $Yb_{14}Mn_{21}Sb_{11}$ [75]. "Higher optical concentration (200-300 Suns and T_h = 1000 ^{o}C) and active cooling on the cold side of the TEG" were projected to achieve an efficiency of 18 % in the aforementioned study [28].

STEG's optimization focuses on the high optical concentration to get maximum efficiency. Over a range of 0.1X-1000X optical concentration, generator of single stage is preferred. Thermoelectric conversion efficiency of 13% is demonstrated for high concentrations when employing selective surfaces and cutting-edge TE materials [76]. A 15.9 % efficiency is achieved at 1273 K by the glass lens based STEG receiving 100 suns solar irradiance and having thermoelectric material (ZT=1), this can be raised up to 23.5% with a material having (ZT=2) [13]. For the value of FOM-ZT=0.8, 1.2, and 1.5, STEG efficiency was found to be 4.5%, 6.8%, and 7.7% [28]. A 4.6 % efficiency is achieved by a flat-panel solar thermoelectric generators (STEGs) under AM 1.5G ($1kW/m^2$) conditions. However, concentrated STEGs demonstrably outperform conventional flat panels [28].

The RSTEG changes the refraction of the transmitted sunlight and the solar energy concentration via lens mounted for the phase change, hence variable efficiency can be achieved by changing phase change material [77]. In a STEG where Spectrally selective (ε = 0.13 and α = 0.954) solar absorber integrated with Fresnel lens, produces good amount of heat[64]. In a Solar pond system with TEG having a control box for controlling the power, four TEMs were used. Each TEM comprises two TE chips, one thermal conduction flat board, one thermal absorber, and 2 cold sinks. The result obtained was approximately 11W [78].

In all these systems efficiency from 1 to18% is achieved, however the cost of the system reaches very high as the higher optical concentration is achieved. The research gap can be identified as (i) almost no work has been done in the field of thermoelectric generator integrated with Giant water lens concentrator. (ii) High cost of presently available solar concentrators such as -parabolic dish TEG, Fresnel lens TEG, solar furnace TEG etc. (iii) Complex design of presently available concentrators, which is not easily adaptable by common public.

Therefore to find out the solution and new exploration, in this project efforts have been made to develop the Bi_2Te_3 based TEG employing a water lens as the solar concentrator at thirteen to twenty-two times lower cost (very low cost) within the efficiency range of presently available thermoelectric system. For this, numerical simulation of a modeled GWLSTEG has been carried out using two different soft-wares. The tracing of the concentrated solar radiation over the absorber surface through the giant water lens has been carried out in Sol-trace, hence transmittance of polythene is optimized, and the thermal and electrical analysis of the TEG module has been conducted by means of COMSOL-multiphysics software. Then for experimenting, a linear low-density polyethylene (LLDPE)/transparent plastic of 400 μm thickness ($\tau_P = 0.95$) has been used to make a parabolic shape and water is poured into this in order to take the shape of a lens. The whole system works as a Plano-convex lens that has been used to concentrate the sun rays over aluminium absorber plate placed at the focus of the giant water lens. The aluminium absorber plate forms the hot junction of the Bi_2Te_3 thermoelectric module that generates electricity owing to Seebeck effect in semiconductors. A four to five-fold increase in the intensity of solar radiation over the receiver plate has been achieved through the water lens concentrator at a relatively much lower cost as compared to the other concentrators of the same size and 13 to 27 times more expensive. The purpose of the whole experiment is to make water lens STEGs more efficient and budget friendly for industrial and domestic use because 60% of households access electricity in India, which means around 40% of households are deprived of electricity. The organization of this work is as follows:

In **Chapter-1** Introduction to TEG is given, **Chapter-2** provides thorough literature review and research gap, **Chapter-3** covers Methodology, in **Chapter-4** Results and Validation are discussed, it also gives brief idea about total cost estimation of the set-up, and finally **Chapter-5** is dedicated to the Conclusion and Future research recommendations.

Chapter 2

LITERATURE SURVEY

Using traditional technology leads to pollution, heat generation, and the release of greenhouse gases, all of which contribute to global warming. Thermoelectric Power Generation converts waste heat into usable electricity, which helps achieve the goal of providing renewable energy options. Both n-type and p-type legs are necessary for a TEG to function properly. The legs are constructed from TE material, with the thermal and electrical connections switching back and forth in a randomized pattern. More conversion efficiency and output power can be achieved with segmented TE legs compared to simplex [36]**.** The TE element's figure of merit is crucial factor [10].

The fundamental issue in focusing TEG is the heat source. Producers aim for optimal efficiency by designing the "concentrator for high optical concentration (0.1X-1000X)", since this is what drives TEG and where losses may be estimated using a numerical model. The thermoelectric conversion efficiency is shown at 13% for this high concentration by using accessible selective surfaces and cutting-edge thermoelectric materials. The RSTEG (Refracted Solar Thermoelectric Generator) is a lens-type concentrator that alters the refraction of the phase change material, which in turn alters the refraction of sunlight, resulting in a peak conversion efficiency of 60-86%. Solar pond is a significant alternative heat source. TEG is used to transfer the heat in the solar pond's LCZ (Low Convective Zone) into power. 11W is generated from the solar pond by a TEG system consisting of two cold sinks and four TEMs[31]**,** [78].

TEG may also use waste heat from sources like cars, furnaces, etc. TEGs have been used in cars for a variety of reasons, including decreasing carbon emissions and increasing overall engine economy. An investigation of the exceptional qualities acquired by the ETC and TEG systems utilized in tiny automobiles powered by a turbocharged SI engine, as well as the associated challenges, were explored [31]. The EGR (Exhaust Gas Recirculation) route was analyzed experimentally for a heavy-duty DE (Diesel engine) and TEM test equipment, and excellent agreement was shown between the simulated and experimental results. The prototype TEG was installed in both vehicles, leading to increased efficiency [32].

The system's efficiency is determined in large part by the absorber's characteristics in addition to the concentrator's transmittance and reflectance. Good amounts of heat may be extracted from the sun using a Fresnel lens and a spectrally selective solar absorber (= 0.13 and = 0.954). The entire system efficiency and cost are greatly impacted by the conversion efficiency of the TE module. High efficiency may be attained by the use of a cogeneration system, which converts waste heat into electricity [38]. “Numerical simulation and modeling of TEG” in steady state may be accomplished with “ANSYS, COMSOL Multi-physics 5.4, and MATLAB”, all of which implement the FEA approach. It is possible to model non-uniform transient heat flow, waste heat flux, and solar energy flux using ray tracing with the help of Sol-Trace Program [34]. TEG has several benefits, including its low noise level during operation, its extended (20–25 year) lifespan, and its lack of potentially harmful byproducts [17]. It has a wide range of applications in rural locales. There have been several advances.

While other studies may focus on certain parts of thermoelectric technology, this one attempt to provide a comprehensive overview of the field by discussing developments in all relevant areas of study. Researchers and businesses can use the information in this review to fine-tune their thermoelectric generator (TEG) project based on factors such as the “local climate, solar radiation, compatibility, availability of waste heat from vehicles and factories, hybridization with other thermoelectric technologies, hot side temperature, materials, modeling and simulation methods, and TEG applications”.

2.1 Thermoelectricity Concept

Thermoelectricity is the process by which an electrical current may be generated directly from heat obtained from both renewable and non-renewable sources using a thermoelectric generator (TEG) and the Seebeck effect. Figure 2.1 (a) depicts a commercial TEG module, and Figure 2.1 (b) depicts charge carrier conduction in a single-stage TEG. Figure 2.2 (a) depicts the conduction of majority of charge carriers in the n-leg, i.e., electrons, whereas Figure 2.2 (b) depicts the conduction of majority of charge carriers in the p-leg, i.e., holes.

In the year 1821, the German scientist- “Thomas Johann Seebeck” used a compass needle to demonstrate the effect that he named after himself, the Seebeck effect, which is simply the induction of voltage within 2 junctions of 2 distinct conductors stored at distinct temperatures [55]. The needle was sandwiched between two metal conductors with temperature-controlled connections. The metals' divergent reactions to the temperature differential resulted in the formation of a current loop and a magnetic field. The TE or Seebeck effect describes the creation of an electric field in a conductor or semiconductor in response to a temperature differential. The magnitude of the deflection depended on the different grades of the conducting material and was insensitive to overall temperature differences between the junctions. Seebeck experimented with several substances, including natural semiconductors like zinc sulfide (ZnSb) and lead sulfide (PbS). It's fascinating to think that if similar components had been used to construct TEG in the early nineteenth century, efficiency levels comparable to modern steam motors may have been attained. The open-circuit voltage generated between a conductor's two nodes is referred to as the Seebeck coefficient [79].

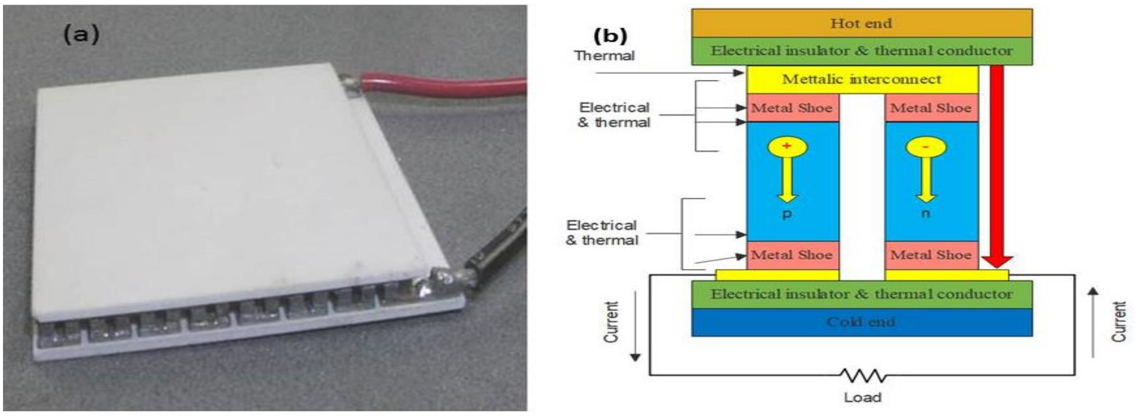

Figure 2.1: *(a) "Thermoelectric Generator module" (b) "Conduction in single-stage (n-leg and p-leg) TEG"*

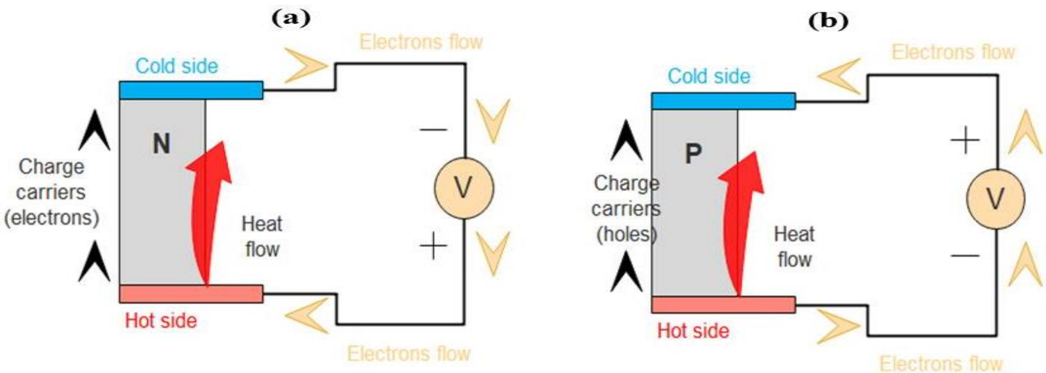

Figure 2.2: *(a) "Charge career flow in n-type leg (b) Charge career flow in p-type leg"* [17]

Thermopiles make up the bulk of TEG. Each thermopile consists of N thermocouples (TCs) wired in series and wired in parallel for electrical and thermal integration, respectively, as shown in Figure 2.3 and Figure 2.4 **(a)**.

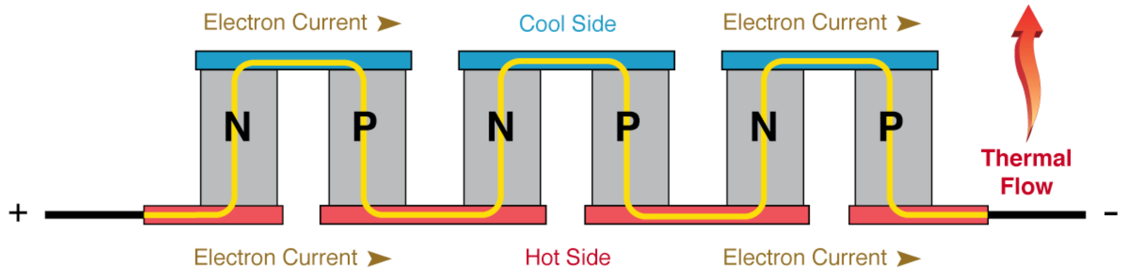

Figure 2.3: *Charge career flow in multi-stage TEG* [17]

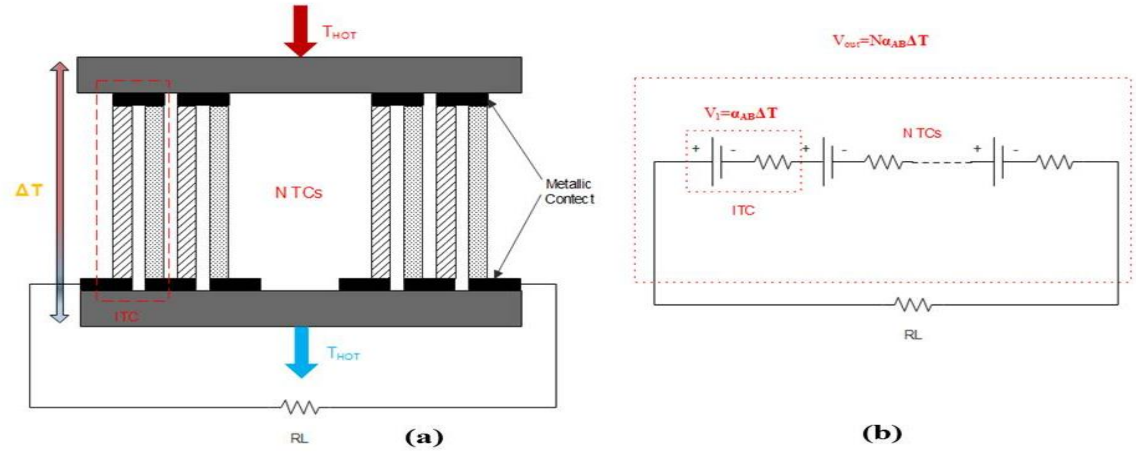

Figure 2.4: *(a) Principle of working (b) Electrical circuit of TEG*

More than one thermopile is linked together to increase power production [37]. Thermocouples are made by joining together two materials with opposing Seebeck coefficients. The Seebeck effect generates a voltage across two thermocouple joints when one of them is heated beyond room temperature and the other is cooled below it [22]. Voltage and power may be expressed as [37]:

$$V_{out} = N\alpha_{AB}\Delta T \quad (2.1)$$

The Seebeck coefficient for a thermocouple made up of two materials A and B is denoted by α_{AB}, and it can be calculated as ($\alpha_{AB} = \alpha_A - \alpha_B$) when total internal resistance is considered; this is because, when connected in series, the internal resistance of each thermocouple is added, making total internal resistance proportional to N. Even if adding more thermocouples (TCs) causes the voltage to rise, it also raises the overall internal resistance Figure 2.4 (b). The internal resistance of a TEG, denoted by R_{TEG}, may be calculated as:

$$R_{TEG} = N\left(\frac{\rho_A L_A}{S_A} + \frac{\rho_B L_B}{S_B} + 2\frac{\rho_C L_C}{S_C}\right) \tag{2.2}$$

The electrical resistivity of the metal contact as well as A and B are denoted with the help of ρ_C, ρ_A and ρ_B. LA and LB denote the flow of the heat via the length of the arms; on the other hand, LC denotes the flow of the heat via the length of the metal. S_C, S_A and S_B respectively denote the metal contacts, A's and B's cross sectional areas. Electrical resistivity of conductors A, B and the metal contact are denoted by, ρ_A, ρ_B *and* ρ_C. Thermocouples' metal contacts (L_C) and arm lengths (L_A and L_B) are the pathways for heat transfer. S_A, S_B, and S_C represent the cross-sectional areas of the A, B, and metal contacts, respectively.

The equation for TEG's total output power (P) is:

$$P = V_{out}^2 \frac{R_L}{(R_{TEG}+R_L)^2} \tag{2.3}$$

TEG's internal resistances are denoted by R_L, while the external load's resistance is denoted by R_{TEG}. The output voltage is denoted by V_{out}. If the resistance of the load, R_L, is equal to the resistance of the TEG itself, R_{TEG}, then the TEG will be able to transmit its maximum possible power. The greatest power output may be expressed as:

$$P_{max} = \frac{V_{out}^2}{4R_{TEG}} \tag{2.4}$$

Various advantages make it extraordinary; such as silent operations, absence of any type of mechanical movement, long operating life [16]**.** Its effectiveness as green technology does not produce any hazardous by-products during its usage [17]**.** It can be extensively used in unattended places and remote areas where the energy conversion technology is less or absent [18].

2.2 Types of TEM based on material

Materials that can conduct both heat and electricity are known as thermoelectric materials. Seebeck, a German physicist, discovered in 1823 that differences in temperature between materials may generate a voltage [80]. French watchmaker Peltier wrote about the anomalous temperature differential he'd discovered on the boundary of two distinct conductors in an essay he published in 1834. These two events demonstrate that either heat can generate electricity or that electricity can be used to generate heat or cool the desired system as shown in Figure 2.5 [81].

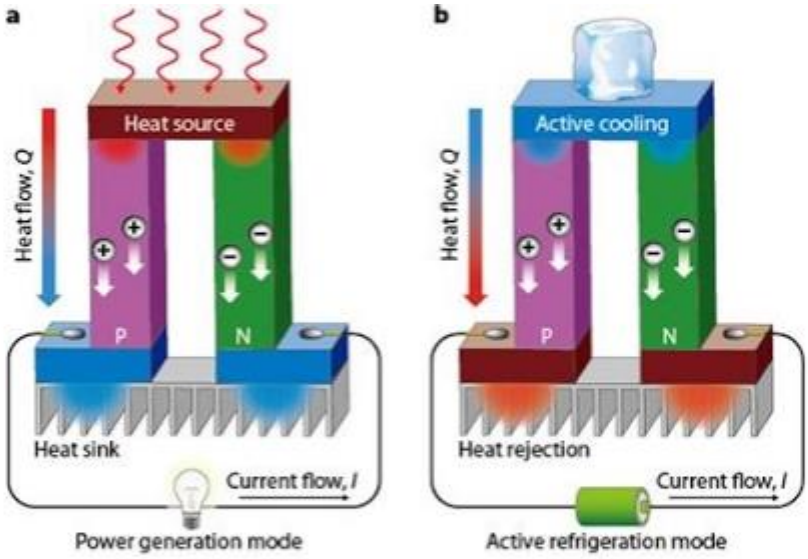

Figure 2.5: *(a) Power generation mode; (b) Active refrigeration mode*[81]

2.2.1 Metal based TEM

Solar cells, gas sensors, optoelectronic devices, passive optics, catalysis, corrosion prevention, environmental protection, etc. may all benefit from the wide range of functional capabilities shown by metal oxide nanostructures. The visual, electrical, chemical, and mechanical properties of metal oxides are largely determined by the oxide's crystal structure, content, native defects, doping, etc. The morphological and structural features of material are greatly influenced by the processing and growth factors [23]. Oxides' band gap and electrical structure may be tuned by changing their size and shape, making them useful in many different contexts [82].

Solar cells and other optoelectronic devices, TCOs, plasmonics, photonic integrated circuits, chemical sensors, catalysis, corrosion prevention, thermal protection, and energy conversion and storage are just a few of the many potential uses. Heavy-doped semiconductors are thought to be the most effective thermoelectric materials. It is generally accepted that a band gap is required for a high thermoelectric power factor and figure of merit to be achieved.

z T = ($S^2\sigma/\kappa$)* T is the dimensionless figure of merit that best describes the thermoelectric efficiency of a material. Where "S is the Seebeck coefficient, κ is the electrical conductivity, σ is the thermal conductivity, and T is the absolute temperature", The first two numbers, S and, describe electrical transport, while is linked to thermal transport. Together, they form the thermoelectric power factor or PF=$S^2\sigma$. It is common practice to utilize the power factor as a filter to narrow down the pool of possible thermoelectric materials. Metals are the most electrically conductive materials, but they also have the lowest Seebeck coefficient [83].

Their Seebeck coefficient is low because the density of states surrounding the chemical potential is symmetrical. Metals typically have an even distribution of hot electrons above and cold empty states below the chemical potential. Therefore, the "number of electrons diffusing from the cold side to the hot side is almost equivalent" to the number of electrons diffusing in the other way when a temperature gradient is present. In semiconductors, however, this issue does not arise since a band gap restricts the diffusion of carriers to only one kind [84]. The typical semiconductor has a Seebeck coefficient that is two orders of magnitude greater than that of a metal. This advantage of semiconductors was initially recognized by Ioffe6 and opened the way for several demonstrative successes using doped semiconductors with high zT values. The influence of band gap on thermoelectric characteristics of materials using two-band toy models for the electronic structure was later researched by numerous groups, including "Chasmar & Stratton" and "Sofo & Mahan," who concluded that the best thermoelectric materials must have band gap bigger than 6-10 kBT [85]. The modern thermoelectric community is mostly concerned with strongly doped semiconductors.

2.2.2 Ceramic based TEM

Modules of thermoelectric ceramics are made out of calcium cobalt oxide, calcium samarium manganese oxide, and other bulk oxide and foam materials, and are essential to energy conversion technologies like thermoelectric power generators. Because of their open porous foam structure, they can make more physical contact with the hot medium, resulting in more efficient electric power generation. Because of how they're built, they may be used to create thermoelectric modules that are both effective and efficient for use with gaseous and liquid waste heat sources [86]

Both traditional (non-oxide) and cutting-edge (oxide) ceramics may be used as thermoelectric (TE) materials. In the business world, standard thermoelectric ceramic materials are used. There are three distinct categories based on the temperatures at which they may function [87]:

i) Workable at temperatures as low as ≤450 K. Bismuth (Bi) non-oxide ceramics, such as Sb_2Te_3, $(Bi\text{-}Sb)_2Te_3$, Bi_2Te_3, etc., based on Antimony (Sb) or Tellurium (Te) or Selenium (Se) alloys.

ii) Lead (Pb) alloy non-oxide ceramics, such as PbTe, can withstand temperatures from room temperature to 850 kelvins.

iii) Ceramics made of Silicon and Germanium (SiGe) can withstand temperatures up to 1300 K without oxidation.

Traditional thermoelectric ceramics materials continue to be widely used for thermoelectric power generating technology's commercial and practical applications due to their comparatively high ZT≥1 [88]. However, they are poisonous, expensive, and have poor thermal stability, making them unsuitable for use in efficient thermoelectric power production. Since they are stable at high temperatures and in air, non-toxic, highly durable, lacking in security elements, lightweight, small thermal expansion, and low cost (cheap), the novel thermoelectric ceramics (oxide ceramics) are alternative TE materials and promising candidates for power generation applications. Thermoelectric ceramics with new applications include doped ZnO, $NaCo_2O_4$, $Ca_3Co_4O_9$ and $SrTiO_3$ oxides.

2.2.3 Polymer based TEM

The inherent low heat conductivity, lightweight, simple process ability, possibly ultralow cost, and environmentally-benign features of polymers make them a particularly appealing candidate for exploitation as a next-generation thermoelectric material. The thermoelectric performance may be effectively enhanced by using polymer materials due to their poor heat conductivity. Unfortunately, they have poor electrical conductivity [89]. Polymers with a high doping level may exhibit great electrical conductivity, but their impaired Seebeck coefficient leads to an extremely low ZT. To meet this need, conjugated polymer composites are now the focus of much research and development.

However, polymer TE materials often have a low figure-of-merit due to their poor electrical conductivity. Chemical or electrochemical doping, molecular structure modification, and production of "polymer-based composites or blends, the simplest and most cost-effective way for altering polymer characteristics, have all been tried to improve the TE performance of organic TE materials". Functional TE inks/paste may be made from solution-processed polymer/inorganic or organic hybrids, allowing for the efficient fabrication of TE generators at scale [88].

Electrical conductivity of polymer thermoelectric materials; Polymers often have inherently low carrier mobility (typically 1 cm^2/V-s) and narrow to moderate energy gaps (~1-3 eV) between their lowest unoccupied molecular orbital (LUMO, conduction band) and their highest occupied molecular orbital (HOMO, valence band).There is a wide variation in the electrical conductivity and Seebeck coefficient of polymer thermoelectric materials, from 10^{-8} S/cm to 10^4 S/cm and 10 μV/K to 1×10^3 μV/K", respectively. Unlike in inorganic TE materials, the correlation between electrical conductivity and the Seebeck coefficient is negative in conducting polymers. Similar efforts were performed with polymer/inorganic particle composites for several inorganic materials. Iodine-doped polyacetylene was the first semiconducting polymer, with electrical conductivity of $1–3 \times 10^4$ S/cm.

Conjugated polymers include the category of conducting polymers. In their natural, undoped condition, conjugated polymers may act as either semiconductors or insulators [87]. They are organic macromolecules with a backbone chain of alternating double and single bonds (Peierls instability); their overlapping -orbitals generate a system of delocalized π-electrons, which may lead to advantageous optical and electrical characteristics. Several hundred monomers make up the repeating units of the conjugated polymer chain. Also, they are hardly soluble unless you introduce some pliable side-chain substituents.

2.2.4 Semiconductor based TEM

Heavily doped semiconductors in the 150-250μVK^{-1} Seebeck coefficient region are ideal thermoelectric materials. At reasonable amounts of the carrier concentration, the electrical resistivity is seen to fall within the range of 0.5-3 (Ω-cm) Good thermoelectric materials are unusual because they have a high value of the 'power factor,' S^2. This is because most semiconductors do not acquire such favorable values of S. Since the demonstration of relevant capabilities throughout a multi-year period between the late 1940s and the mid-1950s, researchers have been focusing on the issue of synthesizing and characterizing semiconducting substances with high ZT values [90].

In terms of thermoelectric effects, semiconductors' band structure surpasses that of metals. Because the Fermi energy is below the conduction band, the state density is not uniform in that region. As a result, the system is receptive to charge transport into a lower energy state because the average electron energy of the conduction band is greater than the Fermi energy. In contrast, metals have conduction bands where the Fermi energy is located. Since the average conduction electron energy is therefore near to the Fermi energy, the forces pushing for charge transport are less. Thermoelectric properties make semiconductors a natural choice.

2.3 TE Properties

2.3.1 Seebeck Coefficient

Thomas Seebeck discovered in 1821 that a closed circuit comprised of two dissimilar metals would allow an electric current to flow continuously so long as the junctions of the metals were kept at two different temperatures.

In 1821, German physicist — Estonian Thomas Johann Seebeck discovered that the temperature difference between junctions of two metals would cause a compass needle to be deflected by the closed loop formed by the combination of the two metals. This discovery is known as the Seebeck effect, which is the change directly from the difference in temperature to the power. This is because, depending on the temperature differential, various metals react in various ways, generating loop currents and magnetic fields. Seebeck labels this event as thermomagnetic because he fails to recognize the presence of electric currents. The word “thermoelectric” was first used and later refined by Danish scientist Hans Christian Orsted. This phenomenon generates a voltage on the order of microvolts per kelvin. At normal temperature, the Seebeck coefficient of a copper-nickel alloy is 41μV/K. Seebeck voltage is directly proportional to the junction temperature difference. The junction voltage increases as the temperature difference increases [91].

The Seebeck coefficient may be calculated from this formula:

$$S = -\frac{\Delta V}{\Delta T} = -\frac{V_{hot} - V_{cold}}{T_{hot} - T_{cold}} \tag{2.5}$$

When one end of a conductor is heated and the other is cooled, electrons with greater thermal velocities at the hot junction diffuse to the cold junction. Seebeck found that an EMF was generated when he heated or cooled one end of a metal bar relative to the other. He played around with junctions, which are just mechanical connections between dissimilar conducting materials. He discovered that by heating one of two electrically linked junctions and cooling the other, he could force a compass needle to swerve along the wire connecting the junctions. In his mind, he had found a technique to convert heat into a magnetic field. Subsequent research confirmed that the variation in emf V (Lenz's Law) was caused by the diffusion of electrons in the circuit.

An actual temperature sensor may be built using an amplified version of the Seebeck effect experiment. To calibrate your device, you'll need an external method of monitoring the temperature gradient between the two nodes.

2.3.2 Thermal Conductivity

A material's heat conduction properties are quantified by its thermal conductivity. The symbol for this is often written as λ or κ.

Materials with low thermal conductivity allow for slower heat transmission compared to those with high thermal conductivity. Metals, for instance, have great thermal conductivity and transfer heat extremely efficiently, whereas insulating materials like Styrofoam have the opposite property. Heat sink applications make extensive use of high thermal conductivity materials, whereas thermal insulation makes use of low thermal conductivity materials. Thermal resistance is defined as the inverse of thermal conductivity [92].

Where q is the heat flow, k is the thermal conductivity, and ΔT is the temperature gradient, we get the defining equation for thermal conductivity: $q=-k\Delta T$. Fourier's Law of Thermodynamics describes this phenomenon. Several techniques exist for determining a material's thermal conductivity, but each one is only applicable to a certain class of substances. Measurement methods may be broken down into two broad classes: steady-state and transient. The steady-state methods use the material's steady-state state to infer its thermal conductivity, whereas the transient methods use the system's instantaneous state as it approaches steady state. Since steady-state methods do not include time, no intricate signal analysis is necessary (steady state implies constant signals). The time needed to attain steady state also prevents quick measurement, therefore a well-engineered experimental apparatus is normally necessary [9].

The experimental investigation of fluids' thermal characteristics is more challenging than that of solid materials. This is because, without certain precautions, other forms of energy movement than thermal conduction are also present: convective and radiative. An insulating barrier layer may also contribute to seemingly lower heat conductivity. The capacity of a substance to transport heat (i.e., an intense attribute) is measured by its specific thermal conductivity. Absolute thermal conductivity, on the other hand, is a component attribute that may be used to evaluate the heat-transfer efficiency of several components (i.e., a broad property). Size and form, such as thickness and area, are considered when identifying a component, as opposed to merely the material itself. Components of the same material but with various dimensions, or components of different dimensions composed of different materials, may be compared and contrasted in terms of their thermal-transfer capabilities in this fashion [93].

"Thermal conductivity" (λ) refers to a material's "ability to transport heat," and it is expressed as "watts per square meter of surface area for a temperature gradient of 1 K per unit thickness of 1 m". Therefore, the formula for determining specific thermal conductivity is:

$$\lambda = \frac{P}{(A\Delta T/t)} = \frac{Pt}{A\Delta T} \tag{2.6}$$

Where:

λ= specific thermal conductivity (W/ (K m))

P= power (W)

A= area (m^2) = 1 m^2 during measurement

t = thickness (m) = 1 m during measurement

Δt = temperature difference(K, or °C) = 1 K during measurement

2.3.3 Electrical Conductivity

The capacity of a substance to conduct electricity is quantified by its electrical conductivity. Specific conductance is another name for electrical conductivity. A material's conductivity comes from its very nature. The symbol for electrical conductivity is "σ" and the SI unit for it is "Siemens per meter" (S/m). The Greek letter γ is often employed in the field of electrical engineering. Conductivity is sometimes represented by the Greek letter. Specific conductance, a measure of water conductivity relative to that of pure water at 25°C, is often reported [94].

2.3.4 Relationship between Conductivity and Resistivity

The reciprocal of electrical resistivity (ρ) is electrical conductivity (σ):

$$\sigma = 1/\rho \tag{2.7}$$

When the material's cross section is constant, the resistivity is:

$$\rho = RA/l \tag{2.8}$$

In this equation, R represents the material's electrical resistance, A its cross-sectional area, and l is its length.

A metallic conductor's electrical conductivity rises with decreasing temperature. Resistance in superconductors reduces to zero below a specific temperature, allowing an electrical current to flow around a loop of superconducting wire without any external power being provided. Band electrons or band holes are responsible for conduction in many materials. Whole ions, bearing their net electrical charge, go across electrolytes. The conductivity of electrolyte solutions depends critically on the concentration of the ionic species present in the solution [95].

2.3.5 Materials with Good and Poor Electrical Conductivity

Materials like metals and plasma have excellent electrical conductivity. Silver is the finest conductor because of its low resistance to electricity. Glass and distilled water, two common electrical insulators, conduct electricity very poorly. Most elements that aren't metals on the periodic table are terrible at conducting heat and electricity.

Semiconductors have a conductivity that falls somewhere in between that of an insulator and a conductor.

The best Conductors include the following:

- “Silver
- Copper
- Gold
- Aluminum
- Zinc
- Nickel
- Brass”

Materials such as the following are not good electrical conductors.

- “Rubber
- Glass
- Plastic
- Dry Wood
- Diamond
- Air
- Pure Water (not salt water, which is conductive)”

There is a close and crucial relationship between electrical conductivity and electrical conductance. Different from electrical conductance, which is a characteristic of a specific electrical component like a wire, electrical conductivity is a property of the substance itself (like silver).

One definition of electrical conductivity is the amount of voltage needed for a certain quantity of electric current to flow. The ease with which mobile electrons may be formed is governed by the number of electrons in the outermost shell. The number of atoms per unit volume is another, less crucial component since it controls how many electrons are available to move in response to an electric field. Copper and aluminum are examples of conductors because of their great electrical conductivity. Electrical insulators, or simply insulators when there's no chance of mistake with thermal insulation, are materials with poor conductivity like rubber and glass. Semiconductors are different kinds of material that fall somewhere in the middle, and examples include silicon and germanium. Because the electrons in their outermost shell are free to move about, metals in general have high conductivity (another way of saying metals tend to be conductors). In general, the conductivity of nonmetals is rather poor.

2.3.6 Figure of Merit (Z)

Since σ, S and κ vary with temperature, the issue of what values should be utilized to calculate the figure of merit, Z, arises if ΔT is big. Since the whole pair is affected by the Joule heating and thermal conduction processes, it is clear that average values of and are necessary. However, it may be argued that the value of S at the cold junction should be used instead, given the confined nature of the Peltier effect. Taking into consideration the Thomson effect reveals that this conclusion is incorrect [96].

For the whole element, the amount of Thomson cooling is denoted by ∫γdTI, which is equal to ∫TdSI by Kelvin's second relation. Each junction is responsible for half of this cooling. Therefore, an overall rate of cooling should be used in place of the Peltier cooling $S_C T_C I$.

$$S_C T_C I + \frac{1}{2} I \int_c^H T dS \tag{2.9}$$

Cold and hot junctions are denoted by the subscripts C and H, respectively, in this case. Now, in the formula for the total cooling, the Thomson component is negligible in comparison to the Peltier term. As a result, it is not too far off to say

$$\int_C^H T dS = T_C \int_C^H dS = (S_H - S_c) T_c \tag{2.10}$$

It is then found that

$$S_c T_c I + \frac{1}{2} I \int_C^H T dS = (\frac{S_H + S_c}{2}) T_c I \tag{2.11}$$

If the average value of the Seebeck coefficient, S, is utilized instead of the value at the cold junction, then the Thomson effect will be accounted for. The mean values of all parameters are factored into the figure of merit, (Z) [97].Z, as described by Eq (2.12)., is a figure of merit used to compare thermoelectric materials, however, it may be a pain to work with. Therefore, the quality indicator Z is defined for a certain material as:

$$Z = S^2 \frac{\sigma}{K} \tag{2.12}$$

In all but extreme cases, a thermoelectric device's figure of merit, Z, will be exactly equal to the average of the elemental figures of merit, Zp and Zn. Z is best understood as a convoluted mean of Zp and Zn. The fact that Zp and Zn values in modern thermocouples that are optimal for thermoelectric applications are seldom substantially divergent justifies the use of a single figure of merit, as stated by Eq (2.12)[98].

2.3.7 Thermoelectric Efficiency

Thermoelectric effect describes a set of occurrences where a change in one temperature causes a change in another, or vice versa. The Seebeck effect (which generates a voltage from temperature differences), the Peltier effect (which uses electric current to propel heat movement), and the Thomson effect are all particular names for these processes (upon presence of electric current and a temperature gradient, reversible heating and cooling within a conductor will occur). While the thermoelectric effect is nonzero in all materials, it is often too modest to be practically relevant. However, low-cost materials with a significant thermoelectric effect (and other essential qualities) are being studied for use in power production and refrigeration, among other potential uses. Bismuth telluride (Bi_2Te_3)is the foundation of almost all thermoelectric materials [99].

As a potential method for the regeneration of energy from waste heat, thermoelectric materials are employed in thermoelectric systems for cooling or heating in specialized applications. A device's thermoelectric efficiency is calculated by dividing its total power output to the load by its total heat output [100]. An expression for the efficiency of a thermoelectric generator (η) to produce electricity is

$$\eta = \frac{energy\ provided\ to\ the\ load}{heat\ energy\ absorbed\ at\ hot\ junction} \tag{2.13}$$

Typically, the figure of merit ZT of a thermoelectric device is used to represent its maximum efficiency, which is defined as:

$$\eta_{max} = \frac{(T_h - T_c)}{T_H} \times \frac{\sqrt{1+ZT}-1}{\sqrt{1+ZT}+\frac{T_c}{T_H}} \tag{2.14}$$

In which the temperature of the surface being cooled (T_C) is subtracted from the temperature at the hot junction (T_H).With knowledge of the temperature dependent characteristics S, κ and σ, as well as the heat and electrical current flowing through the material, the efficiency of a single-leg thermoelectric device may be determined. A real-world thermoelectric device consists of two materials (usually an "n-type and a p-type) connected by metal". Then, the combined efficiency of both legs is added to the electrical and thermal losses from the interconnects and the environment, yielding the maximum efficiency(η_{max})[101].

When these losses are disregarded, an imprecise estimate for ZT is

$$ZT = \frac{(S_p - S_n)^2 T}{[(\rho_n k_n)^{\frac{1}{2}} + (\rho_p k_p)^{\frac{1}{2}}]^2} \tag{2.15}$$

In this notation, the subscripts n and p denote characteristics of n-type and p-type semiconducting thermoelectric materials, respectively; denotes the electrical resistivity averaged throughout the temperature range; T denotes the average temperature difference between the hot and cold surfaces.

2.4 Governing parameters of thermoelectric material selection: intrinsic material properties

Having a narrow band gap semiconductor, high carrier mobility, and low thermal conductivity is what Slack outlined as necessary for a successful thermoelectric material back in 1995. An excellent thermoelectric material, according to Mahan, is often a semiconductor with a small band gap and high mobility carriers. [91]

Rapid industrialization has brought with it the dilemma of diminishing energy resources, particularly fossil fuels, which threatens the steady progress of civilization over the long run. The future power demands can't be met without investing in and developing renewable and sustainable energy sources, and the rising need for energy is driving this effort. Thermoelectric devices can use the Seebeck effect for converting the waste heat generated or produced from exhaust system of the engine, industrial processes, and furnaces into useful electricity, while “solar cells, fuel cells, and other emerging energy conversion technologies still fall short in efficiency, cost, and long-term stability”. Thermoelectric (TE) materials, with their simple design, absence of moving parts, lack of vibration, absence of noise, absence of pollution, and high stability, play a pivotal role in the quest for sustainable energy-efficient technologies. In addition, TE materials present possibilities for the improvement of “smart sensors, energy harvesting, the novel concept of thermal power wave sources, automobiles, wood stoves, and diesel power plants, and can mitigate some of the negative effects of global warming and the resulting climate change” [102].

There have been several developments in TE materials since 1990, and they may generally be split into two groups. “Skutterudite (CoSb, etc.), clathrate (SrGaGe, etc.), half Heusler (FeVSb, etc.), and silicide” are all examples of intermetallic compounds (FeSi, MgSi, etc.). Various compounds based on metal oxides make up the second group of TE materials. $NaCo_2O_4$, Y_2O_3, $Ca(Mn,In)O_3$, (Zn,Al)O, and Fe_2O_3 are some of the most common oxides used today. The study of oxides was pioneered in Japan, and it has since expanded to include a wide range of materials. A metal oxide is a good TE material choice because (a) it is stable at high temperatures, (b) it has a short mean free path of phonons, and (c) it is inexpensive.

Choosing the right materials is an important part of creating anything with a physical form. When designing a product, the primary focus should be on finding the most cost-effective materials without sacrificing desired properties. It is necessary to consider the qualities and prices of potential materials before making a final decision on which one to use. Using a material index or performance index that takes into account the required material qualities may greatly aid the material selection process. To reduce heat loss for a given temperature differential, a thermal blanket's thermal conductivity must be low. Understanding the materials' qualities and how they will perform under normal use is crucial for any designer. Materials vary in a wide range of critical ways, including their “strength, durability, flexibility, weight, heat and corrosion resistance, castability, weldability, hardenability, machinability, electrical conductivity etc. as shown in Figure 2.6.

A system's or a material's intrinsic quality cannot be artificially added. Materials' chemical makeup and 3D structure are primary determinants of their intrinsic qualities [103]. An object's intrinsic properties are those that it has by its nature, unaffected by other influences such as its environment. Properties that are contingent on the object's context are said to be extrinsic (or relational).

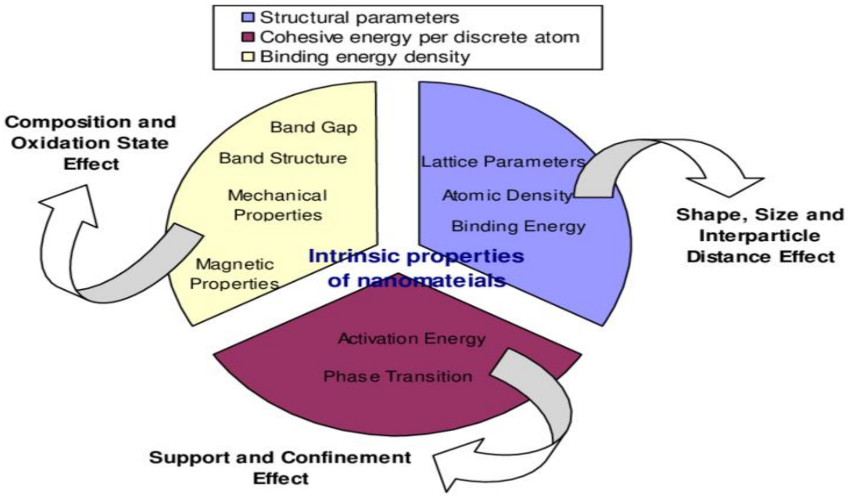

Figure 2.6: Intrinsic properties of nanomaterial [103]

2.4.1 Energy Gap and Band Structure of Semiconductor

A band gap, also known as an energy gap, is a region of the energy spectrum in a solid's electronic band structure where no stable electronic states may exist. The band gap, as shown in Figure 2.7 of the electronic band structure of solids, is the energy difference (in electron volts) between the valence band and the conduction band in insulators and semiconductors. It's the work done by an atom to release a valence electron so it may travel freely in the crystal lattice and act as a charge carrier to carry electricity. In chemistry, it is associated with the HOMO/LUMO gap. In a solid, current can only flow if electrons are moving from the valence band to the conduction band. If both bands are filled, however, current cannot go through the solid (see carrier generation and recombination). This means that the band gap plays a crucial role in defining a solid's electrical conductivity. Band gaps determine whether a material is an insulator, semiconductor, or conductor; in the latter case, the valence and conduction bands overlap, making the band gap very narrow or nonexistent[104].

The energy-band structure of a solid is unique to each kind of material. The vastly different electrical properties of different materials may be traced back to this underlying difference in band structure. Electrons are restricted to certain energy levels inside semiconductors and insulators. Band gap describes the energy separation between the valence band's upper and lower energy levels. Electrons may hop from one frequency range to another. There is, however, a critical energy threshold below which an electron cannot go from the valence band to the conduction band. Varying materials have different energy needs. Absorbing either a phonon (heat) or a photon provides electrons with enough energy to enter the conduction band (light).

At absolute zero, a semiconductor acts like an insulator, but at temperatures over its melting point, it permits thermal excitation of electrons into its conduction band. On the other hand, an insulator has a huge band gap. There may not be a band gap in conductors if the valence and conduction bands overlap [105]. The band gap has a significant impact on the conductivity of intrinsic semiconductors. Only electrons with enough thermal energy to be stimulated over the band gap and the electron holes left behind when this happens are accessible as charge carriers for conduction.

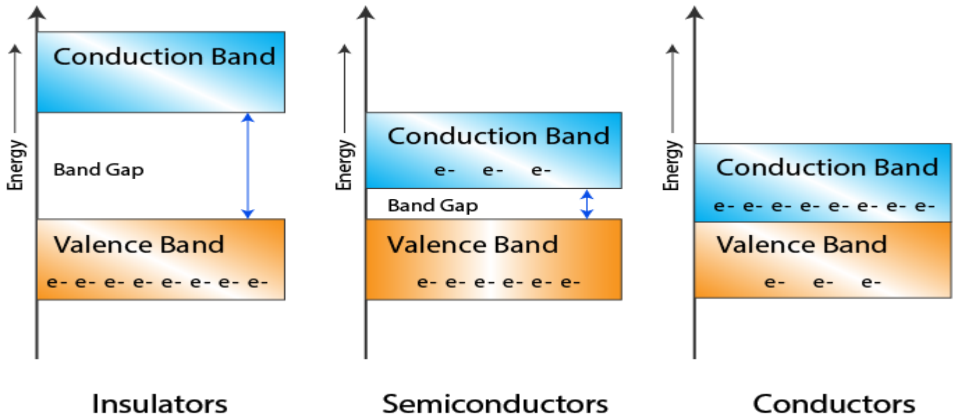

Figure 2.7: *Classification of Energy Bands*[105]

As the temperature of a semiconductor increases, the energy of its band gap typically decreases. To a lesser degree, the band gap will be influenced by the interaction between the lattice photons and the unbound electrons and holes. An empirical expression may be used to explain the connection between band gap energy and temperature:

$$E_g(T) = E_g(0) - \frac{\alpha T^2}{T+\beta} \tag{2.16}$$

where $E_g(0)$, α and β are material constants.

Due to the existence of continuous energy levels, the band gap in a typical semiconductor crystal remains unchanging. Size-dependent changes to the band gap in a quantum dot crystal allow for the generation of a broad spectrum of energies between the valence and conduction bands. It is also known as the impact of quantum confinement [106]. Pressure also affects the size of the band gap. The electrical band structure determines whether a band gap is direct or indirect.

2.4.2 Concentration of Charge Carrier

The number of charge carriers in a given volume is referred to as the charge carrier density. The SI unit of measurement is the, per cubic meter. In theory, it may vary depending on location, just like any other density. Carrier concentration, on the other hand, is often reported as a single quantity that stands in for the average carrier density across the material as shown in Figure 2.8 [107].

Semiconductors are distinguished from other materials by the ease with which thermal stimulation (increased temperature) may promote certain electrons from the valence to the conduction band. As a result, it gains conductivity as the temperature rises. As a result, there is a temperature-dependent change in the inherent carrier concentration of a semiconductor, with more “freed” electrons and holes present at higher temperatures (vacancies). To be clear, only free electrons are meant to be considered charge carriers.

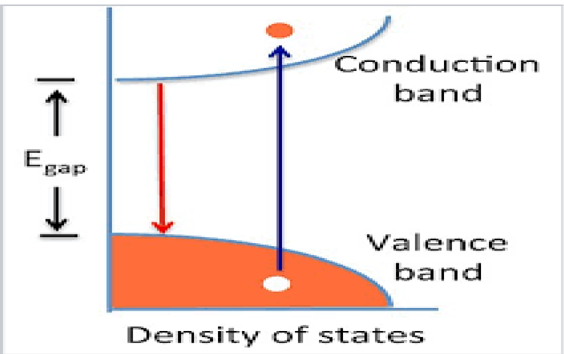

Figure 2.8: *Relation between density of state and energy gap*[107]

The band gap also affects the intrinsic carrier concentration since it controls how readily the electrons may flow through the material. Since the band gap and temperature at which the most electrons are free for conductivity must be taken into account to achieve maximum conductivity, we may deduce that the intrinsic carrier concentration is already related to solar cell efficiency[108].

The hole population in p-type semiconductors far outnumbers the electron population. Boron and gallium are frequent choices for doping silicon to make it p-type. In p-type semiconductors, the Fermi level lies below the intrinsic Fermi level, putting it "closer to the valence band" than the conduction band. An n-type semiconductor is a common electronic material. An impurity is introduced into a semiconductor material (often silicon or germanium) during production. "Phosphorus, arsenic, antimony, bismuth, or any other chemical element" might be employed as impurities. Donor impurities are what they are termed. Diffusion due to difference in charge carrier concentration is shown in Figure 2.9.

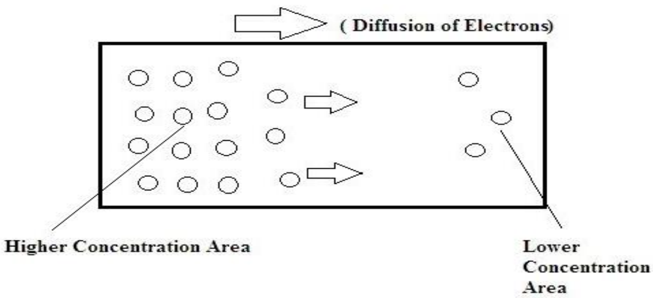

Figure 2.9: *Diffusion of electrons*[108]

2.4.3 Mobility

Mobility is the rate of drift per electric field strength. By applying an electric field, electrons may be "drifted" or have their velocity altered. This electron drift velocity in meters per second Electron mobility is a quantitative measure of the influence of electric field on electron motion.

When an electric field is applied to a metal or semiconductor, electron mobility describes how rapidly the electron may travel through the material. For holes, a comparable quantity known as hole-mobility exists. Carrier mobility may mean either electron or hole mobility. The mobility of electrons and holes in a fluid subject to an applied electric field are subsets of the more general phenomenon of electrical mobility of charged particles in a fluid. When an electric field E is applied across a material, the electrons in that material will move at a mean speed, known as the drift velocity. After that, we may characterize electron mobility as

$$V_d = \mu E \tag{2.17}$$

The standard unit of measure for electron mobility is the centimeter squared per second $cm^2/(V\cdot s)$. This is not the same as the $m^2/(V\cdot s)$ mobility unit used in the SI system. $1m^2/(V\cdot s)=10^4 cm^2/(V\cdot s)$ is the relationship between them. The product of carrier mobility and concentration determines the conductivity. A large number of electrons with low mobility may provide the same conductivity as a small number of electrons with high mobility. Since most metals' electrical behavior is based on conductivity alone, it often does not matter whether of these two is true. As a result, mobility plays little role in the physics of metals. However, the presence of numerous low-mobility electrons against a small number of high-mobility electrons may have a profound effect on the operation of transistors and other semiconductor devices. This means that mobility is a crucial metric for semiconductor materials. Increased portability almost usually improves gadget performance, everything else being equal [108].

The mobility of a semiconductor changes with the concentrations of impurities, defects, electrons, holes, temperature, and the donor and acceptor concentrations. The electric field has a role as well, especially at high fields when the velocity is saturated. The Hall Effect or inference from transistor behavior may be used to find it. Mobility is often tested experimentally and is found to be highly dependent on both impurities in the material and temperature. Values for mobility are often shown in the form of a table or chart. Electrons and holes in a substance have distinct mobilities.

2.5 Selection of TEG According to Operating Temperature

2.5.1 Low Temperature (<250 ^oC) TEGs:

In this temperature range, the most common origins are “ovens, air compressors, furnace doors, electrical circuits, and refrigeration/air conditioning condensers”. TEG also claimed a low temperature range (250^{o}C) for the materials used, which includes metallic and buffer connections [22]. As was previously mentioned, bismuth telluride/selenite has a high ZT in the low temperature range (100-250°C) [109]. Therefore, these materials have seen extensive application in the production of TEGs. In order to get a low temperature for TEG's input, many attempts were made to build organic material-based TEGs [110] as an alternative to bismuth telluride/selenite [29]. Table 2.1summarizes the performance of a variety of TE materials throughout a low-temperature range.

Table 2.1: Various low temperature range TE material

Thermo elements type	**T_h/T_c**	**Interconnect material**	**Buffer layers at the ends**	**Efficiency (%)**	**Remarks**	**Ref.**
p-type Bi_2Te_3	150°C/24°C	N/A	Nickel	5.8	Analyses of thermoelectric and efficiency performance under conditions of extreme temperature variation	[111]
$MgAg_{0.965}Ni_{0.005}Sb_{0.99}$	245°C/20°C	Silver	N/A	8.5	Mg-Ag based materials have excellent thermoelectric conversion efficiency.	[112]

p-type poly[Cu_x(Cu-ett)] and n-type poly[Na_x(Ni-ett)]	147°C /67°C	The cold end has silver attached to it, whereas the hot end has aluminum.	Gold	N/A	Organic thermoelectric materials	[113]

2.5.2 Mid Temperature range (250-650 °C) TEG

Automotive exhausts, gas turbine exhausts, drying and baking oven, steam-boiler exhausts, etc. are all examples of sources that contribute to the mid-temperature range (250-650°C) stated by the summary of several TEGs [114]. BiCuSeO, $Ca_3Co_4O_9$, In_2O_3, $NaCo_2O_4$, $CaMnO_3$, $LaNiO_3$, and $SrTiO_3$ are popular thermodynamic materials due to their cheap cost and simplicity of manufacture. These materials show their greatest thermoelectric performance at temperatures >650 °C [115]. In

Table 2.2, it is shown how different types of TE materials perform in the moderate temperature range.

Table 2.2: Various mid temperature range TE material

Types of thermoelements	**T_h/T_c**	**Interconnect material**	**Buffer layers at the ends**	**Efficiency (%)**	**Remark**	**Ref.**
p-type ZnSb n-type Constantan	420 °C /20 °C	N/A	N/A	5.8	Thermoelectric generators use thermocouples, which	[116] [73]

					are made from a direct connection between p and n wires.	
n-type PbTe	500°C/100°C	Stripe of Ag	Ag/Fe/Ag + Fe	6	The production of the contacts is done through diffusion bonding.	[22], [117]
Skutterudite of p type and n type	500°C /40°C	Aluminum	Molybdenum	7	Brazing is used to create the connections	[118]
Skutterudite of p type and n type	550°C /70°C	N/A	Co_2Si in p-type and $CoSi_2$ in n-type	9	Energy harvesting materials	[119],[120], [36], [121]
p & n type skutterudite	550°C /90°C	N/A	N/A	10	TEM and modules	[122], [123], [124], [116], [125]
Sb_2Te_3/PbTe as p-type and Bi_2Te_3/Pb	600°C /10°C	Copper (Cu)	$Co_{0.8}Fe_{0.2}$ for PbTe side and	11	Thermoelectric materials for use in	[126], [127]

Te as n-type			Ni at Bi_2Te_3/Sb_2Te_3 sides		environmental energy research, contact creation using liquid In-Ga eutectic alloys, and segmented thermoelectric devices	

2.5.3 High Temperature range (>650 °C) TEG

This heat comes from a variety of industrial processes and facilities, such as hydrogen factories, steel heating furnaces, metal refining furnaces, etc. Natural radioactive decay also generates very hot heat (800-1000°C) (e.g., Pu_{238}). Those TEG that operates at such high temperatures is called "radio-isotope thermoelectric power generators" (RTG). Iron di Silicide (b-$FeSi_2$) was suggested in 1964 for use in thermoelectric power production at temperatures over 600 °C because of its stability with regard to evaporation and oxidation sublimation and the presence of hazardous components [83]. "Performance of High temperature range TE material" is summarized in Table 2.3.

Table 2.3: High temperature range TE material

Thermoelement	**T_h/T_c**	**Materials interconnected**	**Buffer layers at the ends**	**Efficiency (%)**	**Remark**	**Ref.**
n-$Fe_{0.93}Co_{0.07}Si_{1.99}Al_{0.01}$/p-	700°C	$TiSi_2$	N/A	3	Thermo electric generators made of Fe-Si_2	[88]

$MnSi_{1.73}$						
n & p-type SiGe alloys	$870^oC/31^oC$	Molybdenum	Pressure contact	7	Thermo electric power generators	[22]
n & p-type SiGe alloys	553^oC /44^oC	Molybdenum	Carbon	N/A	Thermoelectric module, Linear Shaped Si-Ge materials,	[117]
n & p-type SiGe alloys	$1000^oC/300^oC$	With Ti layer, hot shoes connected. p and n type SiMo (i.e. $MoSi_2$ in the Si matrix)"	N/A	N/A	Si-Ge Unicouple materials	[3]
n- type $Ca_{0.92}La_{0.08}MnO_3$ & p type $Ca_{2.75}Gd_{0.25}Co_4O_9$ p-type	773^oC /383^oC	Connection among the p and n type are made through Pt wire.	N/A	1.1	Fabrication of all oxides thermoelectric generators	[128]
Segmented leg of p-type ($Yb_{14}MnSb_{11}$/ $Ce_{0.9}Fe_{3.5}Co_{0.5}$	$1000^oC/152^oC$	N/A	N/A	15	Generation of New Space-Based Nuclear Technologies	[129], [130]

Sb_{12}) and n-type (La$_3$-xTe$_4$/(Ba, $YbCo_4Sb_{12}$)						
Segmented leg of n-type [$CoSb_3$ + $Bi_2(Te/Se)_3$] and p type [$Zn_{4-x}CdxSb_3$ +Zn_4Sb_3 + $(Bi/Sb)_2Te_3$]	700^{o}C /27^{o}C	N/A	N/A	15	High efficiency Segmental thermoelectric Uni-couples	[131], [35]
n-type $MnSi_{1.75}Ge_{0.01}$ and p-type $Mg_2Si_{0.53}Sn_{0.4}Ge_{0.05}Bi_{0.02}$	735^{o}C /50^{o}C	Copper on cold side and Mo on hot side	Cu on n-type and Ni/Pb/ Ni on p-type	5.3	Materials based on silica: characterization, assembly, and design	[132][133]

Table 2.4 provides a high-level summary of TE performance based on the performance of various materials, and it includes theoretical and experimental analyses from a small number of researchers. Several possible TE materials have been used by several research organizations throughout the world. Table 2.4 provides a summary and analysis of a wide variety of TE material and studies.

Table 2.4: Thermoelectric performance of miscellaneous TEG materials

TEG (Material) study	Methodology	Research Findings	Ref.
Temperature Evaluation-dependent thermoelectric performance based upon materials	Finite difference method/ Domenicali's equation.	A single TE filament provides a 2 µW of peak power output, hot surface temperature of 398.15 K and 6 mv of open circuit voltage.	[134]
High TE performance of MgAgSb-based materials, Sb_2Te_3-Te nano composites, W-Ni-Al_2O_3	Synthesis Process Composition Optimization can achieve high ZT at room temperature for obtaining phase pure samples.	By Ni alloying to Ag site and enhancing the phase purity, ZTs of 1-1.5 at room temperature in MgAgSb based materials $MgAg_{0.965}Ni_{0.005}$ $Ag_{0.99}$ can be achieved. When kept at the room temperature ZT can be compared with the best p type $Bi_{0.4}Sb_{1.6}Te_3$.	[135], [136], [83]
High-Performance Spectrally-Selective Solar Absorber Based on Yttria-Stabilized Zirconia Cermet with High-Temperature Stability	Substrate of Stainless steel mechanically polished is layered with tungsten Infrared reflector.	Spectrally selective absorber achieves solar absorptance ~0.95	[82]

Providing Power Supply to a Vehicle by Maximum Power Point Controller for TEG.	Maximum Power Point Controller (MPPT)	With the help of a cascade voltage controller, charge voltage is controlled through adaption of the step size and lowering the oscillation at the MPP in respect of the power gradient.	[137]
Under different temperature conditions, research over TEG's electrical performance(thermo-elements)	To hike thermal conductivity are connected in parallel and to hike operating voltage, these thermo-elements are connected in series electrical link for TEM.	Because of the mismatch temperature condition, the results from the experiment are 11% less in comparison with the theoretical maximum power, which is the significant power loss of the module when connected in series.	[138]

As FOM is a very important aspect, by alloying Ni with Ag, materials like $MgAg_{0.965}Ni_{0.005}Ag_{0.99}$ is formed that achieve ZT (FOM) of 1-1.15 at room temperature. Some materials, such as yttria-stabilized zirconia cermet, may boost the solar absorptance of a receiver to as high as ~0.95, making it more effective as a solar collector.

For TEG applications, continuous research is being carried out to produce some substitute material as most of the materials available till now are inorganic, which raises the cost of the raw materials and processing techniques. These available materials are also toxic as well as brittle by nature. The potential of conducting polymers(CP) has been exhibited for many years in memory devices, transistors, displays used in electronic devices, sensors, super-capacitors, etc. [139]**.** Thus, it can bring a great breakthrough in the thermoelectric field. Their ability in order to emerge as wearable devices, compatibility mixing with inorganic material (can carry the thermal electricity to the smart technologies), providing ease in patterning over many kinds of subtracted which has large area as well as flexible and free standing films [82]. Many researches are conducted to improve the CP's TE performance [140]**.** This resulted in compiling the ongoing trends in the field of organic thermoelectric by various groups of researchers.

2.6 Various Modeling and Simulation Techniques for TEG Systems

In order to enhance the design of practical devices, the performance of each kind of geometry is quantitatively (through simulations and modeling) examined. Such methods are often implemented using computational fluid dynamics (CFD) and finite element analysis (FEA) programs. The smallest element, with a substrate size of only 90 mm^2 (4.15% of the system's total), may nonetheless achieve optimum efficiency. At a fixed TE leg length, it is possible to improve performance in order to reduce the cross-sectional area of the thermoelectric components.

Table 2.5 includes simulation and modeling tools utilized by researchers on different thermoelectric Generator projects. For TEG modeling and simulation prior to actual execution of TEG project, sophisticated popular tools are accessible, such as MATLAB, ANSYS, COMSOL-MULTIPHYSICS, etc. The active-cooling mechanism in the TEG/LED system's cold side temperature (35.7°C) was calculated using the MATLAB Simulink tool. Many TEGs for car exhaust are analyzed using CFD software like ANSYS and COMSOL multi-physics. These aids excel in Finite Element Analysis in three dimensions [119].

Popular modeling and simulation tools for thermoelectric systems include COMSOL, ANSYS, ABAQUS, IMHO, etc. They may be used for many purposes. Software based on equations, like COMSOL. COMSOL-intuitive Multiphysics's interface makes it possible to quickly and simply perform finite element analysis (nanometer scale) on a wide range of complicated physics phenomena using a large number of simultaneous equations. In COMSOL, working with targets of nm size is straightforward, however in ABAQUS, it is not feasible. If a problem with geometric modeling in COMSOL arises, the geometry, however, may be brought in from other programs. It has a built-in model viewer as well. It is easy to model and generate a mesh. Researchers that have experience with equation-based programs like MATLAB often gravitate toward COMSOL [141].

For "structural analysis, general physics phenomena", computational fluid dynamics (CFD) simulations, and time savings, ANSYS, an element-based program, is preferred. When solving a complicated flow issue, ANSYS provides superior solution control, making it considerably easier to achieve convergence. There are two different ANSYS modelers available: workbench and classic. The CAD programming utilized in industry is called workbench, and traditional "ANSYS is used for APDL. The ANSYS workbench (ANSYS-Design Xplorer, ANSYS-Space Claim, ANSYS-Autodyn, ANSYS-CFD, ANSYS-FLUENT, and ANSYS-Mechanical)" is available with the ANSYS student version. While ANSYS WB's user interface is more intuitive, the quality of its meshes is subpar. ANSA and Hyper-mesh both produce high-quality mesh. Both ANSYS (for stress/strain analysis) and COMSOL (for complex multi-physics analysis) may be used in tandem on a single project, however, this choice depends on the specifics of the problem at hand. Adding fluid dynamics to COMSOL would position it at the forefront of numerical simulation technology.

ABAQUS is the market leader in the automotive sector, whereas ANSYS is the market leader in the energy sector. Since ANSYS APDL is over 20 years out of date, it has been superseded by ABAQUS CAE. Parametric design language such as ANSYS is highly helpful, however the same outcomes may be achieved using python and ABAQUS. There is no way for ANSYS to provide an API (application programming interface) for RST. Therefore, it would be difficult for anybody to create a model using ANSYS output (file.rst). ABAQUS's well-organized database and great API make it a powerful tool. Most people would rather use ABAQUS than ANSYS to create UMATs.

There are several different paid ANSYS versions, such as ANSYS-CFX, ANSYS-FLUENT, etc. Different ABAQUS releases include TOSCA, fe-safe, Simpack, XFlow, and XFEM. Tokens may be acquired in increments proportional to the needs of product development, therefore it is not necessary to buy all of them at once. While COMSOL has widespread acceptance in the academic community, NASTRAN is preferred for aeronautical applications. When designing a new product, it's important to consider not just one but all of the software packages that will be used to create it, including those for electromagnetics, acoustics, explicit, CFD, multi-body, fatigue, optimization, and so on.

includes simulation and modeling tools utilized by researchers on different thermoelectric Generator projects.

Good software packages for TEG analysis include MATLAB, ANSYS, COMSOL-MULTIPHYSICS, etc. The cold side temperature of the TEG/LED system was calculated to be 35.7^{0}C using the MATLAB Simulink tool to simulate the active-cooling process. Many cars exhaust-based TEGs undergo CFD study using ANSYS, whereas COMSOL multi-physics is optimal for 3D Finite element modeling.

Table 2.5: Various models of TEG

S.No.	Modelling in Various Research	Simulation Technique	Software	Assumptions	Ref.
1.	TEG module with high-power LED and active-cooling computational modeling for autonomous energy recycling. The suggested LED/TEG module's active cooling mechanism shows significantly greater cooling capacity at 87.5 % of operating temperature than the passive-cooling LED device. The passive cooling heat sink is received at a temperature that is 35.7 ^{o}C higher than that of one of the TEG/LED modules.	Numerical Simulation	MATLAB /Simulink	(i) “Uniform air circulation through DC fan” (ii) “Assume that interconnected metals and ceramic plates possess high thermal conductivity”	[121]
2.	Exhaust heat exchangers in automobiles: experimental and numerical study. Maximum heat transmission of 1737W is achieved by the serial plate construction,	Numerical Simulation: CFD Analysis	ANSYS	The heat outlet and inlet are both constant.	[142]

	which is aided by 7 baffles. It also causes a maximum pressure decrease of 9.7 kPa in a suburban driving cycle.				
3.	For the purpose of designing thermal-concentrated solar TEG, ANSYS is utilized for simulation and modeling. The most efficient performance from the smallest component of the TEG system is 4.15 %.	Numerical Simulation:3-D Finite element scheme	ANSYS	Not Available	[38]
4.	The research and development of an improved TEG system powered by the exhaust of internal combustion engines. The ETEG 3-D numerical model is developed. The engine's fuel consumption rate was reduced by 0.6% thanks to the ETEG (Exhaust based TEG) technology, which is utilized to recover waste heat. When used in conjunction with a waste heat recovery system, TEG modules achieve efficiencies of about 4%.	Numerical Simulation:3-D Numerical model	FLUENT (ANSYS)	It is believed that the engine would not suffer any noticeable performance loss due to the higher jacket water temperature.	[143]

5.	Analysis and design of the TE Module using ANSYS to extend its useful life. The feasibility of strengthening the TEMs' framework is explored. Von Mises stresses are 13% lower and efficiency is 42% higher for TE modules with a circular geometry than those with a rectangular one. Shear stresses are also reduced. ANSYS	Numerical Simulation :Finite element method	ANSYS Workbench	(i) Set of P-type or N-type TE elements is considered isolated. (ii) Due to the same location Stresses existed on a P-N pair in both rectangular and circular layout designs	[26]
6.	Concentrated solar TEGs are designed by modeling and simulation (using a geometrical equivalent model), and then investigated using a numerical technique that takes into account TE characteristics.	Numerical Simulation- three-dimensional finite element scheme	ANSYS	(i)- Steady-state-TEG (ii)- Identical-p-type and n-type elements (ii)-Temperature dependent-TE material properties (iv)-Material properties of the electrode, substrate, solar absorber- constants. (v)-Vacuum environment-	[144]

				convective losses neglected" (vi)-Radiation heat transfer only takes place between the environment and hot-side surface (vii)-Heat sink and the solar absorber are not incorporated in the computational process, however with the help of boundary conditions their effect is described	
7.	Simulation and Modelling (mathematical modelling) of TEG under Mediterranean climatic conditions	Numerical Simulation- MATLAB/SIMULINK environment	MATLAB	(i)-The Seebeck factor (α), electrical conductivity (s) and thermal conductivity (k) are constants and temperature independent. (ii)-These are calculated at the average temperature (T) (iii)-Model is valid for n number of legs (iv)-Hot side temperature > ambient	[49]

				temperature, Cold side temperature< ambient temperature Weather-Autumn and spring”	
8.	Seebeck coefficient, temperature dependency of TE materials, the Thomson effect, and the influence of heat transfer from the side surface are all accounted for in the theoretical modeling of TEG.	Numerical simulation-finite element method	MATLAB	One-dimensional linear temperature distributions	[145]
9.	The purpose of this study is to apply a Transient Heat Transfer Mathematical Model” to the TEG-Solar Pond System.	Numerical simulation-MATLAB/SIMULINK environment	MATLAB	(i)-One dimensional Conductive heat transfer takes place though the infinite size solar pond (ii)-Across the layers of the pond, physical properties are constant (iii)-Throughout the year, the temperature of the aquifer is constant (iv)-Average ambient temperature =UCZ temperature	[146]

				(v)-Heat exchanger provides $T_h \sim T_L$ and $T_c \sim T_{am}$ (vi)-Heat exchanger-No heat loss”	
10.	Multiphysics simulations of electricity and heat transfer using TEG	Numerical transient simulation	ANSYS CFX	Glass fibres is used to insulate sides of the hot block –no leakage of heat flux	[147]
11.	Wearable TEG thermal model development, manufacturing, and experimental testing with no heat sink.	Numerical FEA simulations	Comsol-Multiphysics	Human body distributes uniform heat	[148]
12.	TEG Modeling and simulation for heat extraction from ocean	Numerical simulation	N/A	Heat flow between energy storage material (thermal resistance) and seawater	[149]
13.	Prototype TEG modeling and fabrication for use with hot exhaust gases	Mathematical simulation	N/A	At any cross section of exhaust-uniform temperature distribution”	[150]
14.	Geometrical model and Multiphysics simulation are used to study the “dynamic electrical and thermal performance of TEG	Numerical Simulation	ANSYS 15.0	Uniform temperature over the surface of heater	[151]

15.	Different boundary conditions are used to create two separate three-dimensional models of a TEG. Numerical model	Numeric Simulation	ANSYS FLUENT	Two different thermal boundary conditions: (i)-Fixed temperature at boundaries (ii)- Fixed convective heat transfer	[152]

2.7 Environmental Impact of various TEG Systems

Here, we take a look at the work of a diverse set of researchers and writers that have studied the environmental effect and performance of thermoelectric generators using a variety of theoretical and practical approaches. Various models of TEG's Effect on environment are summarized in Table 2.6.

Table 2.6: Various models of TEG's effect on environment and cost

TEG (Environment and cost) study	Methodology	Research Findings	Ref.
Wet flue-gas thermoelectric generator's analysis (concerning their performance)	Wet flue gases	At the same gas temperature of 150 °C and mass flow rate of flue gas, the maximum production of "wet flue gas, with humidity of 30%, is 5.8 times that of dry flue gas". This means less gas is used as a fuel source.	[153]
CO_2 life cycle scenarios of life cycle	4 scenarios for automobiles incorporated with TEG integrated with an exhaust pipe	The thermoelectric figure of merit is improved by a factor of 1.9 if the $LCCO_2$ is reduced to zero, which is the case for the typical driving pattern. For TEGs to be financially viable during their expected lifespan, their present price must be decreased by 10-40%.	[114]

Passenger automobile	bismuth telluride (Bi-Te) material based thermoelectric generators integrated with the exhaust	By 0.07~0.30%, CO_2 emission in the city is reduced.	[154]
Hybrid commercial vehicles	Waste heat recovery technology	By turning waste heat into power, fuel efficiency may be increased by as much as 20%.	[155]
Heavy duty vehicles	Waste heat recovery	20% increase in fuel efficiency	[156]

0.07~0.30 % CO_2 emission of the city is reduced in japan by using TEG integrated with exhaust of automobiles, that shows TEG can be a good environment friendly technology.

2.8 Applications

When working in diverse temperature ranges, TEG finds use in a wide variety of industries, including “remote power, aircraft, communication, military, biomedical, healthcare”, etc. [157]. Classifications of a few of them are given in Table 2.7.

Table 2.7: Various applications of TEGs

Applications	Methodology	Research Findings	Ref.
Microprocessor’s thermoelectric cooling i.e.	air cooling technique	obtained negative temperature gradient	[55]
Thermoelectric refrigerators and air conditioners	For heat dissipation, charge carriers are used rather than refrigerant in the	a solar Peltier refrigerator might reduce the temperature in about 44 minutes from	[158]

	thermoelectric material	271^{o}c to 51^{o}C	
Aerospace	Solar TEG (TEG and a thermal collector)	Only 0.081% of maximum efficiency was received due to the solar power radiation loss of 10%, free convection and re-radiation loss of the absorber by 70%, while only the remaining 20% was conducted through the legs.	[10]
	Spacecraft (radioisotope thermo-electric generator)	For producing 2.7We power, 865K of maximum hot junction temperature is operated by the RTGs	[159]
	cascaded thermoelectric modules (CTMs)	For generating 108We of electric power and for achieving decrease of 43% amount of 238 PuO_2 fuel needed.	[160]
TE infrared sensors	Seebeck effect	A low cost potential and 3900V/W (high responsivity) are provided. Though, many TE infrared sensors are capable of operating within the range of 7-14 µm.	[161]
Biomedical	In comparison with lithium-ion or Ni-Cd batteries, safer materials are	A fit bit belt typically produces 300mV of open-circuit voltage from a temperature gradient of 1.5K, and it has an approximate efficiency of	[14]

	fabricated out	0.1%	
Automobile	Waste heat recovery	Bi_2Te_3-based TEG is touted as the most efficient globally, has η_{te}=7.2% and an approximate output density of 1W/cm^2 is produced when operating at Tc=30 ^{0}C and T_h=280 ^{0}C. The efficiency of the fuel hikes by 16%.	[162]
	24 TEG module integrated with exhaust pipe	A 301^{o}C of temperature difference produced a 12.41W of total output power.	[163]
	TEG integrated with SUV and CNG generators	Under same conditions for simulation, 3 and 7 factors of increase in power for SUV and CNG respectively in generator based upon QW and Bi_2Te_3	[164]

2.9 Concentrated Solar Power

Currently, a wide variety of solar technology options are on the market. Each has its own set of benefits, however, since it is built on a separate set of ideas and scientific principles. The most effective and advantageous technology to employ under any particular set of circumstances may be determined by careful analysis and comparison of available options.

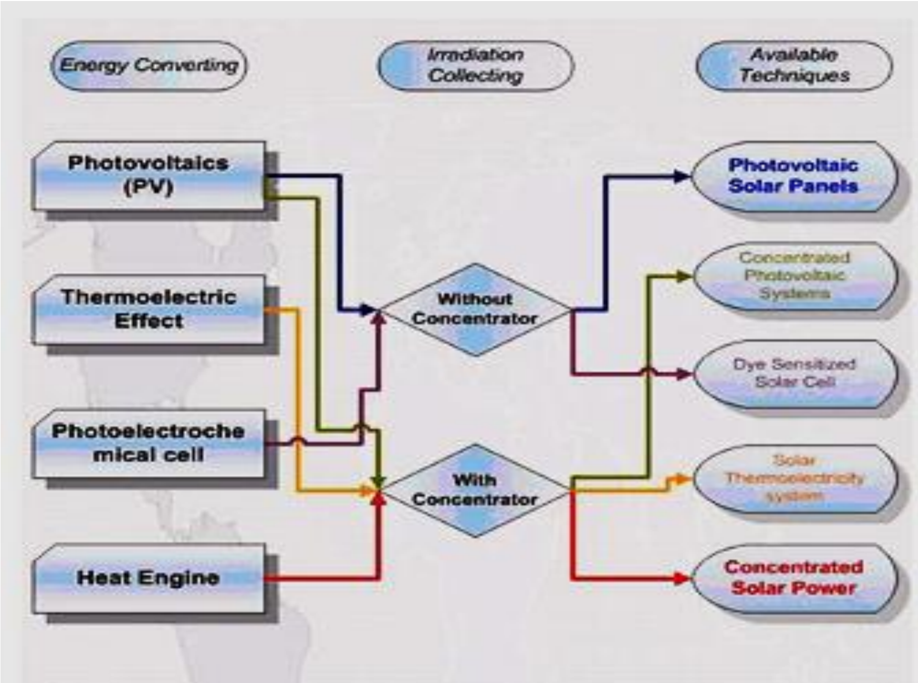

Photovoltaic Solar Panels	Most commonly used techniques in today's market
Concentrated Photovoltaic Systems	The highest efficiency ever achieved in lab
Dye Sensitized Solar Cell	Biomimics techniques based on cheap organic materials
Solar thermoelectricity system	Based on the application of thermoelectricity materials
Concentrated Solar Power	Commonly used based on the application of mature heat engine

Figure 2.10: *Overview of solar technologies*[76]

"Concentrated solar power (CSP) and non-concentrated photovoltaic solar panels (PV)" are the two most developed technologies in this area. They are already being used commercially, and their future expansion is anticipated to be swift [76]. The overview of solar technologies is shown in Figure 2.10.

The field of Concentrated Solar Power (CSP) focuses on the focused use of solar energy. In this manner, steam is produced to power the turbine. In addition, because some of the heat is stored, this sort of plant may operate continuously. When there isn't enough sunlight, it may still generate steam and power plants [165]. Since CSP plants need a lot of direct sun irradiation, they are best suited for the Sun Belt, the region of the world that is between 40 degrees north and south of the equator. In most of these areas, the technological capability of CSP-based energy production is far greater than the electricity demand, opening up possibilities for electricity export through high-voltage lines.

This summary focuses on three crucial facets of CSP growth [166]:

a) Process and Technology Status;

b) Performance and Costs;

c) Potential and Barriers.

Numerous technological studies have recently focused on various renewable energy options. Each summary provides policymakers with information on the technical details, prices, market potential, and obstacles that stand in the way of a swifter switch to renewable energy.

2.9.1 Solar Energy

Each photon of sunshine that makes it to Earth includes energy that keeps our world going, therefore the sun's contributions to Earth go well beyond daylight illumination [167]. Each hour, enough solar radiation reaches Earth's surface to potentially meet global energy demands for almost a whole year. This is because solar energy is the ultimate source accountable for all of our weather systems and energy sources on Earth.

What is the source of all this vitality? Any star in the cosmos, including our own Sun, is analogous to a huge nuclear reactor. Massive quantities of energy are generated by nuclear fusion processes in the Sun's core and radiated outward from the surface of the Sun into space. Photovoltaic and solar thermal collectors are two methods that may be used to gather sunlight and transform it into usable energy [168]. As the price of solar panels continues to drop, more and more people in more and more locations can take advantage of this renewable energy source. As a sustainable energy source that produces no harmful byproducts, solar power is poised to become more significant in the world's energy future.

2.9.2 Solar Geometry

(a) Horizontal Coordinates

Horizontal, or alt-azimuth, is the first coordinate system to be covered. In this model, someone standing on Earth would see the horizon as a level surface. The zenith is the vertical line that is perpendicular to the surface and immediately above the head of the observer. The altitude angle characterizes the inclination of an object with respect to the horizontal. Positive things are those that are above the plane, while bad things are those that lie below. The angle of azimuth defines how far a body is from the plane that runs parallel to the zenith and marks the celestial north and south poles. This plane is set at an azimuth of zero degrees. It's a left-handed system since positive angles move in a clockwise direction. Figure 2.11 shows that the angle of height is denoted by γ_s. The direction normal to the Sun may be calculated using these two angles [76].

(b) Equatorial Coordinates

The equatorial coordinate system is discussed next. The basic plane of the equatorial coordinate system is perpendicular to the equator of the sky. In this reference frame, the axis of planetary rotation serves as the normal vector. Each region of the sky may be thought of as a coordinate system similar to our own. Like latitude, declination (δ) indicates the inclination above or below the celestial equator. Hour angle is the other coordinate that acts like a latitude (H). The hour angle divides a full 360 degrees into 24 equal segments using hour, minute, and second measurements. 15 degrees of arc correspond to one hour. If you stick to these points in space, tracking the Sun's apparent motion becomes much easier. Throughout the day, the hour angle shifts by exactly 1 degree every 4 minutes. There are not more than four tenths of one degree of declination every day. Eq (2.18) and (2.19) may be used to make the transformation between the two sets of coordinates. Given an observer's "latitude (Φ), declination (δ), and hour angle (H)", these equations will provide the sun's height and azimuth angle (H).

$\text{Sin}\alpha = \sin\alpha \times \sin\Phi + \cos\delta \times \cos\Phi \times \cos H$ ……………..…………………………...(2.18)

$\text{Cos}\gamma \times \cos\alpha = \cos\Phi \times \sin\delta - \sin\Phi \times \cos\delta \times \cos H$ …………………………………...(2.19)

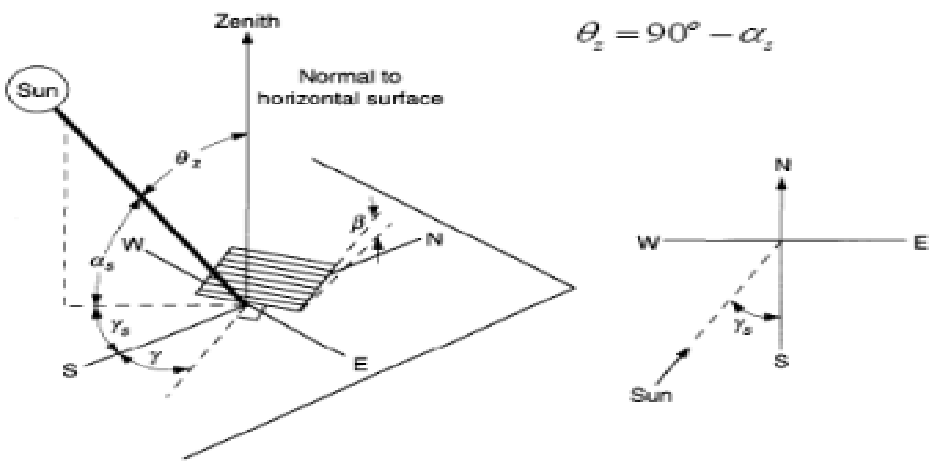

Figure 2.11: *Solar geometry*[76]

2.9.3 Solar Irradiance

Radiant radiation from the Sun is Earth's principal energy source. The irradiance of the sun is measured and reported. Total solar irradiance (TSI) is the sum of all radiation measurements; spectral irradiance is the sum of all radiation measurements broken down by wavelength. Atmospheric regions get light of varying wavelengths. The surface is heated to a habitable temperature by the sun's visible light and infrared rays. At increasing altitudes, ultraviolet light of the UV-A, UV-B, and UV-C varieties is absorbed [169]. Wavelengths shorter than 120 nm (EUV) are absorbed by the atmosphere over 60 miles, along with soft X-ray radiation. Although it is totally absorbed by our atmosphere, extreme ultraviolet (EUV) radiation poses a serious threat to humans and technological devices in outer space.

over the course of the sun's 11-year cycle, the sun's total irradiance increases at solar maximum and decreases at solar minimum. The Sun's radiation at various wavelengths shifts as it revolves and when solar flares cause adjustments. The Earth's changes are distinct from those witnessed on other worlds.

Solar energy is a plentiful resource in India. India receives over 200 megawatts per square kilometer (MW/km2) of solar radiation annually (megawatt per square kilometer). This is equivalent to 657,4,000,000,000,000 MW, given a landmass of 3,287,000,000 square kilometers. However, 87.5% is utilized for agricultural purposes, 6.7% is used for habitation and industrial purposes, and 5.8% is either barren, snow-bound, or otherwise uninhabitable. As a result, just 0.413%, or 12.5%, of the total land area is theoretically suitable for solar energy installations. Even if just 10% of this land is put to use, the resulting 8 GW of solar power would be enough to displace 5,909,000 barrels of oil annually [170].

Solar energy, however, is a diffuse kind of power. Approximately the same amount of energy is generated by burning 1 kilogram of coal or 1/2 liter of kerosene as is gathered by 1 m^2 of a solar collector in a single day. As a result, expansive regions are required for gathering. Furthermore, solar energy conversion efficiency is poor. As a result, the available energy would be far less than what was previously estimated. Solar energy, however, is clearly a viable option for satisfying energy needs[171].

2.9.4 Apparent Solar Day

The time it takes for the Earth to complete one revolution on its axis relative to the apparent sun. True solar day is another name for it.

2.9.5 Direct Solar Radiation

Radiation obtained by the actinometer originates only from the sun, as opposed to diffuse sky radiation, effective terrestrial radiation, or any other source.

2.9.6 Solar Absorption Index

The Ionospheric absorption is a function of solar zenith angle at different latitudes and local times. Air mass penetrable by sunlight at any particular time and latitude is called the solar air mass. Approximately 1367 watts per square meter is the solar constant, which is the rate at which energy is received from the sun just outside the planet's atmosphere on a surface normal to the incident radiation when the earth is at its mean distance from the sun.

2.10 Solar Collectors

In order to heat a material, solar collectors convert sun energy into heat (water, solar fluid, or air). As a result, solar energy may be put to use to warm water and even swimming pools. Not all sun collectors can generate the high temperatures required by solar cooling methods [172]. Concentrating solar power, by collecting light from a wide region using optical equipment like a mirror or other optical equipment, they concentrate a large amount of sunlight on a tiny area. The solar concentrator is most effective when positioned such that its surface is directly towards the sun [10]. In the Figure 2.12, mentioned below, variety of solar energy concentrating devices can be seen.

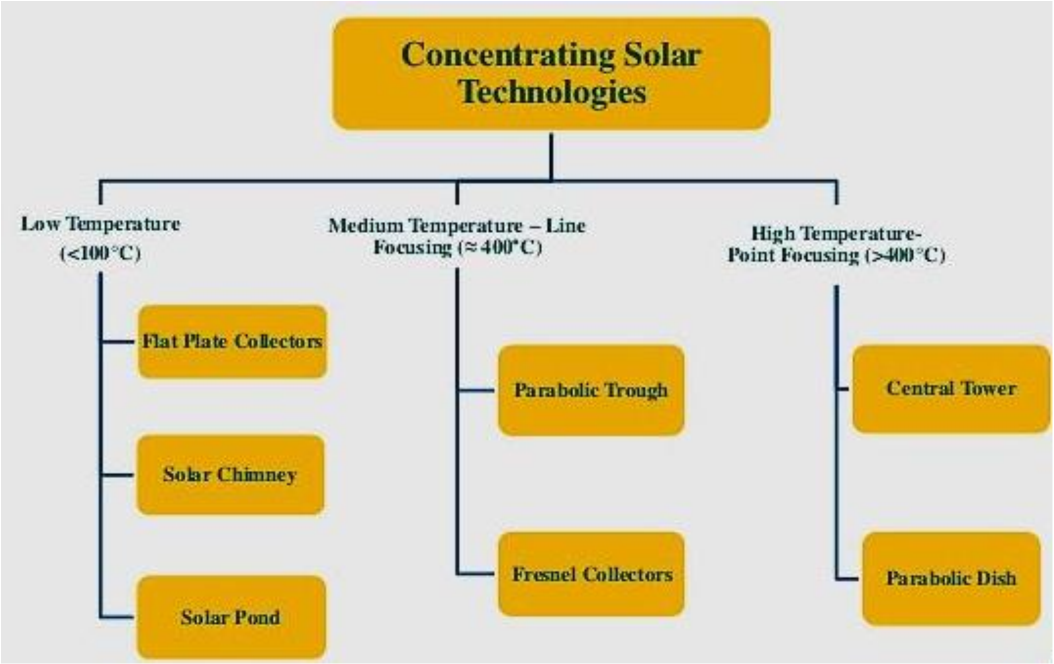

Figure 2.12: *Concentrating solar technologies classification*

Concentrators need to move toward the direction of the sun so that they may maximize their exposure to sunlight throughout the day. A tracker can help you do this effectively. To follow the sun's revolving course, tracking may be done on a single axis from East to West or from North to South.

A receiver is a component of any solar energy conversion system since it must be able to transform the solar radiation into another form of energy. This might be a solar cell or a heat absorber (to collect thermal energy) (to convert light to electric energy). In the former, energy from the absorbed thermal radiation is transferred to a generator through the heating of a medium (fluid). In the second scenario, an electric current is produced when light triggers a photovoltaic effect in the solar cell's material. In both cases, the quantity of energy available for the conversion is limited to what can be supplied by the solar source per unit area of the converter.

There are two ways we can get the extra power we need. The first possibility is to expand the size of the system (for example by increasing the number of receivers). That is to say, we need to increase the size of the plant, which might include buying more land, more supplies, more money, etc. It has been done to some degree, but it is not always enough, particularly when land space is limited, to supply the energy needs. The second strategy involves focusing on the flow of radiation. A concentrator (often an optical device) positioned between the light source (the sun) and the receiver may accomplish this. An aperture, the cross-sectional area via which sunlight enters the system, is one defining feature of a solar collector, which is otherwise defined as a system for processing sunlight that consists of a concentrator and a receiver.

Common types of concentrators include mirrors and lenses, which focus and guide rays of sunlight in different directions. Concentrating optics come in a wide variety of shapes and sizes. Concentrating collectors, which use mirrors of varying shapes, is one kind of example.

First and foremost, the act of focusing light indicates that the energy flow is enhanced as a result of the confined space. Several significant advantages result from this:

- Increasing heat collector temperatures.
- Reducing the receiver's surface area reduces the amount of heat lost by convection.
- More efficient energy conversion with a smaller footprint is possible.

The following are now standard at large-scale CSP plants [Mendelsohn et al., 2012]:

2.10.1 Flat Plate Collectors:

When it comes to solar-powered home heating systems, flat-plate solar collectors are the gold standard. This technique is based on a rather straightforward concept. A dark, flat surface gets heated by the sun and absorbs as much energy as it can before transferring that heat to a fluid such as water, air, or another substance.

A flat-plate solar collector as shown in Figure 2.13 consists mostly of the following parts [73]:

- Black surface: “absorbent of the incident solar energy”
- Glazing cover: a thin, transparent covering that allows radiation to reach the absorber but prevents the surface from losing heat by radiation and convection.
- Heating fluid: filled tubes that go from the collector to the heat source.
- A framework to shield and keep the parts in place.

- To prevent heat from escaping via the sides and bottom of the collector, insulation is used.

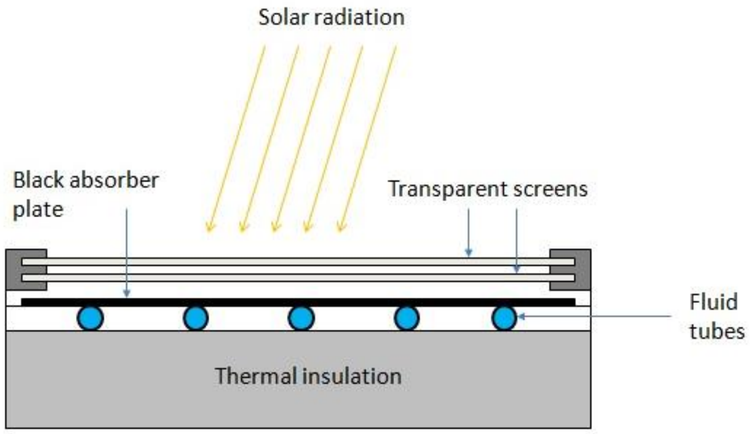

Figure 2.13: *Flat plate collector* [73]

While most flat-plate systems work and are most efficient between 30 and 80°C (Kalogirou, 2009), several novel forms of collectors that make use of vacuum insulation may reach even higher temperatures (up to 100^{o}C). With the application of selective coatings, the temperature of stagnant fluid in flat-plate collectors has been demonstrated to rise over 200 ^{o}C.

The flat-plate collectors have a number of benefits [173]:

- Producing this is a breeze.
- Affordable price.
- Get beam and scattered radiation data.
- Affixed for good (There is no need for high-tech tracking or positioning instruments.).
- Minimal upkeep is required.

2.10.2 Evacuated or Vacuum Tube Collector

Heat is transferred from the tubes to a circulating heat transfer fluid (often 50% Propylene Glycol) in the evacuated or vacuum tube collector, which consists of many rows of parallel clear glass tubes linked to a header pipe [174]. These glass cylinders are for transporting liquids. Since the sun's rays are always perpendicular to the heat-absorbing tubes, these collectors are effective even when the sun's rays are weak, such as in the early morning, late afternoon, or when clouds are present. In places where winters are often foggy and chilly, evacuated tube collectors prove to be invaluable as shown in Figure 2.14.

One or more rows of clear glass tubes are supported by a metal framework in an evacuated tube collector. Depending on the manufacturer, the length and diameter of each tube may be anywhere from 5 feet (1500 millimeters) to 8 feet (2400 millimeters) and 1 inch (25 millimeters). Each tube is either a "twin-glass tube", in which the outer tube is thicker and the inner tube is thinner, and coated with a particular coating that absorbs solar radiation but prevents heat loss, or a "thermos-flask tube", in which the outer tube is thicker and the inner tube is thinner. The borosilicate or soda lime glass used to make the tubes is durable, heat-resistant, and very transparent to the sun's rays [67].

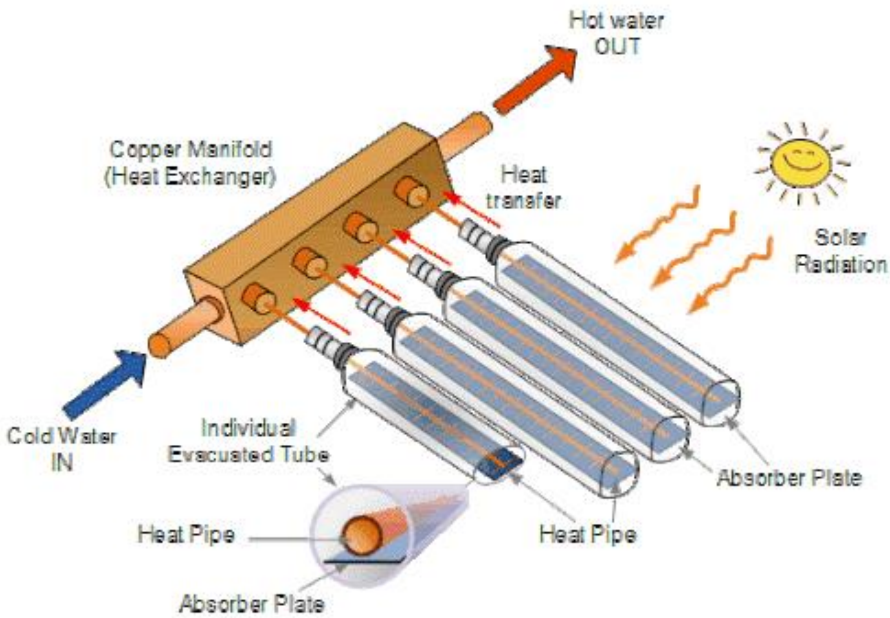

Figure 2.14: *Tube collectors* [174]

Each glass tube has a metal heat pipe running through it, and a flat or curved aluminum or copper fin connected to it. The fin is coated with a selective material that allows heat to be transferred to the fluid in the pipe. Through convection, the fluid within the copper heat pipe warms a "hot bulb", which in turn warms a copper manifold inside the header tank.

Because they can pull heat from the air even on cloudy, humid days, evacuated tube collectors are a contemporary, efficient alternative to traditional flat plate collectors. The vacuum within the glass tube improves performance even when the sun is not at its optimal angle, resulting in greater overall efficiency. The vacuum tube's arrangement is crucial for this sort of solar thermal collector [175]. The way the fluid is cycled around the solar hot water panel may be affected by the vacuum tube configuration used, which can be either a “single wall tube, double wall tube, direct flow, or heat pipe”[125].

2.10.3 Solar Air Collectors

In solar air heating, insolation (sunlight) is converted into heat by an absorber and then utilized to warm air. Heating or conditioning air using solar energy is a renewable heating method that may be used in the context of either space heating or process heating. It targets the highest demand for building energy in heating climates—space heating and industrial process heating—and is often the most cost-effective of all solar technologies, particularly in commercial and industrial applications. There are two basic types of solar air collectors [176]:

- Transpired Solar Collectors and Unglazed Air Collectors (commercial, industrial, agricultural, and process uses for heating ambient air)
- Glass-Enclosed Solar Arrays (heating systems that recycle warm air are the most common.)

There are a few different ways to categorize solar collectors for air heating, including the air distribution methods they use and the materials they're made of (glazed vs. unglazed). For instance:

- Through-pass collectors
- Front-pass
- Back pass
- Combination front and back pass collectors
- Unglazed

- Glazed

In solar air heating, an “unglazed air collector” is an absorber that doesn't have any kind of cover, such as glass or glazing. Transpired solar collectors dominate the market for unglazed collectors. Instead of using the building's recirculated air, unglazed air collectors warm the air outside. To take full use of the “lower sun angle during the winter heating months and the sun's reflection off the snow”, transpired solar collectors function best when running at flow rates of 4 to 8 CFM per square foot (72 to 144 $m^3/h.m^2$) of collector area [177].

To catch the boundary layer of heat and move it evenly into an air cavity behind the outside panels, a transpired solar collector's exterior is covered with thousands of tiny micro-perforations. Ventilation air heated by the sun enters the building's ventilation system via air outlets along the collector's top and is dispersed throughout the structure using either traditional methods or a solar ducting system.

Recirculating the conditioned air from the building via solar collectors serves the same purpose as a traditional forced air furnace. A simple and effective collector for use in a number of air conditioning and industrial applications may be built by using a surface to absorb the sun's heat energy and directing air to come into contact with it.

A basic solar air collector uses an absorber material, which may or may not have a selective surface, to soak up solar heat and then transmit it to the air by convection. The resulting hot air is ducted into the building or the processing area, where it is utilized to fulfill the respective heating requirements. Solar air heat technologies provide a sustainable way to generate thermal energy while lowering the carbon footprint associated with using traditional heat sources like fossil fuels. Space heating, extending the growing season in a greenhouse, preheating ventilation makeup air, and providing process heat are just some of the uses for solar air heat equipment. Together, solar thermal and photovoltaic (PV) technologies may enhance the system's overall efficiency by warming air for space heating and cooling PV panels to boost the latter's electricity output.

2.10.4 CPC Collector

The term "compound parabolic concentrator" (CPC) refers to a specific form of concentrating collector that does not create an image of the light source when incoming solar radiations are reflected off the reflector and then concentrated on the absorber's apparent surface. It's the perfect solar energy collector since it concentrates light from a wide area onto a tiny one, wasting as little energy as possible in the process [176].

It's the perfect solar energy collector since it concentrates light from a wide area onto a tiny one, wasting as little energy as possible in the process. It took more than a decade for this innovation, which was first developed in 1965 for the reflection of Cerenkov radiation onto a sensor, to become the gold standard for collecting solar thermal energy. By reflecting all of the incoming energy on the aperture to the receiver throughout a range of incidence angles within the acceptance angle, CPC reflectors were invented by Winston (1974) to improve the efficiency of low concentration solar collectors. The shape of the absorber might be either flat, round, or cylindrical. Through a process of multiple internal a reflection, the collector's absorptive bottom surface receives all radiation that enters the aperture within the acceptance angle. Smaller concentration ratios, as stated by Pereira (2004), Concentrating photon sources (CPCs) may concentrate a huge amount of diffuse radiation incident on their apertures without having to follow the sun. Concentrated solar power (CSP) system deployment is primarily constrained by the technology's high price tag. Reliability and ease of production are essential in order to reduce overall system costs. The primary challenge that must be overcome to commercialize CSP technology is lowering its price. Because it is a non-imaging type concentrator, where the incoming rays are simply collected on the absorber surface after reflection from the reflector, the compound parabolic concentrator (CPC) is useful for solar energy collecting. Since concentrating solar collectors produce no carbon dioxide emissions, they are a green option for home hot water and space heating [178]. Various CPCs are shown in Figure 2.15.

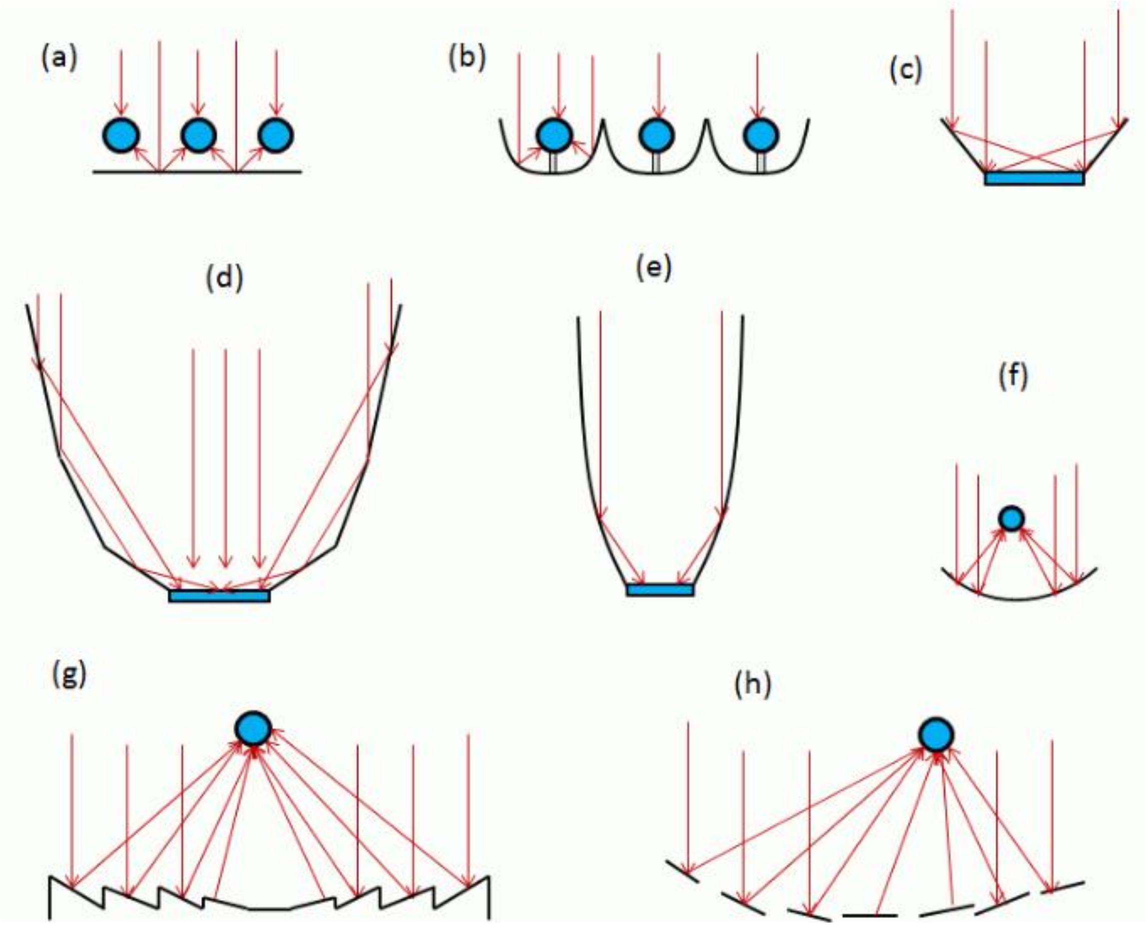

Figure 2.15: *"Types of concentrating sunlight collectors: (a) tubular absorbers with diffuse back reflector, (b) tubular absorbers with specular cusp reflectors, (c) plane receiver with plain reflectors (V-trough), (d) multisectional planar concentrator, (e) compound parabolic concentrator (f) parabolic trough, (g) fresnel concentrator, (h) array reflectors (heliostats) with central receiver. (Concentration of light on the receiver is achieved by shaping the reflectors/mirrors around the receiver, represented by blue circles)* [178]

2.10.5 Parabolic Trough

Parabolic troughs are a special kind of solar thermal collector that is flat on one side and curved like a parabola on the other two, and they are coated with shiny metal mirrors as shown in Figure 2.16. When items to be heated are placed at the focal line, sunlight entering the mirror perpendicular to its symmetry plane is concentrated there. When the focal line of a trough is aligned with the Sun, as it is in a solar cooker, the food within the trough will be cooked.

At its focal line, a tube may be used to transport fluid throughout the length of the trough for different applications. The tube is positioned such that the sun's rays may focus on it, heating the fluid to a very high temperature. The heated fluid may be channeled into a heat engine, which then utilizes the heat energy to power mechanical or electrical systems. This parabolic trough solar collector is the most well-known and widely-used design.

The thermal efficiency of a typical turbine generator, which uses heated steam to generate electricity, is between 60% and 80% when the heat transfer fluid is water. Comparable to PV (Photovoltaic Cells) but less efficient than Stirling dish concentrators, the total efficiency from collector to grid is about 15 %. Thermocline tanks, which employ a combination of silica sand and quartzite rock to displace a major %age of the volume in the tank, are an efficient way for large-scale solar thermal power plants to store the energy they generate. This is followed by the addition of the heat transfer fluid, which is commonly a nitrate salt in liquid form [50].

Figure 2.16: *Parabolic trough at Harper Lake in California* [50]

2.10.6 Parabolic Dish:

Parabolic solar dish collectors are far more compact than their long trough counterparts, and they resemble enormous satellite TV or radar dishes. A curved parabolic shaped dish, often known as a “solar concentrator,” is the major solar component of this kind of solar heating system as shown in Figure 2.17.

Paraboloidal solar dishes, ranging in size from a few feet to several meters in diameter, are created by stamping thin sheets of metal or aluminum-coated mylar. The sun's rays are captured by the parabolic dish, which then concentrates the light into a tiny target area in front of it. The surface area of the parabolic solar dish is maximized by covering it with a large number of miniature mirror reflectors, which focus the sun's rays on the center, where the heat absorber is positioned.

More than 90% of the sunlight that strikes these highly polished mirrors is reflected, enhancing the dish's efficiency by almost 20% in comparison to the parabolic trough collector. For the reflecting surface of a solar dish collector, mirrors are often utilized rather than a single highly polished dish because of their low cost, ease of cleaning, and durability in the harsh outdoor environment. Additionally, broken mirrors may be replaced individually. In addition to a solar dish collector, a thermal receiver is needed to transform the concentrated sun beam into heat. A modest evacuated tube or a more complicated solar heat engine like a Stirling Engine may serve as the solar receiver.

In order to convey the strong heat generated by focusing the sunlight on the receiver, thermal oil or a similar fluid is often utilized within the receiver rather than water. Similarly, to trough collectors, solar dish collectors may function independently or in networks to serve bigger, more industrial loads [179].

Figure 2.17: *Parabolic dish solar concentrator [179]*

2.10.7 Solar Tower

The solar power tower is a concentrating solar power installation that uses a tower to capture the sun's rays for use as an energy source. To concentrate the sun's beams onto a collection tower, it employs a system of flat, moveable mirrors (called heliostats) (the target) as shown in Figure 2.18. One potential approach to clean, renewable power is concentrated solar thermal.

These concentrated beams of light were originally used to boil water, which then turned a turbine. Several systems have been designed and put into operation where molten salts (40 % potassium nitrate, 60 % sodium nitrate) are used as the working fluids. The liquid sodium used in these systems is relatively new. Due to the large heat capacity of these working fluids, the energy may be stored until it is needed to boil water and power turbines. Even when the sun isn't shining, energy may be produced using these designs [180].

The design of the solar tower comprises the following:

- Some concentrating solar power towers utilize air cooling instead of water cooling to save scarce desert water.
- Instead of using curved glass, which is more costly, flat glass is utilized.
- The heat is stored in molten salt tanks so that power may be generated even when the sun isn't out.
- Turbines driven by steam heated to 500 °C are linked to generators to create power.
- The plant's operations, including the positioning of the heliostat array, alarms, and data collecting and transmission, are supervised and controlled by the control systems.

Installations typically use between 150 and 320 hectares (1,500,000 and 3,200,000 square meters).

Figure 2.18: *Solar tower* [180]

2.10.8 Compact Linear Fresnel lens Reflector (CLFR)

To concentrate sunlight on a stationary absorber, Linear Fresnel reflectors employ long, thin segments of mirrors focused at a central point. The absorber channels the focused energy into a thermal fluid (typically, this refers to oil that can remain liquid even when heated to extremely high temperatures.). After passing through the heat exchanger, the fluid is used to produce steam. The CLFR uses a number of absorbers near the mirrors as opposed to only one in conventional LFRs as shown in Figure 2.19.

The system's reflectors, situated at its foundation, focus the sun's beams into its absorber. The use of “Fresnel reflectors” is a crucial component that makes all LFRs superior to conventional parabolic trough mirror systems. Because of the Fresnel lens effect, these reflectors may employ a focusing mirror with a wide aperture and a short focal length while yet using a very little amount of material. Since sagged-glass parabolic reflectors are so costly, this significantly lowers the system's overall price. However, thin-film nanotechnology has drastically decreased the price of parabolic mirrors in recent years. The angle of the incident rays (the rays of sunlight impacting the mirrors) varies during the day, posing a significant problem for any solar concentrating technique. Using a computer-controlled solar tracker system, a CLFR's reflectors rotate in a north-south direction around a single axis. This permits the system to optimize energy transmission by keeping the sun's rays at the optimal angle of incidence with respect to the mirrors. The mirrors' focal point is the absorber. It is positioned above the reflector segments and runs parallel to them, allowing the radiation to be transferred to a thermal fluid. The absorber for the CLFR system consists of a glass-covered air chamber that is inverted, housing insulated steam tubes [180].

Figure 2.19: *Linear Fresnel lens reflector* [180]

2.11 State-of-Art of Solar Energy Based Thermoelectric Generator

Solar power plays significant role in the future of solar projects for diversified and secure energy. Concentrated solar power has the potential to fill an important need in India's energy market**.** To penetrate larger renewable energy, the stage is set by the base load and dispatchable power, unlocked by the concentrated solar power to use hybrid methods and easily add storage [181]**.** It produces electrical power from the heat generated by concentrating solar radiation, one of its exciting applications. Solar TEG uses a heat sink, TEG and collector. Different collector alternatives, like parabolic dishes, fresnel lenses, solar furnace [75] and flat plates [35] and parabolic troughs, may be used to alter the solar flux at the hot end of a TEG [182]**.** The efficiency of TEG combined with the efficiency of optical-to-thermal conversion is the efficiency of solar TEG. Modern solar TEG systems achieve efficiencies of around 5% for materials with a temperature differential of roughly 100 ^{o}C (ZT=1). Compared to other forms of solar electrical technology, such as solar cells, which demonstrate an efficiency of 18 %, solar TEG technologies face a significant economic hurdle in their substantially lower conversion efficiency. Improving the solar collector design and the figure of merit (ZT) of TE materials will lead to higher efficiencies and a higher conversion rate in the future [55].

2.11.1 Parabolic Dish Collectors based Thermoelectric Generator

A solar dish collector is a kind of concentrated solar collector that uses reflective lenses and metal plates to concentrate the sun's rays onto a tiny receiving area (anodized aluminium) as shown in Figure 2.20. In more technical terms, it can also be called a point focusing collector. Received solar energy's intensity can be magnified several times by concentrating the sunlight at one spot through a lens or mirror acting as a single sun, which directs its light to the same focal length. It results in achieving more power per square meter. Solar dish collectors' concentration can be more than one thousand suns which help in attaining temperature at target's focal point. It may lead to a generation of 100s to1000s ^{o}C temperature, which depends on the location and size of the dish. A parabolic solar dish highly resembles a radar dish or big satellite TV dish, which is very small compared to long trough collectors, which was not the case with the previous solar collector as its shape resembles a lot with the long trough. The most significant component used for solar heating is a curved parabolic dish, also termed "parabolic solar concentrator". Targeting the systems with high optical concentration, the optimization and design were described, maximizing its efficiency for single TEG over a high difference in temperature, through a "range of optical concentrations of 0.1 – 1000x using multiple material systems of dish strips". High-concentration solar thermoelectric generators may achieve a 13 % conversion efficiency with a temperature differential of 35 ^{o}C and an output power of 5.5 watts [76].

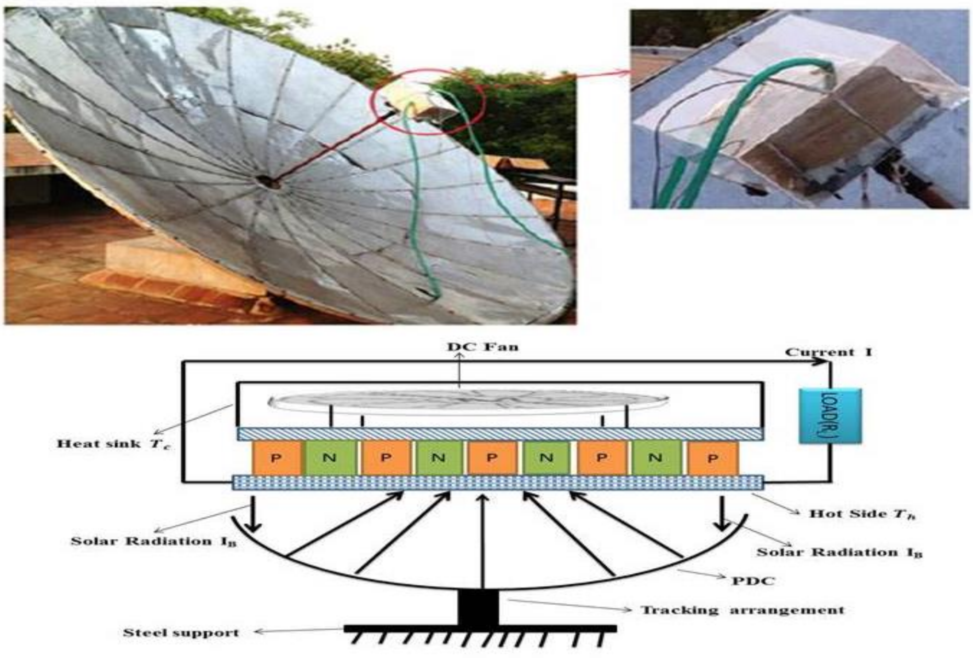

Figure 2.20: *Parabolic dish concentrated solar thermoelectric power generation* [183]

Design and construction of the concentrated STE system are made with the conventional parabolic concentrator. At the concentrator's focus, the receiver is mounted with concentrating the solar rays at the centre. For obtaining maximum efficiency, manual tracking can be used. This maximum efficiency should be present throughout the day. For attaining high temperature, solar dish concentrators are brought into the application, reflecting the incident flux over aperture area (the reflective surface) onto a smaller area (which is the receiver), and the solar radiation is concentrated. It is crucial to understand the complete phenomena involved in figuring out the efficiency of complete system.

This study incorporates theoretical and experimental analysis from various researches of the parabolic dish (concentrating type) solar collector for evaluating the feasibility and efficiency of the collector studies, which are used in various applications with implying many different techniques. These obtained data can be utilized to optimize the thermodynamics of those solar power systems, which are efficient, and hike the efficiency of existing ones.

Without a doubt, the CSP is an exceptional renewable technology. Additionally, a thermoelectric generator based on the Seebeck effect will be the primary emphasis of this article. Table 2.8 summarizes the findings of a number of writers that labored over the optimization and design of the TEG-Concentrator, a component of the CSP system that makes use of several material systems to achieve optimal efficiency throughout a wide temperature range.

Table 2.8: Various CSP (Concentrated Solar Power) technologies for TEGs

TEG using Concentrating Solar Power (CSP)	**Methodology**	**Research Findings**	**Ref.**
Experimental as well as theoretical observation over the "heat pipe cooled TEG with water heating" by utilizing the	Water-based cooling for a heat pipe	For the lab set up of TEG comprising of 60^{o}C, maximum generated power is 1.27W	[127]

concentrated STE			
Energy and exergy study of heat-pipe based annular TEG systems	An annular Thermoelectric Generator's Thermal Model	At 1000W/m^2 of "solar radiation and 308K" of T_{water}, the solar TEG generates a total system exergy of 5.02%, an electrical exergy of 2.63%, and a power output of 1.92%.	[184]
Combined generation of both power as well as heat in TE system	Fresnel lens collectors using both passive as well as active methods for cooling.	Generation of 1.4 W of power at a 37^{o}C temperature difference. Its thermal power, thermal efficiency and total efficiency were 76.1W, 18.05% and 18.39%, respectively.	[113] [64]
Solar Parabolic Dish TEG	Solar Parabolic Dish	When the radiation of solar beam reaches 950 W/m^2 of maximum value, 0.78% of maximum efficiency is received. When the radiation of solar beam reaches the value of 431 W/m^2, 0.22% of minimum overall efficiency is received.	[183]
Solar thermal energy co-generator using a flat-plate solar collector	Using a single system for generating thermal energy as well as electrical power.	The hybrid system enhances overall efficiency as well as performance of the TEPG system.	[38]
Experimental study on solar parabolic dish	A satellite dish antenna that has a polished	At a 950W/m^2 solar beam radiation, 602K of maximum temperature was derived from	[185]

TEG	aluminum sheet concentrator surface.	the receiver plate, whereas the minimum temperature derived for the 430W/m^2 was 375K. The maximum output power obtained was 11W.	
Development of STEG	devices using a wide variety of materials with a magnification range of 0.1 to 1000X	The system generated 5.5W of electricity at a temperature differential of 35^{o}C.	[76]
The impact of a fluctuating heat source on STEG	PCM (phase change material)	The STEG's efficiency, temperature difference, and peak power output all decrease by 32.87 %, 30.71 %, and 52.11 %, respectively, when the height of the PCM is raised by 5-20 mm.	[34]
Vacuum enclosed concentrated STEG	attached with a spectrally selective absorber coating	At a temperature of 642 K on hot side, peak efficiency and peak power output were 2.21% and 0.91 W, respectively.	[64]
Refraction-Assisted STEG	based on PCM	At 1.5kW/m^2 and 1kW/m^2 solar intensities, the RTEG's maximum energy conversion efficiencies are 86% and 60% greater, respectively, than the average STEG.	[77]
Performance of thermoelectric	transient model couples with solar	In terms of producing power, this approach shows the most	[146]

generators	pond	promise. With an annual average LCZ temperature of 80 ^{o}C and a heat extraction rate of 15 %, this system generates around 4.384 kWh/m^2. Overall, the extracted heat contribution to 't' is between 1% and 1.5%.	

As can be seen in Table 2.8, parabolic dish concentrators are not as effective as Fresnel lens solar cookers. If radiation is lowered from 950 W/m^2 to 430 W/m^2 in a parabolic dish collector, the temperature drops from 602 K to 375 K, which indicates a reduction of 520 W/m^2 results in a temperature drop of 227 K. At a temperature differential of 350 C, a concentration range of 0.1 to 1000X may provide a respectable quantity of electricity (5.5 W). While a solar pond-based thermoelectric plant shows maximum potential of producing 4.384KWh/Year m^2, a co-generation system with a Fresnel lens indicates greater performance of the overall system, giving 1.4 W electrical power and 76.1 W thermal power. When compared to conventional flat-plate TEG, annular TEG may provide an additional 50% of usable power.

2.11.2 Fresnel lens based Thermoelectric Generator

Fresnel lenses for solar concentrators were first created with concentrating photovoltaics in mind. Plano-convex “solar concentrator Fresnel lenses” are designed to face the sun and direct sunlight onto the integrated photovoltaic cells. Figure 2.21depicts how these lenses are used in solar furnaces as solar energy concentrator. The purpose of this setup is to concentrate all of the parallel lights into one concentrated area. Shorter focal length Fresnel lenses have found use in detectors and sensors. Fresnel lenses are used in conjunction with TEGs to focus sunlight onto the hot side of the device, where it may be converted into energy [75]. Fresnel lenses hold considerable potential for increasing the efficiency of TEGs, which generate electricity from solar energy, by concentrating solar radiation so that a larger portion of the hot side may be used. High-efficiency STEGs may be achieved with increased optical concentration. Therefore, this method may be used for both solar thermal and concentrated photovoltaic projects [186].

Fresnel lenses, parabolic troughs, parabolic dishes, and heliostat conjunctions inside the central receiving system all fall under this category. Relevant features employed in STEGs include optical efficiency, the necessity for a tracking device, and the amount of concentration obtained [13]. The maximum efficiency of concentrated TEG is 7.4% after adjusting concentrating lenses and enhancing optical concentration [74]. The combination of a phase change lens and an optical lens allowed for the creation of a design that generates solar energy with double the focus strength of previous designs. At 1 kW/m^2 and 1.5 kW/m^2 solar intensities, the mechanism offered an efficiency of 60% for peak energy conversion of RSTEG, which is greater than the conventional STEG by 86% [77].

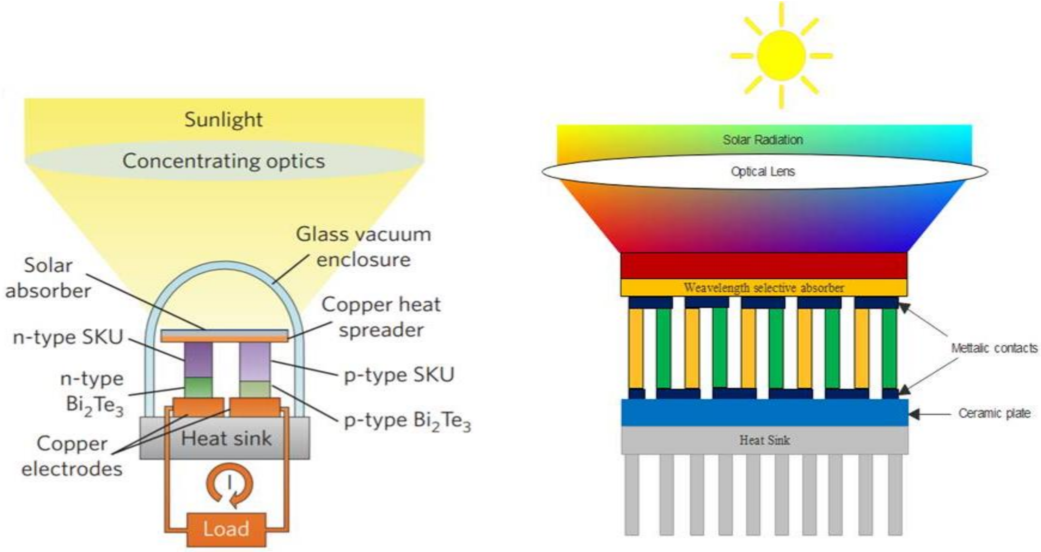

Figure 2.21: *Thermoelectric power generation through optical concentration* [74]

2.11.3 Solar Furnace based Thermoelectric Generator

As seen in Figure 2.22, a solar furnace uses a curved mirror that acts as a parabolic reflector to concentrate sunlight and heat it for industrial use. The light is focused along the focal length by the curved mirror. The produced heat may be used to create nanomaterial, hydrogen fuel, melt steel, or generate power, and the focal length temperature can reach 6330°F (i.e., 3500°C). The solar furnace allows for the concentration of solar energy, which is then used to generate very high temperatures. It consists of parabolic mirrors or heliostats used to focus sunlight at a certain point. It is mechanically constructed and optically complicated, with an automated control system. Solar water pasteurization, solar-powered grills, and affordable solar cookers are all products of the same solar furnace idea.

Higher efficiency of 15% in converting solar energy shows the promise of STEGs [187]. STEGs were analyzed during their lifetimes and put through their paces at HFSF at NREL to optimize the performance of the prototype model [75] [188].

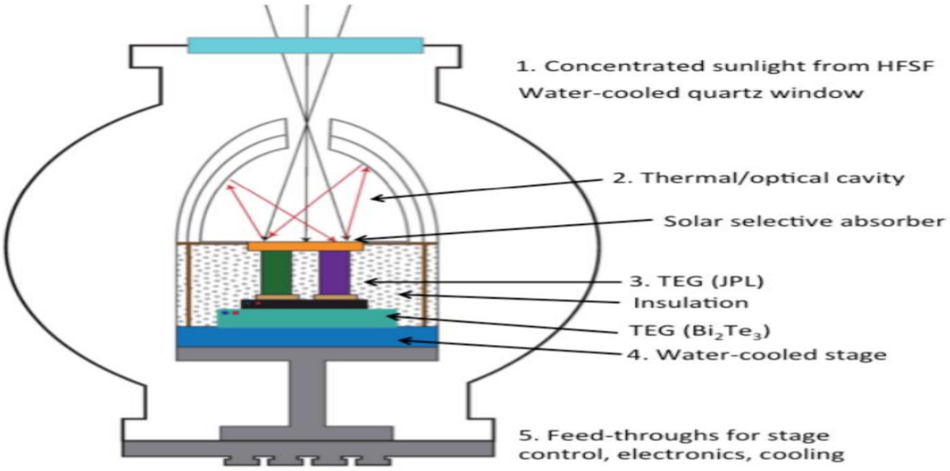

Figure 2.22: *Highly efficient TE power generation through HFSF (high flux solar furnace)*[75]

2.11.4 Waste heat recovery from automobiles, industries and human body through TEGs

The energy created in industrial operations is usually just spilled, squandered, or lost without being put to good use. It is termed Industrial Waste Heat [189]. Energy consumption for any power-using equipment or system may be reduced thanks to the widespread availability of waste heat recovery solutions [26]**.** Figure 2.23 depicts heat from a recuperative burner, while Figure 2.24 depicts heat from a vehicle's exhaust system being put to use.

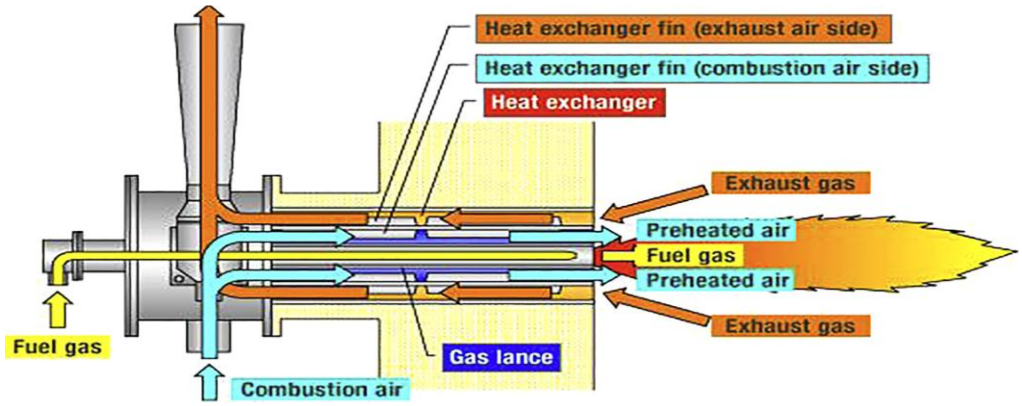

Figure 2.23: *Waste Heat recovery through Recuperative burner* [26]

In contrast to alternative recovery systems where these desired properties are not necessary, the TEG system's waste heat recovery technology prioritizes durability, Fand the TEG system's lack of chemical reaction and absence of moving components make this possible [51].

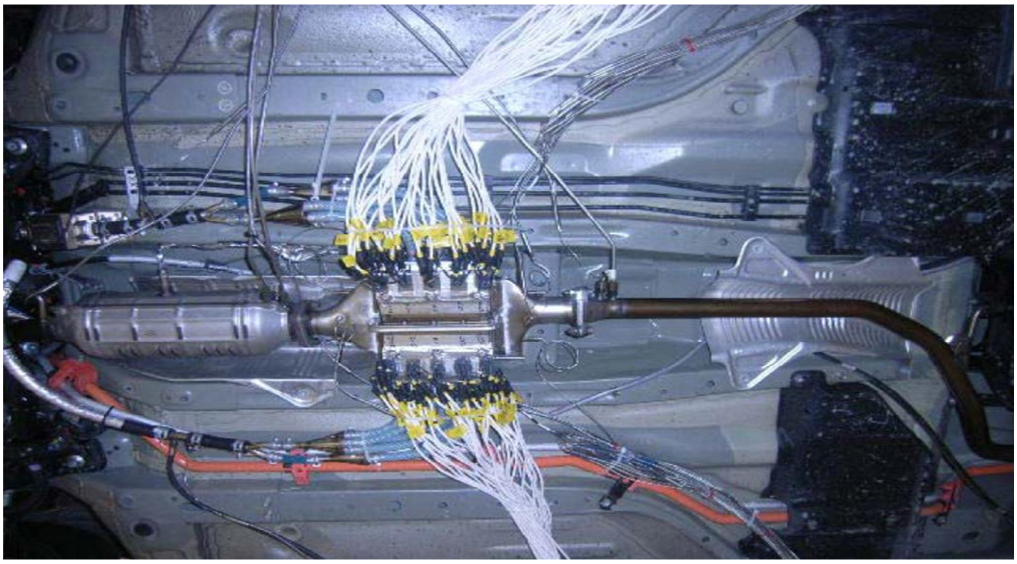

Figure 2.24: *Exhaust heat recovery system through TEG in Honda Car* [51]

Demand for energy recovery methods has been on the rise for quite some time for reasons that have to do with both environmental protection and the global energy problem [190]. Energy recovery methods include heat recovery ventilation, heat recovery steam generators, and water heat recycling. Many experiments are included in Table 2.9, where TEGs are used to convert heat into electricity from the byproducts (smoke) of an automobile's exhaust pipe. The performance of a thermoelectric module (TM) and the characteristics of a TEG system may be determined using the two test benches that have been established. The effects of the primary operating conditions, flow rates, load resistance, hot and cold side temperature, power output, and voltage were investigated in the lab tests.

TEGs are effective enough to use on live things as shown in Figure 2.25. They are more efficient than human solar cells as well. Inconspicuous devices worn by humans have a maximum power output of 10 mW at 22°C and ZT=1. In contrast, by attaching TEG to the body of a big animal like a cow, many milliwatts of power may be generated. TEG scavengers will compete with battery scavengers solely based on fabrication cost, which drops considerably [191].

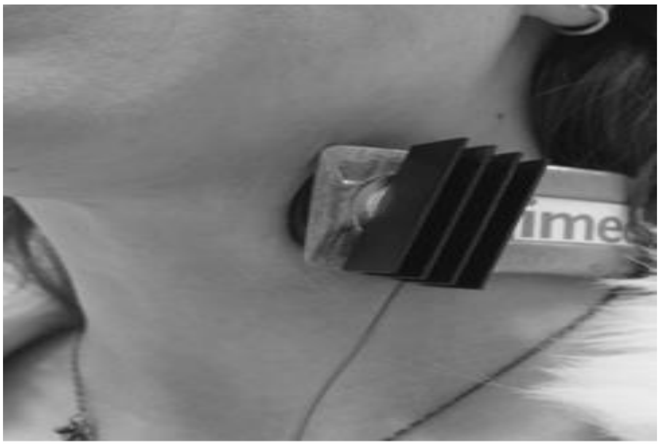

Figure 2.25: *Extracted heat from body utilized in TEG* [191]

Table 2.9: Waste heat recovery from different systems through TEG

TE waste heat recovery technology study	Methodology	Research Findings	Ref.
Thermoelectric power generation is used by Energy harvesting system for the applications of automotive	TEG and heat pipes for thermal energy recovery	When the mass flow rate in the lower duct is less than that in the upper duct, both the maximum power output and the heat transfer rate of TEG increase dramatically.	[192]
Exergy and Energy analysis of an advanced ATEG based on the cookstove.	ATEG thermodynamic modeling at an assumed 30 ^oC in the atmosphere.	Variation in the cold junction temperature between 30 and 150°C causes the combustion air temperature to gradually travel through the TEG's annular fins.	[193]
A study to harvest energy from a table lamp by using a TEG.	Peltier and joule heats, a small heat sink, and a 1D TEG model are all simulated.	The maximum power output of the lamp is around 1 mW, while its waste heat output is about 10W. Therefore, the effectiveness of waste heat recovery is as low as 0.01 %, even when the temperature difference between the surrounding	[194]

		air and the heat source (the lamp tubes) is as high as 86 K.	
Harvesting body heat for generating power, wearable TEG is used	Miniaturized accelerometer	The created wearable TEG features a low internal resistance (1.8 Ω) and an open-circuit voltage of 37.2 mV at a temperature of ΔT=50 K. The related power density and output power are determined to be 16.7 $\mu W/cm^2$ and 192.6 W, respectively.	[53]
With humidified flue gas, exergy and energy analysis of TEG system.	Heating using flue gas that has been humidified	As module area rises, exergy efficiency first decreases but later soars.	[195]
Development of stove-powered TEG	cooking/water heating stove design.	In order to analyze the stove's temperature, the heat sink's efficiency, and the TE's location with any degree of precision, theoretical analysis is required, especially with regard to the cooling and combustion system via numerical simulation. The batteries available have an electrical power of 5 W.	[196]
For stoves of solid fuel, TEG is used in a combined power and heat system.	Maximum Power Point Controller (MPPT)	Experiments show that the suggested CHP system can efficiently power a standard solid fuel stove. The average electrical	[197]

		output is 27 $W_{electrical}$ and the average thermal output is 600 $W_{thermal}$ after burning for 2 hours. TEG has a modest efficiency of about 5%.	
An analytical study of Marine engine applications of TEG	A test rig evaluates TEG's efficiency.	The effectiveness of the TEG's power conversion ranges from 0.2 % for the $Si_{80}Ge_{20}$ TEM to 1.3 % for the Bi_2Te_3 potential. The TEG's power output is between 0.05 and 0.35 watts.	[198]
Wet flue-gas TEG’s performance analysis	Wet flue gases	With the same mass flow rate, the maximum power output of the wet flue gas is 5.8 times higher than that of the dry flue gas at 30% humidity and 150°C gas temperature.	[199]
Heat exchangers for thermoelectric generators	A hot block and electric heater are included in the model.	The TEG heat exchanger system showed 2.094, 2.07, and 1.72 W for zigzag, spiral, and straight lines, respectively, at heater temperatures of 175, 200, and 250 ^{o}C. Assume a thermal resistance of 0.478 for the exchangers, 0.483 for the condenser, and 0.581 for the evaporator.	[196]

Since it can be seen in Table 2.9, even low-grade heat (waste heat) may be used to generate electricity, as 10W of heat from a table lamp can be converted into 1 mW of electrical power using a thermoelectric generator (TEG). At a temperature of 50 Kelvin, the human body generates 192.6 microwatts of electricity, proving that not only humans but also other creatures are capable of generating large amounts of energy.

Thermoelectric generators (TEGs) based on cook stoves have sufficient merit to be the most promising choice for electrical power production, particularly in rural regions; nevertheless, numerical modeling is necessary to determine the size, position where TEG is to be put, and module rating. The average TEG efficiency of modern cook-stoves is 5%. Even while marine engines generate very little power individually, when combined their TEGs may generate a substantial quantity of energy.

2.11.5 Hybrid TEG

Hybrid solar thermoelectric generator (HSTEG) systems have been the subject of much investigation for their potential to improve electrical and thermal efficiency [200]. In comparison to standalone solar panels, hybrid systems are gaining popularity because of their superior performance, stability, and efficiency. The electricity efficiency of a hybrid solar photovoltaic-TEG system is 15.6% and 12.2%.

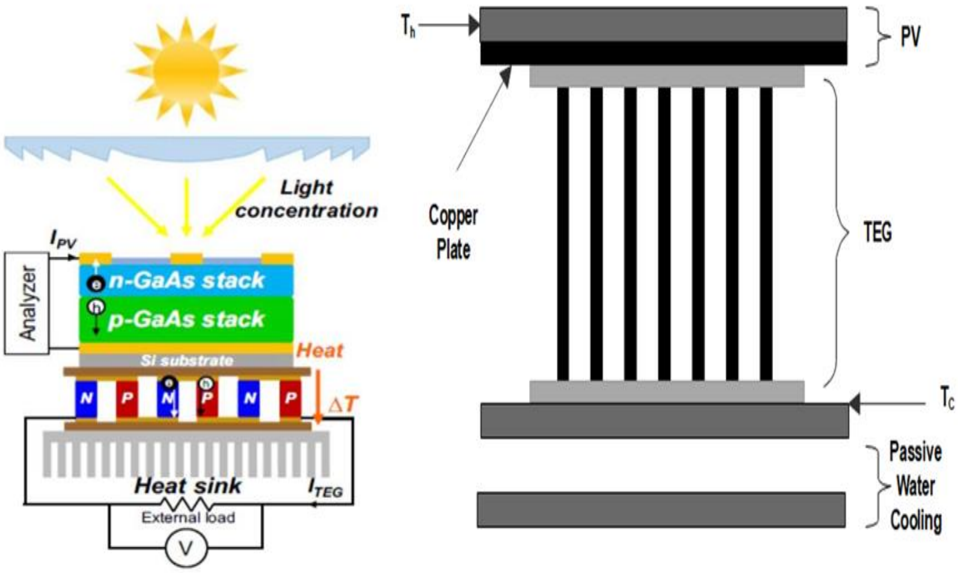

Figure 2.26: *Hybrid concentrated photovoltaic and thermoelectric system and schematic of different layers* [201]

Most research and application have gone into photovoltaic systems, the simplest of which is a solar panel connected to a heat extractor that uses either air or water to dissipate heat. A solar photovoltaic module made of crystalline silver is implemented, boasting a 14 % conversion efficiency. The heat is removed, resulting in a cooler environment [26]. The TEG-PV system has been shown in Figure 2.26 to be the most effective hybrid system. Integrating photovoltaic and thermoelectric systems into the power grid allows for the use of a broader range of solar energy. High-frequency (short-wavelength) radiations are used to generate electricity from PV cells using the "spectrum beam splitting" approach. Long-wave radiations may be utilized to generate thermal energy of moderate to high quality, which in turn can be used by a thermoelectric device to generate electricity, as seen in Figure 2.27. Six Bi_2Te_3 TEG modules linked in series provide 20W of electricity and 200W of heat energy, which is stored in water at roughly 50^oC in a different solar hybrid system. The chilly side of this system is kept at a constant 50 ^oC by using the flow of water. These hybrid systems may be used in lieu of photovoltaic/thermal ones in places like India, Mexico, China, and West Asian nations, where copious solar radiations are accessible throughout the year. Table 2.10 summarizes the results of testing several hybrid TEG configurations.

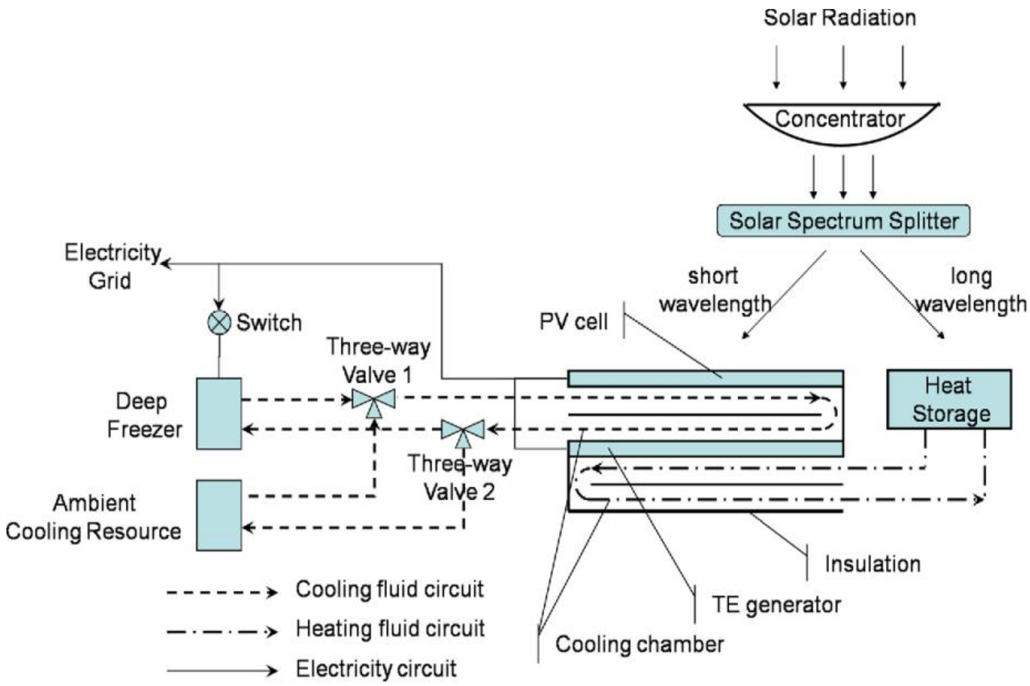

Figure 2.27: *Schematic of the PV–TE hybrid power system* [200]

Table 2.10 provides a summary of the results obtained using various Hybrid TEG configurations.

Table 2.10: Performance of different combinations of Hybrid TEG

Hybrid TEG study	Methodology	Research Findings	Ref.
TEGs with Solar hybrid systems	Hybrid system with non-concentrated sunlight	The hybrid concentrating system's electrical and thermal stability will be enhanced by PV's operation at greater temperature thanks to the incorporation of TEG.	[201]
Theoretical analysis and comparison of Solar PV-TGS were done in different conditions	Using a 1D steady-state model and MATLAB, we analyzed the performance of PV-TGS.	Power P rises as light intensity rises, while η falls. PV-TCS has lower T_{cell} than PV-TGS, but it also has lower and P.	[202]
Hybrid solar TEG's performance analysis	In order to concentrate sunlight on a solar selective coated TEG, the vacuum-enclosed HSTEG makes use of a parabolic trough collector.	The estimated maximum electrical efficiency of the V-HSTEG and the B-HSTEG are 15.6 and 12.2 %, while the corresponding thermal efficiency is 60.3 and 61.9 %.	[182]
The thermoelectric generator system and photovoltaic cell are applied with the algorithm of lock-on mechanism MPPT.	MPPT algorithm/ fixed step hill climbing algorithm	When compared to the method used by traditional fixed-step hill-climbing converters, the one used by SEPIC converters is superior and much faster.	[203]

Similarly effective is a hybrid system. By raising temperatures and reducing losses, a hybrid PV-TEG system improves the system's total efficiency. Both the electrical and thermal efficiency of a parabolic trough-based hybrid solar TEGs were found to be significantly enhanced. For example, Table 2.10 displays that the electrical efficiency of a V- HSTEG is 15.6% and that of a B-HSTEG is 12.2%.

Summing up the advantages of TEG, it can be seen that TEGs are appropriate for integrating with flexible heat source and bulky solar concentrators, have a long operational lifetime, and are independent of the position at which they are deployed or installed. From this critical literature survey main findings are as follows:

- Solar furnaces are more effective than parabolic dish concentrators (efficiency-15 %). If radiation is lowered from 950 W/m^2 to 430 W/m^2, the temperature in a parabolic dish collector drops from 602 K to 375 K, which indicates a reduction of 520 W/m2 results in a temperature drop of 227 K.
- Concentrations of 0.1 to 1000X on polished Al dish strips at 350°C temperature difference provide a respectable amount of electricity (5.5 W). The maximal potential of the Solar Pond-based thermoelectric plant is 4.384 KWh/Year m^2. Fresnel lens-based cogeneration systems have greater overall performance, generating 1.4 W of electrical power and 76.1 W of thermal power.
- With a total system exergy efficiency of 5.02 %, annular TEG can produce 50% more power than conventional flat plate TEG.
- The table lamp's 10W of heat generates 1 mW of energy via TEG, demonstrating that even low-grade heat (waste heat) may be used to generate electricity. At a temperature of 50 ^oC, the human body produces 192.6 microwatts of electricity, with an associated open-circuit voltage of 37.2 millivolts.
- Thermoelectric generators (TEGs) based on cookstoves have the potential to be the most effective electrical power generating option, especially in rural regions; however, numerical modeling is necessary to determine the module rating, mounting position, and TEG size. The thermoelectric generators (TEGs) in the stove are functioning at an average efficiency of 5%.
- The power output of marine engines is modest, but this may be greatly improved by increasing the number of thermocouples in TEGs.

- By raising temperatures and reducing losses, hybrid PV-TEG systems improve the system's overall efficiency. Both the electrical and thermal efficiency of a parabolic trough-based hybrid solar TEG were found to be significantly enhanced. For example, the electrical efficiency of a V- HSTEG is 15.6% and that of a B-HSTEG is 12.2%.
- The efficiency of a TEG is heavily dependent on the solar absorber material. The key to increased efficiency is a high Figure of merit. The efficiency of TEG is 5% for materials with ZT=1 for a temperature differential of 100 ^{o}C and increases with increasing ZT>1. The best ZT of 1.8 at 790 ^{o}C was reached by n-type (La_3-xTe_4/(Ba,YbCo_4Sb_{12}) and p-type ($Yb_{14}MnSb_{11}$/$Ce_{0.9}Fe_{3.5}Co_{0.5}Sb_{12}$) high temperature materials, which together generate an 848 ^{o}C temperature differential and provide 15% efficiency. The highest ZT of 2.2 was attained at 600 ^{o}C in p-type Sb_2Te_3/PbTe and n-type Bi_2Te_3/PbTe, both mid-temperature materials, and this temperature difference of 590 ^{o}C yields 11% efficiency. The best ZT was attained by the low-temperature material $MgAg_{0.965}Ni_{0.005}Sb_{0.99}$ at 48 ^{o}C, and the material's efficiency increases to 8.5% with a temperature difference of 225 ^{o}C.
- Since FOM is crucial, alloying Ni with Ag produces materials like $MgAg_{0.965}Ni_{0.005}Ag_{0.99}$ with a room-temperature ZT (FOM) of 1-1.15. Some materials, like yttria-stabilized zirconia cermet, may boost the solar absorptance of a receiver to as high as 0.95 %, while others, can improve its reflectivity of a collector.
- The cold side temperature of the TEG/LED system was calculated to be 35.70°C using the MATLAB Simulink tool to analyze the active-cooling process. Many types of automotive exhaust-based TEG employ CFD analysis; the maximum heat transfer via the exhaust's serial plate is found 1737 W, and this can be calculated using ANSYS and COMSOL- multi-physics 3D Finite element analysis.
- As far as environment aspect is concerned, 0.07~0.30 % CO_2 emission in the city is reduced in Japan by using TEG integrated with exhaust of automobiles, therefore it is very environmentally friendly power solution.
- Application area of TEG is diversified like Aerospace, Biomedical, Automobile, Rural areas etc.

- For the low and mid-temperature range, materials with higher ZT should be discovered. TE technology could be scaled up if thermoelectric materials of higher figure of merit are economically viable.
- For thorough analysis, numerical simulation of human body is required so that exact waste heat, temperature characterization and produced electricity can be quantified for different age groups.
- There is a need to improve the design of effective heat sink for human body based TEG.
- The unconverted heat from cooling side can further be utilized for heating and other purpose.
- The power electronic circuit can be improved to get smooth DC voltage and an active temperature control mechanism can also be developed to control temperature of hot side. More work should also be done on cost reduction.

2.12 Research Gaps

- Limited work in the application of Giant Water Lens
- High cost of presently available solar concentrators
- Almost no work in the field of thermoelectric generator performance with Giant water lens concentrator
- Complex design of presently available concentrators, easily adaptable by common public

2.13 Research Objectives

The main objective of this work is to evaluate the performance of TEG integrated with giant water lens so that the feasibility of economically viable giant water lens project can be checked out. Specific objectives of this work are:

- Comparative study of various thermoelectric generators utilizing heat from different concentrators and waste heat from industry and automobiles.
- To develop a mathematical model of the designed system.

- Numerical simulation of Linear low density plastic for transmittance of the material through Sol-Trace
- Testing of the Giant Water lens with aluminium absorber, to determine hot side temperature, Cold side temperature, temperature difference, heat produced after concentration to be measured.
- Numerical simulation of TEG in COMSOL-multiphysics
- Testing of the experimental setup integrating Giant water lens as concentrator and TEG
- To investigate the performance of Giant Water Lens Solar Thermoelectric Generator (GWLSTEG)
- To investigate the optical Concentration of the Water lens (amount of radiation)
- To evaluate the various losses in GWLSTEG
- To observe voltage, current output and calculate power output.
- To achieve the overall efficiency of the GWLSTEG system between 10-15%
- Validation of the mathematical model/simulated results with experimental results.
- To make GWLSTEG economically viable and technologically feasible for common public

Chapter 3

METHODOLOGY

Improvements in the efficiency of STEG can be made: (i) by improving FOM(ZT) of the TE materials, (ii) by improving the solar absorber surface(reduction in emittance at higher temperature) and (iii) by combining optical and thermal concentration in a proper ratio. The efficiency of the STEG may be evaluated by knowing the thermal concentration for a certain shape of the thermoelectric components, given a known hot side temperature as well as optical concentration. At ZT = (1.5-2) motionless STEGs with a low optical concentration (<3) may achieve efficiency within the range of 8 to 10%. For a device with similar radiative qualities and geometry, the efficiency reaches 14% for ZT = 2 & 10 times the optical concentration, and this corresponds to an ideal absorber temperature of 300^{o}C [131]. In this research(GWLSTEG), third technique of improving efficiency is adopted and a trade-off between thermal concentration (C_{th}~20) and optical concentration (C_{opt}~5) is made in order to achieve 10-15%, accordingly, experimental setup is fabricated.

First of all, the simulation from sol-trace is done to optimize the transmittance of the polythene, after this optimization we got to know that which type of polythene/plastic we need to purchase, and the size of the lens made up of this polythene is decided by the geometrical ratio (C_{geo}). C_{geo} is near100 and we already know the absorber area A_{ab}, which is fixed according to the area of thermoelectric modules, in this way size of lens is obtained. Simulation from COMSOL is done to check the effect of temperature difference on the thermoelectric module, actually the input to the thermoelectric geometry is the temperature difference and we get the developed voltage for the given temperature difference. This developed voltage is compared with the experimental voltage.

3.1 Experimental Setup

The experimental setup of the GWLSTEG can be divided into two halves. The first one is solar concentrator and the second one is thermoelectric generator (TEG). As discussed earlier giant water lens has been used as a solar concentrator in this experiment. The giant water lens collects more energy as compared to smaller one. The collected energy is then transferred to the TEG in order to produce electricity. Schematic diagram of Giant water lens solar TEG is shown in Figure 3.1**.** The actual setup is shown in Figure 3.2 **(a)** and **(b).**

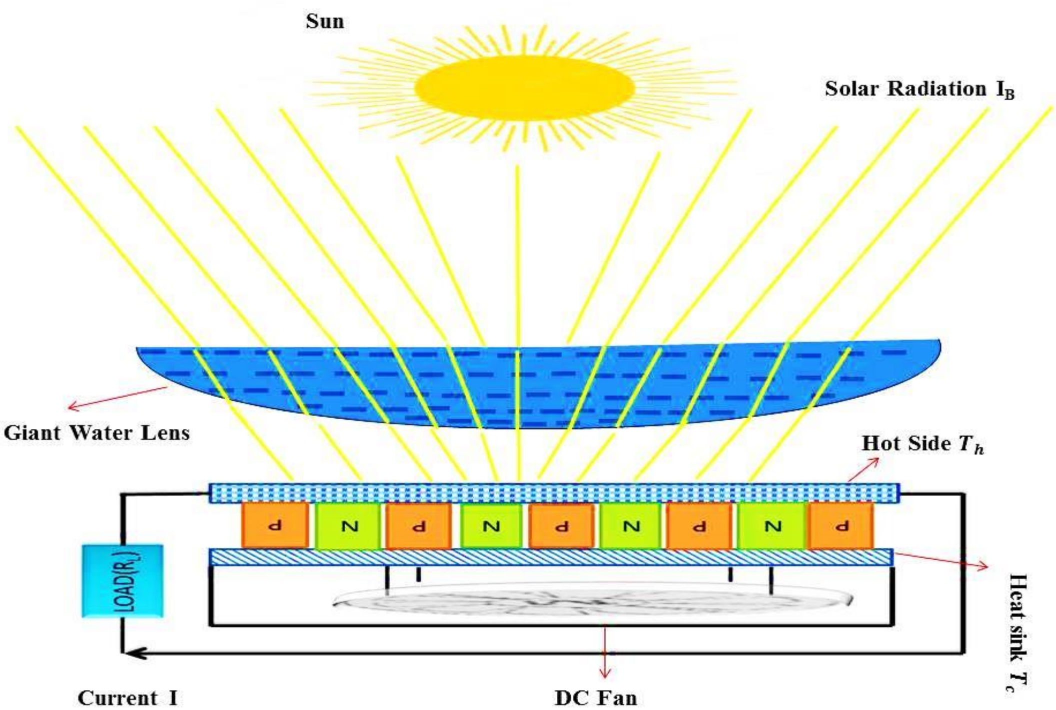

Figure 3.1*: Schematic diagram of the proposed giant water lens solar TEG*

Figure 3.2: *(a) Small and Giant water lens (b) concentrating solar energy on absorber of TEG*

In Figure 3.3 all the instruments to measure the parameters are shown, like solar power meter, Anemometer, Hygrometer, multi-meter and thermal camera, etc. The complete process of fabricating a water lens has been described in next section.

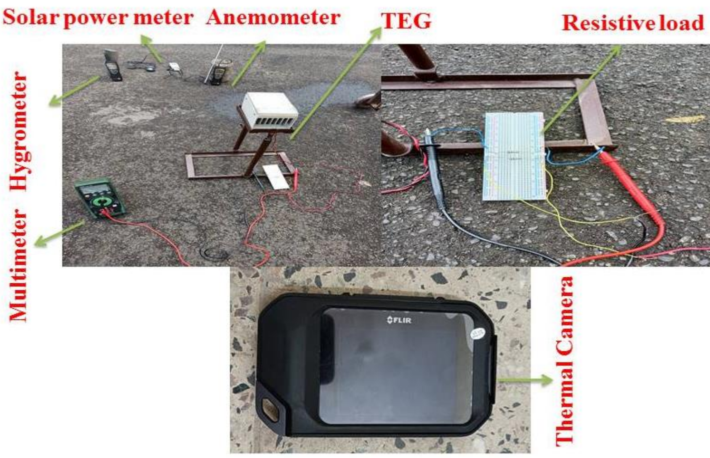

Figure 3.3: *TEG, resistive load and all the instruments*

3.1.1 Fabrication of Lens-Holding Frame

For supporting the parabolic shape type Giant water lens, an iron frame with dimensions (2.2 × 1.4 × 2.14 m) is fabricated, that consists of one square frame of (1.4× 1.4) m and another square frame of (1×1) m as shown in Figure 3.4 **(a)** and **(b).** The parabolic shape type Giant water lens is supported by the frame as shown in Figure 3.4 **(a).** This frame has been designed in such a way that the aluminium absorber placed just under the lens becomes the focal point of the water lens, i.e., at 1.3m as shown in Figure 8.4 **(b).** Teeth gear arrangement is shown in Figure 3.4 **(b)** through which lens can slide and the distance of TEG can be adjusted with focal distance of the lens.

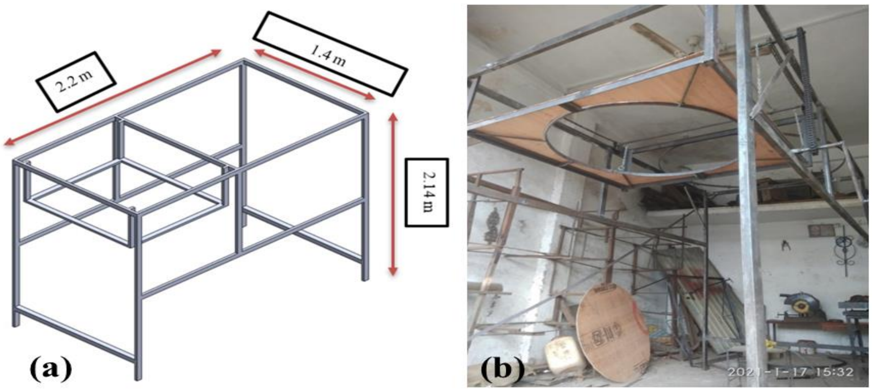

Figure 3.4: *(a) Design of the iron frame (b) Manufacturing in workshop*

3.1.2 Giant Water Lens

Water lens is very economical way to demonstrate yet another way to collect and focus the sun's power. A lens of water can be manufactured by using transparent plastic generally and may have different refractive index, depending upon the type of plastic material.Lens produces high temperature on the relatively small area of absorber. The limiting factor is the size of the lens, Water lens is not intended for latitudes very far from the equator. It requires the sun to be primarily overhead and will produce good amount of heat for could be five-six hours on a clear sky day. The overall form gets more intricate when water is spilled over an impermeable surface, such as plastic foil. Determining the water lens's form is the first step in extracting and analyzing its attributes.

Water lens requires only two materials: water and transparent plastic sheets [116][204][205]. For this setup, a frame of length 1.50 meter and breadth of 1.50 meter was made as shown in Figure 3.5**.** Plastic sheet was mounted on the top of the frame. The obtained lens had a depth of 0.16 meter and diameter of 1.40 meter. The complete setup has been installed and tested in open area of Energy Centre, MANIT Bhopal, India (23.25^0N, 77.41^0 E). The transmittance material of the plastic for lens is simulated in Sol-Trace and for ($\tau_P = 0.95$) it is optimized.

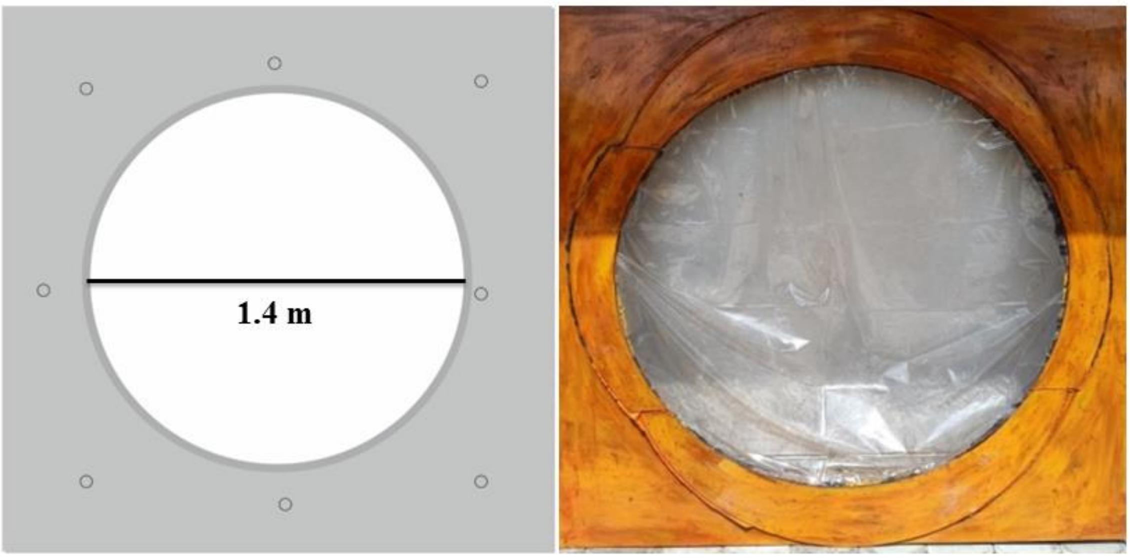

Figure 3.5: *Water lens with frame*

The effectiveness of "geometric optical concentration" (C_{geo}) on STEG efficiency for the four different arrangements is shown in Figure 3.6**.** Once the bismuth telluride STEG concentration becomes sufficiently high for bringing material temperature, at which it is operated, within its limit of (250 °C/523 K), the STEGs immediately stabilize. However, above that concentration, the efficiency only increases extremely slowly due to the radiation losses being insignificant. Total STEG efficiency may be determined by combining the results of the absorber, optics, thermal concentration, as well as TEG. Cascaded bismuth telluride STEG devices have better performance than segmented STEG devices as shown in Figure 3.6. If there is no optical concentration in a "single-stage bismuth telluride STEG" i. e (C_{geo} = 1), the value of efficiency is 4.7%. At a 45 (C_{geo}), the efficiency of a cascaded Bi_2Te_3 STEG may be more than 10%.

At 100 C_{geo} the peak working temperature of (600 °C/873K) is reached for the skutterudite cascaded STEG, and the advantages from growing concentration decline beyond that point [206]. Thus in this project for the single stage Bi_2Te_3 STEG, the diameter 1.4 m and area of the Giant water lens 1.54 m^2 are so decided with (C_{geo} =97~100) as shown in Figure 3.5. The efficiency of these devices can be increased with the help of 2 methods: i) the 1st method involves the improvement of the selective surfaces, and ii) the 2nd method involves the improvement of the TEM's material properties.

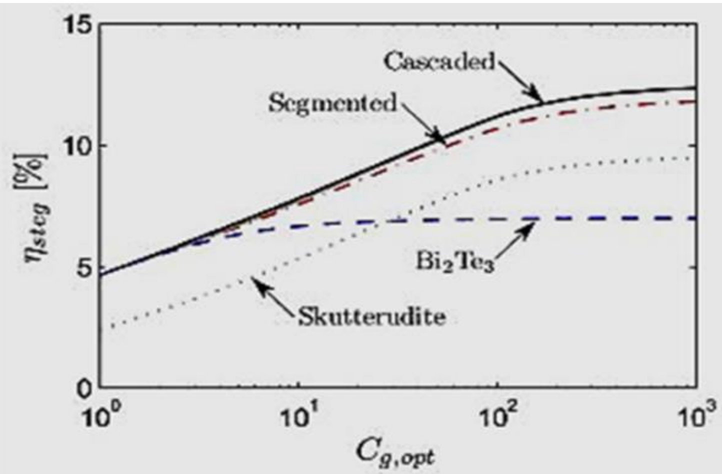

Figure 3.6: *Efficiency for four different STEG architectures: a single-stage bismuth telluride TEG (dashed); a single-stage skutterudite TEG (dotted); a segmented skutterudite and bismuth telluride TEG (dash- dotted); and a cascaded skutterudite and bismuth telluride TEG (solid black)* [206]

3.1.3 Aluminum Absorber Plate

Aluminum, chemically denoted by the symbol Al and atomic number 13, belongs to the boron group of elements. It is a white metal that is ductile and soft and not magnetic. After oxygen and silicon, aluminium is the most common metal in the Earth's crust, and the third most common element overall. About 8% of the crust's mass is made up of it, however it's far less frequent in the mantle below. Due to its high reactivity, pure aluminum is only found in very reducing settings where it may be found in its original state. Instead, it occurs in more than 270 distinct minerals in a mixed form. Bauxite is the primary aluminum ore.

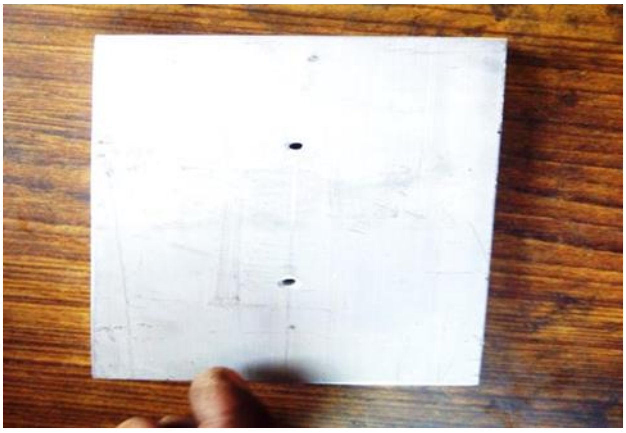

Figure 3.7: *Aluminium absorber plate*

Passivation, a unique property of aluminum, makes the metal very resistant to corrosion. Aluminum and its alloys are used in many critical structural components, including those used in the aircraft industry. Aluminum oxides and sulfates are the most valuable aluminium compounds. Depending on the smoothness of its surface, aluminium may seem either silvery or drab gray. It is a soft, resilient, lightweight, ductile, and malleable metal. It is not magnetic and has a low ignition temperature. A new aluminum film is an effective reflector of visible light (about 92 %) and medium and far infrared radiation (as high as 98 %). The yield strength of pure aluminum is between 7 and 11 Mpa, but that of aluminum alloys may range from 200 to 600 Mpa. The density and rigidity of aluminum are around one-third of those of steel. It can be machined, cast, drawn, and extruded with ease. Aluminia has an atomic structure known as face-centered cubic (fcc). The energy required to cause a stacking fault in aluminum is around 200mJ/m^2.

Despite being just a third as dense as copper, aluminium is an excellent thermal and electrical conductor (59 % as much, respectively). The threshold temperature for superconductivity in aluminum is 1.2 K, while the critical magnetic field is at 100 G (10 Milli-teslas). An aluminum plate of dimensions (16 cm ×10 cm ×1 cm), serves as absorber as shown in Figure 3.7.

3.1.4 Aluminum Heat Sink

Figure 3.8: *Aluminium heat sink*

An aluminum plate measuring (16 cm x10 cm) and height of 50 cm serves as the heat sink for the STEG. The module-equipped absorber is linked to the heat exchanger. Figure 3.8 depicts only the heat sink by itself. As much of the heat sink's exposed surface as feasible should be in contact with air or another cooling medium for efficient heat dissipation. Variables such as velocity, material, protrusion design, and surface treatment may affect a heat sink's efficiency. Not only does the method utilized to connect the heat sink have an impact on the die temperature of an integrated circuit, but so do the thermal interface materials. Thermal glue and thermal grease improve the heat sink's effectiveness by sealing any air gaps between the heat sink and the heat spreader.

(a) Drilling

Cutting a hole with a circular cross section into solid materials, drilling requires the use of a drill bit. The drill bit is a rotary cutting device with many cutting points. Hundreds to thousands of rotations per minute are used to force the bit into the workpiece. By doing so, you may remove chips (swarf) from the hole as you drill by pressing the cutting edge on the workpiece.

Figure 3.9: *Drilling for creating holes*

Holes with a cross-section other than a circle may be drilled using specific bits; a square, for example. See Figure 3.9, where an M4 tap is utilized to thread a hole drilled to 3.5 mm in diameter. The four constituents of an M4 tap are as follows:

1- Nylon Pipe 2- Fibre watcher, 3- Spring, 4- plain watcher.

(b) Milling

Milling is a kind of machining in which rotary cutters are used to remove material from a work-piece while the work-piece is fed (or advanced) in a direction at an angle to the cutter's axis as shown in Figure 3.10. It encompasses a broad range of activities, from the milling of a single component to the milling of a whole assembly in a single, massive machine. It is one of the most used methods for adjusting the dimensions and contours of machined components in modern manufacturing and machining facilities.

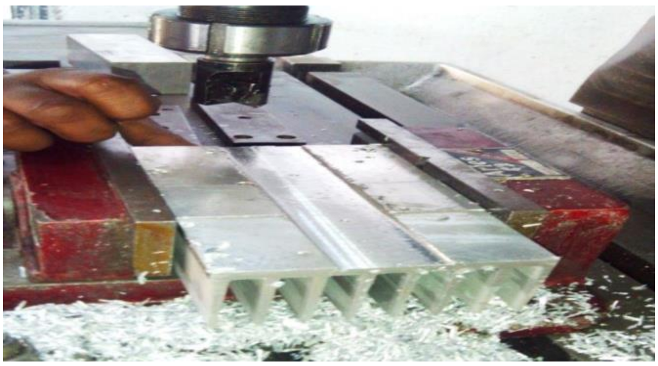

Figure 3.10: *Milling for creating slot to set the modules*

There is a large variety of machine tools suitable for milling. Milling machines were the first of their kind as a category of machine tools (often called a mill). Machining centers, which are essentially mills with added features like “automatic tool changers, tool magazines or carousels, CNC control, coolant systems”, and enclosures, emerged with the development of CNC technology and are typically divided into two categories: “vertical machining centers (VMCs) and horizontal machining centers (HMCs)”. Multitasking machines (MTMs) are a new class of machine tools that were specifically designed to allow for a default machining strategy of using any combination of milling and turning within the same work envelope, which began with live tooling for lathes and the occasional use of mills for turning operations. Here milling is done to create (20 mm x 20 mm x 4 mm) square slot for setting up of modules in this slot as shown in Figure 3.11and in Figure 3.12, smoothening process is accomplished.

Figure 3.11: *Heat Sink & absorber Plate ready, after milling process*

Figure 3.12: *Smoothening of surface of heat sink & absorber plate*

3.1.5 TEG Modules

Specification-Power output = 5 w each at (T_h =230 ^{0}C T_c = 30 ^{0}C)

Full load current = 1.66 A, **Output Voltage =** 6 V (each) R (230) = 4.42 Ω

Max Processing Temperature = 230 ^{0}C

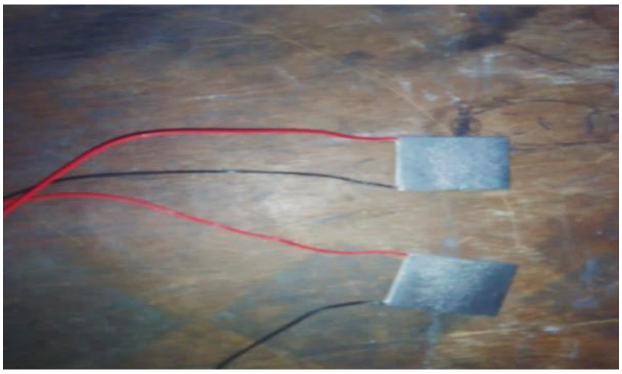

Figure 3.13: *TEG modules*

The thermoelectric module for this STEG is a Tellurex module (20 mm × 20 mm × 4 mm) made from bismuth telluride thermoelectric material (as exhibited in Figure 3.13).

The aluminum absorber of dimensions (16 cm ×10 cm × 1 cm) is used, where the modules are attached with anabond paste (Figure 3.14). Using the aforementioned criteria, the absorber area is already calculated, as (C_{geo}) is the ratio of the water concentrator aperture area to the absorber area. Modules are set between the absorber Plate and Heat Sink (Figure 3.15).

Figure 3.14: *Anabond paste and pasting modules on the absorber*

Figure 3.15: *Modules are set between absorber plate and heat sink*

3.1.6 Glass Wool Filling

Insulating material known as "glass wool" is composed of glass fibers that have been bound together in a wool-like structure as shown in Figure 3.16. The thermal insulation capabilities originate from the action of trapping several little pockets of air between the glass. Rolls and slabs of glass wool, each with its own unique thermal and mechanical qualities, are manufactured. Another form it may take is that of an in-situ spray or adhesive, applied directly to the insulating surface.

Figure 3.16: *Glass wool filling*

3.1.7 DC Fan

12 V,5 W DC fan as shown in Figure 3.17, is used for cooling purposes to maintain cold side temperature between 30 ^{0}C to 50 ^{0}C.

Figure 3.17: *DC Fan*

3.1.8 Drilling for Setting Bracket

Finally, drilling is done for setting bracket to cover whole assembly as shown in Figure 3.18.

Figure 3.18: *Setting of Bracket*

In this way, two thermoelectric modules of dimensions (20 × 20 × 4 mm each) are used for power generation as shown in Figure 3.19 **(a)**. 64 thermocouples in each module connected in series are pasted and fixed to the bottom of a (16 cm × 10 cm x 1 cm) aluminium absorber as shown in Figure 3.19 **(a) and (b)**. The total cross-sectional area of both TE modules would be ($2\times20\times20$ mm$=8\times10^{-4}$ m^2). Bi_2Te_3 thermoelectric material based GWLSTEG is so fabricated. All the specifications of TEG module used in this experiment are shown in Table 3.1. For simplification of analysis, the combination of two modules is considered as single module.

Figure 3.19: *TEG module (b) Aluminium absorber (c) Heat sink (d) DC fan (e) Complete assembly of TEG*

Table 3.1: Specifications of Bi_2Te_3 TEM

Parameters	**Value**
TE module length x width x thickness	20 mm× 20 mm × 4 mm
Alumina Substrate thickness	0.70 mm
Copper Conductor thickness	0.50 mm
N/P type block (length x width x height)	1.40×1.40×1.60 mm
Block Spacing (pitch)	1.00 mm
Two modules-Number of blocks (row x column)	16 × 16 (256 block-128 thermocouple)

The complete TEG assembly consists of the following components:

i. Aluminum absorber
ii. Aluminum Heat sink

iii. TEG module
iv. DC fan

an Aluminium absorber of dimensions of (16 cm x 10 cm x 1cm) and thickness of 1 cm is used to absorb the concentrated solar radiations that have been focused using the water lens. The Aluminum heat sink as shown in Figure 3.19 (C), with specifications as mentioned in

Table *3.2,* is the most widely used product for thermal solutions.

The properties that make an aluminum heat sink popular include (i) Good electrical as well as thermal conductivity (ii) Light weight (iii) Low density with a density ~ 2,700 kg/m^3 (iv) Higher strength within the range of 70 and 700 mega-pascal (v) Easily malleable (vi) Easy machining (vii) Exceptional resistance towards corrosion (viii) non-magnetic, which avoids interference of magnetic fields (ix). Easy to recycle [115][207][115][208][209]. A DC fan of 12 V and 5W is used for cooling purposes to maintain cold side temperature between 30 ^oC to 50 ^oC as shown in Figure 3.19 **(d**). The complete assembly of TEG is shown in Figure 3.19 **(e)**.

Table 3.2: Heat sink specifications

Parameters	**Value**
Length	0.16 m
Breadth	0.10 m
Height of fins	0.05 m
Hole Diameter	0.65 mm

3.2 Instrumentation

During data collecting, researchers use instruments to try to measure a variety of different variables and objects of interest. The term “instrument” refers to the tool used by researchers to gather data, and so encompasses not only the item used to do so, but also its design, selection, construction, and evaluation. Another potential source of skewed findings is investigators' failure to account for the possibility of a shift in calibration of the measuring instrument(s) used. In this research work, all the measurements are made with utmost care to get the most accurate results. Various instruments were brought in application for measuring different parameters. The methodology and requirements of these measurements and instruments are discussed as:

3.2.1 Multi-Meter

Multiple electrical properties can be measured at a time using a multimeter. Because of its ability to measure voltage, current, and resistance, a multimeter is also referred to by its more specific names: voltmeter, ammeter, and ohmmeter. The Rish Multi 15S multimeter integrates a DC voltmeter, an AC voltmeter, an ammeter, and an ohmmeter into one convenient device. VTVMs are amplified analog meters with active electronics, whereas non-amplified analog multimeters include a meter movement, range resistors, and switches. The range of this multimeter is (10µV-1000V) and (100nA-10A).

Figure 3.20: *Multimeter*

The multi-meter is used in this research work to measure the voltage and current generated from the STEG is shown in Figure 3.20.

3.2.2 Solar Power Meter

Through windows to ensure their efficacy or during installation of solar power equipment, a solar power meter may measure solar power or sunshine in units of W/m^2.

When determining the total energy output, efficiency, and optimal location of solar systems, a solar power meter instrument is often used.

- Solar power research
- Identifying high-performance opportunities
- Physics or optical laboratories
- Solar radiation measurement
- Agricultural applications
- Meteorological applications"

Solar radiation received by the absorbent surface is a measure of the system's power production. Instruments can measure the quantity of solar radiation reaching Earth's surface, and these measurements are crucial for providing baseline solar data for use in solar energy conversion applications. Solar power meter used in this research work is shown in Figure 3.21.

Figure 3.21: *Solar power meter*

3.2.3 Thermal Camera

A thermal camera is a camera that detects and reads infrared and infrared radiation emitted by an object to determine its temperature. The use of a thermometer requires physical contact with the individual, which might be risky or impossible in a number of emergency situations. These instruments use thermal radiation to measure temperatures at a distance. As can be seen in Figure 3.22, the FLIR C3-X is a versatile device that may be used as a thermal imaging camera, a digital camera, or even a flashlight. The temperature range of the 128×96 (12,288 pixel) resolution thermal imager is greatly increased from -20 to 300°C (-4 to 572°F).

Figure 3.22: *Thermal camera (FLIR C3-X)*

In this research, the thermal camera is used for taking the temperature readings of both the hot and cold junction of the TEG module.

3.2.4 Digital Hygrometer

A hygrometer is a device that measures the humidity of an area, whether it be air, soil, or a closed environment. Measurements of other values, such as temperature, pressure, mass, or a mechanical or electrical change in a material when moisture is absorbed, are often used as inputs in humidity sensors. These values may be used to calibrate and calculate an accurate humidity reading.

Saturation, the point at which no more water vapor can be dissolved in the air, varies dramatically with temperature, with cold air being able to store far less water vapor per unit volume than warm air. Humidity may be affected by temperature.

Figure 3.23: *Digital hygrometer*

As can be seen in Figure 3.23, the testo 625 is a small thermo-hygrometer with a detachable humidity sensor that may be used to determine both air temperature and relative humidity. The wet bulb temperature and dew point may also be determined. The meter has a big, lighted display that is simple to see, a hold button that locks the current measurement in place, and instant access to the minimum and maximum readings. The testo 625's long-lasting moisture sensor and power-saving sleep mode mean it will continue to provide accurate readings for years to come. The RH scale goes from 0% to 100%.

3.2.5 Digital Anemometer

In addition to construction, mining, renewable energy, and manufacturing, the anemometer is utilized for a wide range of wind monitoring applications. With digital anemometer, there are many other kinds of anemometer used to measure the wind's angle. In this research, digital anemometer as shown in Figure 3.24, is brought into use to measure the speed of wind generated from the DC fan. It allows setting the speed of the fan in accordance with the requirement of the cooling of the cold junction and maintaining the temperature. The range of the anemometer is 0 to 20 m/s.

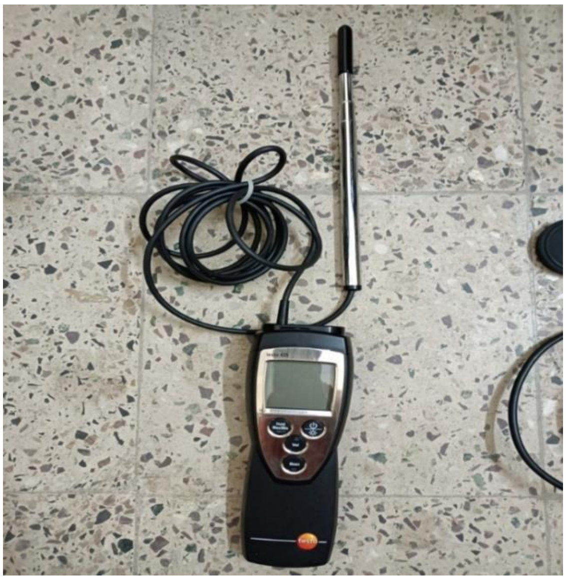

Figure 3.24: *Digital anemometer*

3.3 Uncertainty Analysis

An experimental data is how much accurate, can be determined by an important factor 'Uncertainty'. From **Eq. (1)** the standard uncertainty of the instruments used for this project can be calculated [210]**.**

$$Standard\ Uncertainty = \frac{Accuracy\ of\ instrument}{\sqrt{3}} \quad (3.1)$$

The standard uncertainty and accuracy of all the instruments used are shown in Table 3.3.

Table 3.3: Instruments and their specifications

Instruments	**Observed Parameter**	**Range**	**Accuracy**	**Standard Uncertainty**	**Uncertainty in observed parameter**
Solar power meter (Meco)	Solar radiation	0-2000 W/m^2	±10 W/m^2	1 W/m^2	±1.2 W/m^2
FLIR thermal camera (C3-X)	Temperature	-20 to 300 °C	±0.2°C	0.12°C	±0.25°C
Digital Anemometer	Air velocity	0.2-60 m/s	0.1 m/s	0.06 m/s	±0.10 m/s

(Testo 425)					
Digital Hygrometer (testo 625)	Relative humidity	5-90 %	3%	1.73%	±1.7%
RishMulti 15S multimeter	Voltage	30 V	± 0.01V	0.006 V	± 0.01V
RishMulti 15S multimeter	Current	3A	± 0.001A	0.0006 A	± 0.001A

A function Y, which is dependent on n number of input variables or parameters then the value of uncertainty in the measured value of Y can be computed from **Eq. (3.2)** [210]:

$$U(Y) = \left[\left(\frac{\partial Y}{\partial x_1}\right)^2 u^2(x_1) + \left(\frac{\partial Y}{\partial x_2}\right)^2 u^2(x_2) + \cdots \ldots \ldots + \left(\frac{\partial Y}{\partial x_n}\right)^2 u^2(x_n)\right]^{1/2} \quad (3.2)$$

where, U(Y) is the representation of uncertainty in Y and $u(x_1)\ldots\ldots u(x_n)$ is the uncertainties in the independent variables $(x_1\ldots\ldots x_n)$, which affect the function Y.

3.4 Efficiency of GWLSTEG System

The efficiency of the GWLSTEG system can be broken down into two different components. The first one is the optothermal efficiency of the system (η_{ot}) and the second one is efficiency of the TEG module circuit (η_{te}). To realize the expression for both efficiencies, firstly we need to discuss the water lens. The giant water lens works on the same principle as that of the normal planoconvex lens [211], [212],[116]. Mechanically describing hyper-elastic foils under spatially varying hydrostatic force is necessary since the lens's form dictates its characteristics. For this lens with a diameter of 1.4 meters and a depth of 0.16 meters, we employed a sheet of “linear low-density plastic/polyethylene (LLDPE)” foil measuring 400 µm thick, 1.8 meters in length and breadth, with an elastic modulus of 160 mega-pascal and a Poisson's ratio of 0.435.

To concentrate light traveling in parallel beams into a single point, plano-convex lenses are optimal way. Light may be concentrated, amassed, and collimated with their help. When the object and the receiver are at different distances from the lens, the asymmetry of these lenses reduces spherical aberration. Light from a point source may be collimated by using a planoconvex lens, which focuses the beam to the rear focus. Water lenses have the shape of a Plano convex lens because of the elasticity of the transparent sheet. Water that works as a lens allows the quantity of "solar radiation incident on it to converge at a focal point" avoiding the absorption of the thermal energy, meaning that water that acts as a lens allows the absorber at the focal point to remain at its starting temperature. The focal length is the most crucial aspect of any lens. Each lens' focal length may be determined with a quick application of the thick lens Eq (3.3) [211].

$$f = R_c/(n-1) \tag{3.3}$$

Where refraction index is denoted by n and curvature radius is denoted by R_c, i.e., 0.156 meters. The refractive index is defined as the %age change in the light's speed between traveling through the medium and a vacuum. When light travels through a material other than a vacuum, the speed of light is reduced because the particles of light are constantly absorbed and reemitted by the atoms of that medium. The value of the refractive index has no units. It's a measure of how much longer a light wave would take to travel through the substance compared to a vacuum. The n-symbolized refractive index is equal to the vacuum speed of light divided by the medium speed of light. Here is the equation for the refractive index [213]:

$$n = c/v \tag{3.4}$$

Where,

- refractive index was denoted with *n*
- light velocity in a vacuum was denoted with *c*
- light velocity in any medium is denoted with *v*

A refractive index of 1 describes a vacuum. The formula can be used to get the refractive index of any substance. When the refractive index or optical density is high, light travels more slowly. Lens has a refractive index of 1.12 because water has a refractive value of 1.333 and plastic has a refractive index of 1.5.

Focal length has an inverse relationship with the optical concentration ratio [211], [214]. The water lens demonstrated a focal length shift of almost 50%, providing the operator with an additional axis of flexibility. Lens optical behavior may be carefully adjusted by replacing water with various clear liquids of varying refractive indices. In this work, a new approach is used by investigating the lens on a broad scale. By adjusting the amount of water, the intensity might be raised by as much as 400%. Over a wide range of wavelengths, the water lens showed a concentration factor of up to 25 that was somewhat typical. Although it filters out the near infrared spectrum, its loss increases as the wavelength increases. As a filter for certain solar energy conversion devices, or to keep things from becoming too hot, this may be quite helpful. While the concentration factor is lower than that of other cutting-edge solar concentrators, the production cost is much lower, and by replacing the current lenses with a water lens array, the savings may be double. Since maximum intensity, shortest focus length, and highest concentration factor are all shown by the 40 liter (V_{max}) water volume, this value is optimal. It also has advantageous optical qualities since its form is a near approximation to that of an ideal aspheric lens.

3.4.1 Volume of water in GWLSTEG

The water lens' shape as shown in Figure 3.25, is parabolic which is given by the equation

$$y = x^2 \tag{3.5}$$

This parabola is rotated about the y-axis to calculate the volume of the water lens. The paraboloid can then be broken down into n number of finite cylinders, as in Figure 3.25, and then the total volume can be calculated by integrating the volumes of these finite cylinders [211].

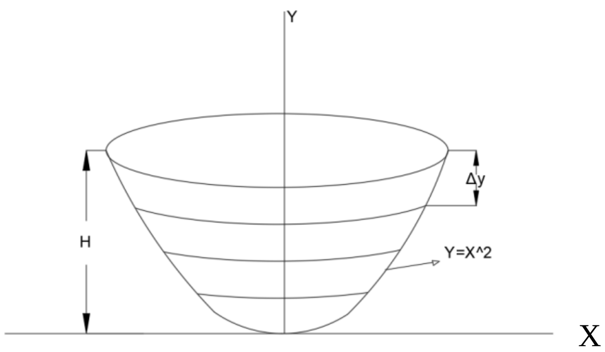

Figure 3.25: *Giant Water Lens schematic*

Consider the small section of the uppermost cylinder and assume its height to be Δy. Therefore, at height y, radius x = $\sqrt{y}$

Volume of the cylinder = $\pi r^2 h$

This Δy is the height of only the uppermost cylinder, therefore to calculate the total volume of all cylinders or the volume of the paraboloid lens, the following steps are followed:

Volume of the paraboloid lens (V) = $\lim_{h \to \infty} \sum_{i=1}^{h} \pi y_i \Delta y$

$$V = \int_0^H \pi y \, \partial y$$

$$V = \left[\frac{\pi}{2} y^2\right]_0^H$$

$$V = \frac{\pi}{2} H^2 \qquad (3.6)$$

Height of the paraboloid H is measured which is 16cm, i.e., H = 0.16m. Therefore, the volume of the paraboloid water lens was calculated as:

V = $\frac{\pi}{2}(0.16)^2$ = 0.040 m^3

Since, 1 m^3 = 1000 litres, the volume of water in the GWLSTEG used in this experiment is about 40 litres.

3.4.2 Optical Efficiency of the Lens

The concentration ratio (C) is often used to describe the light concentration process. From a physics perspective, the concentration ratio is the measure of how much the incoming energy flux on the lens surface is amplified optically on the receiving surface. At the aperture (I_b) and the receiver (I_c), the ratio of the energy fluxes represents the concentration ratio. It is immediately applicable to thermal calculations and is referred to here as the optical concentration ratio C_{opt} (or flux concentration ratio). The optical concentration is shown in Figure 3.26.

$$C_{opt} = \frac{Average\ flux\ over\ the\ absorber}{Flux\ over\ the\ aperture\ (insolation)} = \frac{\frac{1}{A_{ab}} \int I_c dA_{ab}}{I_b} \qquad (3.7)$$

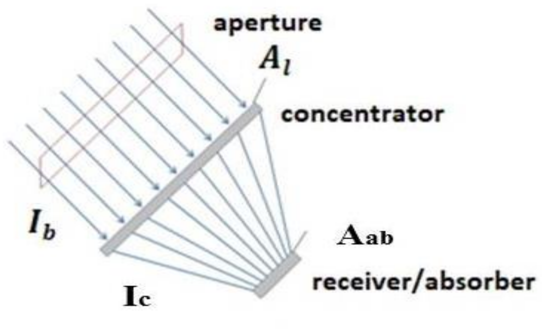

Figure 3.26: *Optical concentration of a lens*

The geometrical concentration ratio (C_{geo}) is defined as the ratio of the aperture area of lens (A_l) to the absorber area (A_{ab}). If the ambient energy flow (insolation/irradiance) is the same over the aperture as it is over the receiver, then the geometric and optical concentration ratios will be the same ($C_{geo} = C_{opt}$). The optical efficiency of the system is given by **Eq. (3.9)** [215] [123].

$$C_{geo} = \frac{area\ of\ the\ aperture}{area\ of\ the\ absorber} = \frac{A_l}{A_{ab}} \tag{3.8}$$

$$\eta_{opt} = \tau_l \alpha_{ab} \tag{3.9}$$

It accounts for the aperture net transmission losses $\boldsymbol{\tau_l}$ and the absorptance $\boldsymbol{\alpha_{ab}}$ of the solar absorber. $\boldsymbol{\tau_l}$ is 0.90 and $\boldsymbol{\alpha_{ab}}$ is 0.94, hence optical efficiency is 84%. Thermoelectric generator (TEG) modules are constructed from numerous TE blocks that are electrically linked in series and thermally coupled in parallel to increase power output. Seebeck effect describes the phenomenon in which the amount of electricity produced is proportional to the degree of temperature difference between the two sides of the TEG module [216]. A thermocouple, consisting of a P-type and N-type thermo-element coupled thermally and electrically respectively in parallel and series, is the simplest thermoelectric power generator. One partner receives heated air while the other gets cooled. The generation of the voltage takes place when there is a large enough difference in the temperature between the cold and hot junctions [217].

3.4.3 Thermoelectric Efficiency of TEG and Opto-thermal Efficiency of GWLSTEG System

In reaction to a change in temperature, a thermoelectric (TE) material produces a voltage. The ZT for a TEM is defined as:

$$ZT = \frac{s^2 T}{k\rho} \tag{3.10}$$

This study took into account the Thomson effect, and the temperature-dependent characteristics of the thermoelectric material (Bi_2Te_3) were used according to the formulas presented by Xuan et al. [110]:

Seebeck coefficient:

$$s = [s_p - (-s_n)] = 2 * (22224 + 930.6\,T - 0.9905T^2)10^{-9}V/K \tag{3.11}$$

Electrical Resistivity:

$$\rho_n = \rho_p = (5112 + 163.4T + 0.6279T^2)10^{-10}\Omega m \tag{3.12}$$

Thermal conductivity:

$$k_n = k_p = (62605 - 277.7T + 0.4131T^2)10^{-4}\mathrm{W/mK} \tag{3.13}$$

Thomson coefficient:

$$\mu = [\mu_p - (-\mu_n)] = 2 * (930.6T - 1.981T^2)\ 10^{-9}\ V/K \tag{3.14}$$

Where, mean temperature, “Thomson coefficient, thermal conductivity, electrical resistivity, and Seebeck coefficient”, respectively are denoted by T, μ, k, ρ, and s for developing the thermal model of the GWLSTEG system. Developed equations for the energy balance for every control volume are as follows.

Incident solar energy on lens Q_i:

$$Q_i = Q_{abs} + h_{conv,l-a}A_l(T_l - T_a) + \varepsilon_l\sigma_{sb}A_l(T_l^4 - T_a^4) + \varepsilon_{lh}\sigma_{sb}A_l(T_l^4 - T_h^4) \tag{3.15}$$

i.e $I_g A_l = Q_{abs} + Q_{conv,l-a} + Q_{rad,l-a} + Q_{rad,l-h}$

Losses are less, therefore may be equated to zero,

$$h_{conv,l-a}A_l(T_l - T_a) + \varepsilon_l\sigma_{sb}A_l(T_l^4 - T_a^4) + \varepsilon_{lh}\sigma_{sb}A_l(T_l^4 - T_h^4) = 0 \quad (3.16)$$

$$\varepsilon_{lh}\sigma_{sb}A_l(T_h^4 - T_l^4) = h_{conv,l-a}A_l(T_l - T_a) + \varepsilon_l\sigma_{sb}A_l(T_l^4 - T_a^4) \quad (3.17)$$

In **Eq (3.16)** the first and second terms represent the convective and radiative heat loss from the water to the environment, while the third represents the radiative heat loss from the top of the absorber to the LLDPE plastic cover. When compared to radiative heat losses, convective heat losses are negligible. Temperature of the absorber surface, surroundings and water lens are respectively denoted by T_h, T_a, and T_1. Stefan–Boltzmann constant is denoted by σ, the net emittance within the plastic cover and the absorber surface is denoted by ε_{lh} and water emittance to its surrounding is denoted byε_w. Convective heat coefficient among the surrounding and the water, absorber surface's area and water lens surface's area are respectively denoted by $h_{conv,l-a}$, A_{ab} and A_l.

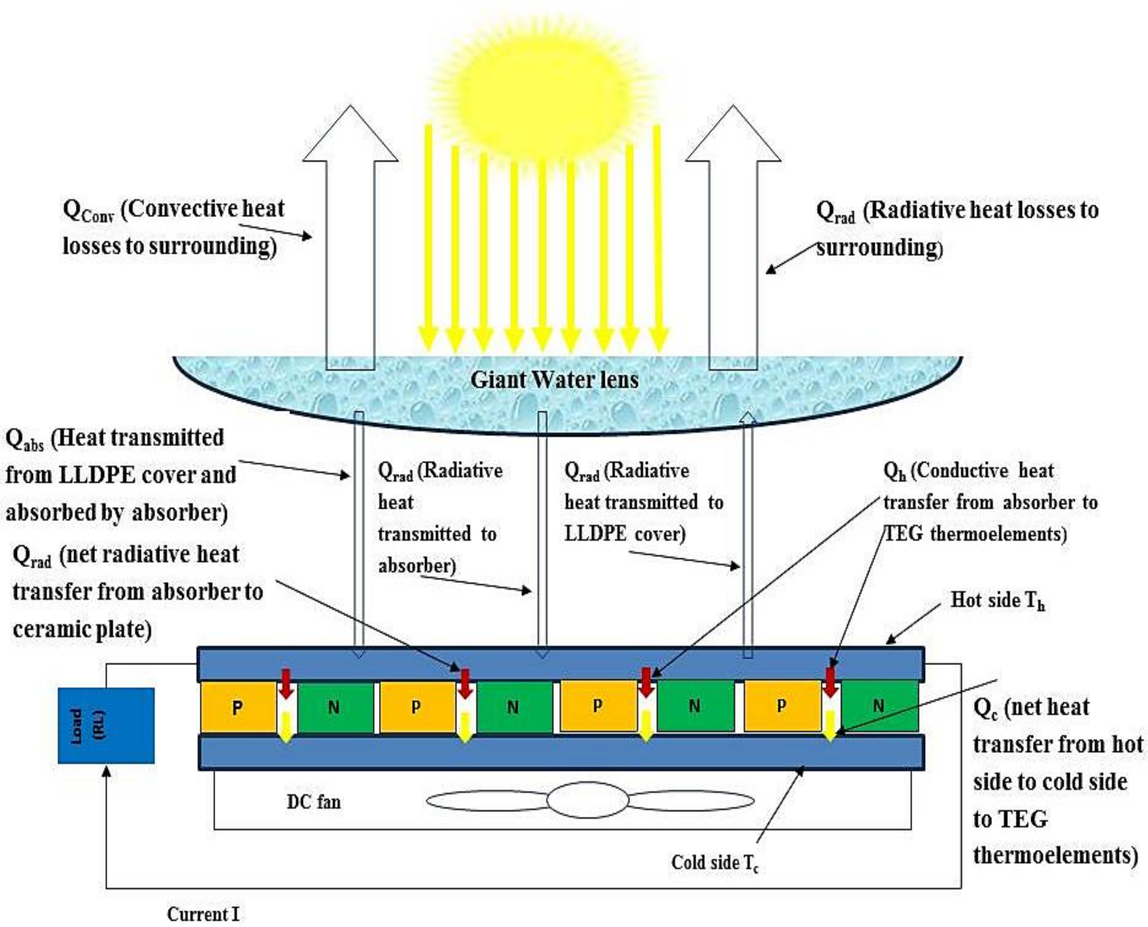

__Figure 3.27:__ Energy balance diagram

Referring the Figure 3.27, using the first rule of thermodynamics under steady-state circumstances, we can write the absorber surface's thermal balance equation as:

$$\tau_l \alpha_{ab} C_{th} I_g A_{ab} = Q_h + \varepsilon_{hl}\sigma_{sb}A_{ab}(T_h^4 - T_l^4) + \varepsilon_{hc}\sigma_{sb}(A_{ab} - A_{mod})(T_h^4 - T_c^4) + h_{conv,h-a}(A_{ab} - A_{mod})(T_h - T_c) \quad (3.18)$$

i.e $$Q_{abs} = Q_h + Q_{rad,h-l} + Q_{rad,h-c} + Q_{conv,h-a}$$

Where ε_{lh} is the net emittance between the plastic cover and the absorber surface and the net emittance of area between the cold and hot side (absorber surface) of the TEG is denoted by ε_{hc}, module's cross-sectional area is denoted by A_{mod} and $h_{conv,h-a}$ is the convective film coefficient between the hot side of the absorber surface and the surroundings. The net emittance ε_{lh} and ε_{hc} are given as, respectively:

$$\varepsilon_{lh} = \varepsilon_{hl} = \frac{1}{\frac{1}{\varepsilon_l} + \frac{1}{\varepsilon_h} - 1} \quad (3.19)$$

$$\varepsilon_{hc} = \frac{1}{\frac{1}{\varepsilon_h} + \frac{1}{\varepsilon_c} - 1} \quad (3.20)$$

$$\varepsilon_l = \frac{1}{\frac{1}{\varepsilon_w} + \frac{1}{\varepsilon_P} - 1} \quad (3.21)$$

Emittance is generally represented as a function of wavelength of radiation i.e $\varepsilon = f(\lambda)$. Black bodies can be defined as ($\varepsilon = 1$) and in case of a gray or natural body ("$0 < \varepsilon < 1$"). The incoming radiation to a body can either be reflected (reflectance termρ_{ref}), absorbed (absorbance term α) or transmitted (transmittance term τ). The transmitted part for earth (a thick body) is zero, if the earth or thick body is in thermodynamic equilibrium, then according to the principle of conservation of energy ($\rho_{ref} + \alpha = 1$) *or* ($\alpha = 1 - \rho_{ref}$). As per Kirchhoff's law, absorptance is equal to emittance ($\alpha = \varepsilon$), thus we get ($\varepsilon = 1 - \rho_{ref}$). In this way, reflectance is associated with emittance and in case of lens or any transparent medium ($\varepsilon = 1 - \tau_l$), emittance is associated with transmittance [218].

In **Equation (8.16)** the term on the left represents the absorbed solar energy by the "selective absorber surface"; the 1st term on the right represents the total heat absorbed at the TEG module's hot side; the 2nd term represents the transferring of the radiative heat within the LLDPE cover and the absorber's top surface; the 3rd and 4th terms represent the radiative and convective heat transfer (A_{ab}-A_{mod}). The convective transferring of heat within the TEG modules' cold side and the absorber's surface via the non-packed could be avoided given that the non-packed space is evacuated. I_c is the concentrated solar radiation on the absorber surface per unit area. The net transmittance of the water and the LLDPE cover is given by [219].

$$\tau_l = \tau_w \tau_P \tag{3.22}$$

Where τ_w is the transmittance of the water and τ_P is the transmittance of the plastic cover. C_{th} is the thermal concentration ratio. When the power flux (W/m^2) on a receiver is increased by means of heat localization from a large highly-conductive absorber to a small absorber area is called thermal concentration. Direct solar radiation are concentrated on absorber by means of a reflective surface or lens, in order to produce high temperature on the absorber [70].

$$C_{th} = \frac{A_{ab}}{A_{mod}} \tag{3.23}$$

Combining Equations (3.17) and (3.18):

$$\begin{aligned} \tau_l \alpha_{ab} C_{th} I_g A_{ab} &= Q_h + h_{conv,l-a} A_l (T_l - T_a) + \varepsilon_l \sigma_{sb} A_l (T_l^4 - T_a^4) \\ &+ \varepsilon_{hc} \sigma_{sb} (A_{ab} - A_{mod})(T_h^4 - T_c^4) + h_{conv,h-a}(A_{ab} \\ &- A_{mod})(T_h - T_c) \end{aligned} \tag{3.24}$$

i.e another form $Q_{abs} = Q_h + Q_{conv,l-a} + Q_{rad,l-a} + Q_{rad,h-c} + Q_{conv,h-a}$

Heat balance schematic for TEG module is exhibited in Figure 3.27. In accordance with the 1st law of thermodynamics, the thermocouple junction's rate for heat transfer is defined. As much heat is absorbed in the hot junction (Q_h) of the TEG module as is transmitted downward from the absorber surface, and Q_c denotes the rejected heat at the TEG module's cold junction to the heat sink. The rates of heat transfer at hot and cold sides are respectively numerically represented as:

$$Q_h = S_h I T_h - \frac{I^2 R}{2} + K(T_h - T_c) - \frac{\mu I (T_h - T_c)}{2} \quad (3.25)$$

$$Q_c = S_c I T_c + \frac{I^2 R}{2} + K(T_h - T_c) + \frac{\mu I (T_h - T_c)}{2} \quad (3.26)$$

Where, the electric current is denoted with I, the thermal conductance was denoted with the help of K, Thomson coefficient was denoted with the help of μ and the Seebeck coefficient was denoted with the help of S. The n as well as p-type materials are respectively denoted with the help of the subscripts n and p. On the other hand, the thermocouple's cold and hot side are respectively denoted with the subscript c and h. the overall electrical resistance, thermal conductance and Seebeck coefficient are expressed as:

$$S = N\left(s_p - (-s_n)\right), \quad (3.27)$$

$$K = N(K_n + K_p) \quad (3.28)$$

$$R = N(R_n + R_p) \quad (3.29)$$

Where

$$K_p = \frac{k_p A_p}{L_p},\ K_n = \frac{k_n A_n}{L_n}$$

$$R_n = \frac{\rho_n L_n}{A_n},\ R_p = \frac{\rho_p L_p}{A_p}$$

The thermocouple number is denoted by N. the n and p-type materials' cross sectional area are represented by A_n and A_p respectively in the thermoelements. Their lengths are respectively denoted with the help of L_n and L_p. s_p, s_n, k_p, k_n, ρ_p, and ρ_n changes along with the change in temperature at TE module's cold and hot junctions.

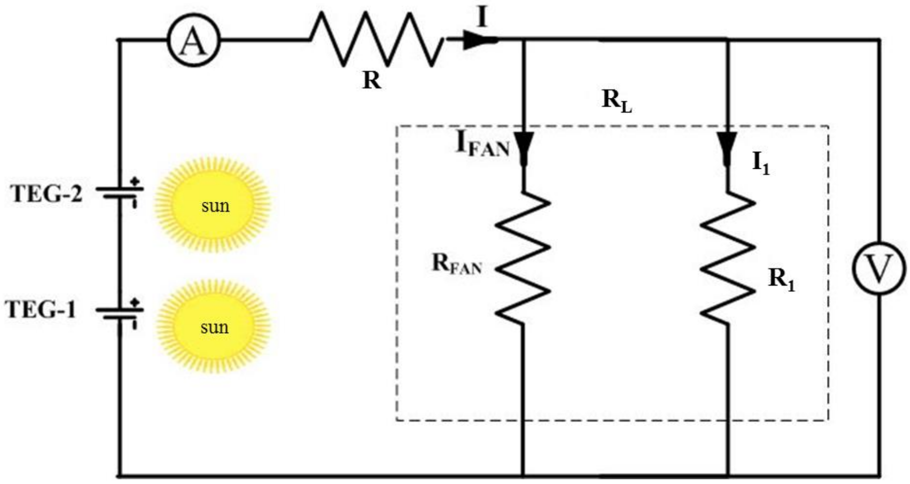

Figure 3.28: *Equivalent electric circuit of GWLSTEG*

From the "Equivalent electric circuit" given in Figure 3.28, the expression of the "Solar TEG's power output" is given as:

$$P_{out} = Q_h - Q_c = (S_h T_h - S_c T_c)I - I^2 R - \mu I(T_h - T_c) = I^2 R_L \qquad (3.30)$$

Where, R_L is the "load resistance", The generation of the electric current from the TEG is dependent over the external load resistance, TEG's internal resistance, thermoelectric element's thermoelectric characteristics, and cold and hot junctions' temperatures. This can be evaluated by solving **Eq (3.30)** for I and is expressed as:

$$I = \frac{(S_h T_h - S_c T_c) - \mu(T_h - T_c)}{R + R_L} \qquad (3.31)$$

Power output is dependent over the current. Thus, with the differentiation of **Eq (3.31),** the current at which "maximum power transferred" occurs can be obtained. Further, condition for the "maximum power transferred" provides the "optimum current" at which the "maximum power transferred" occur:

$$I_{P,max} = \frac{(S_h T_h - S_c T_c) - \mu(T_h - T_c)}{2R} \qquad (3.32)$$

Numerical expression of the TEG system's efficiency is:

$$\eta_{TE} = \frac{P_{out}}{Q_h} = \frac{(S_h T_h - S_c T_c)I - I^2 R - \mu I(T_h - T_c)}{S_h I T_h - \frac{I^2 R}{2} + K(T_h - T_c) - \frac{\mu I(T_h - T_c)}{2}} \qquad (3.33)$$

Numerical expression for STEG system's efficiency, with respect to energy, is:

$$\eta_{sys} = \frac{P_{out}}{Q_{in}} = \frac{(S_h T_h - S_c T_c)I - I^2 R - \mu I(T_h - T_c)}{C_{th} I_g A_{ab}} \quad (3.34)$$

As an alternative notation, the GWLSTEG's energy efficiency may be expressed as the product of its optothermal and thermoelectric efficiencies:

$$\eta_{sys} = \frac{Q_h}{C_{th} I_g A_{ab}} \, X \, \frac{P_{out}}{Q_h} = \eta_{ot}\eta_{te} \quad (3.35)$$

$$\eta_{sys} = \left[\tau_l \alpha_{ab} - \frac{(\varepsilon_{lh} + \varepsilon_{hc})\sigma_{sb}(T_h^4 - T_c^4)}{C_{th} I_g}\right] X \left[\frac{(T_h - T_c)}{T_h} \frac{\sqrt{1 + zT} - 1}{\sqrt{1 + zT} + \frac{T_c}{T_h}}\right] \quad (3.36)$$

TE and opto-thermal efficiencies are given as:

$$\eta_{ot} = \left[\eta_{opt} - \frac{(\varepsilon_{lh} + \varepsilon_{hc})\sigma_{sb}(T_h^4 - T_c^4)}{C_{th} I_g}\right], \quad (3.37)$$

$$\eta_{te} = \left[\frac{(T_h - T_c)}{T_h} \frac{\sqrt{1 + zT} - 1}{\sqrt{1 + zT} + \frac{T_c}{T_h}}\right] \quad (3.38)$$

η_{opt} is the optical efficiency. For finding the GWLSTEG's exergy efficiency, the solar radiation's exergy input's expression was evaluated, as per the Petela. The GWLSTEG generates electrical power, which is a kind of exergy. Therefore, the solar thermoelectric generator's exergy efficiency may be written as:

$$\psi_{sys} = \frac{P_{out}}{Ex_{in}} = \frac{(S_h T_h - S_c T_c)I - I^2 R - \mu I(T_h - T_c)}{Q_{in}\left(1 - \frac{4T_a}{3T_{sun}} + \frac{1}{3}\left(\frac{T_a}{T_{sun}}\right)^4\right)} \quad (3.39)$$

For the validation purpose the error can be calculated as follows:

$$\%\, error = \left[\frac{(\,experimental\ value - theoretical\ value)}{theoretical\ value}\right] X[100] \quad (3.40)$$

3.5 Numerical Simulation and Optimization

Two different soft-wares have been used for overall numerical analysis of GWLSTEG. The first one is COMSOL which has been used for modelling and simulation of TEG, and the second one is Sol-Trace, which has been used to evaluate the solar radiation concentration of water lens over the aluminium absorber for the optimized transmittance of polythene. Following steps were involved in the software simulation of GWLSTEG.

3.5.1 Solar Ray Tracing for Giant Water Lens

For conducting this research, the concentrated solar heat flow distribution is predicted [220][221] using the Sol-Trace software [180]. A method of ray-tracing is utilized by the code [222]. The quantity of rays traced from the sun through the system is set, and as those rays travel through the system they meet the numerous optical interactions set out. It's important to note that not all of these interactions are equally deterministic (for instance, picking a solar angle based on the sun's angular intensity distribution). Determining the form and orientation of the sun is the first stage in developing a Sol-Trace project. After that, groups of optical attributes are developed and assigned to the system's optical components. At last, the geometry of the optical system is developed, which includes the stages and their constituent elements. Each constituent is linked here to a category of optical properties. Complete system definitions may be stored in a file for subsequent review [222]. The Sun-shape profile used and the rays traced are shown in

Figure 3.29 (a) and (b). As can be seen in the Gaussian sun shape profile, at 0 mrad angle of the sun the intensity is 1 and it follows a parabolic curve.

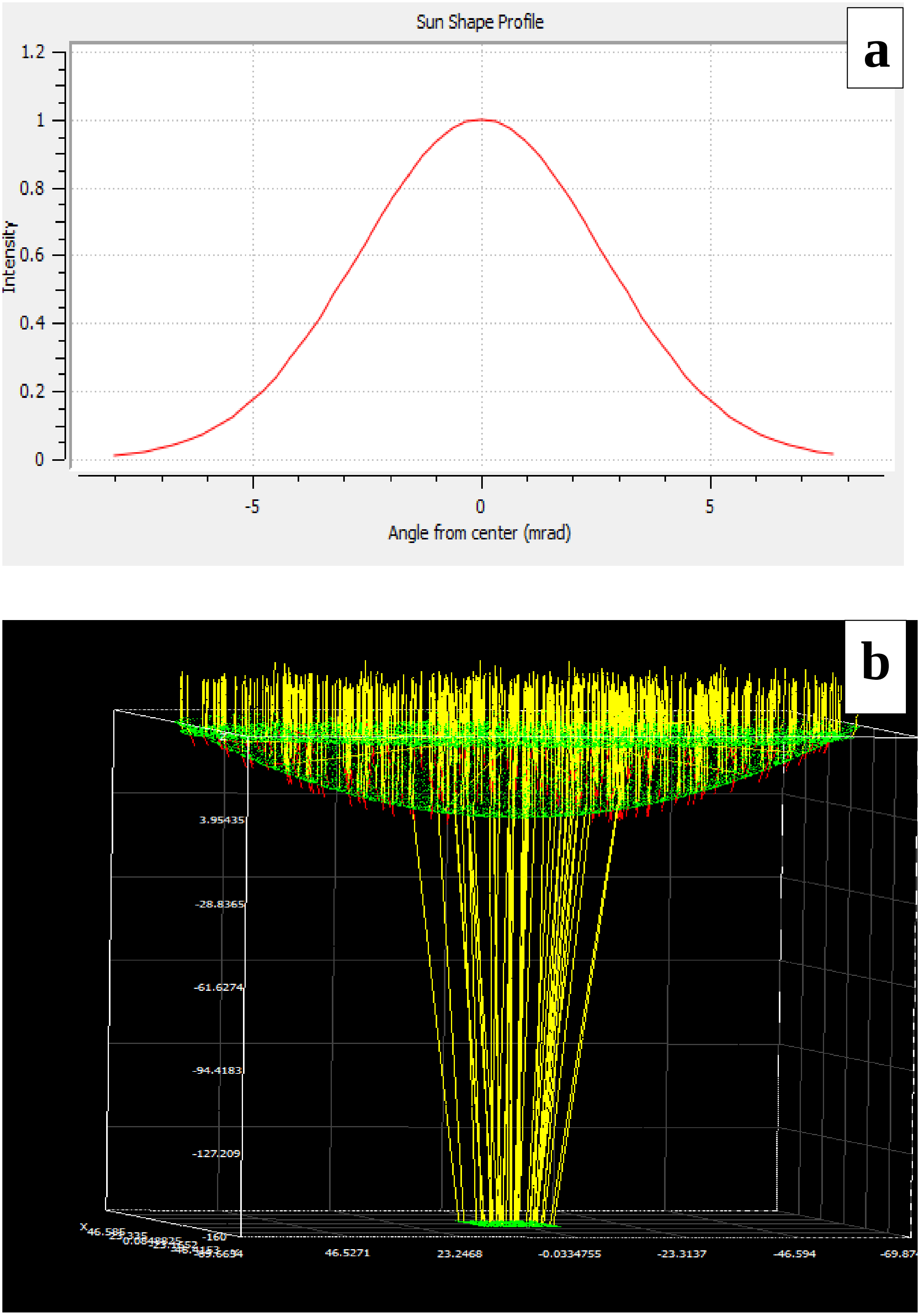

Figure 3.29: *(a) Sun shape profile; (b) Ray tracing in Sol-Trace software*

Table 3.4 and Table 3.5 show the data that has been used in the Sol-Trace to achieve the objectives of this setup.

Table 3.4: Optical properties of water (40 ltr) and LLDPE plastic

Optical Properties	Value
Emittance of water	0.03
Emittance of Plastic	0.02
Emittance of lens	0.10
Transmittance of water	0.94
Transmittance of Plastic	0.95
Transmittance of lens	0.90
Abroptance of absorber	0.94
Effective emittance	0.03
Slope error water	3.0 mrad
Specularity error water	3.0 mrad
Slope error Plastic	3.0 mrad
Specularity error Plastic	3.0 mrad
Refractive Indices of water	1.33
Refractive Indices of plastic	1.5

An ideal lens' surface would be shaped like a circular paraboloid. Slope errors are angular aberrations of the lens surface relative to the ideal shape and can be caused by deformations due to gravitational force of the weight of the lens, deformations due to mounting the lens on a bearing structure, or unavoidable shape tolerances in the fabrication process.

The slope error can be measured at any location on the lens surface. The overall geometrical quality of the mirror can be inferred from the average value of slope error for the entire lens. Deflectometry is one approach that might be used to measure the slope error [223][224].

Table 3.5: Tracing parameters

Parameters	Value
Desired Number of ray intersections	10000
Maximum number of generated sun rays	1000000
Maximum number of CPUs to utilize	16
Seed Value	-1

3.5.2 Development of Multi-Physics Model of TEG Module

Accuracy and complete inclusion of all relevant effects occurring during TEG operation are essential for the model. Since TEGs rely on principles of operation that include electrical production, heat transport, and other phenomena, some of which might be non-linear, multiphysics modeling is crucial. The nonlinearities of TEGs may be effectively addressed by using finite element techniques (FEM). The capability to modify the TEG controlling equations is another feature that should be included in a high-quality software suite. As a result, you may toggle the visibility of individual words to see how they influence the model.

For developing a mathematical model which was identical to that of the experimental model of this study, the use of COMSOL Multiphysics V5.4 [225][226] was made. The thermoelectric effects, electric current and transfer of heat were taken into account in this model to provide a reliable estimate of electrical output obtained from the TEG employed in the intended application. The model generation process begins with including the geometry of the experimental setup. One of the most important conditions for success is to have the geometry as precise as possible, since little changes in the geometry may lead to drastically different outcomes in simulations. When more information on the TEG module's build was needed than what was included in the commercial datasheet, it was necessary to get in touch with the manufacturer. At first, just one module pair was simulated (consisting of a N Type block and a P Type block) to verify the reliability of the build. Bismuth telluride (Bi_2Te_3) was chosen as the semiconductor material for both types P and N. The Seebeck coefficient and other material rameters were calibrated to match the manufacturer's specifications.

(a) .Meshing

After that, we were able to successfully simulate the experimental test cell in multiphysics. Thermoelectric effect, electromagnetic heating, electric current, fluid heat transfer, and other physics and modeling research were all included in the model. In order to fine-tune the mesh, the element size settings were changed to “Extra fine.” as shown in Table 3.6. This mesh size was appropriate for the test since a finer mesh would not have improved the findings and would have increased the calculation time. The model’s overall geometry developed was exhibited in Figure 3.30 (a). The mesh size that is implemented for this study is exhibited in Figure 3.30 (b) along with the detailed parameters that are shown in Table 3.6. The model was programmed to provide estimates for the input power, output power, matching load power, and internal resistance, all in SI units. First test was simulated using a duplicate of the parameters described in the product datasheet to verify the accuracy of the computer model.

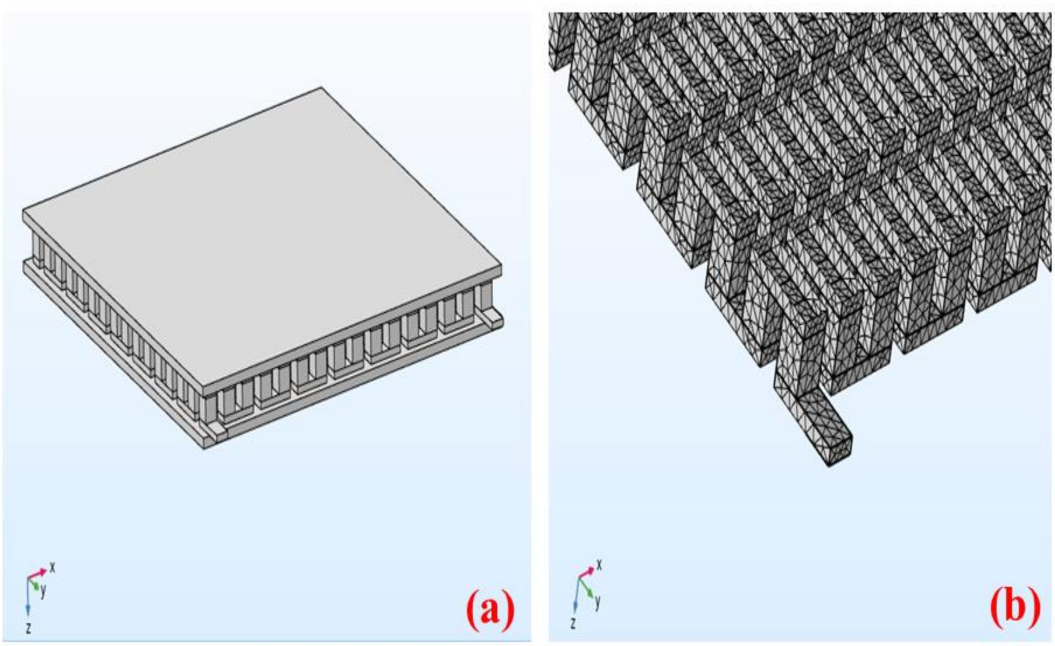

Figure 3.30: *(a) COMSOL model of the TEG (b) Meshing of the TEG model*

The selected mesh's element size parameters in relation to various pre-set mesh sizes, as well as the stored convergence values for the electrical potential, are compared and contrasted.

Table 3.6: Meshing details

Pre-set mesh size parameters	**Coarse**	**Extra fine**	**Extreme fine**
Maximum element size (mm)	0.018	0.00146	0.00015
Minimum element size (mm)"	0.0015	6.25e-5	6.54e^{-7}
Maximum element growth rate	1.2	1.35	1.5
Curvature factor	0.5	0.3	0.1
Resolution of narrow regions	0.6	0.85	1
No. of elements	4.3 million	9.2 million	12 million
Max. temperature obtained	170^{o}C (443 K)	225^{o}C (498 K)	230^{o}C (503 K)

Grid independent test graph, shown in Figure 3.31, shows that for elements with atomic masses of more than 9 million, the maximum temperature attained on the absorber surface follows a nearly constant curve. As a consequence, ultra-precise simulations have been employed, using a total of 9.2 million components and ultra-fine meshing.

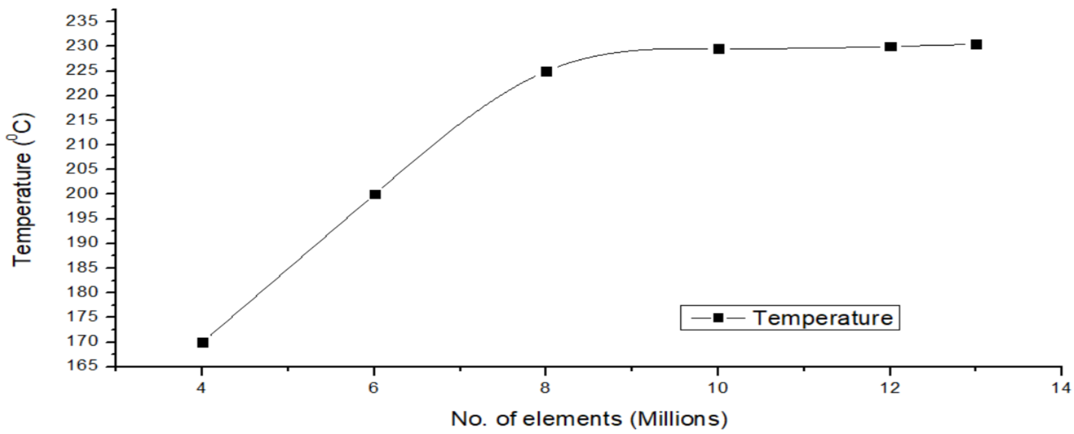

Figure 3.31: *Grid independent test graph*

(b). Thermoelectric modeling of TEG (governing equations)

Since thermoelectric effect is already included in COMSOL-Multiphysics, it was chosen as the platform to create the computer model of this investigation. In addition, it has supposedly been put to use in TEG simulation, with promising results being presented to the academic community. In this research, we assume that the TEG is hermetically sealed, thus we may utilize the equations in "COMSOL-Multiphysics" that explain the "Thermoelectric effect and electromagnetic heating", as well as general transmission of heat in solids and electric currents.

The Thomson, Peltier, Fourier and Joule effect are all taken into account in the inquiry, and the thermoelectric analysis' primary equation was generated using "COMSOL Multiphysics software". In thermoelectric analysis, the heat flow equation has the form [226]:

$$\rho_d C_H \frac{\partial T}{\partial t} + \nabla.\vec{q} = \dot{q} \tag{3.41}$$

Here, ρ_d (kg/m^3) signifies the density, C_H (J/kgK) denotes the specific heat capacity, heat generation rate per unit volume is signified by $\vec{q}$ (W/m^2) and absolute temperature is signified by T (K). From this equation, we can determine that electric charge is continuous:

$$\nabla.\left(\vec{J} + \frac{\partial \vec{D}}{\partial t}\right) = 0 \tag{3.42}$$

Where, electric flux and electric current density vector are respectively signified by $\vec{D}$(C/m^2) and $\vec{J}$ (A/m^2). Using the proper basic thermoelectric equations, the aforementioned two equations are combined:

$$\vec{q} = T[\alpha].\vec{J} - [k].\nabla T \tag{3.43}$$

$$\vec{J} = [\sigma].\left(\vec{E} - [\alpha].\nabla T\right) \tag{3.44}$$

Thermal and electrical conductivity, as well as "Seebeck coefficient" matrix are respectively denoted by [k], [σ], and [α].

$\vec{E}$ is used for representing the electric field intensity and it is evaluated from:

$$\vec{E} = -\nabla\varphi \tag{3.45}$$

φ represents the electric scalar potential. Incorporating the above three equations, the heat flow equation and the continuity equation given above can be rearranged as:

$$\rho_d C_H \frac{\partial T}{\partial t} + \nabla[(T[\alpha].\vec{j}) - [\alpha].\nabla T] = \dot{q} \tag{3.46}$$

$$\nabla\left[\left([\varepsilon_d].\nabla\frac{\partial \varphi}{\partial t}\right) + ([\sigma].[\alpha].\nabla T) + ([\sigma].\nabla \varphi)\right] = 0 \tag{3.47}$$

Dielectric permittivity is defined as the internal electric field to electric displacement ratio of a material. $[\varepsilon_d]$ indicates the dielectric permittivity matrix and its unit is (F/m).

Chapter 4

RESULTS, DISCUSSSION AND VALIDATIONS

To achieve the objective of this research, the result section has been broken down into parts. The results obtained through the simulations have been discussed first and then results from experimental setup and validated. Then both results are compared.

4.1 Simulation Results

Simulation results of the plastic lens are used to fabricate the lens and the experimental values of temperature of the absorber were used for simulation of TE module in COMSOL software.

4.1.1 Temperature distribution on the surface

The temperature profile across the TEG module as obtained in the simulation is shown in Figure 4.1 **(a)** and **(b)**. Maximum value of the temperature obtained on the hot junction is 498K while the minimum value is 308-313K on the cold plate. A maximum temperature difference of 463K is obtained. This is in accordance with the results obtained from the experimental outcomes. These results have been validated by Qusay Doraghi et al. [226][64].

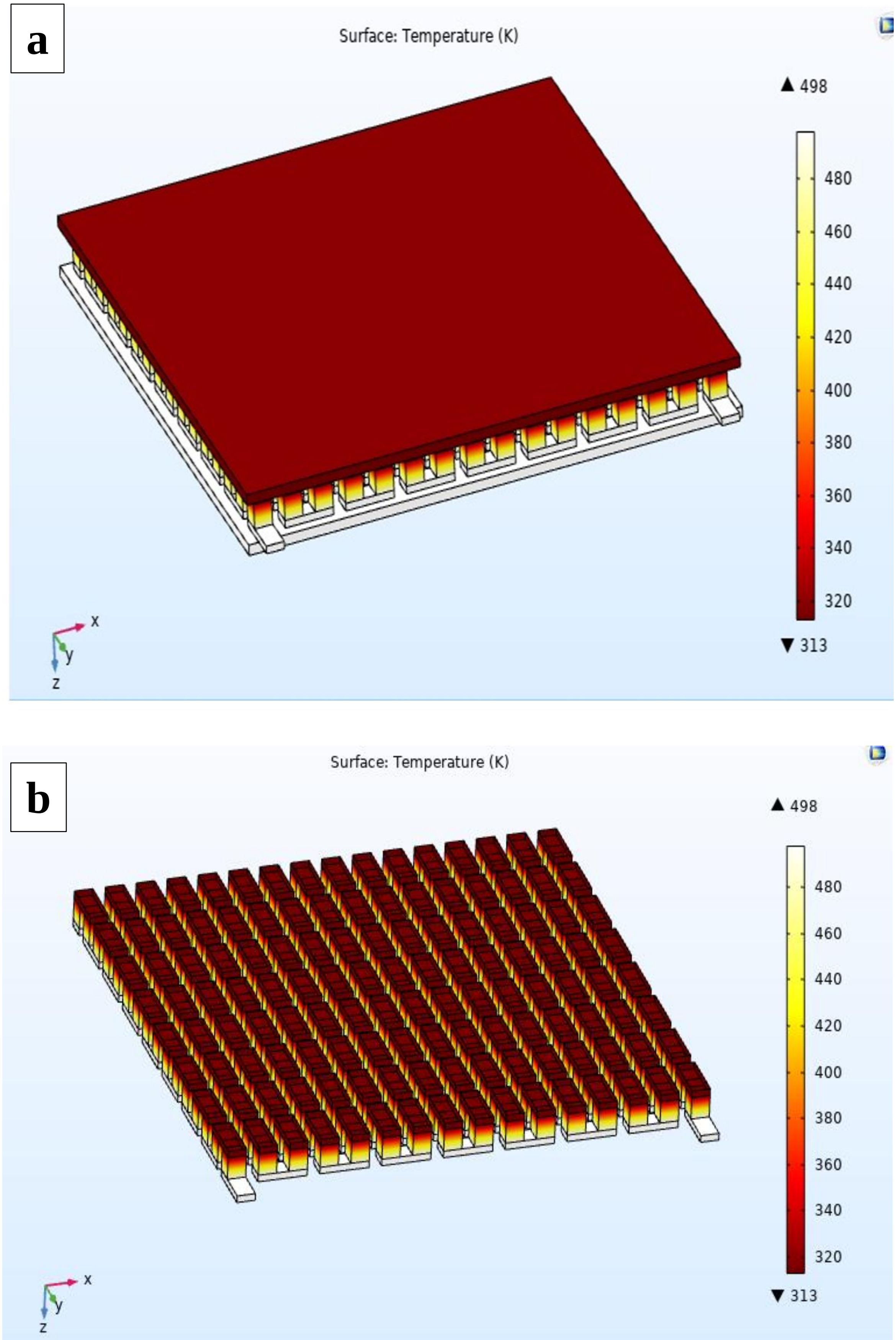

Figure 4.1: *Temperature distribution on (a) Surface of absorber plate (b) TEG module*

4.1.2 Electric potential on surface

Maximum electric potential is recorded 10.9 V and the minimum electric potential is recorded as -1.3×10^{-8}, which can be observed in **Fig. 16**. This is also in accordance with the results obtained from the experimental evaluation of the process. The potential difference obtained across the TEG module as obtained in the simulation is shown. These results have been validated by Qusay Doraghi et al. [226][227].

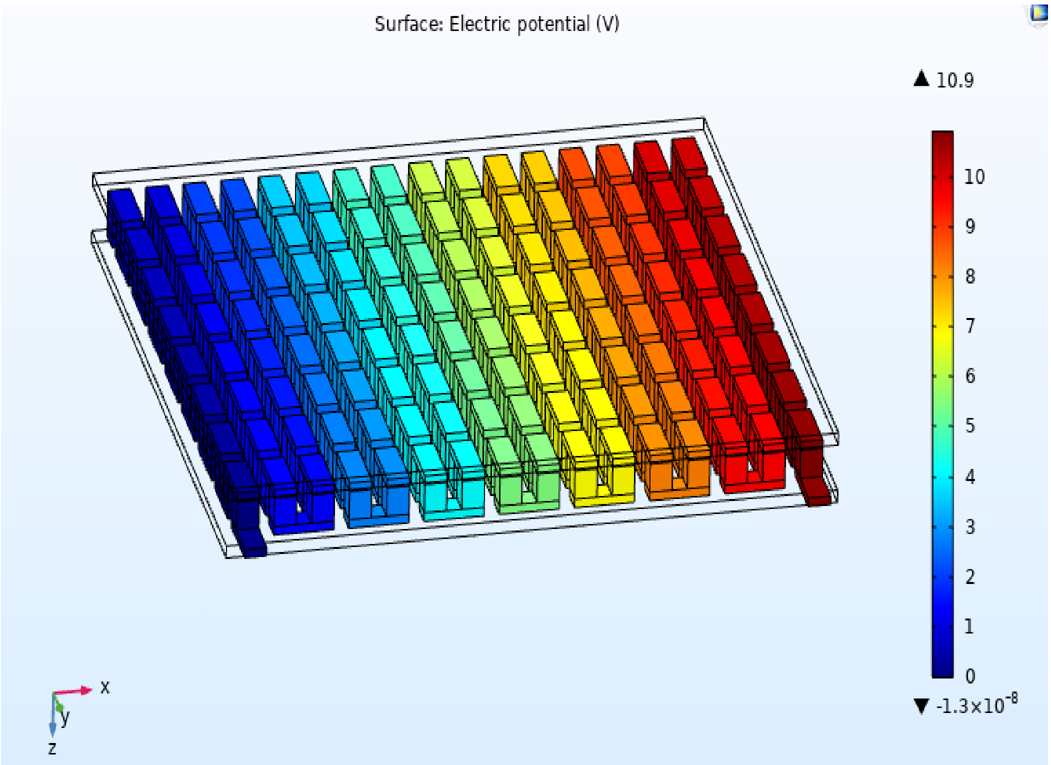

Figure 4.2: Electric potential across the surface

4.1.3 Flux Intensity at surface of water lens

Figure 4.2 **(a)** and **(b)** show the distribution of the flux intensity obtained through the Sol-Trace software [77]. Maximum average flux intensity at the surface of the water lens is observed to be 1203 W/m^2. LLDPE plastic layer is almost unaffected by radiation and shows little to no deviation in flux intensity as represented by a thin outer layer in blue.

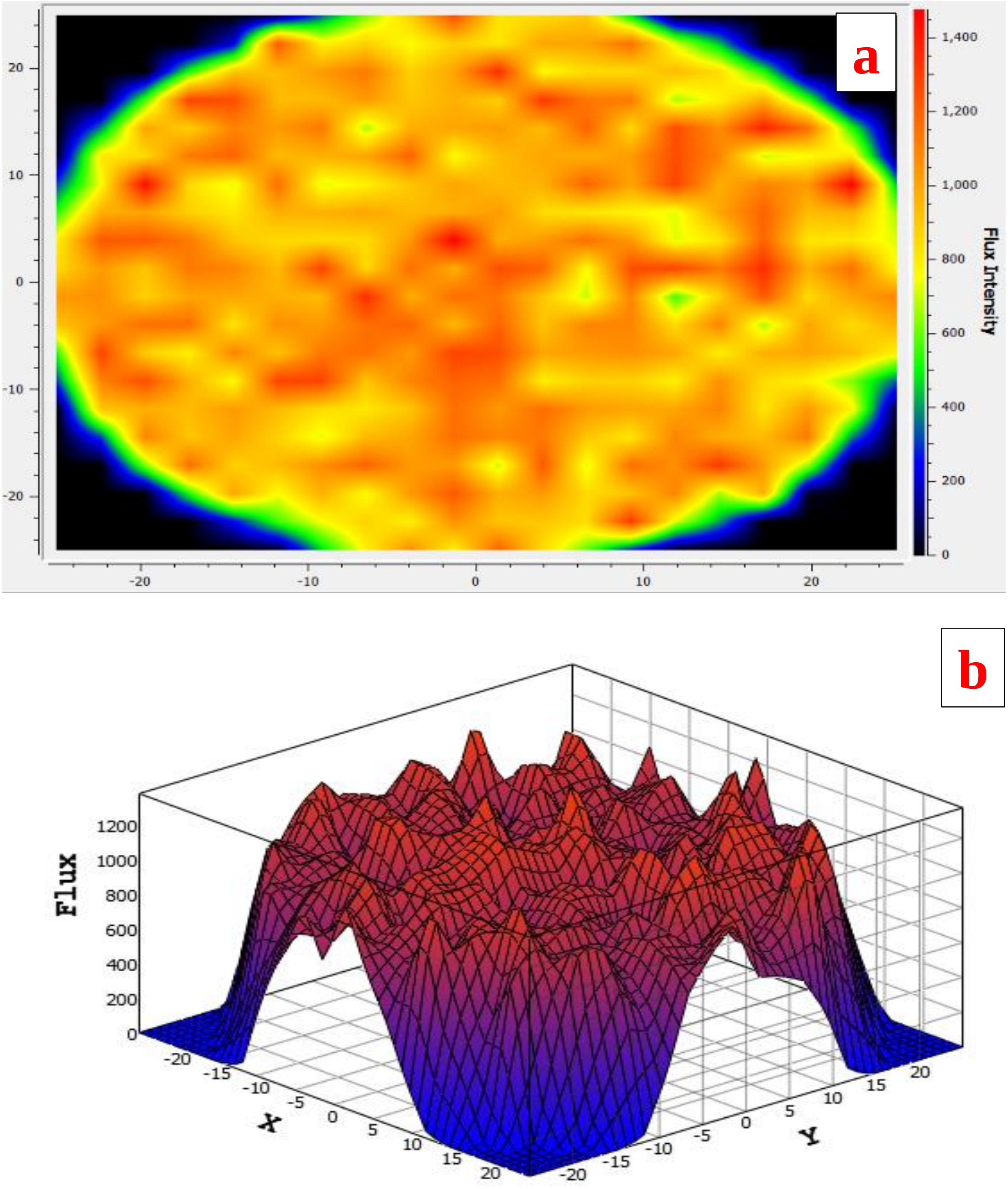

Figure 4.3: (a) Heat flux distribution on the water lens surface (b) 3D graph of heat flux

4.1.4 Flux intensity at the absorber plate

The distribution of the flux intensity that is concentrated on the absorber through the Sol-Trace software was simulated [77]. As shown in Figure 4.4 **(a)** and **(b)**, the maximum value of average flux intensity obtained at the surface of the absorber is 4200 W/m^2.

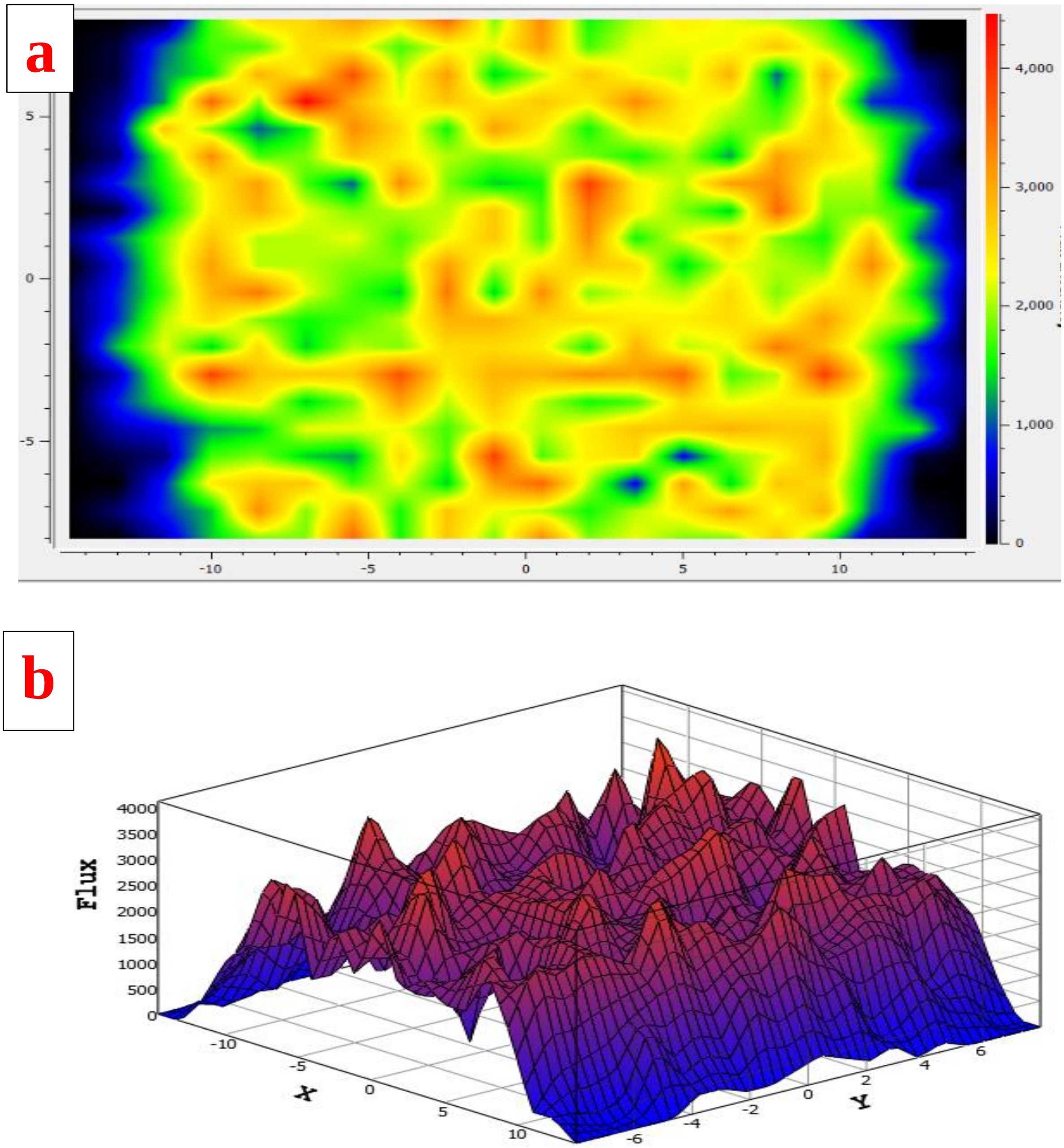

Figure 4.4: *(a) Heat flux distribution on absorber plate (b) 3D presentation of heat flux*

Radiation intensity concentrated on the absorber has increased almost 4 times through the water lens which is in accordance with the experimental observations.

4.2 Experimental Results

Experimental results have been obtained by measuring the different parameters using suitable instruments and have been plotted below in the form of the time gradients of the current inputs and outputs, beam radiation, diffuse radiation, temperatures of the hot and cold junction, average temperature, temperature difference, air velocity, relative humidity, voltage and current. Experiment was conducted between 800 hrs and 1700 hrs on 17th May 2021 and the measurements were taken at every 15 mins intervals. The graphs of these values with respect to time.

4.2.1 Solar irradiance

Maximum energy that is collected from the sun in the form of radiation per unit area is known as solar irradiance [15][228][74]. The graph traced in Figure 4.5 shows the values of the global radiation from the sun (I_g), the beam radiation (I_b), concentrated solar radiation over the aluminium absorber through the water lens (I_c) and the diffused radiation (I_d) with respect to time. With this design, 4580W/m^2 of solar radiation is to give approximately 190 K of temperature difference across the thermoelectric module, while the ambient/cold side temperature is 308K and the hot side temperature is 498 K. The variation of global, beam, diffuse and concentrated radiation with time radiation is shown in Figure 4.5. Most significant sunshine hours can be considered between 1100 hrs and 1500 hrs. Global radiation reaches from 930 W/m^2 at 1100 hrs to 1135 W/m^2 at 1400 hrs and then to 700 W/m^2 at 1500 hrs. Concentrated radiation reaches from 2790 W/m^2 at 1100 hrs to 4580 W/m^2 at 1400 hrs and 2100 W/m^2 at 1500 hrs. Diffuse radiation reaches from 178 W/m^2 at 1100 hrs to 221 W/m^2 at 1400 hrs and 93 W/m^2 at 1500 hrs. Beam radiation reaches from 752 W/m^2 at 1100 hrs to 914 W/m^2 at 1400 hrs and 607 W/m^2 at 1500 hrs. Variation of Solar Radiation, air velocity, Relative humidity, Temperature with respect to time (hrs) is shown in Table 4.1.

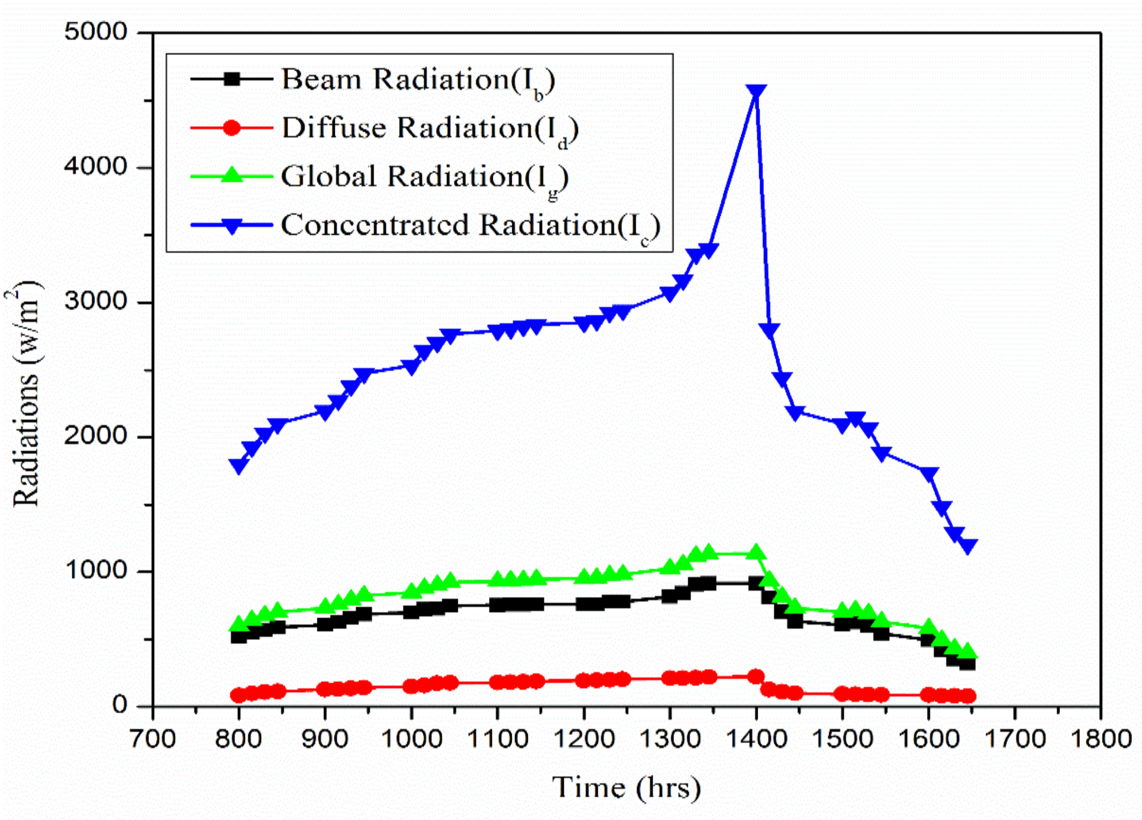

Figure 4.5: *Variation of solar irradiance with time*

Table 4.1: Variation of solar radiation, air velocity, relative humidity, temperature with respect to time (hrs)

Time (hrs)	I_b (W/m^2)	I_d (W/m^2)	I_g (W/m^2)	I_c (W/m^2)	V_a (m/s)	R_{ha} (%)	T_h (K)	T_c (K)	mean T (K)	ΔT (K)	T_a (K)	T_l (K)
800	517	82	599	1797	0.26	44.1	308.5	305	305.25	6.5	302	305
815	547	95	642	1926	0.22	44	313	305.6	308	10	303	305.6
830	569	108	677	2031	0.23	40	324	306.6	313.5	21	303	306.6
845	588	112	700	2100	0.42	38	361	306.7	332.5	57	304	306.7
900	605	127	732	2196	0.48	35	371	307.1	337.5	67	304	307.1
915	628	130	758	2274	0.69	34	376	307.2	340.5	71	305	306.6
930	658	135	793	2379	0.22	34	380	307.9	342.5	75	305	307.3
945	685	140	825	2475	0.26	33	386	308.2	345.5	81	305	307.4
1000	698	147	845	2535	0.39	31	393	308.3	349.5	87	306	307.5
1015	723	157	880	2640	0.52	30	396	308.6	351	90	306	307.8

1030	727	173	900	2700	0.51	29	401	309.2	353.5	95	306	308.4
1045	747	175	922	2766	0.52	29	413	309.5	360	106	307	308.7
1100	752	178	930	2790	0.86	25.3	423	310	365	116	307	309.2
1115	755	180	935	2805	0.99	23.1	426	310.1	366.5	119	307	309.1
1130	757	183	940	2820	0.37	22.2	433	310.2	370	126	307	309.2
1145	759	187	946	2838	0.29	21.1	440	310.5	373.5	133	307	309.5
1200	758	192	950	2850	0.3	20.4	445	311	376	138	307	310
1215	760	195	955	2865	0.07	19.5	446	311.6	376.5	139	307	310.6
1230	778	197	975	2925	0.21	19	449	312.1	378	142	307	311
1245	778	202	980	2940	0.27	18	450.5	312.4	378.75	143.5	307	311.4
1300	815	210	1025	3075	1.21	17	459	312.5	383	152	307	311.5
1315	844	212	1056	3168	0.28	16	463	312.8	385	156	307	311.8
1330	905	215	1120	3360	0.16	14	473	313	390.5	165	308	312.4

1345	914	218	1132	3396	0.18	13.5	483	313.1	395.5	175	308	312.5
1400	914	221	1135	4580	0.19	12.5	498	313.2	403	190	308	312.2
1415	810	125	935	2805	0.18	13	480	313	394	172	308	312.4
1430	705	110	815	2445	0.14	14.5	471	310.8	389	164	307	310.2
1445	633	98	731	2193	0.39	16.5	450	310.3	378.5	143	307	310.3
1500	607	93	700	2100	0.22	19.2	419	309.3	362.5	113	306	310
1515	624	91	715	2145	0.2	21.3	383	309.2	344	78	305	310
1530	603	87	690	2070	0.22	21.2	363	309.2	333.5	59	304	309.9
1545	544	86	630	1890	0.69	23.5	345	308.3	324.5	41	304	309
1600	495	85	580	1740	0.34	24.3	333	308.2	318	30	303	308.8
1615	414	81	495	1485	0.29	25.1	319	308.1	311	16	303	308.5
1630	351	79	430	1290	0.27	26	318	308	310	16	302	308.3
1645	322	78	400	1200	0.33	30	318	308	310.5	15	303	308.2

Maximum concentration of the solar flux (I_c) 4580W/m^2 at the absorber plate is obtained at 1400 hrs (2 PM) of the day for the maximum global radiation from the sun (I_g) is 1135 W/m^2 as traced in Figure 4.5. Beam radiation incident (I_b) on the water lens at this point is 914 W/m^2 and diffused radiation (I_d) is observed as 221 W/m^2 for the central India climatic conditions.

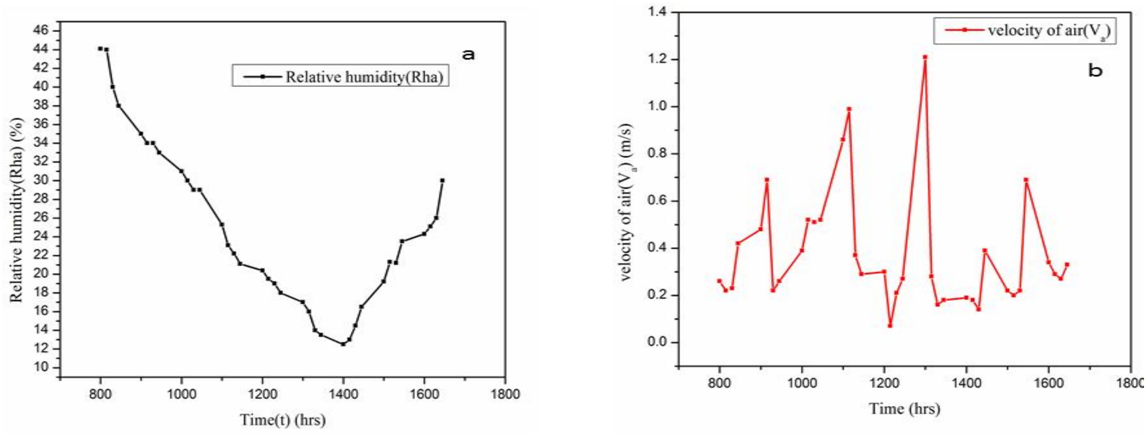

Figure 4.6: *(a) Variation of relative humidity; (b) Velocity of air w.r.t time*

Minimum relative humidity is observed at 1400 hrs i.e., 12.5% when the wind velocity is low as seen in Figure 4.6. The air velocity reaches from 0.86 m/s at 1100 hrs to 0.19 m/s at 1400 hrs and then 0.22 m/s at 1500 hrs. Relative humidity reaches from 25.3 % at 1100 hrs to 12.5 % at 1400 hrs and then to 19.2% at 1500 hrs. As the temperature at the hot junction increases with the increase in the concentrated flux, the effect of air velocity and humidity is accommodated in the temperature of hot and cold side.

4.2.2 Temperature

Graphical presentations, given in Figure 4.7, show the global radiation, distribution of the temperature across the hot and cold junction of the TEG, i.e. Temperature of the hot junction (T_h), temperature of the cold junction (T_c), temperature of the ambience (T_a), average temperature (T), temperature difference between the hot and cold junctions (ΔT), and temperature of water lens (T_a) with respect to time. Figure 4.7 shows gradual increase in all temperatures till 1400 hrs of the day when the values of T_h, T_c, T and ΔT are maximum, i.e. 498K, 308K, 403K and 190K while T_c remain little bit higher than T_a throughout the day by means of DC fan air cooling. Ambient temperature (T_a) reaches from 310 K at 1100 hrs to 313.2 K at 1400 hrs and then to 309.3K at 1500 hrs. Water lens temperature (T_l) reaches 309.2 K at 1100 hrs to 312.2 K at 1400 hrs and then to

310K at 1500 hrs. Hot side temperature (T_h) reaches 423 K at 1100 hrs to 498 K at 1400 hrs and then to 419 K at 1500 hrs. Cold side temperature reaches (T_c) from 307 K at 1100 hrs to 308 K at 1400 hrs and then to 306K at 1500 hrs. Average temperature reaches from 365K at 1100 hrs to 403 K at 1400 hrs and 362.5 K at 1500 hrs. The ΔT reaches 116 K at 1100 hrs to 190K at 1400 hrs and 113K at 1500 hrs.

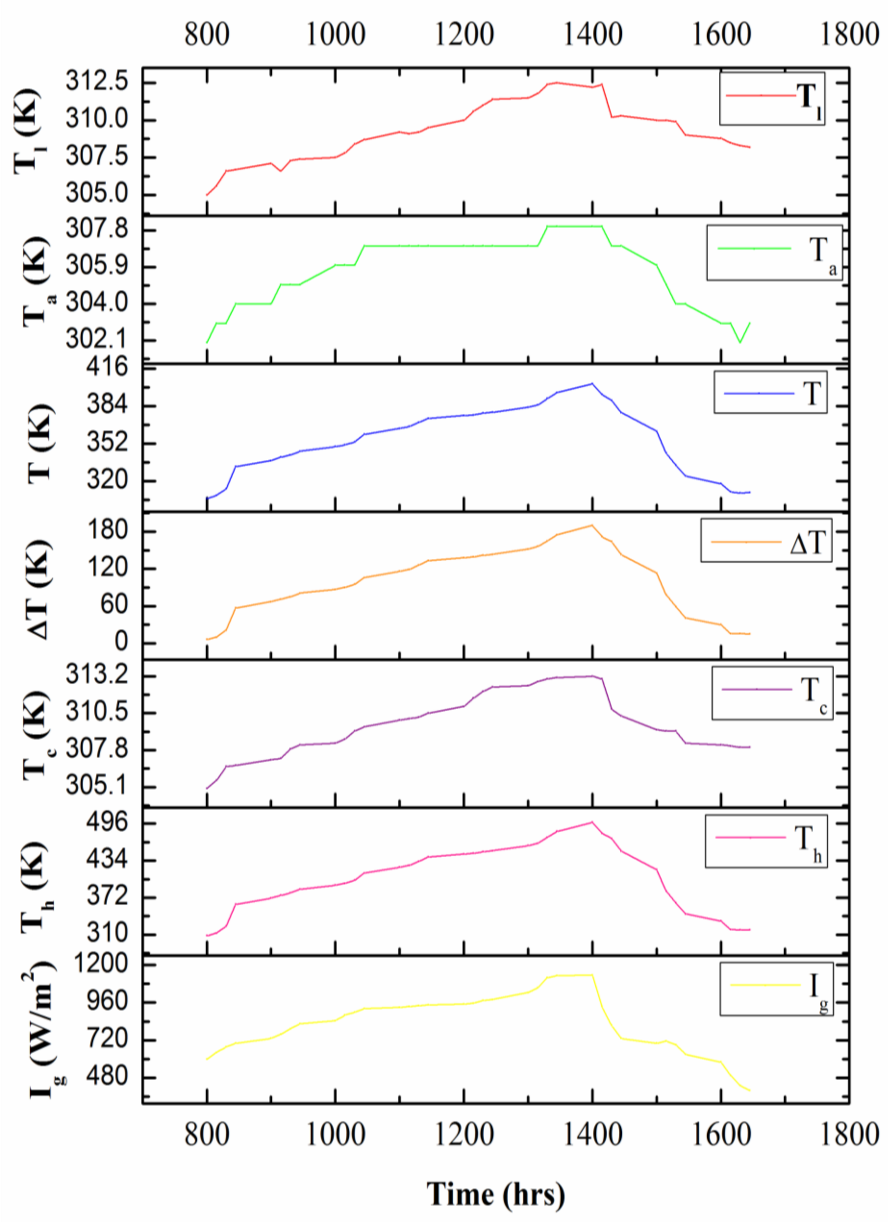

Figure 4.7: *Temperature variations with time*

The reason for all the maxima of temperature can be attributed to the amount of the global incoming radiation (I_g) which increases from the morning time, i.e. 800 hrs to 1400 hrs when it is maximum, i.e. 1135 W/m^2, and thereafter decreases in the evening hours which can be observed in Figure 4.7**.**

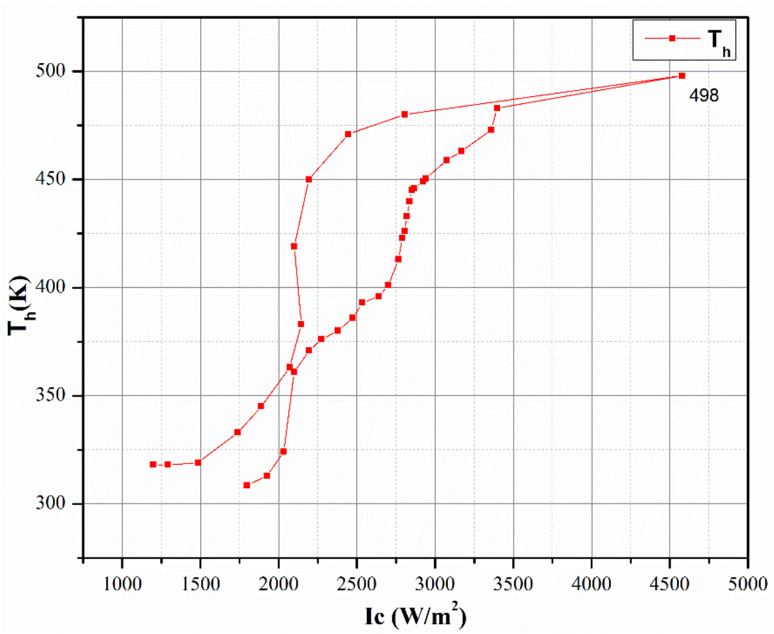

Figure 4.8: *Variation of temperature at hot side of TEG w.r.t. concentrated solar flux at absorber surface*

Figure 4.8 shows the maximum temperature obtained on the hot junction is 498K while the temperature at the cold junction is almost the same throughout the day. Again this maximum value of the temperature at the hot junction is obtained at 1400 hrs when the global incoming radiation and the concentrated radiant flux on the absorber are also maximum, i.e. 1135 and 4580 W/m^2 respectively. Also, maximum temperature difference obtained across the junction is 190K and mimimum is 10 K. These results have been validated by [77] [15][228].

4.2.3 Energy losses

One way to create a greater temperature difference is to use optical means (optical concentration) to focus more sunlight on the thermoelectric generator, which means increasing the heat flow. A ΔT of 247^{o}C (520K) or 200^{o}C (473K) is possible with an optical concentration (C_{opt}) of (40-200), depending on the length of the thermoelectric element. Telkes, in the year 1954, reported an efficiency of 3.35 % using thermoelectric elements built of p-type ZnSb alloy and n-type Bi-based alloy with an optical concentration of 50. However, tracking is necessary for optical concentration by a factor of (40-200), which is undesirable due to the system's poor efficiency [131]. As already discussed thermal concentration is another method for achieving the required temperature differential throughout the thermoelectric device. Through lateral heat conduction inside the extremely thermally conductive absorber substrate, solar energy is converted into heat and thermally concentrated onto the thermoelectric components. Several solar thermal devices have made use of this strategy for heat concentration via conduction. Heat concentration incurs losses, just as optical concentration does. Multiplying the thermal concentration by the optical concentration and then dividing it by the optothermal efficiency (η_{ot}) yields the energy flow concentration through the absorber. Variation of Incident solar power, convective and radiative losses, power output with respect to time is shown in Table 4.2.

Table 4.2: Variation of Incident solar power, convective and radiative losses, power output with respect to time

Time (hrs)	Q_i (W)	$hconv._{(l-a)}$ (W)	$Qconv._{(l-a)}$ (W)	$Qrad._{(l-a)}$ (W)	$Qrad._{(l-h)}$ (W)	Qabs (W)	$Qrad._{(h-l)}$ (W)	$Qrad_{(h-c)}$ (W)	$Qconv_{(h-a)}$ (W)	Q_h (W)	Q_c (W)	P_{out} (W)
800	922.46	6.68	0	0	-0.70	162.16128	0.00733211	0.00637406	0.6607744	2.82011512	2.81902418	0.001090938
815	988.68	6.53	0	0	-1.53	173.80224	0.01589376	0.01007519	0.993472	5.75860642	5.73291536	0.025691062
830	1042.58	6.57	0	0	-3.81	183.27744	0.03961364	0.02233086	2.0984208	12.0842858	11.972211	0.11207488
845	1078	7.29	0	0	-14.21	189.504	0.14760796	0.07276382	6.3212544	32.9062822	32.1157475	0.790534688
900	1127.28	7.52	0	0	-17.55	198.16704	0.18235793	0.08966866	7.6624416	38.7751115	37.6971285	1.077982922
915	1167.32	8.32	-7.69	-0.60	-19.47	205.20576	0.20231475	0.09767683	8.9811024	41.1511818	39.9497717	1.201410105
930	1221.22	6.53	-6.04	-0.61	-20.84	214.68096	0.2165253	0.10512474	7.45104	43.5268104	42.1936666	1.333143826
945	1270.5	6.68	-8.24	-0.81	-23.17	223.344	0.24078083	0.1167462	8.2342656	47.1102865	45.5685591	1.54172732
1000	1301.3	7.18	-8.84	-0.81	-26.04	228.7584	0.27059253	0.13002402	9.4974768	50.7498694	48.9907477	1.759121688
1015	1355.2	7.67	-9.45	-0.82	-27.27	238.2336	0.28332638	0.13637375	10.500768	52.5684421	50.6943663	1.874075871
1030	1386	7.63	-9.41	-0.82	-29.36	243.648	0.30501775	0.14728209	11.029272	55.6161801	53.5439722	2.072207969
1045	1419.88	7.67	-9.46	-0.82	-34.95	249.60384	0.36310708	0.1741857	12.3675712	62.4567866	59.9272024	2.529584133

1100	1432.2	8.96	-11.05	-0.83	-39.95	251.7696	0.41505017	0.19936697	15.8123776	68.7440705	65.7643645	2.979705975
1115	1439.9	9.46	-14.57	-1.04	-41.57	253.1232	0.43191992	0.20727825	17.1148656	70.651522	67.5316135	3.119908518
1130	1447.6	7.10	-10.94	-1.04	-45.43	254.4768	0.47195951	0.22639891	13.6094112	75.1427803	71.687097	3.455683276
1145	1456.84	6.80	-10.47	-1.04	-49.43	256.10112	0.51356933	0.24646974	13.7509232	79.6936104	75.8908275	3.802782842
1200	1463	6.84	-10.53	-1.04	-52.35	257.184	0.54393336	0.26140492	14.347584	82.9826065	78.9254885	4.05711802
1215	1470.7	5.96	-9.19	-1.05	-52.84	258.5376	0.54904939	0.26445303	12.6049648	83.6443784	79.5357889	4.108589542
1230	1501.5	6.49	-11.01	-1.16	-54.64	263.952	0.56768968	0.27372115	14.0252832	85.6378227	81.3736599	4.264162793
1245	1509.2	6.72	-10.36	-1.06	-55.50	265.3056	0.57671849	0.27842543	14.6707512	86.6391803	82.2965965	4.342583863
1300	1578.5	10.29	-15.86	-1.06	-61.07	277.488	0.63451793	0.30598431	23.7924992	92.3737963	87.5793534	4.794442868
1315	1626.24	6.76	-10.42	-1.06	-63.75	285.88032	0.66230113	0.31949438	16.0387968	95.1090793	90.0979287	5.011150584
1330	1724.8	6.30	-5.83	-0.64	-70.78	303.2064	0.73537856	0.35383261	15.820464	101.528875	96.0360194	5.492855518
1345	1743.28	6.38	-5.89	-0.64	-78.38	306.45504	0.81442999	0.39148719	16.98144	108.647001	102.593346	6.05365491
1400	1747.9	6.42	-9.88	-1.06	-90.82	307.2672	0.9435934	0.45252465	18.546736	119.653333	112.741899	6.911434628
1415	1439.9	6.38	-5.89	-0.64	-76.07	253.1232	0.79034571	0.379942	16.6903296	106.493793	100.609483	5.884310432
1430	1255.1	6.23	-5.75	-0.62	-69.77	220.6368	0.72493197	0.34758486	15.5351296	100.653368	95.2019136	5.451454521

1445	1125.74	7.18	0	0	-55.42	197.89632	0.57580417	0.2768521	15.6107952	86.3050477	81.9886502	4.316397444
1500	1078	6.53	7.04	0.72	-37.69	189.504	0.39166463	0.19006989	11.2262336	66.7800251	63.9315391	2.848486072
1515	1101.1	6.46	7.96	0.82	-21.45	193.5648	0.22285282	0.1108672	7.658976	45.315435	43.8796209	1.435814079
1530	1062.6	6.53	7.04	0.72	-14.21	186.7968	0.14768799	0.07603456	5.8614848	34.0760661	33.2312603	0.844805849
1545	970.2	8.32	8.97	0.72	-8.82	170.5536	0.09163317	0.04848913	5.1862704	23.6064815	23.189363	0.417118471
1600	893.2	6.99	6.46	0.61	-5.5941656	157.0176	0.0581212	0.03333147	3.188352	17.2632956	17.0367386	0.226557034
1615	762.3	6.80	4.19	0.41	-2.2659789	134.0064	0.02354264	0.01660256	1.6542464	9.20919497	9.1438069	0.065388071
1630	662.2	6.72	3.11	0.30	-2.0812628	116.4096	0.02162351	0.01644299	1.6357632	9.21439337	9.14888567	0.0655077
1645	616	6.95	2.14	0.20	-2.1017226	108.288	0.02183608	0.02846667	1.585512	8.63419039	8.57666368	0.057526706

Incoming solar energy including various losses like convective, radiative, and conductive for the system at regular intervals of time are observed and calculated throughout the day. In coming radiation heat (Q_i) incident on lens is 1432.2 W at 1100 hrs and 1747.2 W at 1400 hrs. The variation of heat incident on lens and global radiation with respect to time is shown in Figure 4.9 **(a)** and enegy absorbed by the absorber throughout the day is shown in Figure 4.9 **(b).**

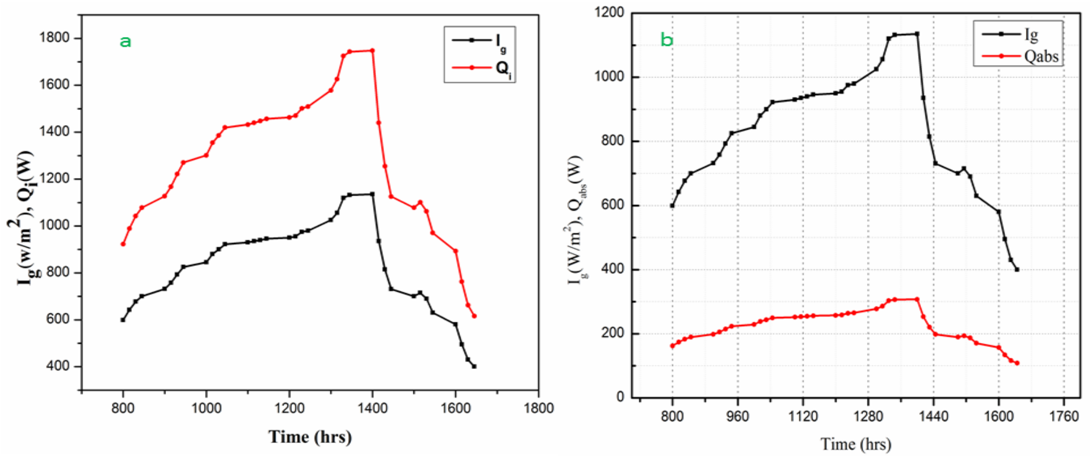

Figure 4.9: *(a)Variation of global radiation and incident solar power (Q_i) on the lens aperture w.r.t time; (b) Variation of global radiation and heat absorbed by the absorber (Q_{abs}) w.r.t time*

Temperature of the water and LLDPE plastic is observed almost equal to that of the surroundings at the beginning of the day, as the ambient temperature starts increasing during the day time with respect to the global radiation, therefore in order to maintain the equilbrium the water in the lens absorbs heat from the surroundings and gets heated up. This is supported by heat losses calculated at every 15-minute time interval.

The temprature difference between water and surrounding $(T_l - T_a)$, convection coefficient $h_{conv(l-a)}$ contributes to convective losses and these losses are represented by $h_{conv,l-a}A_l(T_l - T_a)$. The convective coefficient from lens-water to surrounding varies between 8.968 at 1100 hrs and 6.42 at 1400 hrs. At 800 hrs, the net convectional and radiative heat losses from the water to air are very less, and the heat absorption by water from air starts increasing as it can be seen that the convectional $Q_{conv(l-a)}$ and radiative heat gain $Q_{rad(l-a)}$ by the water from the air varies between -11.04 W to -9.88 W and -0.829 W to -1.067 W during 1100 hrs to 1400 hrs. The negative sign indicates that the heat flows from surrounding ambiance to water. After this, as the ambient temperature cools down, the water in the lens starts losing heat to the surroundings. At 1500 hrs, the convectional and radiative heat losses from the water to air are 7.045808 W and 0.72589803 W respectively further decreasing to 2.14 W and 0.20 W respectively at 1645 hrs. The radiative losses are represented by $\varepsilon_l \sigma_{sb} A_l (T_l^4 - T_a^4)$, depends on fourth order temprature difference between water and surrounding $(T_l^4 - T_a^4)$ and emittance of the lens (ε_l=0.10), which is combination of emittance of water (ε_w=0.03) and emittance of polythene/plastic (ε_p=0.02).

The radiative heat loss from lens to hot side (absorber) $Q_{rad(l-h)}$ varies between -39.94 W and -90.82 W from 1100 hrs to 1400 hrs. The radiative losses between lens and hot side are represented by $\varepsilon_{lh} \sigma_{sb} A_l (T_l^4 - T_h^4)$ .The variation of convective and radiative heat loss from the lens throughout the day is shown in Figure 9.10 **(a)**.

Convective heat loss from hot side to surrounding $Q_{conv(h-a)}$ varies between 15.82 W and 18.54 W from 1100 hrs to 1400 hrs and is represented by $h_{conv,h-a}(A_{ab} - A_{mod})(T_h - T_c)$. The radiative heat loss from hot side to lens $Q_{rad(h-l)}$ varies between 0.415 W at 1100 and 0.943 W from 1100 hrs to 1400 hrs and is represented by $\varepsilon_{hl} \sigma_{sb} A_{ab} (T_h^4 - T_l^4)$. The radiative heat loss from hot side to cold side $Q_{rad(h-c)}$ varies between 0.1993 W and 0.452 W 1100 hrs to 1400 hrs and is represented by $\varepsilon_{hc} \sigma_{sb} (A_{ab} - A_{mod})(T_h^4 - T_c^4)$. The effective emittance is $(\varepsilon_{lh} + \varepsilon_{hc} = 0.03)$ .The variation of all the convective and radiative heat loss from the absorber's hot side throughout the day is shown in Figure 4.10 **(b)**.

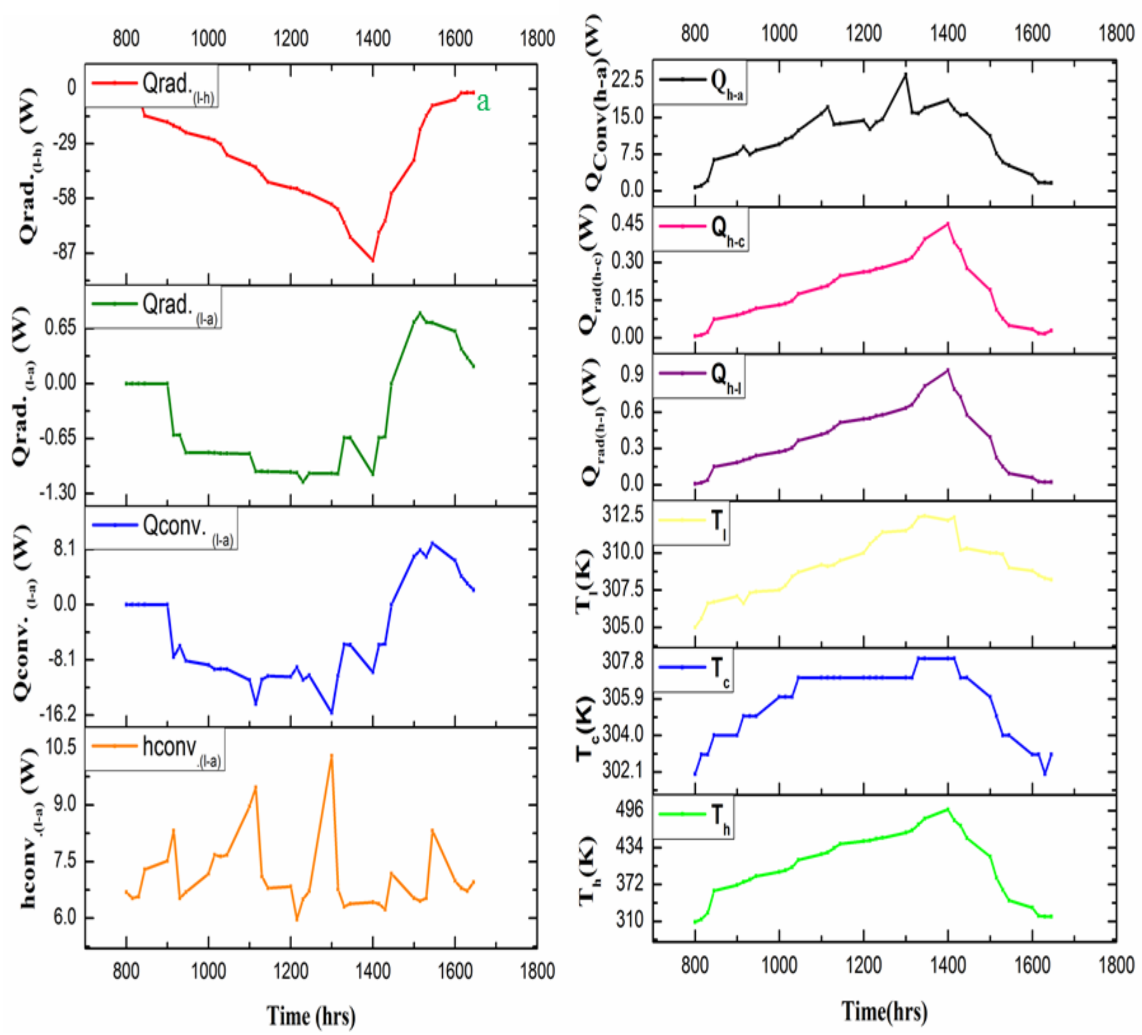

Figure 4.10: *(a) Variation of air convection coefficient, convective (Q_{conv}) and radiative (Q_{rad}) losses from the lens w.r.t time; (b) Variation of hot side temperature, cold side temperature, lens temperature, convective (Q_{conv}) and radiative losses (Q_{rad}) from hot side (absorber) w.r.t time*

Heat absorbed by absorber Q_{abs} varies between 251.76 W and 307.267 W 1100 hrs to 1400 hrs and is represented by $\tau_l \alpha_{ab} C_{th} I_g A_{ab}$, where transmittance of lens $(\tau_l = 0.90)$ which is a combination of transmittance of water $(\tau_P = 0.94)$ and transmittance of Plastic $(\tau_P = 0.95)$ and $\alpha_{ab} = 0.94$ is the absorptance of absorber. The variation of energy absorbed by the absorber with respect to global radiation throughout the day is shown in Figure 4.11.

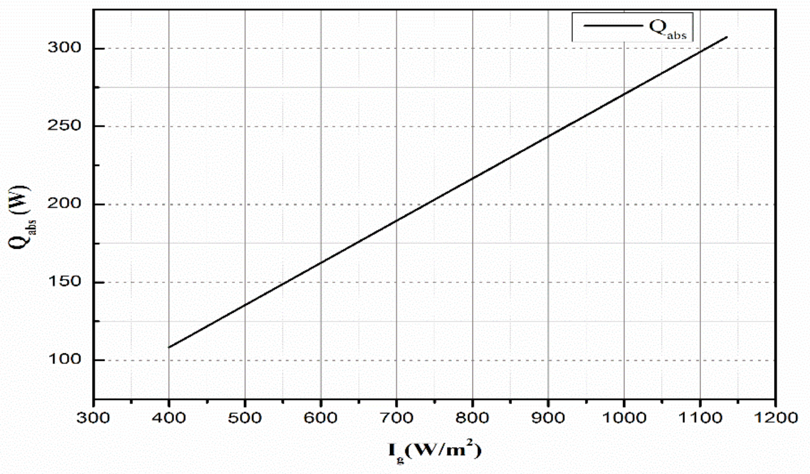

Figure 4.11: *Variation of heat absorbed by absorber (Q_{abs}) w.r.t global radiation*

Net heat transferred to module hot side Q_h is 68.74 W at 1100 hrs and 119.65 W at 1400 hrs. The heat rejected from cold side Q_c is 65.76 W at 1100 hrs and 112.74 W at 1400 hrs, therefore generated electrical power P_{out} is 2.97 W at 1100 hrs and 6.91 W at 1400 hrs that will be delivered to load, which is equal to the difference Q_h- Q_c as shown in Figure 4.12.

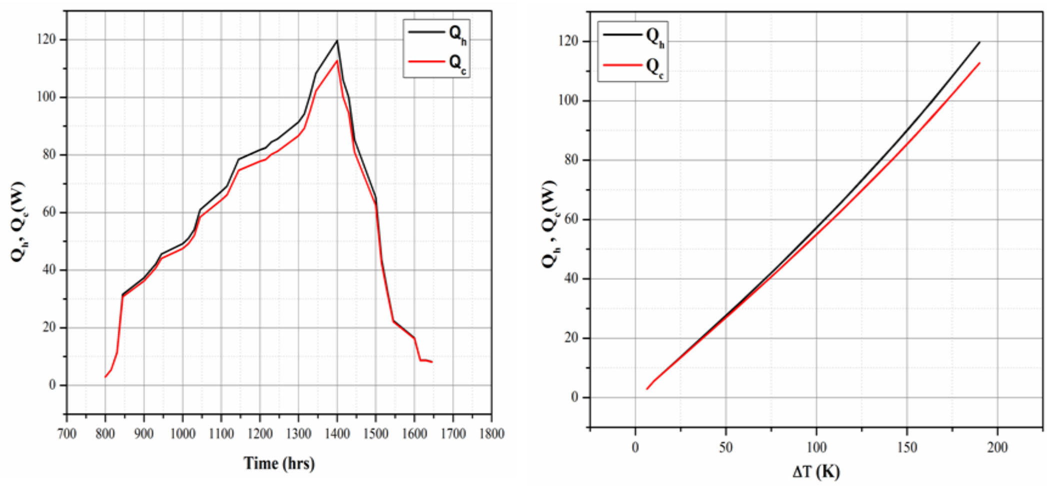

Figure 4.12: *Variation of heat input to the module (Q_h) and heat rejected from the module (Q_c) w.r.t time and ΔT*

Losses due to convection and radiation grow in proportion to the increment of the temperature difference. For each combination of geometry of thermoelectric element and sun intensity, there exists a maximum thermal concentration. However, upon a very low level of thermal concentration, the TE efficiency of the thermoelectric device gets reduced, since the temperature differential between the solar absorber and the surroundings is not as great as required. The highest temperature achieved will be too high if the thermal concentration is high enough, but it makes η_{ot} too small. Furthermore, following a high temperature of around 498K, the ZT falls with a further increase in temperature. Opto-thermal efficiency improves with increasing incoming solar flux; at 1135 W/m^2 because the thermal concentration drops and leads to lowering radiation losses from the absorber. We determined that a thermal concentration of around 20 is appropriate for the thermal needs of the selected element size.

4.2.4 Voltage, current and power output

The maximum values of open circuit (V_{oc}), Load voltage (V_L), current (I) and power (P) are 11.1V, 5.5 V, 1.24 A and 6.9 W respectively which are obtained at 1400 hrs. The no load voltage/open circuit voltage reaches from 6.8 V at 1100 hrs to 11.49 V at 1400 hrs and then to 6.6 V at 1500 hrs because at this instant of the day the temperature at the hot junction also reaches its maximum value which is 498K. The load voltage reaches from 3.3 V at 1100 hrs to 5.5 V at 1400 hrs and then to 6.14 V at 1500 hrs. The load current reaches from 0.88 A at 1100 hrs to 1.24 A at 1400 hrs and then to 0.87 A at 1500 hrs. The value of power reaches from 2.9 W at 1100 hrs to 6.9 W at 1400 hrs and then to 2.84 W at 1500 hrs. The variation in open circuit (V_{oc}), Load voltage (V_L), current (I) and power (P) with respect to time is shown in Table 4.3 and graphically represented in Figure 4.13.

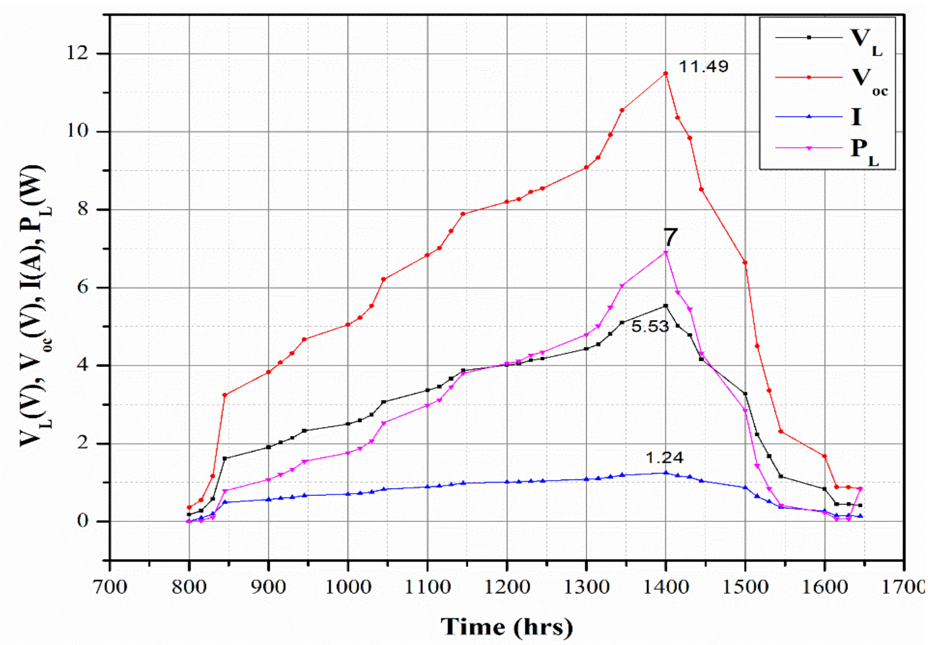

Figure 4.13: *Variation in open circuit (V_{oc}), Load voltage (V_L), current (I) and power (P) with respect to time*

Table 4.3: Variation of Current, voltage, power, efficiency with respect to time

Time (hrs)	**I (A)**	**I_p (A)**	**V_L (V)**	**P_L (W)**	**V_{oc} (V)**	**η_{ot} (%)**	**η_{ot} (%)**	**η_{te} (%)**	**η_{syst} (%)**
800	0.006127589	0.006127589	0.178037	0.0010909	0.356091465	0.8398950	83.9894988	0.14007107	0.117644991
815	0.093414435	0.093414435	0.2750224	0.0256911	0.55010818	0.8398451	83.9845131	1.08385909	0.910273775
830	0.192576108	0.192576108	0.5819771	0.1120749	1.164541225	0.8396745	83.9674490	2.23949587	1.880447552
845	0.489530914	0.489530914	1.6148821	0.7905347	3.241503862	0.8389742	83.8974194	5.72624468	4.804171513
900	0.56527421	0.56527421	1.9070088	1.0779829	3.833083668	0.8387911	83.8791137	6.61618508	5.549597401
915	0.592797025	0.592797025	2.0266804	1.2014101	4.076049472	0.8387283	83.8728343	6.94444932	5.824506469
930	0.621700731	0.621700731	2.1443498	1.3331438	4.31544306	0.8386918	83.8691784	7.28356825	6.108668847
945	0.664181549	0.664181549	2.3212438	1.5417273	4.676176757	0.8386035	83.8603514	7.7814631	6.525562305
1000	0.703311967	0.703311967	2.5011969	1.7591217	5.044137557	0.8384815	83.8481501	8.24359582	6.912102596
1015	0.723575437	0.723575437	2.5900214	1.8740759	5.226255579	0.8384707	83.8470689	8.48023492	7.110428416
1030	0.756776578	0.756776578	2.7382031	2.072208	5.53075691	0.8383851	83.8385065	8.8673791	7.434278204
1045	0.824620412	0.824620412	3.067574	2.5295841	6.210648883	0.8381356	83.8135642	9.65820419	8.094885172

1100	0.885609955	0.885609955	3.3645805	2.979706	6.828109299	0.8378845	83.7884476	10.3621125	8.68225321
1115	0.903367097	0.903367097	3.4536442	3.1199085	7.014113959	0.8378123	83.7812290	10.5662152	8.852504946
1130	0.943839988	0.943839988	3.661302	3.4556833	7.449411917	0.8376232	83.7623192	11.0298023	9.238818246
1145	0.982978212	0.982978212	3.8686339	3.8027828	7.886406181	0.8374289	83.7428893	11.4757354	9.610112401
1200	1.010123794	1.010123794	4.0164562	4.057118	8.199511228	0.8372846	83.7284575	11.7834992	9.866142157
1215	1.015472352	1.015472352	4.0459886	4.1085895	8.262223922	0.8372673	83.7267294	11.8439799	9.916576986
1230	1.031357565	1.031357565	4.1345145	4.2641628	8.450538526	0.8372295	83.7229543	12.0232833	10.06624802
1245	1.039210137	1.039210137	4.1787351	4.3425839	8.544792768	0.8371963	83.7196307	12.1117343	10.13989927
1300	1.082581	1.082581	4.4287151	4.7944429	9.08005082	0.8370541	83.7054066	12.5979044	10.54512707
1315	1.102332119	1.102332119	4.5459535	5.0111506	9.332569459	0.8370143	83.7014294	12.8178824	10.7287508
1330	1.141495141	1.141495141	4.8119833	5.4928555	9.90873132	0.8368823	83.6882349	13.244255	11.08388319
1345	1.186574462	1.186574462	5.101791	6.0536549	10.5433235	0.8365871	83.6587137	13.7355369	11.49097345
1400	1.249447134	1.249447134	5.5315943	6.9114346	11.4979943	0.8360655	83.6065459	14.4089375	12.04681497
1415	1.173318762	1.173318762	5.0150996	5.8843104	10.35276606	0.8359899	83.5989917	13.5917456	11.36256226
1430	1.140581681	1.140581681	4.7795389	5.4514545	9.838696376	0.8357913	83.5791272	13.24107	11.06677077

1445	1.03659927	1.03659927	4.1639982	4.3163974	8.513367633	0.8362625	83.6262526	12.0823395	10.10400776
1500	0.870449261	0.870449261	3.2724321	2.8484861	6.636332252	0.8373204	83.7320443	10.1859494	8.5289037
1515	0.643072009	0.643072009	2.2327423	1.4358141	4.495567405	0.8384698	83.8469812	7.53413577	6.317145405
1530	0.504917331	0.504917331	1.6731568	0.8448058	3.359332921	0.8389125	83.8912549	5.9070615	4.955508024
1545	0.362122671	0.362122671	1.1518706	0.4171185	2.30811031	0.8392405	83.9240458	4.22937511	3.549462706
1600	0.270926219	0.270926219	0.8362315	0.226557	1.674174551	0.8394329	83.9432881	3.15566344	2.648967653
1615	0.14796784	0.14796784	0.4419073	0.0653881	0.884074289	0.8396690	83.9669008	1.71903736	1.443422398
1630	0.148455618	0.148455618	0.4412612	0.0655077	0.882782003	0.8396226	83.9622636	1.7222481	1.446038489
1645	0.138953246	0.138953246	0.4140004	0.8282148	0.8396179	83.9617877	0.01613975	0.01355122	0.000483813

In this project, two Bi_2Te_3 TEG modules (20 mm × 20 mm × 4 mm) were used for experiment. Bismuth telluride alloy is the material of which module is made and the length of the TE element is 1.60 mm. Specifications of TEG according to the supplier are as figure of Merit of TE material (Z=1), rated power 10 W, rated voltage 12V, rated current 1.66 A at T_h= 230 ^{0}C (503 K) and T_c= 30^{0}C (303 K). The internal resistance of TEG module is 2.5 Ω at the maximum processing temperature 503 K. However, in this research, 4.42 Ω internal resistance for two modules connected in series, is obtained because temperature reaches to maximum value of 498K. The change in internal resistance with mean temperature can be seen inFigure 4.14**.**

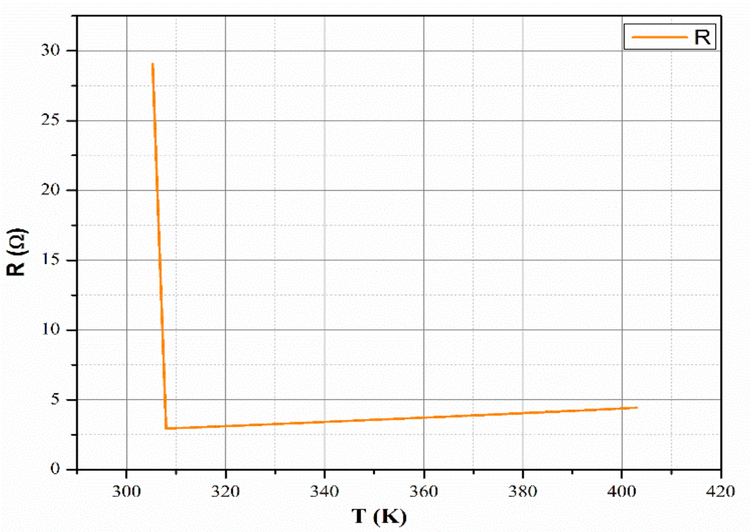

Figure 4.14: *Variation of internal resistance of TEG with mean temperature*

Open circuit test and load tests (R_{fan}=96 Ω, R_1=4.63 Ω, R_L= $R_{fan}\|R_1$=4.42 Ω,) are performed to analyse the performance of TE module, but the TEG produces open circuit voltage (6.8-11.49 V) and load voltage in the range (3.3-5.5 V), current in the range (0.88-1.24 A) and Power in the range (2.97-6.91≈7 W).

GWLSTEG concentrates solar radiation that starts to raise the temperature of hot side. Voltage build-up process starts at T_h =308.5K with a value of 0.35 V and reaches the value of 11.49 V at 498 K instead of a rated voltage of 12 V, current of 1.24 A instead of 1.66 A and power of 6.94≈7 W instead of 10 W for the global radiation 1135 w/m^2. The decrement in ΔT takes place due to increased air velocity and relative humidity therefore all the performance parameters do not match with the supplier's specification. The GWLSTEG system provides hot side temperature (T_h=498 K), Cold

Side Temperature (T_c=308 K), Average receiver temperature (T=403 K), maximum open circuit Voltage 11.49 V, maximum load Voltage 5.5 V Current 1.24 A, Power 7 W with the maximum overall efficiency of 12.04%. The change in current with respect to ΔT can be seen in Figure 4.15**.**

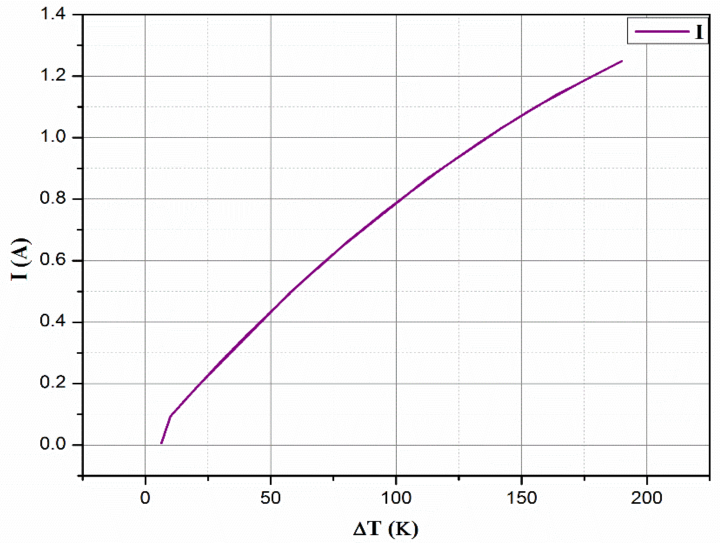

Figure 4.15: *Variation in load current with ΔT*

Maximum power to the load is transferred in the case only when internal and load resistances of the TEG are equal. At this operating point, the generator's internal resistance and the load will both dissipate the same amount of power (i.e., 50 % of electrical efficiency) [114]. To obtain maximum electrical power output the load resistance is kept equal to the internal resistance of TEG. The variation of current with changing internal resistance is shown in Figure 4.16. As the resistance decreases Current increases. The operating internal resistance is 4.42 Ω which is why maximum current is obtained at this point. Further discussion about the results and optimization of load is as follows:

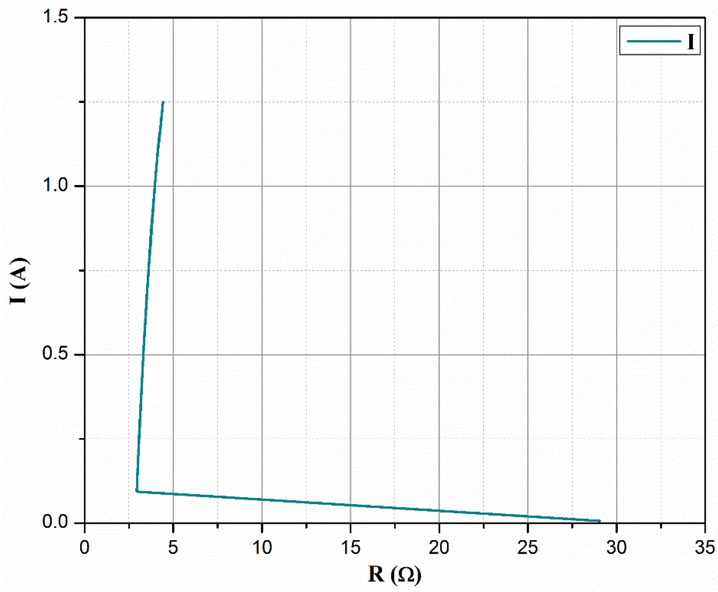

Figure 4.16: *Variation in load current with internal resistance*

Device was kept under sunshine for an hour so that it could achieve steady state. As the incoming solar radiation increases during the day, the hot side temperature increases, and the DC fan maintains cold side temperature between (302-308) K during (1100 hrs-1400 hrs). At the beginning of the day around 800 hrs when T_h =308.5 K and T_c = 302 K, no open circuit voltage build up process starts up at ΔT =6.5 K and is observed as 0.35 V as shown in Figure 4.17. As time passes after 800 hrs solar radiation increases, which leads to increased hot side temperature that raises open circuit voltage. The maximum no-load voltage is achieved as 11.49 V at 1400 hrs when the global radiations are observed as 1135 W/m^2. Due to the change in concentrated radiation on the absorber plate, hot side temperature changes and hence all the maximum values are obtained at highest hot side temperature as shown in Figure 4.17**.** The no-load test and load test were conducted simultaneously on the TEG after each 15 minute interval. For every instantaneous global radiation value open circuit voltage was observed, at the same moment TEG was loaded with load (R_L) consecutively and hence all other parameters like voltage, current and power of TEG were observed and calculated as shown in Figure 4.17. The maximum load voltage 5.5 V, load current of 1.24 A, and power of 7 W were observed.

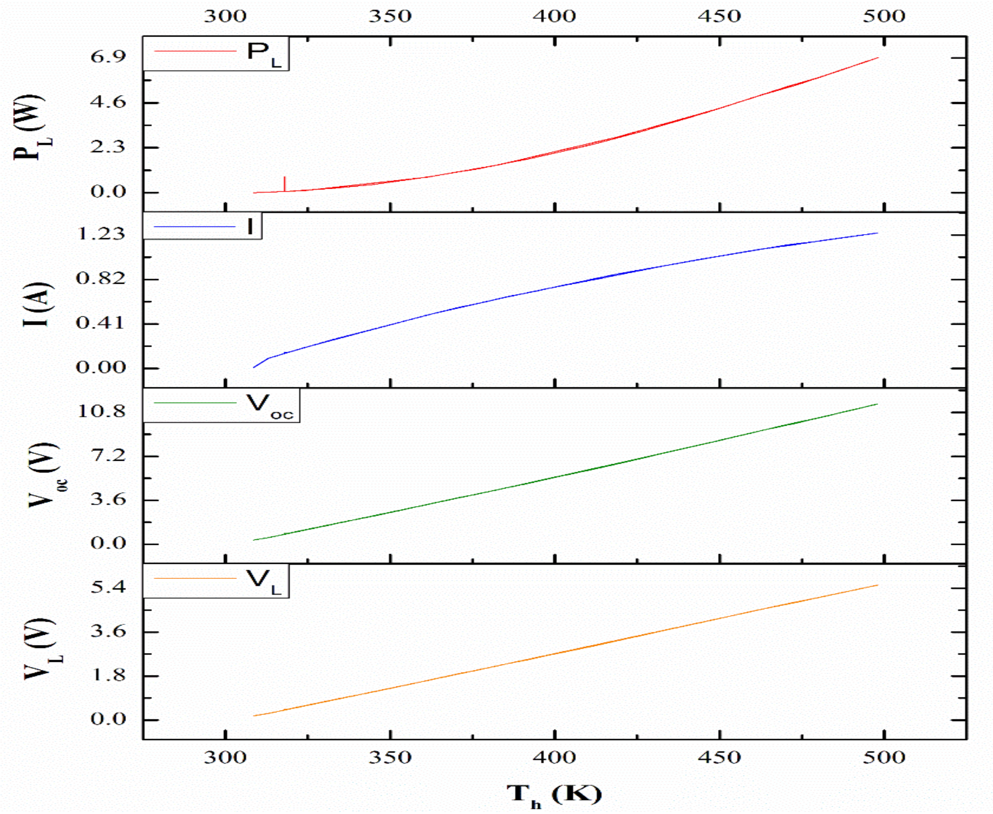

Figure 4.17: *Variation of open circuit (V_{oc}), Load voltage (V_L), current (I) and power (P) with respect to hot side temperature (Tc: 302-308 K, R $_{fan}$=96 Ω R_1=4.63 Ω R_L= 4.42 Ω)*

Based on the phenomena of the TE, 5 effects are there that are under simultaneous operation inside the circuit. These effects are Fourier, Joule, Thomson, Peltier, and Seebeck effects. The electrical power output of a thermoelectric generator is $P_{out} = Q_h - Q_c$ as per Eq (3.30). From Eq (3.25) and (3.26) it can be seen that Q_h and Q_c depend on T_h, T_c, S_h, S_c, K, I and μ. The key role is played by hot and cold side temperature. However, the effect of other factors can't be neglected.

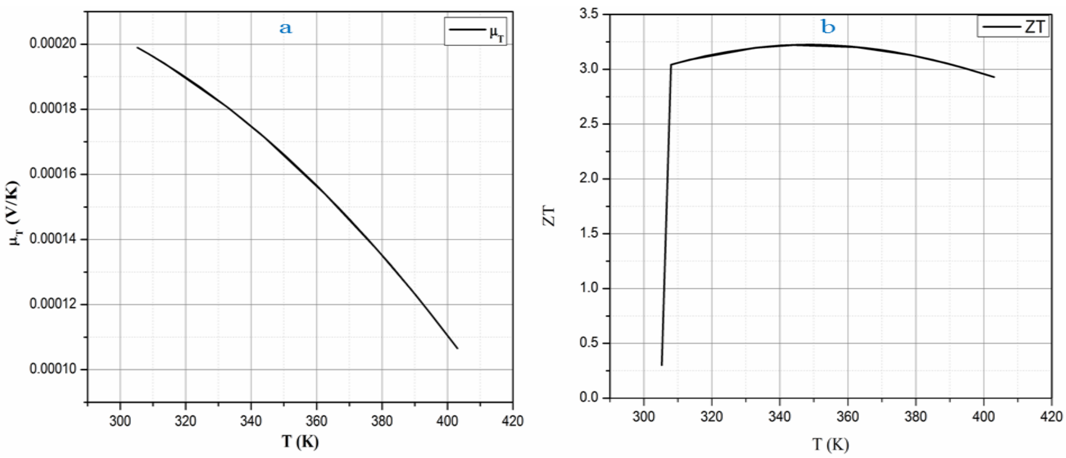

Figure 4.18: *Variation of (a) Thomson coefficient; (b) Figure of merit with mean temperature*

In Equation (3.25) and (8.24), Reversible Peltier heat is represented by the 1st term, irreversible Joule heating by the 2nd, irreversible Fourier heat conduction from the heated side to the cold side by the 3rd, and reversible Thomson heat by the 4th. In the presence of a temperature gradient, a single conductor carrying a current along its length will either release or absorb heat, this action is known as the Thomson effect. When an electric current moves through a conductor, it creates Joule heat, also known as the Joule effect. Conductive heat transfer across connections of different temperatures is what the Fourier effect is all about. Figure 4.18 exhibits the figure of merit (ZT) and Variation of Thomson coefficient (μ_T) along with the mean temperature. Thomson effect drastically decreases both power and efficiency. As average temperature rises, μ_T falls. The value of μ_T is 0.0193 at 1100 hrs and 0.0136 at 1400 hrs and gradually decreases.

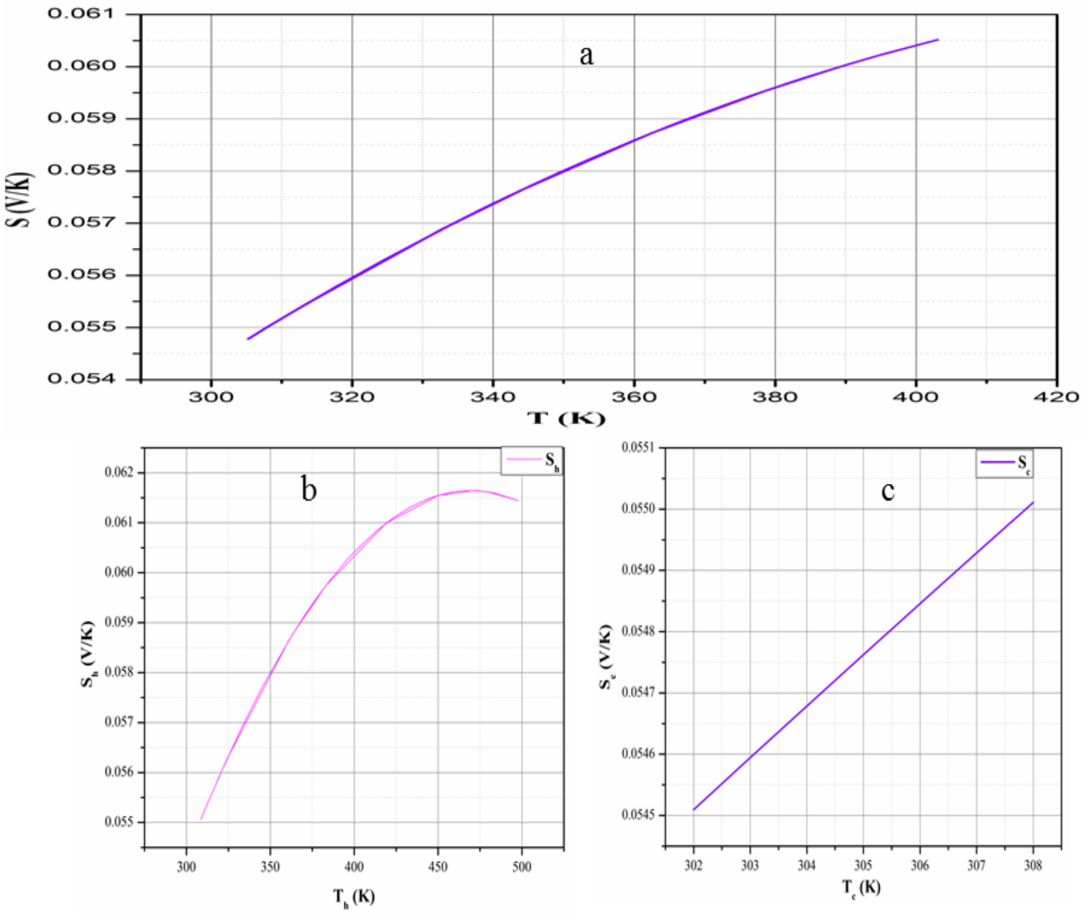

Figure 4.19: *Variation of Seebeck coefficient with (a) mean temperature, (b) hot side temperature, (c) cold side temperature*

In Eq (3.30) first term is $(S_h T_h - S_c T_c)I$ where Seebeck coefficient is denoted with S, which is TEM property. There is a unique Seebeck coefficient (S) for every type of TEM. This is the magnitude of the thermoelectric voltage caused by a temperature gradient across the material. Volts per kelvin (V/K) is the unit for thermo-power (S). Then, we may quantify the performance of this device, technique, or system by calculating the figure of merit using the values for electrical and thermal conductivity. Since the Seebeck coefficient of a suitable thermoelectric material is between 100 and 300 μV/K, multiple thermoelectric couplings must be coupled in series to produce even a few volts at the load. Because of their low Seebeck coefficient, metals have a poor thermoelectric figure of merit at low temperatures. Bi_2Te_3 semiconductor is employed in this project, and its Seebeck coefficient rises steadily with mean temperature from 0.00045 V/K at 1100 hours to 0.00047 V/K at 1400 hours, then back down to 0.00045 V/K at 1500 hours as shown in Figure 4.19 **(a)**. The variation of S_h and S_c with mean temperature is shown in Figure 4.19 **(b)** and **(c).**

Unlike the thermal conductivity (k), which has a negative effect on the figure of merit (ZT), the electrical conductivity (σ) and the Seebeck coefficient of the thermoelectric material both have positive effects on ZT. The variation of (k) can be seen in **Fig. 33.** It changes as 1.63 W/mK at 1100 hrs, 1.77 W/mK at 1400 hrs and 1.62 W/mK at 1500 hrs as shown in Figure 4.20. Thermal conductivity is found to be reduced in nanostructured Bi_2Te_3 as compared to ordinary material. Thus the increased figure of merit is obtained and hence improved efficiency. For a long time, the worth of ZT was rather lower value. To improve the thermoelectric figure of merit, however, new methods have been developed since the late 1990s to boost thermal and electrical conductivity along with the Seebeck coefficient.

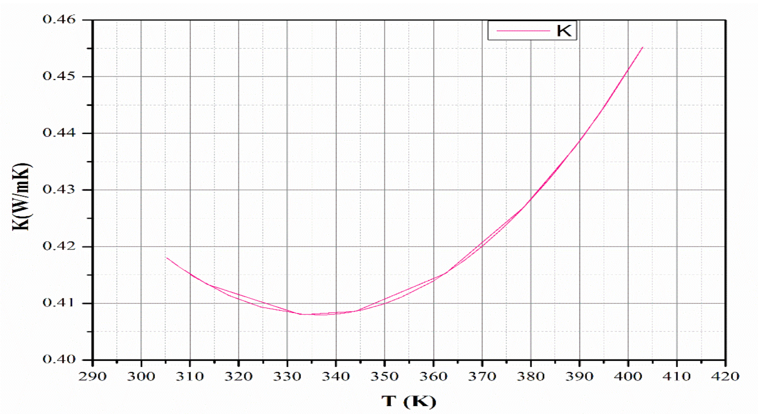

Figure 4.20: *Variation of thermal conductance with mean temperature*

If the difference in the temperature within the cold and the hot side is at its maximum then P_{out} will be maximum and so as the efficiency of a GWLSTEG. This will happen at the instant of maximum radiation. However maximum power transfer to the load R_L is so important in designing TEG systems. TEGs inherently do not work as "regulated power supplies" [229]. At any given ΔT, the load voltage decreases and increases respectively with the decrease and increase in the load resistance [230]. Because every TEG has a considerable amount of internal resistance, it refers that when electrical load draws more current, the dissipation of available power will be more in the TEG as exhibited in Figure 4.21.

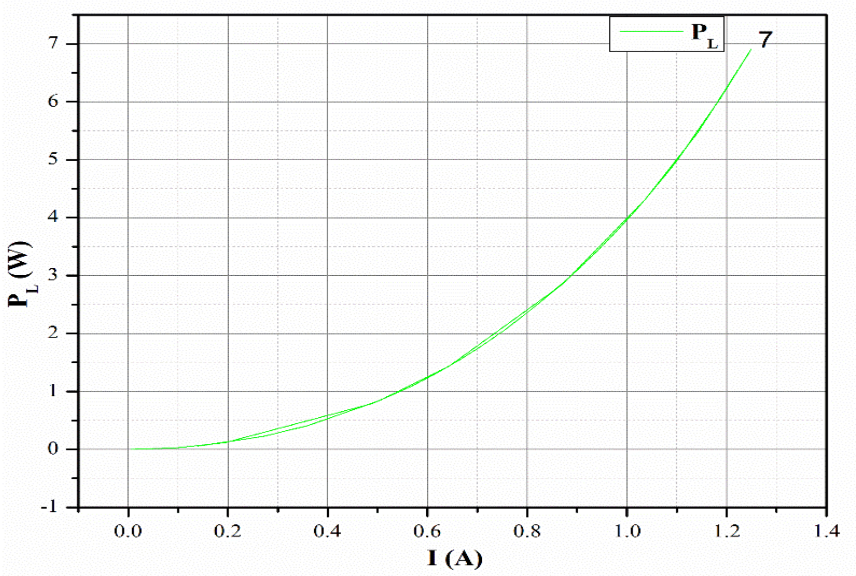

Figure 4.21: *Variation of output power with load current*

Moreover, there will be a considerable voltage drop across this internal resistance. Analysis of the voltage drop with the help of electrical model of TEG system is accomplished in this article. According to the voltage divider rule, the voltage across a series circuit made up of a no-load voltage (such as the open-circuit voltage output of a TEG) and the module's internal resistance R along with the electrical load R_L will drop as a function of this resistance. Thus, if we consider no-load voltage 12 V, the internal resistance is 4.42 Ω and the Full load R_L= 4.42 Ω (R_L=R_{fan}ǁ R_1), then from the voltage divider rule there would be a 6.2 V drop across the load.

$$V_L = V_{NL}\frac{R_L}{R+R_L} V_L = 12V\frac{4.42\Omega}{4.42\Omega+4.42\Omega} = 6\,V \qquad (4.1)$$

Consequently, the highest possible load power transmission is of paramount importance. If the resistance of the load is equal to the resistance of the voltage source, then the maximum amount of power will be transmitted from the source to the load [229], [230]**.** Here it is to be noted that this point of operation will not provide the maximum amount of voltage or current, but the greatest power can be derived at that point. The following formulas may be used to calculate load voltage, current, and power for a range of load resistances, for a given no-load voltage:

$$V_L = V_{NL} \frac{R_L}{R+R_L} \tag{4.2}$$

$$I_L = \frac{V_L}{R_L} \tag{4.3}$$

$$P_L = V_L . I_L \tag{4.4}$$

The variation of Load voltage with current (V-I characteristics) can be seen in Figure 4.22 **(a)** and power delivered to load with load voltage (P-V characteristics) can be seen in Figure 4.22 **(b)**. Load voltage increases with an increase in output current. The demand for load power at the required load current is fulfilled. The maximum power is delivered to the load at maximum voltage.

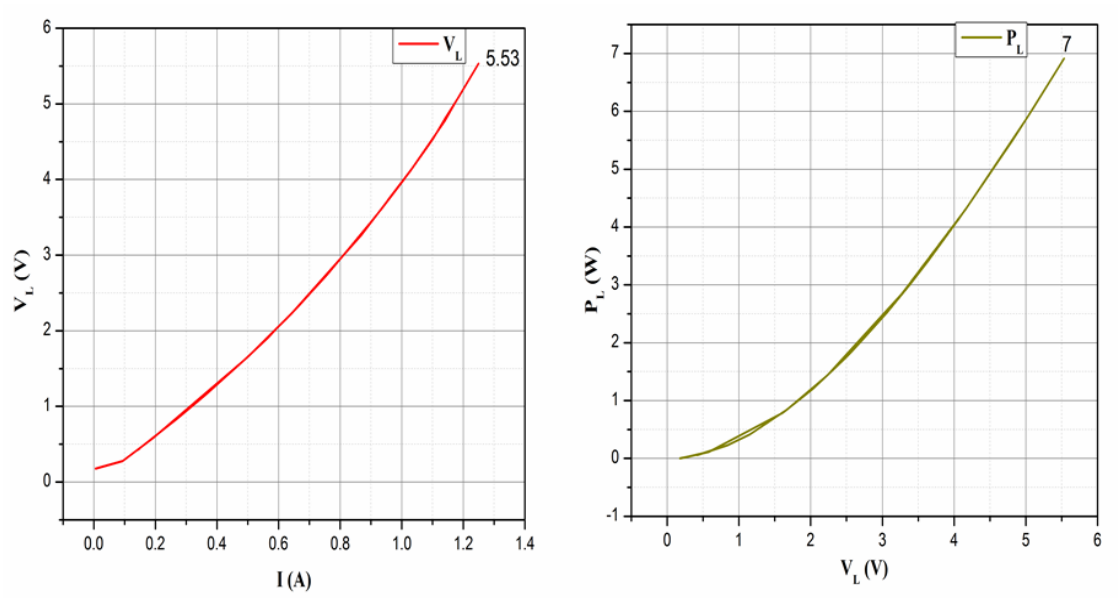

Figure 4.22: *(a)Variation of load voltage with current; (b) output power with load voltage*

It is fairly tricky to match the loads. It can be easily done when a TEG is customised for a particular project, then the optimization of the pallet configuration can be done for the specific application [231]**,** [232]. On the other hand, the best job of load-matching is the series/parallel module combination, for which the designer is left to arrive at. The fact that operating conditions might change over time, making our design suitable for one set of conditions but not another, would further complicate issues in many situations [120],[233]. The TEG has to be built for the worst case scenario due to the dynamic nature of the surrounding environment and/or the resistance of the loads. [233], [234].

Sometimes maximum power transfer couldn't be the priority, especially in those systems whose heat source is not waste heat. The efficiency of the power conversion process may be more of a concern here since it happens at a somewhat different operating point. To improve power transmission, however, TEG must make certain concessions[28],[234]. A significant power boost can be achieved by sacrificing a little bit of efficiency. Almost all TEG system layouts will be imperfectly matched [184], [232]. A given resistance with series/parallel combination is the sole approximation for a discrete construction block (in this case, individual TEG modules). In most cases, external load resistance should be greater than interior resistance (efficiency is a much more slippery slope when it is the other way around). Maximum power output, also known as optimum load matching, is where we often find the necessary load resistance. In the special case the optimal value of the load resistance must be [235]:

$$R_{L,opt} > R \tag{4.5}$$

Theoretical foundation for GWLSTEG's best performance is laid by the findings of the optimum load resistance calculations. Therefore, if there is any difference in operating circumstances, it will be necessary to investigate the range of module resistance that may provide results according to varying ambient states. It is thus obvious that while building a TEG system, one should do so with the worst-case scenario in mind, ensuring that the system can generate enough power during periods even when ΔT is low and high current demand, as well as at all other operational points.

4.2.5 Efficiency of the system

Figure 4.23 shows variation of "hot side temperature, cold side temperature, temperature difference between hot and cold side", optothermal, thermo-electrical, overall system efficiency and exergy efficiency of the system w.r.t. time and global radiation throughout the day. As the change in Global Incoming radiation takes place, the change in hot side temperature, cold side temperature, ΔT occurs, as a result of which variation in optothermal, Thermoelectric and overall System efficiency takes place. As the Global Incoming radiation increases, the concentrated flux at the absorber surface increases which leads to increase the hot side temperature and so as the ΔT. The overall system efficiency of the system (η_{sys}) is a product of two different efficiencies, i.e. optothermal efficiency (η_{ot}) and thermoelectric efficiency (η_{te}) of the TEG module. η_{ot} is the combination of the optical efficiency of water lens and thermal efficiency of the absorber. Optical efficiency η_{opt} of the water lens almost remains constant throughout the day while the optothermal efficiency decreases gradually since morning and reached almost minimum value i.e 83.60% at 1400 hrs, thermoelectric efficiency gradually increases and reaches its maxima at 1400 hrs, i.e. 14.4%, after which it starts decreasing because ΔT decreases. Consequently, the overall system efficiency is achieved maximum at 1400 hrs with a value of 12.04 % and exergy efficiency of 2.05% for the maximum incoming global radiation from the sun i.e.1135W/m^2, and T_h=498K, T_c =398K, ΔT=190K at 1400 hrs.

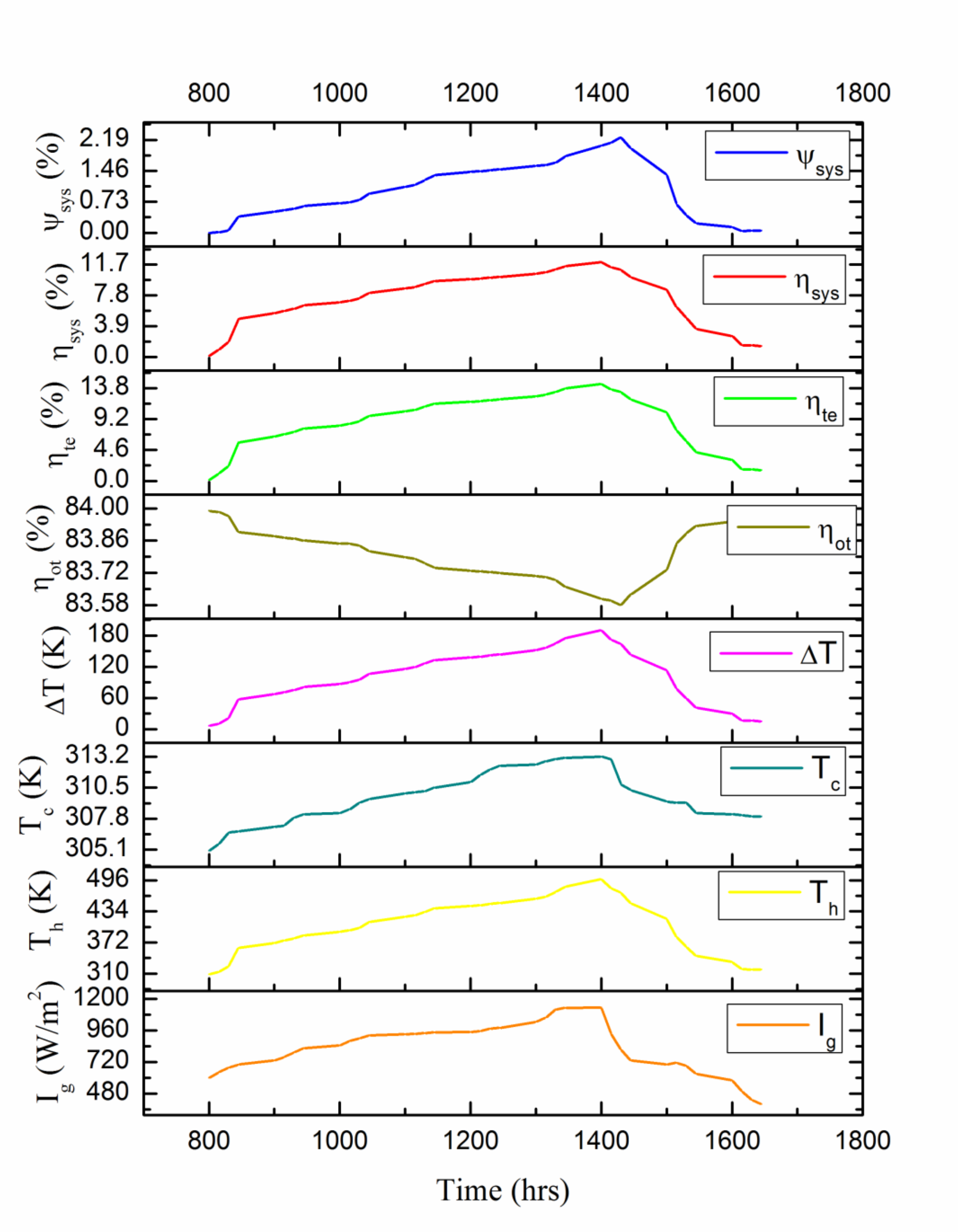

Figure 4.23: *Variation of global radiation, hot side temperature, cold side temperature, ΔT, optothermal, thermoelectrical, overall System Efficiency and exergy efficiency of the system w.r.t. time*

Optothermal efficiency (η_{ot}) is the function of optical efficiency (η_{opt}) which is the first term and ε_{lh}, ε_{hc}, σ_{sb} , $(T_h^4 - T_c^4)$, C_{th}, I_g which are the factors of second term. Optothermal efficiency is directly proportional to the $(T_h^4 - T_c^4)$, this factor of temperature difference becomes maximum at 1400 hrs and optothermal efficiency is inversely proportional to the global radiation therefore with increase in global radiation the second term in optothermal efficiency decreases, hence due to the net effect of first and second term the optothermal efficiency decreases with increase in global radiation. At 1400 hrs it is observed as almost minimum (83.60%). The thermoelectric efficiency (η_{te}) mainly depends on temperature difference $(T_h - T_c)$ and $\sqrt{1+zT}$. ΔT and mean T gradually increase with global radiation, because with the increase in global radiation, the concentrated radiation (I_c) on the absorber surface increases which lead to increase in the temperature of the hot side, which can be seen in Figure 4.23, and hence there is an increase in the overall efficiency of the system (η_{sys}) between 1100 hrs to 1400 hrs. ΔT increases from 116K to 190K from 1100 to 1400 hrs and then decreases from 190K to 15K from 1400 hrs to 1645 hrs. The duration 1100 hrs to 1645 hrs can be considered effective sunshine hours. The maximum concentrated heat flux, i.e. 4580W/m^2 is a direct result of the maximum heat flux incident on the water lens at 1400 hrs. The overall efficiency of the GWLSTEG system could be enhanced for the higher value of global radiations (more sunshine) with less wind velocity and relative humidity [236]**.**

The simulated results obtained are much closer to the experimental data, as can be observed in Table 4.4, which proves that methodology adopted for the simulation of the experiment is quite correct.

Table 4.4: Experiment and simulation results comparison

Parameter	**Experimental Value**	**Simulated Value**	**Previous Study** [216]
Maximum Solar irradiance at the lens surface	1135 W/m^2	1203 W/m^2	-
Maximum Solar irradiance at the reveiver plate	4580 W/m^2	4200 W/m^2	-
Maximum temperature of the hot junction of TEG	225^{o}C (498K)	225^{o}C (498K)	250^{o}C
cold junction of TEG	35^{o}C (308K)	35^{o}C (308K)	50 ^{o}C
Maximum temperature difference	190^{o}C (463K)	190^{o}C (463K)	200^{o}C
Maximum electric potential across the surfaces	11V	10.9V	10.1V

The error between the experimental voltage and simulated voltage is 0.90 %, which is very less, and if we consider power and efficiency for the global radiation of 1135 W/m^2 ,the experimental power output of TEG is 6.9 W and theoretically for this radiation, developed hot and cold side temperature should be 503K and 303 K respectively, therefore for the temperature difference of 200 K power developed should be 10W, hence the error between experimental and theoretical power is almost 30%. From the **Eq.(3.36)** the expression of overall system efficiency is $\eta_{sys} = \left[\tau_l \alpha_{ab} - \frac{(\varepsilon_{lh}+\varepsilon_{hc})\sigma_{sb}(T_h^4 - T_c^4)}{C_{th} I_g}\right] X \left[\frac{(T_h - T_c)}{T_h} \frac{\sqrt{1+zT} - 1}{\sqrt{1+zT} + \frac{T_c}{T_h}}\right]$, Putting the value of hot and cold side temperature 503K and 303 K in the above expression, the value of efficiency is obtained 12.63%, Which is theoretical efficiency as shown in Table 4.5**.**

Table 4.5: Validation of thermoelctric model

Parameters	**Experimental value**	**Theoretical value**	**% Error**
Power	6.9 W	10 W	-30%
Overall efficiency of the system (η_{sys})	12.04 %	12.63 %	-4.7%

From **Eq. (3.40)** the error between the experimental value of efficiency and theoretical efficiency is found to be 4.7 % that is a good agreement between the experimental and theoretical values hence mathematical and numerical model for the developed system is valid for the central Indian climatic conditions.

4.3 Total Cost Estimation of SETUP

When conducting the same experiment with different concentrators, the number of concentrators to focus the solar radiation increases the complexity of setup design to focus the same amount of solar radiation over the absorber plate. So, the total cost of the setup has been estimated, in

Table ***4.6***. The total cost only seems to be increasing for the other concentrators as per the complexity of their design.

Table 4.6: Comparison of cost of the giant water lens

Particulars	**Water lens (PVC clear Sheet) ($)**	**Parabolic dish Concentrator ($)** [237]	**Fresnel Lens ($)** [238]	**Parabolic Trough ($)** [61]
Concentrator	11.52	156	182	260
Plywood	95.72	-	-	-
Hardware Items	-	23.09	23.09	23.09
Teeth gear freewheel	92.04	92.04	92.04	92.04
Iron pipe	45.77	-	-	-
Total Cost ($)	**245.05**	**271.13**	**297.13**	**375.13**

The cost of GWLSTEG system would be least as compared to other systems and if compare only concentrator part the cost of water lens is only 11.52 $ i.e thirteen times less as compared to parabolic dish, sixteen times less as compared to fresnel lens and twenty two times less as compared to parabolic trough.

Chapter 5

CONCLUSION AND FUTURE SCOPE

A prototype of solar concentrating thermoelectric generator using giant water lens is fabricated and the potential of thermoelectric cells combined with concentrating solar energy as a power generation system is tested and illustrated. Water lenses are comparatively cheaper, easily available, easy to fabricate and do require not much special care or maintenance. A four to five times increase in the flux intensity of the solar radiation on the absorber plate on the TEG has been achieved in this research by using a water lens as a concentrating device. As compared to the previous experiments conducted using different types of solar concentrators and with almost the same amount of solar irradiance, the water lens can concentrate enough heat flux (4580W/m^2) on the absorber plate to achieve a maximum temeperature of 498K and the Bi_2Te_3 TEM is found able to provide a power output of about 6.9~7 W with an overall system efficiency of 12.04% and exergy efficiency of 2.05%.

5.1 Conclusion

The following conclusions are drawn:

- GWLSTEG technology without maximum power point tracking achieves maximum overall system efficiency of 12.04 % for the global radiation of 1135 W/m^2 and a minimum efficiency of 8.68 % at minimum global radiation of 930 W/m^2 during 1100 hrs and 1400 hrs for the 10 W capacity TEGs with passive/forced air cooling.
- The parameters are achieved as hot side temperature 225^{o}C (498K) and cold side temperature 35^{o}C (308K) that's why ΔT=190^{o}C (463K) instead of 2000^{o}C (473K) is achieved i.e ΔT decreased by 50C (278K) and hence maximum Power output approximately 6.94 W ≈7 W at 11 V voltage and 1.24 A current with an overall system efficiency of 12.04 % are obtained with passive air cooling and without any maximum power point tracker.
- Combination of thermal and optical concentration and improved figure of merit caused improved efficiency (12.04 %).
- Power transfer to the load can be maximized only when the load resistance

would be equal to internal resistance of the TEG module.

- Maximum power output 7W is achieved just near to rated power of 10W as specified by supplier, however not matched with the supplier's specifications. This Power gap is mainly caused by the reduction in ΔT due to dynamic ambient conditions, like increased air velocity and humidity.
- Experimental and theoretical values of generated power and efficiency of the GWLSTEG are within 30% and 4.7% accuracy. The experimental results show considerable agreement with the mathematical and numerical model.
- Performance can also be improved by using selective surface absorber (black paint or any other coating) and by incorporating maximum power point solar tracker however, it increases the cost of GWLSTEG power generation.

5.2 Author's Contribution

The major contributions of the author in this work are as follows:

- Performed experiment of Giant Water Lens Solar Thermoelectric Generator (GWLSTEG) on load condition and achieved no load voltage 11.49 V.
- Performed experiment of Giant Water Lens Solar Thermoelectric Generator (GWLSTEG) on loaded condition and achieved load voltage 11 V, current 1.24 A and power output almost 7 W.
- By ensuring trade-off between thermal concentration (20) and optical concentration (~5), and improved figure of merit efficiency (12.04 %) is achieved as ensured through energy analysis.
- Developed economically viable and technologically feasible power generation technology for common public that can impact social life of rural and urban areas.
- Conducted multiple experiments with plastic of different thicknesses and transmittance and also find the appropriate plastic material with the help of Simulation.

5.3 Future Scope

Further investigation of the GWLSTEG can be carried out with various aspects. It is observed that the perspective applications for such power system strongly depend on the development of the types of concentrator (lens design), thermoelectric material, various absorbers, absorber coating, various substrates, various heat sinks, cooling techniques, therefore research for exploring the modern and efficient technology in above-said areas for development of state-of-the-art GWLSTEG system is recommended.

More experiments need to be conducted on water lens in future in order to increase their efficiency. The numerical simulation methodology as presented in this article also provides a more precise, accurate and less costly means to conduct further experiments on the GWLSTEG. The increased controllability of water lenses may help reduce costs and boost performance in solar thermal applications. Solar energy conversion technologies such as solar cells, thermoelectric, thermo-photovoltaic, Stirling engines, and more, will benefit in the future from research into water lenses. Lenses' interactions with various liquids and their performance at elevated temperatures should also be investigated. GWLSTEG could be a feasible renewable power system. As observed, the GWLSTEG is capable of generating enough power that can be utillized in domestic and industrial sectors, as compared to other STEGs at the same cost and facilities without harming environment.

LIST OF PUBLICATIONS

I. Sanjeev Kumar Bhukesh, Suresh Kumar Gawre & Anil Kumar (2023) Review on advancement in solar and waste heat based thermoelectric generator, **Energy Sources, Part A: Recovery, Utilization, and Environmental Effects**, 45:2, 4982-5002, DOI: 10.1080/15567036.2023.2206370 **(SCIE) IF; 2.90**

II. Sanjeev Kumar Bhukesh, Suresh Kumar Gawre & Anil Kumar (2023) Performance Evaluation of Bi_2Te_3 Semiconductor based Parabolic Dish Concentrated Solar Thermoelectric Generator, **Journal of Semiconductor optoelectronics,** 42:1, 645-673 **(Scopus)**

https://bdtgd.cn/article/view/2023/645.php
https://www.scopus.com/sourceid/13218

III. Sanjeev Kumar Bhukesh, Anil Kumar, Suresh Kumar Gawre "Bismuth telluride (Bi_2Te_3) thermoelectric material as a transducer for solar energy application" in the journal **"Materials Today Proceedings"** 2020, https://doi.org/10.1016/j.matpr.2020.02.646 **(Scopus)**

IV. Sanjeev Kumar Bhukesh, & Anil Kumar (2023) Simulation, Modeling and Experimental Performance Investigation of Novel Giant Water Lens Solar Thermoelectric Generator, **Energy Conversion and Management, Elsevier (SCI) IF; 10.4 (communicated)**

REFERENCES

[1] Ahiska R, Dişlitaş S. Computer controlled test system for measuring the parameters of the real thermoelectric module. Energy Convers Manag. 2011;52(1):27-36, doi:10.1016/j.enconman.2010.06.023.

[2] Najjar YSH, Kseibi MM. Thermoelectric stoves for poor deprived regions – a review. Renew Sustain Energy Rev. 2017;80(January) 2016:597-602, doi: 10.1016/j.rser.2017.05.211.

[3] Varma VS, Kalamdhad AS. Bio-conversion of organic waste using composting technologies- A review. Int J Environ Technol Manag. 2014;17(6):483-507, doi: 10.1504/IJETM.2014.066518.

[4] Warkhade GS, Babu AV. Experimental investigations on the feasibility of higher blends of biodiesel in variable compression ratio diesel engine. Int J Ambient Energy. 2020;41(14):1617-27, doi: 10.1080/01430750.2018.1525574

[5] Sakthivel P, Subramanian KA, Mathai R. Comparative studies on combustion, performance and emission characteristics of a two-wheeler with gasoline and 30% ethanol-gasoline blend using chassis dynamometer. Appl Therm Eng. 2019;146:726-37doi: 10.1016/j.applthermaleng.2018.10.035.

[6] Munda US, Pholane L, Kar DD, Meikap BC. Production of bioenergy from composite waste materials made of corn waste, spent tea waste, and kitchen waste co-mixed with Cow Dung. Int J Green Energy. 2012;9(4):361-75, doi: 10.1080/15435075.2011.621492.

[7] Motghare KA, Rathod AP, Wasewar KL, Labhsetwar NK. Comparative study of different waste biomass for energy application. Waste Manag. 2016;47(A):40-5, doi: 10.1016/j.wasman.2015.07.032.

[8] Yadav P, Heynen AP, Palit D. Pay-As-You-Go nancing: A model for viable and widespread deployment of solar home systems in rural India. Energy Sustain Dev. 2019;48:139-53, doi: 10.1016/j.esd.2018.12.005.

[9] Champier D. Thermoelectric generators: a review of applications. Energy Convers Manag. 2017;140:167-81, doi: 10.1016/j.enconman.2017.02.070.

[10] Xi H, Luo L, Fraisse G. Development and applications of solar-based thermoelectric technologies. Renew Sustain Energy Rev. 2007;11(5):923-36, doi: 10.1016/j.rser.2005.06.008.

[11] Paddock B. A Guide to online information about: Peltier Thermoelectric Coolers; 2001. p. 1-16 [Internet]. StudFiles. [cited 2021 Aug 13]. Available from: https://studfile.net/preview/429756/

[12] Luo D, Wang R, Yu W, Zhou W. Performance optimization of a converging thermoelectric generator system via multiphysics simulations. Energy. 2020;204:117974, doi: 10.1016/j.energy.2020.117974.

[13] Baranowski LL, Snyder GJ, Toberer ES. Concentrated solar thermoelectric generators. Energy Environ Sci. 2012;5(10):9055-67, doi: 10.1039/c2ee22248e.

[14] Allen D, Haugeto R, Kajor M, Namazian M. Small thermoelectric generators. In: Int. Conf. Thermoelectr ICT, proc.; 2002-Janua,2. p.424-6, doi: 10.1109/ICT.2002.1190351.

[15] Mahmoudinezhad S, Cotfas PA, Cotfas DT, Rosendahl LA, Rezania A. Response of thermoelectric generators to Bi2Te3 and Zn4Sb3 energy harvester materials under variant solar radiation. Renew Energy. 2020;146:2488-98, doi: 10.1016/j.renene.2019.08.080.

[16] Elghool A, Basrawi F, Ibrahim TK, Habib K, Ibrahim H, Idris DMND. A review on heat sink for thermo-electric power generation: classi cations and parameters affecting performance. Energy Convers Manag. 2017;134:260-77, doi: 10.1016/j.enconman.2016.12.046.

[17] Tellurex. 2010. Frequently asked questions about our power generation technology. *Technology*. [cited October 15, 2021]. Available from: https://pdfcoffee.com/seebeck-faq-pdf-free.html .

[18] Bharti M, Singh A, Samanta S, Aswal DK. Conductive polymers for thermoelectric power generation. Prog Mater Sci. 2018;93:270-310,

doi: 10.1016/j.pmatsci.2017.09.004.

[19] Sharma Y. Synthesis and characterisation of CZTSe bulk materials for thermoelectric applications. Nanosystems: Phys Chem Math. 2020;11(2):195-204, doi: 10.17586/2220-8054-2020-11-2-195-204.

[20] Ando Junior OH, Maran ALO, Henao NC. A review of the development and applications of thermoelectric microgenerators for energy harvesting. Renew Sustain Energy Rev.2018;91(April)2017:376-93, doi: 10.1016/j.rser.2018.03.052.

[21] Kim HS, Liu W, Chen G, Chu CW, Ren Z. Relationship between thermoelectric gure of merit and energy conversion ef ciency. Proc Natl Acad Sci U S A. 2015;112(27):8205-10, doi: 10.1073/pnas.1510231112.

[22] Aswal DK, Basu R, Singh A. Key issues in development of thermoelectric power generators: high gure-of-merit materials and their highly conducting interfaces with metallic interconnects. Energy Convers Manag. 2016;114:50-67, doi: 10.1016/j.enconman.2016.01.065.

[23] Chen G et al. ’Thermoelectric energy conversion using nanostructured materials,’*Micro- Nanotechnol*. Sens Syst Appl *III*. 2011;8031:80311J, doi: 10.1117/12.885759.

[24] T. Generators. Power where you need it. Technology. [cited Dec 15, 2020] Available from: https://www.globalte.com/products/thermoelectric-generators-tegs/overview

[25] Link C. Accessed Concentrating solar thermoelectric generators with a peak efficiency;2019.[cited,October15,2021].Available,from:https://www.osti.gov/biblio/1388454

[26] Jouhara H, Khordehgah N, Almahmoud S, Delpech B, Chauhan A, Tassou SA. Waste heat recovery technologies and applications. Therm Sci Eng Progr. 2018;6(January):268- 89, doi: 10.1016/j.tsep.2018.04.017

[27] Wang X, Liang R, Fisher P, Chan W, Xu J. Critical design features of thermal-based radioisotope generators: a review of the power solution for polar regions and space. Renew Sustain Energy Rev. 2020;119(October):109572,

doi:10.1016/j.rser.2019.109572.

[28] Karami Rad M, Omid M, Rajabipour A, Tajabadi F, Aistrup Rosendahl L, Rezaniakolaei A. Optimum thermal concentration of solar thermoelectric generators (STEG) in Realistic Meteorological Condition. Energies. 2018;11(9), doi: 10.3390/en11092425

[29] Stiller E, "March06.intro 31(March). p. 1-42; 2010 [Online cited October 15, 2021]. Available from; Papers2://publication/uuid/404677AC-FC6C-4F43-8A36-3280346ED166.

[30] Pourkiaei SM, Ahmadi MH, Sadeghzadeh M, Moosavi S, Pourfayaz F, Chen L et al. Thermoelectric cooler and thermoelectric generator devices: a review of present and potential applications, modeling and materials. Energy. 2019;186:115849, doi: 10.1016/j.energy.2019.07.179.

[31] Arsie I, Cricchio A, Pianese C, Ricciardi V, De Cesare M. Modeling analysis of waste heat recovery via thermo-electric generator and electric turbo-compound for CO2 reduction in automotive SI engines. Energy Procedia. 2015;82:81-8, doi: 10.1016/j.egypro.2015.11.886

[32] Lan S, Yang Z, Chen R, Stobart R. A dynamic model for thermoelectric generator applied to vehicle waste heat recovery. Appl Energy. 2018;210(June):327-38, doi: 10.1016/j.apenergy.2017.11.004

[33] Li W, Paul MC, Siviter J, Montecucco A, Knox AR, Sweet T et al. Thermal performance of two heat exchangers for thermoelectric generators. Case Stud Therm Eng. 2016;8:164- 75, doi: 10.1016/j.csite.2016.06.008

[34] Shittu S, Li G, Xuan Q, Xiao X, Zhao X, Ma X, Akhlaghi YG. Transient and non-uniform heat ux effect on solar thermoelectric generator with phase change material. Appl Therm Eng. 2020;173(October):115206, doi: 10.1016/j.applthermaleng.2020.115206

[35] Kraemer D, McEnaney K, Chiesa M, Chen G. Modeling and optimization of solar thermoelectric generators for terrestrial applications. Sol Energy. 2012;86(5):1338-50, doi:10.1016/j.solener.2012.01.025

[36] Tian H, Jiang N, Jia Q, Sun X, Shu G, Liang X. Comparison of segmented and traditional thermoelectric generator for waste heat recovery of diesel engine. Energy Procedia. 2015;75:590-6, doi: 10.1016/j.egypro.2015.07.461.

[37] Jaziri N, Boughamoura A, Müller J, Mezghani B, Tounsi F, Ismail M. A comprehensive review of Thermoelectric Generators: technologies and common applications. Energy Rep, no. xxxx. 2019;6:264-87, doi: 10.1016/j.egyr.2019.12.011.

[38] Sathawane NS, Dr. Walke PV, Sathawane NS, Walke PV. a Review on Solar Thermoelectric Cogenerator with Evacuated Tube Solar Collector. Int J Adv Res Sci Eng,2014;8354(3).p. 36-41,

Available,from: http://www.ijarse.comwww.ijarse.com.

[39] Ritz F, Peterson CE. Multi-mission radioisotope thermoelectric generator (MMRTG) program overview. In: IEEE Aerosp Conf. proc. 5. p. 2950-7; 2004, doi: 10.1109/AERO.2004.1368101.

[40] Enescu D. Thermoelectric Energy Harvesting: Basic Principles and Applications. Green Energy Advances [Internet]. 2019 Feb 20; Available from: https://www.intechopen.com/books/green-energy-advances/thermoelectric-energy-harvesting-basic-principles-and-applications, doi:10.5772/intechopen.83495

[41] Huang J. Aerospace and aircraft thermoelectric applications. Progr Manag. 2009.

Available,from:chromeextension://efaidnbmnnnibpcajpcglclefindmkaj/https://www1.eere.energy.gov/vehiclesandfuels/pdfs/thermoelectrics_app_2009/thursday/huang.pdf

[42] Pursiheimo E, Holttinen H, Koljonen T. Inter-sectoral effects of high renewable energy share in global energy system. Renew Energy. 2019;136:1119-29, doi: 10.1016/j.renene.2018.09.082

[43] M. and A.J. Azarbayjani. Assessment of solar energy conversion technologies-application of thermoelectric devices in retrofit an office building, *Sixt. Symp. Improv Build Syst Hot Humid Clim*, 2008; no. ESL-HH-08-12-29;p.1-8;

http://txspace.di.tamu.edu/handle/1969.1/90769.

[44] Dalola S, Ferrari V, Guizzetti M, Marioli D, Sardini E, Serpelloni M, Taroni A. Autonomous sensor system with power harvesting for telemetric temperature measurements of pipes. IEEE Trans Instrum Meas. 2009;58(5):1471-8, doi: 10.1109/TIM.2009.2012946.

[45] Nuwayhid RY, Shihadeh A, Ghaddar N. Development and testing of a domestic woodstove thermoelectric generator with natural convection cooling. Energy Convers Manag. 2005;46(9-10):1631-43, doi: 10.1016/j.enconman.2004.07.006

[46] Ismail BI, Ahmed WH. Thermoelectric power generation using waste-heat energy as an alternative green technology. Recent Pat Electr Eng. 2009;2(1):27-39, doi: 10.2174/1874476110902010027.

[47] Zubi G, Fracastoro GV, Lujano-Rojas JM, El Bakari K, Andrews D. The unlocked potential of solar home systems; an effective way to overcome domestic energy poverty in developing regions. Renew Energy. 2019;132:1425-35, doi: 10.1016/j.renene.2018.08.093.

[48] Harb A. Energy harvesting: state-of-the-art. Renew Energy. 2011;36(10):2641-54, doi: 10.1016/j.renene.2010.06.014

[49] Al-Nimr MA, Tashtoush BM, Jaradat AA. Modeling and simulation of thermoelectric device working as a heat pump and an electric generator under Mediterranean climate,Energy.2015;90:1239-50,

doi: 10.1016/j.energy.2015.06.090.

[50] Thornsberry C. Methicillin-resistant staphylococci. Clin Lab Med. 1989;9(2):255-67, https://pubmed.ncbi.nlm.nih.gov/2659244/

[51] Orr B, Akbarzadeh A, Mochizuki M, Singh R. A review of car waste heat recovery systems utilising thermoelectric generators and heat pipes. Appl Therm Eng. 2016;101:490-5, doi: 10.1016/j.applthermaleng.2015.10.081

[52] Ferrari C, Melino F. Thermo – Photo – Voltaic generator development. Energy Procedia. 2014;45:150-9, doi: 10.1016/j.egypro.2014.01.017

[53] Wang Y, Shi Y, Mei D, Chen Z. Wearable thermoelectric generator to harvest body heat for powering a miniaturized accelerometer. Appl Energy. 2018;215(October) 2017:690-8, doi: 10.1016/j.apenergy.2018.02.062.

[54] Kim CS, Lee GS, Choi H, Kim YJ, Yang HM, Lim SH et al. Structural design of a exible thermoelectric power generator for wearable applications. Appl Energy. 2018;214(August) 2017:131-8, doi: 10.1016/j.apenergy.2018.01.074.

[55] Hamid Elsheikh MH, Shnawah DA, Sabri MFM, Said SBM, Haji Hassan M, Ali Bashir MB, Mohamad M. A review on thermoelectric renewable energy: principle parameters that affect their performance. Renew Sustain Energy Rev. 2014;30:337-55, doi: 10.1016/j.rser.2013.10.027.

[56] Penders J, Gyselinckx B, Vullers R, De Nil M, Nimmala VSR, van de Molengraft J et al. Human++: from technology to emerging health monitoring concepts. Proceedings of the 5th int work. Wearable Implant. Body Sens. Networks, BSN2008, conjunction with 5th Int. Summer Sch. Symp. Med, ISSS-MDBS 2008. p. 94-8; 2008, doi: 10.1109/ISSMDBS.2008.4575026.

[57] He W, Zhang G, Zhang X, Ji J, Li G, Zhao X. Recent development and application of thermoelectric generator and cooler. Appl Energy. 2015;143:1-25, doi: 10.1016/j.apenergy.2014.12.075

[58] Lamba R, Manikandan S, Kaushik SC. Performance analysis and optimization of concentrating solar thermoelectric generator. J Electron Mater. 2018;47(9):5310-20, doi: 10.1007/s11664-018-6410-7.

[59] Kumar B, Chauhan YK, Shrivastava V," no. July 2014. A comparative study of maximum power point tracking methods for a photovoltaic-based water pumping system. International Journal of Sustainable Energy. 2014;33(4):37-41, doi: 10.1080/14786451.2013.769990

[60] Kumar S, Saket RK, Dheer DK, Holm-Nielsen JB, Sanjeevikumar P. Reliability enhancement of electrical power system including impacts of renewable energy sources: A comprehensive review. IET Gener Transm Distrib. 2020;14(10):1799-815, doi: 10.1049/iet-gtd.2019.1402.

[61] M. Tecpoyotl-Torres, J. Campos-Alvarez, F. Tellez-Alanis, J. Sánchez-Mondragón, "Parabolic solar concentrator," Proc. SPIE 6330, Nonlinear Optical Transmission and Multiphoton Processes in Organics IV, 63300H (14 September 2006); https://doi.org/10.1117/12.679614

[62] Silver/glass Mirrors for Solar Thermal Systems. 1985. [cited October 15, 2021]; Available,from;chromeextension://efaidnbmnnnibpcajpcglclefindmkaj/https://www.nrel.gov/docs/legosti/old/2293.pdf

[63] Sinha B. 'Study of Solar Thermoelectric Generators Coupled with Concentrated Solar Power Systems,' [master's thesis on the Internet]. *San Fr. State Univ.*, no.; January 2017 [cited 2022 Nov 15].

Available,from:chromeextension://efaidnbmnnnibpcajpcglclefindmkaj/https://scholarworks.calstate.edu/downloads/qb98mg968

[64] Cheruvu P, Kumar VP, Barshilia HC. Experimental analysis and evaluation of a vacuum enclosed concentrated solar thermoelectric generator coupled with a spectrally selective absorber coating. Int J Sustain Energy. 2018;37(8):782-98, doi: 10.1080/14786451.2017.1365866

[65] Watzman S. ' Design of a solar thermoelectric generator' [Undergraduate Honors Thesis on the Internet]. Ohio State Univ; 2013 [cited 2022 Nov 15].

Available,from;chromeextension://efaidnbmnnnibpcajpcglclefindmkaj/https://core.ac.uk/download/pdf/159578913.pdf

[66] Realpe Á, Reina R, Figueroa A, Herrera A, Acevedo M. Modeling of a solar collector of parabolic dish and a plate heat exchanger to improve the industrial drying process of calcium propionate. Int J ChemTech Res. 2016;9(7):523-31

[67] O'Gallagher J, Winston R. Development of compound parabolic concentrators for solar energy. Int J Ambient Energy. 1983;4(4):171-86, doi: 10.1080/01430750.1983.9675885.

[68] Thakkar V. Performance analysis methodology for parabolic dish solar concentrators for process heating using thermic Fluid\n," *IOSR J. Mech*. Civ Eng. 2015;12(1):101-14, doi: 10.9790/1684-1212101114.

[69] Chakraborty O, Roy S, Das B, Gupta R. Effects of helical absorber tube on the energy and exergy analysis of parabolic solar trough collector – A computational analysis. Sustain Energy Technol Assess. 2021;44(February):101083, doi: 10.1016/j.seta.2021.101083

[70] Kraemer D, McEnaney K, Ren Z, Chen G. Solar thermoelectric power conversion Apr 2015; 2012. p. 1-16, doi: 10.1201/b11892-28.

[71] Kraemer D, Chen G. High-accuracy direct ZT and intrinsic properties measurement of thermoelectric couple devices. Rev Sci Instrum. 2014;85(4):045107, doi: 10.1063/1.4870278.

[72] Mcenaney K, Kraemer D, Ren Z, Chen G. 'Modeling of concentrating solar thermoelectric generators Modeling of concentrating solar thermoelectric generators,' vol. Journal of Applied Physics. 2011;110(7):074502, doi: 10.1063/1.3642988

[73] Weinstein L, Kraemer D, McEnaney K, Chen G. Optical cavity for improved performance of solar receivers in solar-thermal systems. Sol Energy. 2014;108:69-79, doi: 10.1016/j.solener.2014.06.023.

[74] Kraemer D, Jie Q, McEnaney K, Cao F, Liu W, Weinstein LA et al. Concentrating solar thermoelectric generators with a peak efficiency of 7.4%. Nat Energy. 2016;1(11), doi: 10.1038/nenergy.2016.153.

[75] Olsen ML, Warren EL, Parilla PA, Toberer ES, Kennedy CE, Snyder GJ et al. A high- temperature, high-ef ciency solar thermoelectric generator prototype. Energy Procedia. 2014;49:1460-9, doi: 10.1016/j.egypro.2014.03.155

[76] Maslamani Abdu TM, Omer I, MMA. Development of solar thermoelectric generator. Eur. Sci. J. 2014;10(9):1857–7881,

https://doi.org/10.19044/esj.2014.v10n9p%25p

[77] Kim MS, Kim MK, Jo SE, Joo C, Kim YJ. Refraction-Assisted Solar Thermoelectric Generator based on Phase-Change Lens. Sci Rep. 2016;6:27913, doi: 10.1038/srep27913,

[78] Chang, H. , Guan, J. , Yang, M.. "A New Design of Mobile Thermoelectric Power Generation System". World Academy of Science, Engineering and Technology, Open Science Index 80, International Journal of Electrical and Computer Engineering,2013;7(8):978-983,doi: doi.org/10.5281/zenodo.1335542

[79] Lv S, He W, Jiang Q, Hu Z, Liu X, Chen H, Liu M. Study of different heat exchange technologies in uence on the performance of thermoelectric generators. Energy Convers Manag. 2018;156(October):167-77,

doi: 10.1016/j.enconman.2017.11.011

[80] Kraemer D, Sui J, McEnaney K, Zhao H, Jie Q, Ren ZF, Chen G. High thermoelectric conversion efficiency of MgAgSb-based material with hot-pressed contacts. Energy Environ Sci. 2015;8(4):1299-308, doi: 10.1039/C4EE02813A.

[81] He R, Kraemer D, Mao J, Zeng L, Jie Q, Lan Y et al. Achieving high power factor and output power density in p-type half-Heuslers Nb1-xTixFeSb. Proc Natl Acad Sci U S A. 2016;113(48):13576-81, doi: 10.1073/pnas.1617663113

[82] Cao F, Kraemer D, Tang L, Li Y, Litvinchuk AP, Bao J et al. A high-performance spectrally-selective solar absorber based on a yttria-stabilized zirconia cermet with high- temperature stability. Energy Environ Sci. 2015;8(10):3040-8, doi: 10.1039/C5EE02066B

[83] Cao F, Kraemer D, Sun T, Lan Y, Chen G, Ren Z. Enhanced thermal stability of W-Ni- Al2O3 Cermet-based spectrally selective solar absorbers with tungsten infrared re ectors. Adv Energy Mater. 2015;5(2):1-6, doi: 10.1002/aenm.201401042

[84] Liu EY, Lin FH, Yang ZR, Liu CJ. A facile energy-saving route of fabricating thermoelectric Sb 2 Te 3 -Te nanocomposites and nanosized Te. R Soc Open Sci. 2018;5(10):180698, doi: 10.1098/rsos.180698

[85] LeBlanc S. Thermoelectric generators: linking material properties and systems engineering for waste heat recovery applications. Sustain Mater Technol. 2014;1-2:26-35, doi: 10.1016/j.susmat.2014.11.002

[86] Fu T, Yue X, Wu H, Fu C, Zhu T, Liu X et al. Enhanced thermoelectric performance of PbTe bulk materials with figure of merit zT >2 by multi-functional alloying. J Mater. 2016;2(2):141-9, doi: 10.1016/j.jmat.2016.05.005.

[87] Zhang X, Zhao LD. Thermoelectric materials: energy conversion between heat and electricity. J Mater. 2015;1(2):92-105, doi: 10.1016/j.jmat.2015.01.001

[88] Rowe DM. CRC Handbook of Thermoelectrics(1st ed). CRC Press; 1995. https://doi.org/10.1201/9781420049718

[89] Chen WH, Lin YX. Performance comparison of thermoelectric generators using different materials. Energy Procedia. 2019;158(2018):1388-93, doi: 10.1016/j.egypro.2019.01.339.

[90] Han M-K, Jin Y, Lee D-H, Kim S-J. Thermoelectric Properties of Bi2Te3: CuI and the Effect of Its Doping with Pb Atoms. Materials 2017;10:1235. https://doi.org/10.3390/ma10111235.

[91] Dunham MT, Hendricks TJ, Goodson KE. Thermoelectric generators: A case study in multi-scale thermal engineering design 51. Elsevier Ltd; 2019.

[92] Richner P, Gaspar PD, Gonçalves LC, Almeida D. 'Experimental results analysis of the energy conversion ef ciency of thermoelectric generators,' *Renew*. Energy Power Qual J. 2011;1(9):278-82, doi: 10.24084/repqj09.312

[93] Lee HS, Attar AM, Weera SL. Performance prediction of commercial thermoelectric cooler modules using the effective material properties. J Electron Mater. 2015;44(6):2157-65, doi: 10.1007/s11664-015-3723-7.

[94] Öhlund T, Andersson M. Effect of paper properties on electrical conductivity and pattern definition for silver nanoparticle inkjet ink. Proceedings of the LOPE-C. 2012;2012(January)2012:115-119,Availablefrom: https://urn.kb.se/resolve?urn=urn:nbn:se:miun:diva-16589

[95] Reif-Acherman S. Studies on the temperature dependence of electric conductivity for metals in the nineteenth century: A neglected chapter in the history of superconductivity. Rev Bras Ensino Fis. 2011;33(4):4602-302, doi: 10.1590/S1806-11172011000400020

[96] Wang S. ‘Characterization and analysis of electrical conductivity properties of nanotube composites’, [master's thesis on the Internet]. *Florida State University*, no.; July 2005 [cited 2022 Dec 20].

Available from: http://purl.flvc.org/fsu/fd/FSU_migr_etd-1258

[97] Tserng, Hua Quen. "Temperature dependence of thermoelectric figure of merit and maximum thermal efficiency of a thermoelectric generator." [master's thesis on the Internet], Rice University, no. (1966), [cited 2023 Jan 05].

Available from: https://hdl.handle.net/1911/89370.

[98] Nicolaou MC. ‘Thermoelectric figure of merit of degenerate and nondegenerate semiconductors’. [dissertation on the Internet]. Northeastern University Boston, Massachusetts, no; December, 2009, [cited 2023 Feb 02].

Available,from:chromeextension://efaidnbmnnnibpcajpcglclefindmkaj/https://repository.library.northeastern.edu/files/neu:1624/fulltext.pdf

[99] Saikhedkar NK, Dewangan A. Experimental analysis of Waste heat recovery using TEG for an internal combustion engine. Int Jour of Inn Sci, Eng & Tech.2015;2(6):711-20.

Available,from:chromeextension://efaidnbmnnnibpcajpcglclefindmkaj/https://ijiset.com/vol2/v2s6/IJISET_V2_I6_101.pdf

[100] Hudge PG, Pawar RN, Watode BD, Kumbharkhane AC. Dielectric relaxation behaviour of triethylene glycol [TEG] + water mixture as a function of composition and temperature using TDR technique.2018;56:269-75. http://nopr.niscpr.res.in/handle/123456789/44207

[101] Li G, Shittu S, Diallo TMO, Yu M, Zhao X, Ji J. A review of solar photovoltaic-thermoelectric hybrid system for electricity generation. Energy. 2018;158:41-58, doi: 10.1016/j.energy.2018.06.021

[102] Yuping Wu. Metal oxides in energy technologies. London: Elsevier; 2018:49-72, https://doi.org/10.1016/B978-0-12-811167-3.00003-1

[103] Qin Y, Xiao Y, Zhao LD. Carrier mobility does matter for enhancing thermoelectric performance. APL Mater. 2020;8(1), doi: 10.1063/1.5144097

[104] Zhang Q, Gu B, Wu Y, Zhu T, Fang T, Yang Y et al. Evolution of the intrinsic point defects in bismuth telluride-based thermoelectric materials. ACS Appl Mater Interfaces. 2019;11(44):41424-31, doi: 10.1021/acsami.9b15198

[105] Zwolenski P, Tobola J, Kaprzyk S. A theoretical search for efficient dopants in Mg 2X (X = Si, Ge, Sn) thermoelectric materials. J Electron Mater. 2011;40(5):889-97, doi: 10.1007/s11664-011-1624-y.

[106] Perumal S, Roychowdhury S, Biswas K. High performance thermoelectric materials and devices based on GeTe. J Mater Chem C. 2016;4(32):7520-36, doi: 10.1039/C6TC02501C.

[107] Bulusu A, Walker DG. Review of electronic transport models for thermoelectric materials. Superlattices Microstruct. 2008;44(1):1-36,

doi: 10.1016/j.spmi.2008.02.008

[108] Savenije TJ, Kroeze JE, Yang X, Loos J. The effect of thermal treatment on the morphology and charge carrier dynamics in a polythiophene-fullerene bulk heterojunction. Adv Funct Mater. 2005;15(8):1260-6,

doi: 10.1002/adfm.200400559.

[109] Shtern YI, Sherchenkov AA, Rogachev MS, Babich AV. Investigation of thermoelectric properties and thermal stability of semiconductor materials for the application in middle temperature thermoelectric generators. In: Proceedings of the 2018 IEEE conf. Russ:1642-5, doi: 10.1109/EIConRus.2018.8317416.

[110] Manikandan S, Kaushik SC. The in uence of Thomson effect in the performance optimization of a two stage thermoelectric generator. Energy. 2016;100:227-37, doi: 10.1016/j.energy.2016.01.092

[111] Nadgorny M, Xiao Z, Chen C, Connal LA. Three-Dimensional Printing of pH-Responsive and Functional Polymers on an A ff ordable Desktop Printer. ACS Appl Mater Interfaces. 2016;8(42):28946-54, doi: 10.1021/acsami.6b07388

[112] Kwan TH, Wu X. The Lock-On Mechanism MPPT algorithm as applied to the hybrid photovoltaic cell and thermoelectric generator system. Appl Energy. 2017;204:873-86, doi: 10.1016/j.apenergy.2017.03.036.

[113] Banakar A, Motevali A, Emad M, Ghobadian B. Co-generation of heat and power in a thermoelectric system equipped with Fresnel lens collectors using active and passive cooling techniques. Renew Energy. 2017;112:268-79, doi: 10.1016/j.renene.2017.05.052.

[114] Kishita Y, Ohishi Y, Uwasu M, Kuroda M, Takeda H, Hara K. Evaluating the life cycle CO2 emissions and costs of thermoelectric generators for passenger automobiles: A scenario analysis. J Clean Prod. 2016;126:607-19, doi: 10.1016/j.jclepro.2016.02.121.

[115] Mamur H, Bhuiyan MRA, Korkmaz F, Nil M. A review on bismuth telluride (Bi2Te3) nanostructure for thermoelectric applications. Renew Sustain Energy Rev. 2018;82(October):4159-69, doi: 10.1016/j.rser.2017.10.112

[116] Mondol AS, Vogel B, Bastian G. Large scale water lens for solar concentration. Opt Express. 2015;23(11):A692-708, doi: 10.1364/OE.23.00A692

[117] Sun L, Liao B, Sheberla D, Kraemer D, Zhou J, Stach EA et al. A microporous and naturally nanostructured thermoelectric metal-organic framework with ultralow thermal conductivity. Joule. 2017;1(1):168-77,

doi: 10.1016/j.joule.2017.07.018

[118] Laird. Product information assembly information performance and properties. Thermoelector. Handb. [Online cited Feb 25, 2023]

Available,from;chromeextension://efaidnbmnnnibpcajpcglclefindmkaj/https://www.lairdthermal.com/sites/default/files/ckfinder/files/resources/Handbooks/Thermoelectric-Assemblies-Handbook-1120.pdf

[119] Lee SW, Yang Y, Lee HW, Ghasemi H, Kraemer D, Chen G, Cui Y. An electrochemical system for ef ciently harvesting low-grade heat energy. Nat Commun. 2014;5(May):3942, doi: 10.1038/ncomms4942

[120] Manikandan S, Kaushik SC. Thermodynamic studies and maximum power point tracking in thermoelectric generator-thermoelectric cooler combined system. Cryogenics. 2015;67:52-62, doi: 10.1016/j.cryogenics.2015.01.008.

[121] Tsai HL, Le PT. Self-suf cient energy recycling of light emitter diode/thermoelectric generator module for its active-cooling application. Energy Convers Manag. 2016;118:170- 8, doi: 10.1016/j.enconman.2016.03.077

[122] Hafez AZ, Soliman A, El-Metwally KA, Ismail IM. Design analysis factors and speci cations of solar dish technologies for different systems and applications. Renew Sustain Energy Rev. 2017;67:1019-36, doi: 10.1016/j.rser.2016.09.077.

[123] Kurt L, Millar J, Lehtonen M, Märss M. Optimization of concentrated solar thermoelectric generator system for highest yearly electric output; *2015* 56th Int Sci Conf. Power Electr Eng Riga Tech Univ RTUCON 2015. p. 1-6 2015, doi: 10.1109/RTUCON.2015.7343170.

[124] Li G, Pei G, Su Y, Ji J, Wang D, Zheng H. Performance study of a static lowconcentration evacuated tube solar collector for medium-temperature applications. Int J Low Carbon Technol. 2016;11(3):363-9, doi: 10.1093/ijlct/ctt083.

[125] Shah PK, Srinivasan K, Srinivasa Murthy SS. Geometry of ideal CPC collectors with gap between absorber and re ector. Int J Sol Energy. 1990;9(1):13-21, doi: 10.1080/01425919008941470

[126] Atouei SA, Rezania A, Ranjbar AA, Rosendahl LA. Protection and thermal management of thermoelectric generator system using phase change materials: an experimental investigation. Energy. 2018;156:311-8, doi: 10.1016/j.energy.2018.05.109

[127] Date A, Date A, Dixon C, Akbarzadeh A. Theoretical and experimental study on heat pipe cooled thermoelectric generators with water heating using concentrated solar thermal energy. Sol Energy. 2014;105:656-68, doi: 10.1016/j.solener.2014.04.016

[128] Bensaid S, Brignone M, Ziggiotti A, Specchia S. High ef ciency Thermo-Electric power generator. Int J Hydrog Energy. 2012;37(2):1385-98,

doi: 10.1016/j.ijhydene.2011.09.125

[129] Sahu AK, Sudhakar K. Effect of UV exposure on bimodal HDPE oats for oating solar application. J Mater Res Technol. 2019;8(1):147-56, doi: 10.1016/j.jmrt.2017.10.002.

[130] Tawiah S, Marfo SA, DB Jnr. Solar power for sustainable offshore petroleum exploration and production in Africa Soc. Pet. Eng. SPE/AAPG Africa Energy Technol. Conf. 2016 Dec 5, 2018;42027:459-66, doi: 10.2118/AFRC-2588537-MS

[131] Kraemer D, Poudel B, Feng HP, Caylor JC, Yu B, Yan X et al. High-performance at- panel solar thermoelectric generators with high thermal concentration. Nat Mater. 2011;10(7):532-8, doi: 10.1038/nmat3013

[132] Moosbrugger C, editor. Engineering properties of magnesium alloys. ASM International; 2017 Nov 1,[Online cited March 1, 2023], doi: 10.1002/9780470905098.ch1

[133] Bux SK, Yeung MT, Toberer ES, Snyder GJ, Kaner RB, Fleurial JP. Mechanochemical synthesis and thermoelectric properties of high quality magnesium silicide. J Mater Chem. 2011;21(33):12259-66, doi: 10.1039/c1jm10827a

[134] 134. Markov M, Hu X, Liu HC, Liu N, Poon SJ, Esfarjani K, Zebarjadi M. Semi-metals as potential thermoelectric materials. Sci Rep. 2018;8(1)(1):9876, doi: 10.1038/s41598- 018-28043-3,

[135] Zhao H, Sui J, Tang Z, Lan Y, Jie Q, Kraemer D et al. High thermoelectric performance of MgAgSb-based materials. Nano Energy. 2014;7:97-103, doi: 10.1016/j.nanoen.2014.04.012

[136] Wang J, Liu S, Li L. Experiments and modeling on thermoelectric power generators used for waste heat recovery from hot water pipes. Energy Procedia. 2019;158:1052-8, doi: 10.1016/j.egypro.2019.01.254.

[137] Carstens JH, Gühmann C. Maximum Power Point controller for thermoelectric generators to support a vehicle power supply. Mater Today Proc. 2015;2(2):790-

803, doi: 10.1016/j.matpr.2015.05.099

[138] Jaworski M, Bednarczyk M, Czachor M. Experimental investigation of thermoelectric generator (TEG) with PCM module. Appl Therm Eng. 2016;96:527-33, doi: 10.1016/j.applthermaleng.2015.12.005

[139] Sun T, Peavey JL, David Shelby MD, Ferguson S, O'Connor BT. Heat shrink formation of a corrugated thin lm thermoelectric generator. Energy Convers Manag. 2015;103:674-80, doi: 10.1016/j.enconman.2015.07.016

[140] Zhang G, Fan L, Niu Z, Jiao K, Diao H, Du Q, Shu G. A comprehensive design method for segmented thermoelectric generator. Energy Convers Manag. 2015;106:510-9, doi: 10.1016/j.enconman.2015.09.068

[141] Yu C, Chau KT. Thermoelectric automotive waste heat energy recovery using maximum power point tracking. Energy Convers Manag. 2009;50(6):1506-12, doi: 10.1016/j.enconman.2009.02.015

[142] Liu X, Li C, Deng YD, Su CQ. An energy-harvesting system using thermoelectric power generation for automotive application. Int J Electr Power Energy Syst. 2015;67:510-6, doi: 10.1016/j.ijepes.2014.12.045.

[143] Niu Z, Diao H, Yu S, Jiao K, Du Q, Shu G. Investigation and design optimization of exhaust-based thermoelectric generator system for internal combustion engine. Energy Convers Manag. 2014;85:85-101, doi: 10.1016/j.enconman.2014.05.061

[144] Chen WH, Wang CC, Hung CI, Yang CC, Juang RC. Modeling and simulation for the design of thermal-concentrated solar thermoelectric generator. Energy. 2014;64:287-97, doi: 10.1016/j.energy.2013.10.073

[145] Shen ZG, Wu SY, Xiao L, Yin G. Theoretical modeling of thermoelectric generator with particular emphasis on the effect of side surface heat transfer. Energy. 2016;95:367-79, doi: 10.1016/j.energy.2015.12.005

[146] Ding LC, Akbarzadeh A, Date A. Transient model to predict the performance of thermoelectric generators coupled with solar pond. Energy. 2016;103:271-89, doi: 10.1016/j.energy.2016.02.124

[147] Li W, Paul MC, Montecucco A, Knox AR, Siviter J, Sellami N et al.

Multiphysics simulations of a thermoelectric generator. Energy Procedia. 2015;75:633-8, doi: 10.1016/j.egypro.2015.07.473

[148] Francioso L, De Pascali C, Sglavo V, Grazioli A, Masieri M, Siciliano P. Modelling, fabrication and experimental testing of an heat sink free wearable thermoelectric generator. Energy Convers Manag. 2017;145:204-13, doi: 10.1016/j.enconman.2017.04.096.

[149] Falcão Carneiro J, Gomes de Almeida F. Model and simulation of the energy retrieved by thermoelectric generators in an underwater glider. Energy Convers Manag. 2018;163(February):38-49, doi: 10.1016/j.enconman.2018.02.031

[150] Mostafavi SA, Mahmoudi M. Modeling and fabricating a prototype of a thermoelectric generator system of heat energy recovery from hot exhaust gases and evaluating the effects of important system parameters. Appl Therm Eng. 2018;132:624-36, doi: 10.1016/j.applthermaleng.2018.01.018

[151] Li W, Paul MC, Montecucco A, Siviter J, Knox AR, Sweet T. Multiphysics simulations of thermoelectric generator modules with cold and hot blocks and effects of some factors. Case Stud Therm Eng. 2017;10(October):63-72, doi:10.1016/j.csite.2017.03.005.

[152] Niu Z, Yu S, Diao H, Li Q, Jiao K, Du Q et al. Elucidating modeling aspects of thermoelectric generator. Int J Heat Mass Transf. 2015;85:12-32, doi:10.1016/j.ijheatmasstransfer.2015.01.107.

[153] Zhao Y, Wang S, Liang Z, Ge M. Performance analysis of wet ue-gas thermoelectric generator. Energy Procedia. 2017;142:148-53, doi: 10.1016/j.egypro.2017.12.024

[154] Kishita Y, Uwasu M, Takeda H, Hara K, Ohishi Y, Kuroda M. Assessing the greenhouse gas emissions and cost of thermoelectric generators for passenger automobiles: A life cycle perspective. Proceedings of the ASME eng tech. conf. 2014;4(6):1-9, doi: 10.1115/DETC2014-34483.

[155] Avaritsioti E. Thermoelectric Generator: An Electronic Device for the Reduction of CO_2 Emissions in Commercial Vehicles. International Journal of Energy and Environment,2016;10:219–224. http://www.naun.org/cms.action?id=12157

[156] Saidur R, Rezaei M, Muzammil WK, Hassan MH, Paria S, Hasanuzzaman M. Technologies to recover exhaust heat from internal combustion engines. Renew Sustain Energy Rev. 2012;16(8):5649-59, doi: 10.1016/j.rser.2012.05.018.

[157] Amarantidis GA, Dixon R, Hubbard PD, Harrington I. Integrated thermoelectric model for on-board aircraft generators. IFAC PapersOnLine. 2016;49(21):598-602, doi: 10.1016/j.ifacol.2016.10.666.

[158] Dai YJ, Wang RZ, Ni L. Experimental investigation on a thermoelectric refrigerator driven by solar cells. Renew Energy. 2003;28(6):949-59, doi: 10.1016/S0960- 1481(02)00055-1.

[159] Rinehart GH. Design characteristics and fabrication of radioisotope heat sources for space missions. Prog Nucl Energy. 2001;39(3-4):305-19, doi: 10.1016/S0149-1970(01)00005-1..

[160] M. S. El-Genk and H. H. Saber, "Thermal and performance analyses of efficient radioisotope power systems," Energy Convers. Manag., vol. 47, no. 15–16, pp. 2290–2307, 2006, doi: 10.1016/j.enconman.2005.11.022.

[161] Hirota M, Nakajima Y, Saito M, Uchiyama M. 120 × 90 element thermoelectric infrared focal plane array with precisely patterned Au-black absorber. Sens Actuators A. 2007;135(1):146-51, doi: 10.1016/j.sna.2006.06.058.

[162] European Commission. Critical raw materials for the EU [Technical report]," *Eur.Commusion*, 39. p. 1-84; 2010, doi: 10.1002/eji.200839120.IL-17-Producing

[163] Karri MA, Thacher EF, Helenbrook BT. Exhaust energy conversion by thermoelectric generator: two case studies. Energy Convers Manag. 2011;52(3):1596-611, doi: 10.1016/j.enconman.2010.10.013

[164] Gou X, Yang S, Xiao H, Ou Q. A dynamic model for thermoelectric generator applied in waste heat recovery. Energy. 2013;52:201-9, doi: 10.1016/j.energy.2013.01.040.

[165] Li G, Pei G, Yang M, Ji J, Su Y. Optical evaluation of a novel static incorporated compound parabolic concentrator with photovoltaic/thermal system and preliminaryexperiment.EnergyConversManag.2014;85:204_211,doi:10.1016/j.en

conman.2014.05.082.

[166] Guiqiang L, Gang P, Yuehong S, Jie J, Riffat SB. Experiment and simulation study on the flux distribution of lens-walled compound parabolic concentrator compared with mirror compound parabolic concentrator. Energy. 2013;58:398-403, doi: 10.1016/j.energy.2013.06.027.

[167] Guiqiang L, Gang P, Yuehong S, Yunyun W, Jie J. Design and investigation of a novel lens-walled compound parabolic concentrator with air gap. Appl Energy. 2014;125:21-7, doi: 10.1016/j.apenergy.2014.03.042.

[168] Vaidya SD. Sun Focus: concentrated solar thermal progress in india (magazine). Proj Manag Unit MNRE. 2016;4(1):1-23. Available from:chrome-extension://efaidnbmnnnibpcajpcglclefindmkaj/https://www.undp.org/sites/g/files/zskgke326/files/migration/in/Sun-Focus-jul-sep-2016.pdf

[169] Sakhare V, Kapatkar VN. Experimental analysis of parabolic solar dish with copper helical coil receiver. Int J Innov Res Adv Eng. 2014;1(8):199-204.

Available from: https://api.semanticscholar.org/CorpusID:114251287

[170] Babalola PO. Design and construction of parabolic solar heater using polymer matrix composite. In: Proceedings of the ICCEM. p. 298-314; 2012. Available from:chromeextension://efaidnbmnnnibpcajpcglclefindmkaj/http://eprints.covenantuniversity.edu.ng/1977/1/Design%20and%20construction%20of%20parabolic%20solar%20heater%20using%20polymer%20matrix.pdf

[171] Sagade A, Shinde N. Performance evaluation of parabolic dish type solar collector for industrial heating application. Int J Energy Technol Policy. 2012;8(1):80-93, doi: 10.1504/IJETP.2012.046015.

[172] Sallaberry F, Serrats EM. 'R2.4 Topic report for WP2 solar thermal collectors. Concentrating / tracking collector component characterization,' Proj. IEE; 2012. Available,from:chromeextension://efaidnbmnnnibpcajpcglclefindmkaj/http://www.estif.org/solarkeymarknew/images/downloads/QAiST/qaist%20d2.1%20r2.4%20concentrating%20tracking%20collector%20component.pdf

[173] SCI. 'Parabolic Solar Cooker Designs; 2019. p. 4211500.

[174] McEnaney K, Weinstein L, Kraemer D, Ghasemi H, Chen G. Aerogel-based solar thermal receivers. Nano Energy. 2017;40:180-6, doi: 10.1016/j.nanoen.2017.08.006

[175] Patel DK, Brahmbhatt PK, Panchal H. A review on compound parabolic solar concentrator for sustainable development. Int J Ambient Energy. 2018;39(5):533-46, doi: 10.1080/01430750.2017.1318786.

[176] Kulal MSD, Patil PR. 'Performance analysis of parabolic solar dish collector for various reflecting materials' [Undergraduate Thesis on the Internet]. Dibrugarh Univ. Assam; 2018 [cited 2023 April 15].

Available,from;chromeextension://efaidnbmnnnibpcajpcglclefindmkaj/https://jecassam.ac.in/wp-content/uploads/2018/10/PERFORMANCE-ANALYSIS-OF-A-SOLAR-PARABOLIC-TROUGH.pdf

[177] Ngo LC. Exergetic analysis and optimisation of a parabolic dish collector for low power application. Angew Chem Int Ed 6(11). 1967;2012:951-2

[178] Vatcharasathien N, Hirunlabh J, Khedari J, Daguenet M. Design and analysis of solar thermoelectric power generation system. Int J Sustain Energy. 2005;24(3):115-27, doi: 10.1080/14786450500291966.

[179] Sagade AA, Shinde NN. 'Performance evaluation & analysis of low cost parabolic dish type solar collector for domestic & industrial heating application,' *30th ISES Bienn*. Sol World Congr.; *2011*. SWC *2011* 5. p. 3428-38, doi: 10.18086/swc.2011.23.15.

[180] Jafrancesco D, Cardoso JP, Mutuberria A, Leonardi E, Les I, Sansoni P et al. Optical simulation of a central receiver system: comparison of different software tools. Renew Sustain Energy Rev. 2018;94(December) 2017:792-803, doi: 10.1016/j.rser.2018.06.028.

[181] N. Resources and D. Council. Concentrated solar power: heating up India's solar thermal market under the national solar mission(September), 2012.

[182] Sundarraj P, Roy SS, Taylor RA, Maity D. Performance analysis of a hybrid solar thermoelectric generator. Energy Sources Part Recover Util Environ Eff.

2016;38(20):2977-84, doi: 10.1080/15567036.2016.1180331.

[183] Muthu G, Shanmugam S, Veerappan AR. Solar parabolic dish thermoelectric generator with acrylic cover. Energy Procedia. 2014;54:2-10, doi: 10.1016/j.egypro.2014.07.244.

[184] Manikandan S, Kaushik SC. Energy and exergy analysis of solar heat pipe based annular thermoelectric generator system. Sol Energy. 2016;135:569-77, doi: 10.1016/j.solener.2016.06.031.

[185] Eswaramoorthy M, Shanmugam S, Veerappan A. Experimental study on solar parabolic dish thermoelectric generator. Int J Energy Eng. 2013;3(3):62-6, doi: 10.5963/IJEE0303001.

[186] Lertsatitthanakorn C, Jamradloedluk J, Rungsiyopas M. Electricity generation from a solar parabolic concentrator coupled to a thermoelectric module. Energy Procedia. 2014;52:150-8, doi: 10.1016/j.egypro.2014.07.065.

[187] Goupil C, Ouerdane H, Zabrocki K, Seifert W, Hinsche NF, Müller E. Thermodynamics and thermoelectricity. Contin Theor Model Thermoelectr Elem. 2016:1-74, doi: 10.1002/9783527338405.ch1.

[188] Suleebka KP. High temperature solar thermoelectric generator. Appl Energy.1979;5(1):53-9, doi: 10.1016/0306-2619(79)90005-9.

[189] Temizer İ, İlkılıç C. The performance and analysis of the thermoelectric generator system used in diesel engines. Renew Sustain Energy Rev. 2016;63:141-51, doi: 10.1016/j.rser.2016.04.068.

[190] Krushi P, Wango S. Smart power generation from waste heat by thermo electric generator *Int. J. Mech*. Prod Eng. 2016:45-9.

[191] Leonov V, Vullers R.J.M 2007. Thermoelectric generators on living beings. Available,from:https://www.researchgate.net/publication/228995659_Thermoelectric_generators_on_living_beings

[192] Huang K, Yan Y, Li B, Li Y, Li K, Li J. A novel design of thermoelectric generator for automotive waste heat recovery. Automot Innov. 2018;1(1):54-61, doi: 10.1007/s42154-018-0006-z.

[193] Drahansky M et al. We are IntechOpen, the world's leading publisher of Open Access books Built by scientists, for scientists TOP 1 %. Intech. 2016;i, no. tourism,:13, doi: 10.5772/57353.

[194] Weng CC, Huang MJ. A study of using a thermoelectric generator to harvest energy from a table lamp. Energy. 2014;76:788-98, doi: 10.1016/j.energy.2014.08.078

[195] Zhao Y, Wang S, Ge M, Li Y, Yang Y. Energy and exergy analysis of thermoelectric generator system with humidi ed ue gas. Energy Convers Manag. 2018;156(October):140-9, doi: 10.1016/j.enconman.2017.10.094.

[196] Gao HB, Huang GH, Li HJ, Qu ZG, Zhang YJ. Development of stove-powered thermoelectric generators: a review. Appl Therm Eng. 2016;96:297-310, doi: 10.1016/j.applthermaleng.2015.11.032.

[197] Montecucco A, Siviter J, Knox AR. A combined heat and power system for solid-fuel stoves using thermoelectric generators. Energy Procedia. 2015;75:597-602, doi: 10.1016/j.egypro.2015.07.462.

[198] Nour Eddine A, Chalet D, Faure X, Aixala L, Chessé P. Optimization and characterization of a thermoelectric generator prototype for marine engine application. Energy. 2018;143:682-95, doi: 10.1016/j.energy.2017.11.018.

[199] Li Y, Wang S, Zhao Y. Experimental study on the in uence of the core ow heat transfer enhancement on the performance of thermoelectric generator. Energy Procedia. 2017;105:901-7, doi: 10.1016/j.egypro.2017.03.410.

[200] Li Y, Witharana S, Cao H, Lasfargues M, Huang Y, Ding Y. Wide spectrum solar energy harvesting through an integrated photovoltaic and thermoelectric system. Particuology. 2014;15:39-44, doi: 10.1016/j.partic.2013.08.003

[201] Kil TH, Kim S, Jeong D, Geum D, Lee S, Jung S et al. A highly-ef cient, concentrating- photovoltaic/thermoelectric hybrid generator. Nano Energy. 2017;37(April):242-7, doi: 10.1016/j.nanoen.2017.05.023

[202] Wu SY, Zhang YC, Xiao L, Shen ZG. Performance comparison investigation on solar photovoltaic-thermoelectric generation and solar photovoltaic-

thermoelectric cooling hybrid systems under different conditions. Int J Sustain Energy. 2018;37(6):533-48, doi: 10.1080/14786451.2017.1345906.

[203] Vanden Eynde NW, Chowdhury S, Chowdhury SP. Modeling and simulation of a stand- alone photovoltaic plant with MPPT feature and dedicated battery storage. IEEE PES Gen Meet PES. 2010;2010:1-8, doi: 10.1109/PES.2010.5589830.

[204] Rangwala A. 'Water Lenses for low-cost concentrator photovoltaics' [master project report on the Internet]. Washington University, St. Louis; 2017 [cited 2023 May 5]

Available,from;chromeextension://efaidnbmnnnibpcajpcglclefindmkaj/https://openscholarship.wustl.edu/cgi/viewcontent.cgi?article=1084&context=mems411

[205] Search H, C Journals, A. Contact, M. Iopscience, I. O. P. Conf, and I. P. Address, "Experimental Analysis of Desalination Unit Coupled with Solar Water Lens Concentrator," vol. 012182, doi: 10.1088/1757-899X/149/1/012182.

[206] McEnaney K, Kraemer D, Ren Z, Chen G. Modeling of concentrating solar thermoelectric generators. J Appl Phys. 2011;110(7), doi: 10.1063/1.3642988.

[207] Sharma H, Sharma YC. Synth Char Bismuth Selenide Thin Films by thermal evaporation technique. NANOSYSTEMS: PHYSICS, CHEMISTRY, MATHEMATICS, 2020;11(1):92-98. doi:10.17586/2220-8054-2020-11-1-92-98

[208] Jagadish P, Khalid M, Amin N, Hajibeigy MT, Li LP, Numan A et al. Recycled carbon fibre/Bi2Te3 and Bi2S3 hybrid composite doped with MWCNTs for thermoelectric applications. Compos B Eng. 2019;175(5):107085, doi: 10.1016/j.compositesb.2019.107085.

[209] Zhao L, He Y, Zhang H, Yi L, Wu J. Enhancing the thermoelectric property of Bi2Te3 through a facile design of interfacial phonon scattering. J Alloys Compd. 2018;768:659-66, doi: 10.1016/j.jallcom.2018.07.324.

[210] Ahmad A, Prakash O, Kumar A, Hussain MS. Drying kinetics and performance analysis of thermal storage-based hybrid greenhouse dryer for uniform drying of tomato akes. J Therm Sci Eng Appl. 2023;15(5):1-10, doi: 10.1115/1.4056242.

[211] Patel AS, Patil PD. Experimental simulation of solar aqua lens concentrator.

IJEAT.2019;9(2):1591-4, doi: 10.35940/ijeat.B2340.129219.

[212] Delin M, Rychwalski RW, Kubát MJ, Kubát J. Volume changes during stress relaxation in polyethylene. Rheol Acta. 1995;34(2):182-95, doi: 10.1007/BF00398438.

[213] Singh S. Refractive index measurement and its applications. Phys Scr. 2002;65(2):167- 80, doi: 10.1238/Physica.Regular.065a00167

[214] De-Jun F, Mao-Sen Z, Liu G, Xi-Lu L, Dong-Fang J. D-shaped plastic optical ber sensor for testing refractive index. IEEE Sens J. 2014;14(5):1673-6, doi: 10.1109/JSEN.2014.2301911.

[215] Duraisamy S, Sundararaj M, Raja K, Poongavanam GK, Selvarasan I. Energy and Exergy Analysis of an Advanced Cookstove-Based Annular Thermoelectric Cogeneration System. InBiomass for Bioenergy-Recent Trends and Future Challenges 2019 Jun 22. IntechOpen. doi:10.5772/intechopen.84237.

[216] Al Musleh M, Topriska EV, Jenkins D, Owens E. Thermoelectric generator characterization at extra-low-temperature difference for building applications in extreme hot climates: experimental and numerical study. Energy Build. 2020;225:110285, doi: 10.1016/j.enbuild.2020.110285.

[217] O'halloran S, Rodrigues MM, "AC. POWER AND EFFICIENCY MEASUREMENT IN A THER-MOELECTRIC GENERATOR degrees in mechanical engineering from Kansas State University. Power and efficiency measurement in a thermoelectric generator 2000, 2000; 2012-3976.

[218] Wigneron JP, Kerr Y. 'Passive Low Frequency Microwaves: Principles, Radiative Transfer, Physics of Measurements,' *microw. remote Sens*. L. Surf Tech Methods. 2016;Nov 2009:219-83, doi: 10.1016/B978-1-78548-159-8.50005-0.

[219] Cheung J, Gardner JL, Migdall A, Polyakov S, Ware M. High accuracy dual lens transmittance measurements. Appl Opt. 2007;46(22):5396-403, doi:10.1364/AO.46.005396.

[220] Said Z, Ghodbane M, Hachicha AA, Boumeddane B. Optical performance

assessment of a small experimental prototype of linear Fresnel re ector. Case Stud Therm Eng. 2019;16:100541, doi: 10.1016/j.csite.2019.100541

[221] Awasthi K, Reddy DS, Khan MK. Design of Fresnel lens with spherical facets for concentrated solar power applications. Int J Energy Res. 2020;44(1):460-72, doi:10.1002/er.4947.

[222] Wendelin T, Dobos A, Lewandowski A. SolTrace: a ray-tracing code for complex solar optical systems. National Renewable Energy Lab.(NREL), Golden, CO (United States); 2013 Oct 1:275–3000. https://doi.org/10.2172/1260924

[223] Günther M, Shahbazfar R, Fend RT, Hamdan M. Advanced CSP teaching materials solar dish technology; 2006. p. 1-63.

[224] Kinoshita GS. The Shenandoah parabolic dish solar collector. *Sandia Natl. Lab.*, no January. p. 1-12; 1985 [Online cited on Feb 15, 2023]. http://prod.sandia.gov/techlib/access- control.cgi/1983/830583.pdf.

[225] A. Khajepour and F. Rahmani, "crossmark," *Appl. Radiat. Isot.*, vol. 119, no. October 2016, pp. 51–59, 2017, doi: 10.1016/j.apradiso.2016.11.001.

[226] Doraghi Q, Khordehgah N, Żabnieńska-Góra A, Ahmad L, Norman L, Ahmad D, Jouhara H. Investigation and computational modelling of variable teg leg geometries. ChemEngineering. 2021;5(3), doi:10.3390/chemengineering5030045

[227] Ming T, Wu Y, Peng C, Tao Y. Thermal analysis on a segmented thermoelectric generator. Energy. 2015;80:388-99, doi: 10.1016/j.energy.2014.11.080.

[228] Lv S, He W, Hu Z, Jinwei M, Chen H, Feiyang S. Experimental investigation of solar thermoelectric (STEG) co-generation system. Energy Procedia. 2019 Feb;158:892–7, doi: 10.1016/j.egypro.2019.01.227

[229] H. P. Garg, *Advances in Solar Energy Technology. Volume 1: Collection and Storage Systems*, vol. 1. 1987.

[230] Duf e JA, Beckman WA. Solar Engenierring of thermal process; John Wiley & Sons;2013. p. 893.

[231] Li P, Cai L, Zhai P, Tang X, Zhang Q, Niino M. Design of a concentration solar thermoelectric generator. J Electron Mater. 2010;39(9):1522-30,doi: 10.1007/s11664- 010-1279-0.

[232] Ong KS. Review of solar, heat pipe and thermoelectric hybrid systems for power generation and heating. Int J Low Carbon Technol. 2016;11(4):460-5, doi: 10.1093/ijlct/ctv022.

[233] Radkowski S, Lubikowski K, Wikary M, Szczurowski K. Seebeck phenomenon, calculation method comparison. J Power Technol. 2015;95:63-7

[234] Zulkifli MN, Ilias I, Abas A, Muhamad WMW. Finite element analysis on the thermoelectric generator for the waste heat recovery of solar application. AIP Conf Proc. 2017;1877, doi: 10.1063/1.4999894.

[235] Moore GA. Modern thermoelectrics. Electron Power UK. 1984;30(9):733, doi: 10.1049/ep.1984.0389.

[236] Shanmugam S, Eswaramoorthy M, Veerappan AR. Modeling and analysis of a solar parabolic dish thermoelectric generator. Energy Sources Part Recover Util Environ Eff. 2014;36(14):1531-9, doi: 10.1080/15567036.2011.555352.

[238] Seller C, Price GL, Sheet ML. ’Solar Fresnel Lense A Explore similar products View all products in Fresnel Lenses Find related products near you This bac millio usin met,’ *indiamart*; 2021, [online cited on April 2, 2023] https://www.indiamart.com/proddetail/solar-fresnel-lense-a-19032890548.html